Aerodynamics 3 (AENG 31101): numerical/potential flow methods and boundary layers

T.C.S. Rendall and C.B. Allen

August 21, 2019

Contents

1 Introduction

The course should be sufficiently self-contained, in terms of lecture notes and handouts, that it is not essential to use/buy a text book to supplement the course notes. However, it is always useful to get a second view of derivations, interpretations etc.

Below is a list of books, all available in the library, that you may wish to refer to at some stage.

1.1 General Aerodynamics

These are good general aerodynamics books. Would help any aerodynamics course and/or project. These all contain a derivation of the fundamental fluid equations.

Bertin and Smith *'Aerodynamics for Engineers'*

F. M. White *'Fluid Mechanics, 3rd Edition'*

J. Anderson *'Fundamentals of Aerodynamics'*

J. Anderson *'Modern Compressible Flow'*

Houghton and Brock *'Aerodynamics for Engineering Students'*

1.2 Complex Potential, Conformal Mapping

These books are more mathematical. All have sections on the complex potential function, and conformal mapping.

Kreyszig *'Advanced Engineering Mathematics*

L.M. Milne-Thomson *'Theoretical Aerodynamics'*

G.K. Batchelor *'An Introduction to Fluid Dynamics'*

G. Lighthill *'An Informal Introduction to Theoretical Fluid Mechanics'*

1.3 Aims of the Course

1. To illustrate the elements of aerodynamics relevant to aircraft design
2. To describe the physical principles involved
3. To demonstrate the mathematical tools used in **classical aerodynamics**, as well as their limitations
4. To show how the concepts derived in earlier courses may be applied to aircraft design

The course divides in to three sections

1. Compressible flow and inviscid tools in 3D. This will cover transonic behaviour in more detail than aero 2, together with the vortex lattice and similar methods. The emphasis here is on how you might use these tools, for example, during your group design project.
2. Complex potential and the Joukowsky transformation. This work allows us to form a model for the inviscid incompressible flow around specific aerofoils in 2D, which we require before we can use it to link to the subsequent boundary layer methods.
3. Laminar and turbulent boundary layers. This will be your first contact with boundary layer behviour. We will take the Joukowsky work and apply this together with boundary layer methods to form a model for a viscous, 2D incompressible aerofoil.

You are expected to have a complete and polished understanding of all topics from fluids 1 and aerodynamics 2. Topics from these courses may appear at any time in any exam question!. Engineering is a complete subject greater than the sum of its parts and you should learn accordingly.

1.4 Role of the Aerodynamicist

To predict forces and moments induced by the flow about an ‘arbitrary shape’. To do this we need to be able to predict the flow about the shape.

Fluid flow is governed by the NAVIER-STOKES equations - governs UNSTEADY, COMPRESSIBLE, VISCOUS, 3D flow.

However, these are non-linear, partial differential equations and hence insoluble analytically.

Hence, we must use physical insight to make assumptions about the flow and/or the shape to reduce the equations to an approximate form which can be solved analytically.

CLASSICAL AERODYNAMICS - Get exact solutions of approximate equations.

COMPUTATIONAL AERODYNAMICS - Get approximate solutions of exact equations.

1.5 Compressible Flow Equations

The Navier-Stokes equations govern all fluid flow, i.e. unsteady, viscous, compressible flow. However, these are insoluble analytically except for a few special cases, so classical methods reduce these equations to simpler ones, which can be solved.

1.5.1 3-D Navier-Stokes Equations in Fixed Axis System

Velocity vector: $\underline{\mathbf{U}} = u\underline{\mathbf{i}} + v\underline{\mathbf{j}} + w\underline{\mathbf{k}}$
Body force vector: $\underline{\mathbf{F}} = f_x\underline{\mathbf{i}} + f_y\underline{\mathbf{j}} + f_z\underline{\mathbf{k}}$
CONTINUITY EQUATION

$$\frac{\partial \rho}{\partial t} + \underline{\nabla}.(\rho\underline{\mathbf{U}}) = 0$$

MOMENTUM EQUATION(S)

$$\frac{\partial(\rho\underline{\mathbf{U}})}{\partial t} + \underline{\nabla}.(\rho\underline{\mathbf{U}}\underline{\mathbf{U}}) = -\underline{\nabla}P + \rho\underline{\mathbf{F}} + \frac{4}{3}\underline{\nabla}(\mu\underline{\nabla}.\underline{\mathbf{U}}) + \underline{\nabla}(\underline{\mathbf{U}}.\underline{\nabla}\mu)$$

$$-\underline{\mathbf{U}}\nabla^2\mu + \underline{\nabla}\mu\times(\underline{\nabla}\times\underline{\mathbf{U}}) - (\underline{\nabla}.\underline{\mathbf{U}})\underline{\nabla}\mu - \underline{\nabla}\times(\underline{\nabla}\times\mu\underline{\mathbf{U}})$$

Note that $\underline{\mathbf{U}} \otimes \underline{\mathbf{U}} = \underline{\mathbf{U}}\underline{\mathbf{U}} = \underline{\mathbf{U}}\underline{\mathbf{U}}^T$ is the vector outer product. This gives a matrix, from which the divergence may be taken to get a vector again (the momentum equation is usually a 3 component vector equation). So

$$\underline{\mathbf{U}} \otimes \underline{\mathbf{U}} = \begin{pmatrix} u^2 & uv & uw \\ vu & v^2 & vw \\ wu & wv & w^2 \end{pmatrix}$$

It is symmetric, so you can take divergence of a row or column and get the same result.

ENERGY EQUATION

$$\rho\frac{\partial e}{\partial t} + \rho\underline{\mathbf{U}}.\underline{\nabla}e + P\underline{\nabla}.\underline{\mathbf{U}} = \underline{\nabla}.(K\underline{\nabla}T) + \Phi$$

Φ = DISSIPATION FUNCTION = $\sum \tau_{ij}\frac{\partial U_i}{\partial X_j}$

Newtonian fluid with constant viscosity, momentum equation reduces to

$$\frac{\partial(\rho\underline{\mathbf{U}})}{\partial t} + \underline{\nabla}.(\rho\underline{\mathbf{U}}\underline{\mathbf{U}}) = -\underline{\nabla}P + \rho\underline{\mathbf{F}} + \frac{1}{3}\mu\underline{\nabla}(\underline{\nabla}.\underline{\mathbf{U}}) + \mu\nabla^2\underline{\mathbf{U}}$$

For example
CONTINUITY EQUATION

$$\frac{\partial \rho}{\partial t} + \frac{\partial \rho u}{\partial x} + \frac{\partial \rho v}{\partial y} + \frac{\partial \rho w}{\partial z} = 0$$

X-MOMENTUM

$$\frac{\partial \rho u}{\partial t} + \frac{\partial \rho u^2}{\partial x} + \frac{\partial \rho uv}{\partial y} + \frac{\partial \rho uw}{\partial z} + \frac{\partial P}{\partial x} - \rho f_x =$$

$$\frac{1}{3}\mu\left\{\frac{\partial^2 u}{\partial x^2} + \frac{\partial^2 v}{\partial x\partial y} + \frac{\partial^2 w}{\partial x\partial z}\right\} + \mu\left\{\frac{\partial^2 u}{\partial x^2} + \frac{\partial^2 u}{\partial y^2} + \frac{\partial^2 u}{\partial z^2}\right\}$$

Above all, remember that the NS equations represent *transport*. Whether the property is mass, momentum or energy, it gets moved from A to B without being destroyed (unless you specify this, eg a chemical reaction dumps energy into the flow). Remember that for momentum what we really mean is that momentum changes are balanced by forces (pressure or viscous), according to Newton's second law. Momentum itself clearly changes (consider freestream flow moving to a stagnation point where the velocity is zero).

1.5.2 Euler Equations

The equations that correctly describe inviscid, compressible and rotational flow are the Euler equations, which may be written for steady flow as:

$$\frac{\partial \rho u}{\partial x} + \frac{\partial \rho v}{\partial y} + \frac{\partial \rho w}{\partial z} = 0$$
$$\frac{\partial \rho u^2}{\partial x} + \frac{\partial \rho uv}{\partial y} + \frac{\partial \rho uw}{\partial z} = -\frac{\partial P}{\partial x}$$
$$\frac{\partial \rho uv}{\partial x} + \frac{\partial \rho v^2}{\partial y} + \frac{\partial \rho vw}{\partial z} = -\frac{\partial P}{\partial y}$$
$$\frac{\partial \rho uw}{\partial x} + \frac{\partial \rho vw}{\partial y} + \frac{\partial \rho w^2}{\partial z} = -\frac{\partial P}{\partial z}$$

These are in the *conservative* form. The left hand side of each equation can be expanded as;

$$\frac{\partial \rho u^2}{\partial x} + \frac{\partial \rho uv}{\partial y} + \frac{\partial \rho uw}{\partial z} = \rho u\frac{\partial u}{\partial x} + \rho v\frac{\partial u}{\partial y} + \rho w\frac{\partial u}{\partial z}$$
$$+u\left(\frac{\partial \rho u}{\partial x} + \frac{\partial \rho v}{\partial y} + \frac{\partial \rho w}{\partial z}\right)$$

From continuity equation, the term in brackets is identically zero. The equations may thus be written as;

$$u\frac{\partial u}{\partial x} + v\frac{\partial u}{\partial y} + w\frac{\partial u}{\partial z} = -\frac{1}{\rho}\frac{\partial P}{\partial x}$$
$$u\frac{\partial v}{\partial x} + v\frac{\partial v}{\partial y} + w\frac{\partial v}{\partial z} = -\frac{1}{\rho}\frac{\partial P}{\partial y}$$
$$u\frac{\partial w}{\partial x} + v\frac{\partial w}{\partial y} + w\frac{\partial w}{\partial z} = -\frac{1}{\rho}\frac{\partial P}{\partial z}$$

You can also think of this as $F = ma$, where force 'is' the gradient of pressure (gradient of pressure has units of force per volume), and density 'is' mass (density has units of mass per volume). Showing that the force per volume is the gradient of pressure can be done through the divergence theorem, by taking the force acting on an element of mass (surface integral of pressure and normal vector)

$$\int p\mathbf{n}ds = \int \nabla p dV \tag{1}$$

the mass per volume is just the density, the acceleration is $\frac{D\mathbf{u}}{Dt}$ and $\mathbf{n}$ is outwards from the volume, giving $-\nabla p = \rho\frac{D\mathbf{u}}{Dt}$, or $F = ma$ (per volume). Remembering that $\frac{D\mathbf{u}}{Dt} = \frac{\partial \mathbf{u}}{\partial t} + \mathbf{u}\cdot\nabla\mathbf{u}$ the equivalence to the above is clear. The minus sign appears because we need the inwards normal to get the force on the volume rather than the outwards normal.

1.5.3 Isentropic and Irrotational Assumptions

If we assume the flow is isentropic (essentially weak shock waves or shock free) then we have the relationship;

$$P = k\rho^{\gamma}$$

so

$$\frac{\partial P}{\partial x} = k\gamma\rho^{\gamma-1}\frac{\partial \rho}{\partial x} = \frac{\gamma P}{\rho}\frac{\partial \rho}{\partial x} = a^2\frac{\partial \rho}{\partial x}$$

where a is the local speed of sound. A similar equation is found for $\frac{\partial \rho}{\partial y,z}$.

If the flow is irrotational, then the vorticity is everywhere zero. Vorticity is a vector,

$$\underline{\omega} = \underline{\nabla} \times \underline{U} = \omega_x \underline{i} + \omega_y \underline{j} + \omega_z \underline{k}$$

and so all three components must be zero, i.e.

$$\omega_x = \frac{\partial w}{\partial y} - \frac{\partial v}{\partial z} = 0$$

$$\omega_y = \frac{\partial u}{\partial z} - \frac{\partial w}{\partial x} = 0$$

$$\omega_z = \frac{\partial v}{\partial x} - \frac{\partial u}{\partial y} = 0$$

We may use these relationships to substitute for some terms in the momentum equations;

$$u\frac{\partial u}{\partial x} + v\frac{\partial u}{\partial y} + w\frac{\partial u}{\partial z} = u\frac{\partial u}{\partial x} + v\frac{\partial v}{\partial x} + w\frac{\partial w}{\partial x} = \frac{\partial \frac{1}{2}\left(u^2+v^2+w^2\right)}{\partial x}$$

$$u\frac{\partial v}{\partial x} + v\frac{\partial v}{\partial y} + w\frac{\partial v}{\partial z} = u\frac{\partial u}{\partial y} + v\frac{\partial v}{\partial y} + w\frac{\partial w}{\partial y} = \frac{\partial \frac{1}{2}\left(u^2+v^2+w^2\right)}{\partial y}$$

$$u\frac{\partial w}{\partial x} + v\frac{\partial w}{\partial y} + w\frac{\partial w}{\partial z} = u\frac{\partial u}{\partial z} + v\frac{\partial v}{\partial z} + w\frac{\partial w}{\partial z} = \frac{\partial \frac{1}{2}\left(u^2+v^2+w^2\right)}{\partial z}$$

So, for irrotational, isentropic flow, the momentum equations become;

$$\frac{\partial \frac{1}{2}\left(u^2+v^2+w^2\right)}{\partial x} = -\frac{a^2}{\rho}\frac{\partial \rho}{\partial x}$$

$$\frac{\partial \frac{1}{2}\left(u^2+v^2+w^2\right)}{\partial y} = -\frac{a^2}{\rho}\frac{\partial \rho}{\partial y}$$

$$\frac{\partial \frac{1}{2}\left(u^2+v^2+w^2\right)}{\partial z} = -\frac{a^2}{\rho}\frac{\partial \rho}{\partial z}$$

Now consider the term

$$\frac{a^2}{\rho}\frac{\partial \rho}{\partial x} = \frac{\gamma P}{\rho^2}\frac{\partial \rho}{\partial x}$$

Using the isentropic relationship $P = k\rho^\gamma$,

$$\frac{\gamma P}{\rho^2}\frac{\partial \rho}{\partial x} = \frac{\gamma k \rho^\gamma}{\rho^2}\frac{\partial \rho}{\partial x} = \gamma k \rho^{\gamma-2}\frac{\partial \rho}{\partial x} = \frac{\partial\left(\frac{\gamma k \rho^{\gamma-1}}{\gamma-1}\right)}{\partial x} = \frac{\partial\left(\frac{\gamma}{\gamma-1}\frac{P}{\rho}\right)}{\partial x}$$

with similar results for y and z terms. The momentum equations are then;

$$\frac{\partial \frac{1}{2}\left(u^2+v^2+w^2\right)}{\partial x} = -\frac{\partial\left(\frac{\gamma}{\gamma-1}\frac{P}{\rho}\right)}{\partial x}$$

$$\frac{\partial \frac{1}{2}\left(u^2+v^2+w^2\right)}{\partial y} = -\frac{\partial\left(\frac{\gamma}{\gamma-1}\frac{P}{\rho}\right)}{\partial y}$$

$$\frac{\partial \frac{1}{2}\left(u^2+v^2+w^2\right)}{\partial z} = -\frac{\partial\left(\frac{\gamma}{\gamma-1}\frac{P}{\rho}\right)}{\partial z}$$

or, as these equations show it does not vary in space;

$$\frac{1}{2}(u^2+v^2+w^2) + \frac{\gamma}{\gamma-1}\frac{P}{\rho} = H$$

where H is constant, equal to the total enthalpy of the flow. This may be used to give an equation for the local speed of sound $a^2 = \frac{\gamma P}{\rho}$. Taking conditions in the undisturbed freestream to be a_∞ and U_∞ we equate local and undisturbed conditions;

$$\frac{1}{2}(u^2+v^2+w^2) + \frac{a^2}{\gamma-1} = \frac{1}{2}U_\infty^2 + \frac{a_\infty^2}{\gamma-1}$$

The continuity equation may be written in the expanded form;

$$\frac{\partial \rho u}{\partial x} + \frac{\partial \rho v}{\partial y} + \frac{\partial \rho w}{\partial z} = \rho\left(\frac{\partial u}{\partial x} + \frac{\partial v}{\partial y} + \frac{\partial w}{\partial z}\right)$$

$$+u\frac{\partial \rho}{\partial x} + v\frac{\partial \rho}{\partial y} + w\frac{\partial \rho}{\partial z} = 0$$

or

$$\left(\frac{\partial u}{\partial x} + \frac{\partial v}{\partial y} + \frac{\partial w}{\partial z}\right) + u\frac{1}{\rho}\frac{\partial \rho}{\partial x} + v\frac{1}{\rho}\frac{\partial \rho}{\partial y} + w\frac{1}{\rho}\frac{\partial \rho}{\partial z} = 0$$

Now

$$\frac{1}{\rho}\frac{\partial \rho}{\partial x} = -\frac{1}{a^2}\left(u\frac{\partial u}{\partial x} + v\frac{\partial v}{\partial x} + w\frac{\partial w}{\partial x}\right)$$

with similar expressions for $\frac{1}{\rho}\frac{\partial \rho}{\partial y}$ and $\frac{1}{\rho}\frac{\partial \rho}{\partial z}$. Substituting these expressions into the expanded continuity equation, we obtain;

$$\left(\frac{\partial u}{\partial x} + \frac{\partial v}{\partial y} + \frac{\partial w}{\partial z}\right) - \frac{u}{a^2}\left(u\frac{\partial u}{\partial x} + v\frac{\partial v}{\partial x} + w\frac{\partial w}{\partial x}\right)$$

$$-\frac{v}{a^2}\left(u\frac{\partial u}{\partial y} + v\frac{\partial v}{\partial y} + w\frac{\partial w}{\partial y}\right) - \frac{w}{a^2}\left(u\frac{\partial u}{\partial z} + v\frac{\partial v}{\partial z} + w\frac{\partial w}{\partial z}\right) = 0$$

Collecting terms, this is equal to

$$(a^2-u^2)\frac{\partial u}{\partial x} + (a^2-v^2)\frac{\partial v}{\partial y} + (a^2-w^2)\frac{\partial w}{\partial z} -$$

$$uv\left(\frac{\partial v}{\partial x} + \frac{\partial u}{\partial y}\right) - uw\left(\frac{\partial w}{\partial x} + \frac{\partial u}{\partial z}\right) - vw\left(\frac{\partial w}{\partial y} + \frac{\partial v}{\partial z}\right) = 0$$

1.5.4 Velocity Potential

As the flow is irrotational we may introduce the velocity potential Φ such that

$$u = \frac{\partial \Phi}{\partial x}, \qquad v = \frac{\partial \Phi}{\partial y}, \qquad w = \frac{\partial \Phi}{\partial z}$$

The modified continuity equation then becomes;

$$(a^2 - u^2)\frac{\partial^2 \Phi}{\partial x^2} + (a^2 - v^2)\frac{\partial^2 \Phi}{\partial y^2} + (a^2 - w^2)\frac{\partial^2 \Phi}{\partial z^2} -$$

$$2uv\left(\frac{\partial^2 \Phi}{\partial x \partial y}\right) - 2uw\left(\frac{\partial^2 \Phi}{\partial x \partial z}\right) - 2vw\left(\frac{\partial^2 \Phi}{\partial y \partial z}\right) = 0$$

This is the **Full Potential Equation**. To make further progress we now introduce the small perturbation assumption. The onset flow is taken as parallel to the $x-$axis, so that at upstream infinity the velocity vector is $(U_\infty, 0, 0)$ in these *wind axes*. The velocity field is then taken as a perturbation of this onflow;

$$u = U_\infty + u', \qquad v = v', \qquad w = w'$$

where the dashes represent perturbation velocities. The local (perturbed) speed of sound is then

$$a^2 = a_\infty^2 + \frac{\gamma - 1}{2}(U_\infty^2 - (U_\infty + u')^2 - v'^2 - w'^2)$$

$$= a_\infty^2 - \frac{\gamma - 1}{2}(2U_\infty u' + u'^2 + v'^2 + w'^2)$$

So

$$a^2 - u^2 = a_\infty^2 - \frac{\gamma - 1}{2}(2U_\infty u' + u'^2 + v'^2 + w'^2)$$
$$-U_\infty^2 - 2U_\infty u' - u'^2$$

Retaining only the first-order terms in the perturbation velocities, this is approximately;

$$a^2 - u^2 \approx a_\infty^2 - U_\infty^2 - 2U_\infty u' - (\gamma - 1)U_\infty u'$$

$$a^2 - u^2 \approx a_\infty^2 - U_\infty^2 - (\gamma + 1)U_\infty u'$$

We may be interested in conditions where $U_\infty \approx a_\infty$, i.e. near sonic or transonic conditions, we cannot drop the $(\gamma + 1)U_\infty u'$ term at this stage. In a similar manner, we obtain the following *linear* approximations

$$a^2 - v^2 \approx a_\infty^2 - (\gamma - 1)U_\infty u' \approx a_\infty^2$$
$$a^2 - w^2 \approx a_\infty^2 - (\gamma - 1)U_\infty u' \approx a_\infty^2$$

Substituting these approximations into the full potential equation, we obtain;

$$(a_\infty^2 - U_\infty^2 - (\gamma + 1)U_\infty u')\frac{\partial^2 \Phi}{\partial x^2} + a_\infty^2 \frac{\partial^2 \Phi}{\partial y^2} + a_\infty^2 \frac{\partial^2 \Phi}{\partial z^2}$$

$$-2U_\infty v^{'}\frac{\partial^2\Phi}{\partial x\partial y} - 2U_\infty w^{'}\frac{\partial^2\Phi}{\partial x\partial z} - 2v^{'}w^{'}\frac{\partial^2\Phi}{\partial y\partial z} = 0$$

The last three terms can be dropped as (generally) being small, to obtain

$$(a_\infty^2 - U_\infty^2 - (\gamma+1)U_\infty u^{'})\frac{\partial^2\Phi}{\partial x^2} + a_\infty^2\frac{\partial^2\Phi}{\partial y^2} + a_\infty^2\frac{\partial^2\Phi}{\partial z^2} = 0$$

This is the **Transonic Small Perturbation** or TSP equation. It has been used as the basis of a number of early CFD codes, and is still used in some industrial applications.

If $U_\infty << a_\infty$ (subsonic), or $U_\infty >> a_\infty$ (supersonic), then we can neglect the term $(\gamma+1)U_\infty u^{'}$ in comparison with $a_\infty^2 - U_\infty^2$ and arrive at the greatly simplified equation

$$(a_\infty^2 - U_\infty^2)\frac{\partial^2\Phi}{\partial x^2} + a_\infty^2\frac{\partial^2\Phi}{\partial y^2} + a_\infty^2\frac{\partial^2\Phi}{\partial z^2} = 0$$

which is generally presented as the **Prandtl-Glauert equation** in the form;

$$(1 - M_\infty^2)\frac{\partial^2\Phi}{\partial x^2} + \frac{\partial^2\Phi}{\partial y^2} + \frac{\partial^2\Phi}{\partial z^2} = 0$$

1.5.5 Perturbation Potential

We can also introduce the perturbation potential ϕ such that $\Phi = U_\infty x + \phi$ and so

$$u^{'} = \frac{\partial\phi}{\partial x}, \qquad v^{'} = \frac{\partial\phi}{\partial y}, \qquad w^{'} = \frac{\partial\phi}{\partial z}$$

It is trivial to show that the Prandtl-Glauert equation can be rewritten in terms of perturbation potential to give;

$$(1 - M_\infty^2)\frac{\partial^2\phi}{\partial x^2} + \frac{\partial^2\phi}{\partial y^2} + \frac{\partial^2\phi}{\partial z^2} = 0$$

the **Prandtl-Glauert equation for perturbation potential**.

We shall see later how to construct real flows by summing solutions to Laplaces equation.

2 Supercritical aerofoils

Key points: *Breguet range, effect of wave drag on $\frac{ML}{D}$, supercritical aerofoil ideas, pros and cons, Korn equation in 2D and for a wing, a CFD method for estimating κ*

2.1 Why Mach 0.8?

A common misconception, often implied in media aviation commentaries, is that commercial aircraft are designed to burn as little fuel as possible flying a given distance. This probably has much to do with many people only encountering aircraft design through paper aeroplanes or models, where the goal is to glide as far as possible or stay aloft for as long as possible. 'If we can get from Heathrow to JFK burning 100kg less fuel', goes the reasoning, 'then that is a good thing'. The truth of course is that commercial aircraft are designed for commerce and nothing else; safety is required, comfort is desired but profit is holy. The logic should read, 'if we can get from Heathrow to JFK making £100 more profit, then we must'. Either that, or the airline eventually fails.

Consider a drive home to see your parents. You 'should' drive at the speed for lowest fuel consumption per mile. Too slow and engine and transmission losses are excessive (an idling car consumes fuel but travels nowhere; the MPG is infinitely poor), too fast and aerodynamic drag dominates with the square of the speed. Now consider driving a taxi (let's assume not on a meter, but paid per journey). You wish to earn your living so the number of journeys you can complete in a day is an important factor. If you drive a little faster than when you drive home you can complete a extra few trips, and the profit here is greater than the extra fuel burnt due to the additional speed required. An obvious point perhaps, but rarely pointed out in environmental discussions.

So is there a magic number we can calculate in advance that represents how profitable an aircraft is? Sadly, no. This depends on everything from the wing and engine design and integration to how big a loan the airline needs to buy the aircraft (and the associated interest payments). Perhaps a heavier aircraft makes more money because although it burns more fuel it is cheaper to maintain. Some US domestic carriers operate rather outdated aircraft because the finance required to buy new ones would, overall, lose them money compared to keeping the old aircraft flying. Banks view airlines as risky and the rates are high.

So we've established we can't calculate profitability directly without taking into account a large number of other factors. However, it turns out that in the broadest terms airlines would like to maximise $\frac{ML}{D}$ - the Breguet range. They want a high $\frac{L}{D}$ because fuel is a large (and ever increasing) cost, but they also want a high speed so that they can operate more flights in a given time with that aircraft, as this means they get a better return on per-hour crew costs. Maximising range also means they can cover more of the potential market in terms of destinations.

So, shall we give up on this seemingly intractable problem? I think not! First, a reminder of Breguet range.

2.2 Breguet Range Reminder

The aircraft is in equilibrium, so weight and lift, and thrust and drag balance, so that

$$W = L = D\frac{L}{D} = T\frac{L}{D} \tag{2}$$

The rate of change of weight can be linked to the mass flow rate of fuel $\dot{m}$, and also the specific fuel consumption S (fuel burn per unit thrust) and thrust T

$$-\frac{dW}{dt} = g\dot{m} = gST \tag{3}$$

Putting these together

$$-\frac{dW}{dt} = gS\frac{W}{\frac{L}{D}} \tag{4}$$

$$\frac{dW}{W} = -gS\frac{dt}{\frac{L}{D}} \tag{5}$$

Integrating

$$\ln\left(\frac{W_1}{W_2}\right) = gS\frac{t_f}{\frac{L}{D}} \tag{6}$$

Where t_f is time elapsed. Range is $t_f V$ so

$$R = \frac{VL}{D}\frac{1}{gS}\ln\left(\frac{W_1}{W_2}\right) = a_0\frac{ML}{D}\frac{1}{gS}\ln\left(\frac{W_1}{W_2}\right) \tag{7}$$

This is handy, but no use unless we can relate it to the transonic behaviour quantitatively.

A useful empirical result is Lock's fourth power law[1*]

$$C_{d_w} = K(M - M_{crit})^4 \tag{8}$$

Why a fourth power? Drag associated with a normal shock varies with the cube, and Lock ascertained that shock height is roughly linear with Mach number, which overall leads to the fourth power. An offset of 0.1 in M_{crit} can give better agreement, so $M'_{crit} = M_{crit} - 0.1$ may sometimes be used (see coursework), but the justification is based on experiment; this uncertainty is the price to be paid for conceptual simplicity.

This is only applicable to aerofoils (ie 2D), but it can tell us a lot. Wave drag for an aircraft will follow a similar curve, but with perhaps a different constant K, a different M_{crit} and an alternative power (not perhaps 4).

Notice the neatness of this result. There's a lot of physics in there; if the thickness goes up M_{crit} goes down, and the wave drag therefore goes up. If C_L goes up (incidence increases) M_{crit} also drops, so again the wave drag rises. A pure increase in M of course achieves a similar drag increase. That's three physical effects for the price of only one aerofoil parameter (M_{crit}).

*CNH Lock carried out a great deal of work relating to aerodynamics and later transonic aerofoils during the first half of the last century, and confusingly was followed by RC Lock working primarily at the NPL, from 1950 through to the 80s, also on transonics - I have no idea if they were related

We shall include some non-compressible drag here in the form of C_{d_0} and induced drag for realism (you'll see it makes a difference). Don't go thinking this analysis is the letter of the law; in reality these parameters interact, but this is beyond what we want to discuss at this point.

So, looking at the Breguet range parameter

$$f = \frac{ML}{D} = \frac{MC_L}{K(M - M_{crit})^4 + C_{d_0} + \frac{C_L^2}{\pi A_R}} \tag{9}$$

which we can differentiate with respect to M to arrive at

$$\frac{df}{dM} = \frac{C_L(K(M - M_{crit})^4 + C_{d_{tot}}) - 4K(M - M_{crit})^3 MC_L}{(K(M - M_{crit})^4 + C_{d_{tot}})^2} \tag{10}$$

where we have kept C_L and $C_{d_{tot}} = C_{d_0} + \frac{C_L^2}{\pi A_R}$ as constants. This is valid if we consider an aircraft at a varying altitude, so that the pressure changes as the Mach number changes to keep the dimensional lift unchanged. If we made different assumptions so that C_L was a function of M, the results would be marginally different.

We would like f to be a maximum so setting the polynomial in the numerator to zero is a sensible choice (we can find $\frac{ML}{D}$ later to check we have a maximum and not a minimum!). So, solve

$$K(M - M_{crit})^4 + C_{d_{tot}} - 4K(M - M_{crit})^3 M = 0 \tag{11}$$

Trivially if $C_{d_{tot}} \approx 0$ then we should fly at the critical Mach number. Now, since $M - M_{crit}$ will be positive but less than one, and $K < 4K$, we know that the (subtracting) cubed term dominates the (adding) quartic term. So, as $C_{d_{tot}}$ goes up, so must M in order to remain at the root of the polynomial. Hence, the optimum $\frac{ML}{D}$ will be with $M > M_{crit}$, i.e. transonic. Compare this to the minimum fuel burnt for a given distance case, which would require flight at the minimum drag speed.

The outcome is that commercial aircraft would burn less fuel over a given distance if operated at their minimum drag speed rather than their maximum range speed. It would be environmentally friendly, but would result in increased non-fuel operating costs. Equivalently, if two identical aircraft with equal fuel set off, one flown at maximum range speed and one at minimum drag speed, the maximum range flight will go further. Perhaps it is clear why one would prefer to be a passenger on the maximum range flight, especially as the fuel cost on the ticket would be the same for both. If flying the same distance, the maximum range flight would arrive sooner, with a higher fuel cost but lower time costs (eg crewing) on the ticket. The minimum drag ticket would be more expensive despite the fuel saving, owing to crewing and similar costs.

If fuel prices soar and crew wages/maintenance costs drop, perhaps we will see some rather slow flying aircraft? Or will passenger demand keep the Mach number up? How much would you pay to arrive 1hr earlier?

We can put some rough numbers in to equation (11). Using K=20 (this constant is the most vague aspect to the method, but you will estimate it using CFD in your coursework) the iteration

$$M_{i+1} = \left(\frac{20(M_i - M_{crit})^4 + C_{d_{tot}}}{80M_i}\right)^{\frac{1}{3}} + M_{crit} \tag{12}$$

converges to the root of interest. For an incompressible C_d of 0.0253 (this is skin friction, pressure and induced drag) and a critical Mach number of 0.69 (corresponds to RAE 2822 at a compressible

C_l of 0.6 - remind yourself how to calculate M_{crit} from aero 2 last year!), we find the optimum Mach number to be 0.765. If M_{crit} rises to 0.73 this becomes 0.804. Using a range of M_{crit} values shows that the optimum cruise Mach number is usually about 10% above the critical Mach number. M_{crit} is the dominant factor; the incompressible drag coefficient does not change the optimal cruise Mach number greatly. This is not surprising as M_{crit} clearly has a big influence on the wave drag according to Lock's result.

2.3 Supercritical Aerofoil Design

So whatever aerofoil we select, it is likely that it will be operating at a transonic speed. This is awkward; compressible subsonic flow is easier to analyse (using a Prandtl-Glauert scaling in 2D, or Göthert's rule in 3D through a panel code). Transonic flow is tricky since it is both supersonic and subsonic, and the shock interacts with the boundary layer.

The transonic aerofoil design problem arises because we wish to limit shock (wave) drag losses at a given transonic speed - which effectively limits the minimum pressure coefficient (= maximum local velocity) that can be tolerated. In turn this limits the lift coefficient and the thickness ratio, since both affect the maximum velocity over the aerofoil section.

A physical understanding of wave drag can come from realising that a shock induces a velocity in the air, as well as heating it (imagine the shockwave from an explosion with the draft of moving air behind it). The velocity produced as the shock front passes increases the kinetic energy of the air left behind (somewhat akin to the kinetic energy left in trailing tip vortices), and the temperature increase raises its internal energy. The main contribution to the wave drag is actually isentropic, as evidenced by the good drag predictions of linear isentropic supersonic theory (Ackeret's C_p). Wave drag is thus not primarily associated with total pressure loss. Two outcomes of this reasoning are that (1) a shock with a higher upstream Mach number will produce more wave drag, and (2) a shock that extends a shorter distance from the aerofoil surface will produce less drag than one that extends a long way, because the taller the shock the greater the mass flow of air passing through it, and the greater the kinetic and thermal energy dumped into it.

It should be noted that transonic drag rise is not entirely the same as wave drag. In 2D subsonic flow the drag rise is also due to form drag arising from shock-induced boundary layer separation - drag due to total pressure loss through the shock itself is actually rather small. Similarly, wave drag in supersonic flow is not only related to losses through a shock, but to the energy lost to the compression and expansion wave systems trailing behind an aerofoil or wing (these induce a velocity in the air which extends away from the object).

2.3.1 Design Idea

The simplest approach to improving transonic performance is to delay the onset of supersonic flow as long as possible - and it turns out that the 'roof top' type pressure distribution typical of the 6-series laminar flow aerofoils is a pretty good way of doing this, by maintaining a constant or gradually increasing velocity distribution over the forward part of the section. However, once the critical Mach number is exceeded large regions of supersonic flow appear aft of the crest (maximum thickness point) of the aerofoil, giving a drag increment due to the high suction levels. This supersonic flow region is then terminated by a strong shock, giving a further rapid drag rise soon after M_{crit} is exceeded. Ex-

tending the roof-top region aft would raise the critical Mach number, but at the risk of early boundary layer separation in the pressure recovery region.

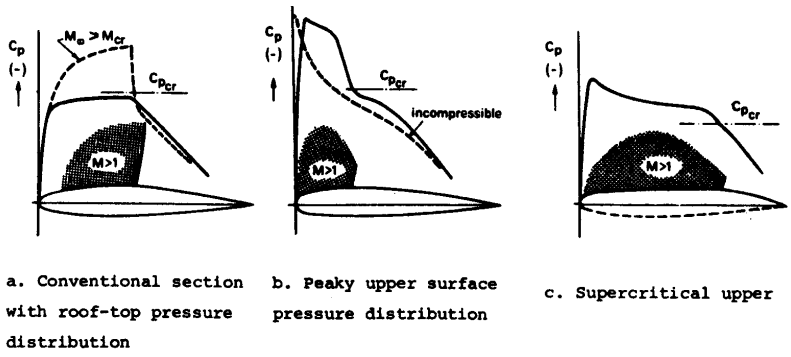

Figure 1: Transonic flows on conventional, peaky and supercritical aerofoils

6-series aerofoils (and similar) therefore have a high critical Mach number, but then a very rapid drag rise - good for high-subsonic cruise but necessitating high sweep or low thickness for transonic and supersonic performance.

However, we can generally tolerate some supersonic flow over the forward part of the aerofoil without drag increase - since it is the terminating shock that causes transonic drag rise (pressure loss through the shock + shock/boundary layer interaction - see your 2nd year Aerodynamics notes), so that some sections can operate efficiently as 'supercritical aerofoils'. A rule of thumb is that the maximum local Mach numbers should not exceed about 1.2 to 1.3 on a well-designed supercritical aerofoil. This produces a considerable increase in available C_l compared with entirely subcritical designs.

Early supercritical sections developed in the UK (by Pearcey at NPL) made use of what is known as a 'peaky' pressure distribution to intentionally create supersonic velocities (up to M = 1.4) near to the leading edge, where the associated suction forces give a thrust (rather than drag) force. The nose profile is then very carefully designed to give a near-isentropic compression (deceleration) around the leading edge followed by a weak shock. Drag rise Mach number is postponed by 0.03 to 0.05 compared to a conventional section. The ideal compression would only occur at one design point (M and C_l), but rate of growth of the shock off-design is slow enough to give a practical design.

2.3.2 Aerofoil Usage

'Peaky' aerofoils and their variants were quite successful, and are found on many older transport aircraft developed during the 60s (BAC1-11, VC-10, DC-9, DC-10, L1011, 727, 737 (-100→500, probable) 747 (-100→400, not -8), A300). As you can see, that is quite an esteemed list of aircraft, all with respectable performance for the era. The aerofoil usage database reports that the VC-10 in fact used a 'Pearcey' aerofoil, and the aircraft test flew around the time of one of Pearcey's first publications. Aircraft developed in the mid-late 70s (A310, 757, 767) switched to 'supercritical' sections, and this has been the norm since (A320/330/340/380 and 737NG/777/787).

In the limit, it is theoretically possible to design entirely shock-free aerofoils using this approach (eg Fig. 69). However, a remarkable (and frustrating result) derived by Cathleen Morawetz[2] (a mathematics graduate student at the Courant Institute in New York in the 1950s) is that if such a route is followed, the aerofoil will only be shockless at an isolated operating point. A small change in lift

or Mach number will produce a shock once more. What is really needed is clearly a transonic aerofoil with good properties across a range of C_l and M.

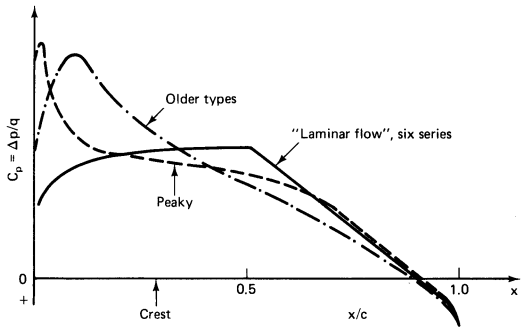

Figure 2: C_p on conventional, peaky and supercritical aerofoils

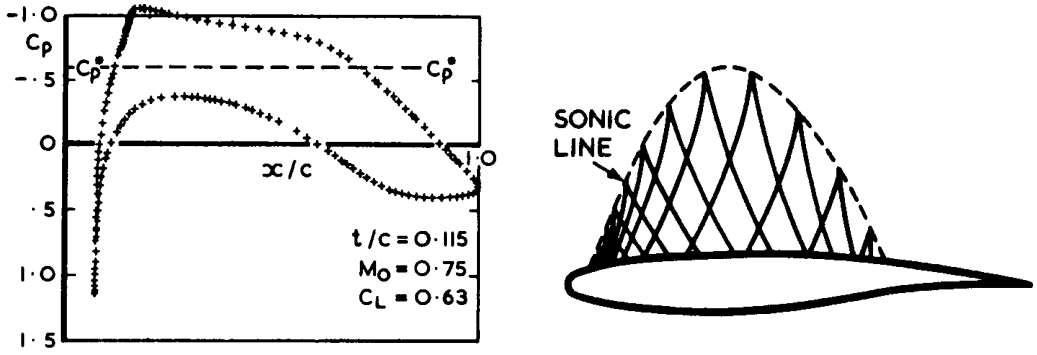

Figure 3: A shock-less lifting aerofoil design with an isentropic compression region

2.3.3 Supercritical: pros and cons

Following on from Pearcey's work, Whitcomb in the US (also linked to the area rule concept and winglets) developed the modern supercritical (aft-loaded) section. In contrast to the peaky section, these aerofoils are designed to have substantial regions of supersonic flow over much of the upper surface. This is achieved by:

1. Forward sonic point located in a region of high curvature, near the leading edge
2. Relatively large leading edge radius to expand the flow
3. Having very small curvature over much of the rest of the upper surface - so that the aft-facing surface has very little vertical projected area, reducing the drag penalty of the supersonic flow region
4. Cambering the aft portion of the wing to carry more load aft (particularly on the lower surface) - reducing peak local velocities and hence increasing critical Mach number
5. Using a thin trailing edge (tangential upper and lower surfaces) to reduce the adverse pressure gradient. This combination leads to significant lower surface curvature, particularly near the trailing edge

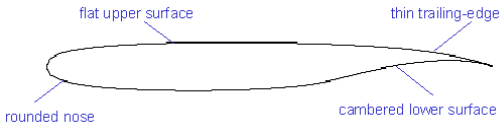

Figure 4: Design features of an early Whitcomb supercritical aerofoil section

Note the similarity of this supercritical profile to many laminar sections (which we will see in coming lectures) - hardly surprising since the need to avoid high peak suction on the upper surface is common to both design cases.

In addition to the aerodynamic performance benefits, it is evident that this section has some structural advantages - plenty of depth for spars and high internal volume fuel.

Set against these are some disadvantages:

1. Too much aft loading can produce large negative pitching moments with trim drag and structural weight penalties (can be alleviated in 2D by tailoring the underside of the nose region to move loading forward, or in 3D by varying camber, twist and thickness across the span)
2. The adverse pressure gradient on the aft lower surface can produce separation in extreme cases
3. The thin trailing edge may be difficult to manufacture, or to integrate control surfaces into (may be possible to use a blunt trailing edge)
4. Supercritical (and especially shock-free) designs are often very sensitive to M and CL and may perform poorly at off-design conditions. The appearance of 'drag creep' is quite common, a situation in which substantial section drag increase with Mach number occurs even at speeds below the design value.
5. Wing root flow separation can be a problem due to high adverse pressure gradients

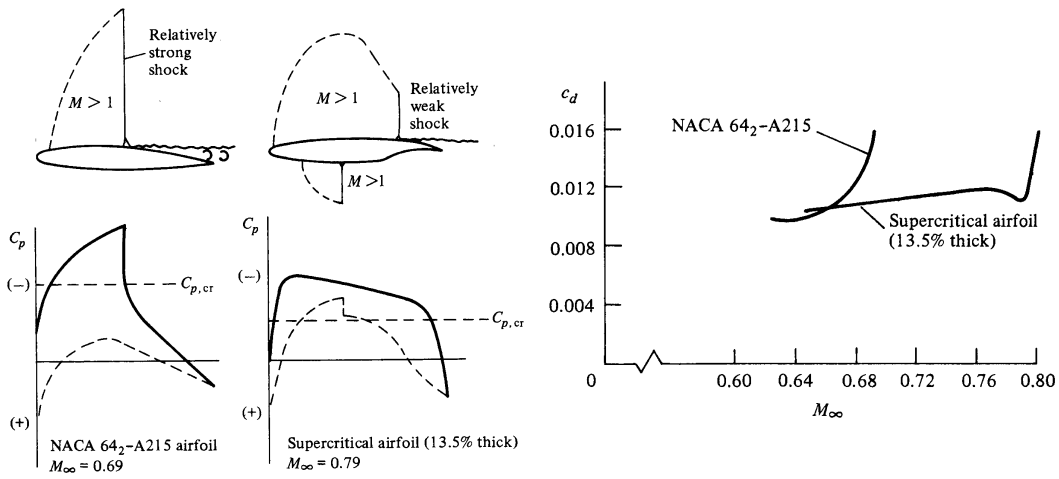

Figure 5: Effect of design for supercritical operation on drag - NASA

The effect of the trailing edge shape on pressure distribution and drag is illustrated in figures 6 and 7. Increasing aft camber and reducing trailing edge thickness improves the drag rise Mach number,

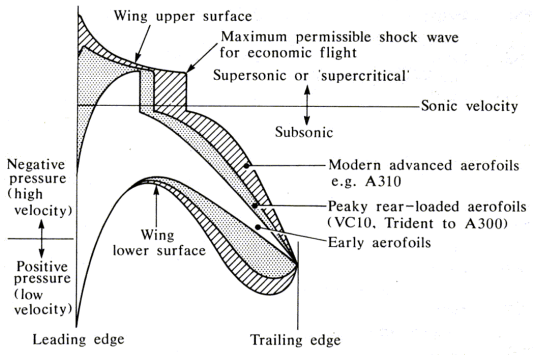

Figure 6: UK development of supercritical aerofoil sections (1)

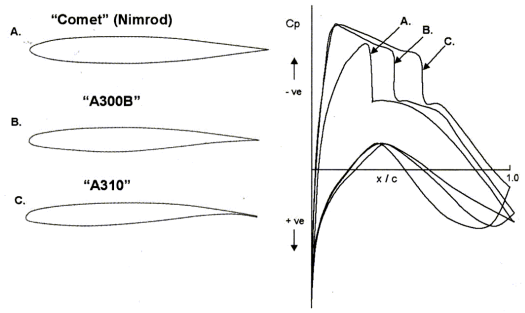

Figure 7: UK development of supercritical aerofoil sections (2)

but also increases form drag at lower speeds. Figure 8 illustrates older and newer wing designs, showing how improvements in supercritical/computational capabilities have enabled an increase in wing thickness (particularly at the root) coupled with an improvement in high-speed drag (or rather the drag-rise lift coefficient).

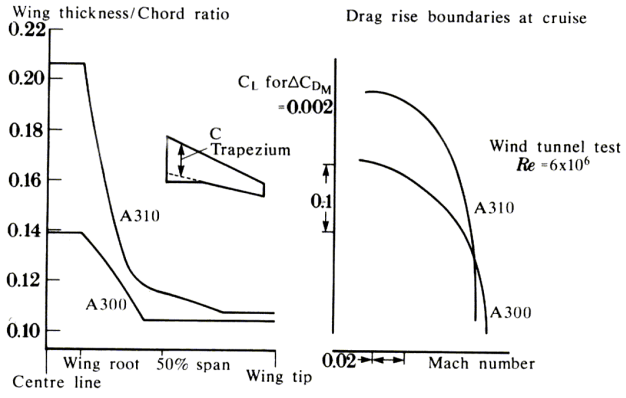

Figure 8: A310 (1980s) wing compared with A300B (1960s) showing increased thickness and improved drag standard at high Mach Number

Off-design performance can be a problem for supercritical sections, particularly at low-speed/high-lift conditions. An alternative to complex variable geometry (eg slats) is to apply a small amount of leading edge droop to reduce the curvature from the stagnation region to the point where the suction peak develops at high lift. This increases maximum lift by delaying stall onset but also ensures that 'peaky' supersonic flow still develops (albeit slightly further aft). Balanced against the increase in

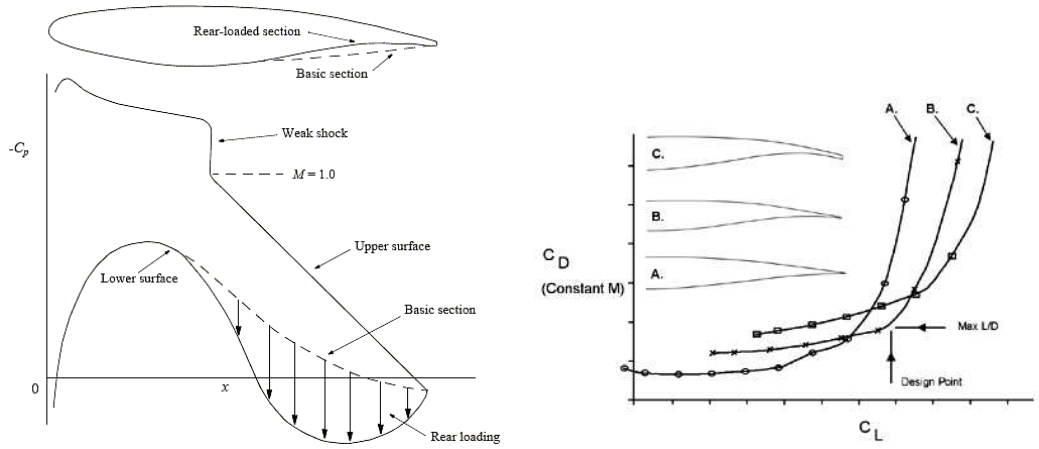

Figure 9: Effect of trailing edge shaping on aft loading and performance - Airbus

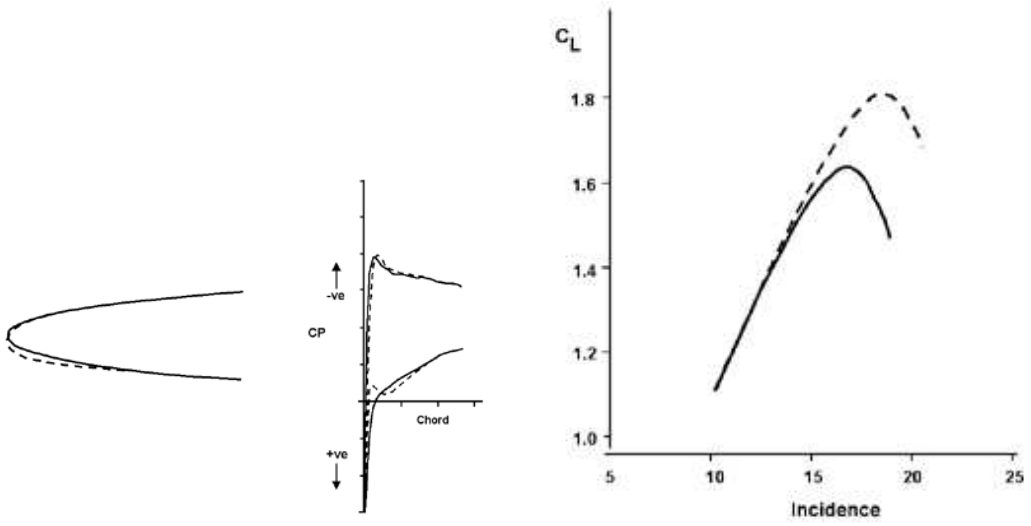

Figure 10: Effect of leading edge droop on pressure distribution and maximum lift

maximum lift is a small loss of lift at low incidence due to the change in leading edge pressure distribution (≈1-2% of design CL). The degree of droop is limited by the suction peak developed on the lower surface under the 'chin' of the droop, which could go supercritical at cruise conditions, leading to an unwanted shock on the lower surface. The BAe146 and Airbus A400M make use of this approach to give improved high-lift performance.

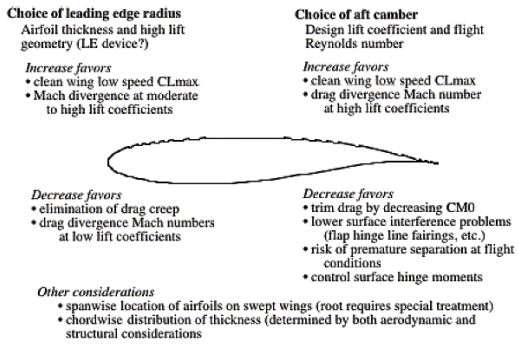

Figure 11: Some design principles for supercritical aerofoils (from Mason[3])

2.4 Korn Equation

Lock's result for wave drag is very powerful but the influence of C_L and thickness are implicit through M_{crit}. It would be preferable to have a way of understanding their mutual effects in a single result. This can be done through the 'Korn equation', which is an empirical result first noticed by Korn (you'll hear of him again later) in the 70s.

For an aerofoil the beguilingly simple Korn equation states

$$M_{dd} + \left(\frac{t}{c}\right) + \frac{C_L}{10} \approx \kappa \tag{13}$$

where κ is the 'technology factor' and M_{dd} is the drag divergence Mach number. Don't doubt it, this approximate result is a gem, if you know how to estimate κ! What this all allows us to do is simultaneously assess how 'good' an aerofoil is in terms of drag divergence, thickness and lift, and then trade these parameters off against each other if we wish to.

The validity of the Korn equation is illustrated by two figures below (from Mason[3]), showing the variation of drag rise Mach number with thickness and lift coefficient. With the appropriate 'technology factor' applied, the thickness and lift effects are well matched - apart from an overly optimistic prediction at high lift.

In 3D it would be convenient to have a similar result. For a swept wing with a reasonable aspect ratio much of the flow is 2D and hence design rules for 2D supercritical aerofoils can be applied to the 3D wing - eg a roof-top pressure distribution over the forward section.

For an untapered wing the equivalent 2D flow is that of an infinite yawed wing, and can be related to the 3D flow by a number of (relatively) simple geometric transformations (see your 2nd year Aerodynamics notes for an introduction, or ESDU 90008 for a more detailed treatment).

The equivalent freestream Mach Number is the familiar component normal to the leading edge

$$M_{2D} = M_\infty \cos(\Lambda) \tag{14}$$

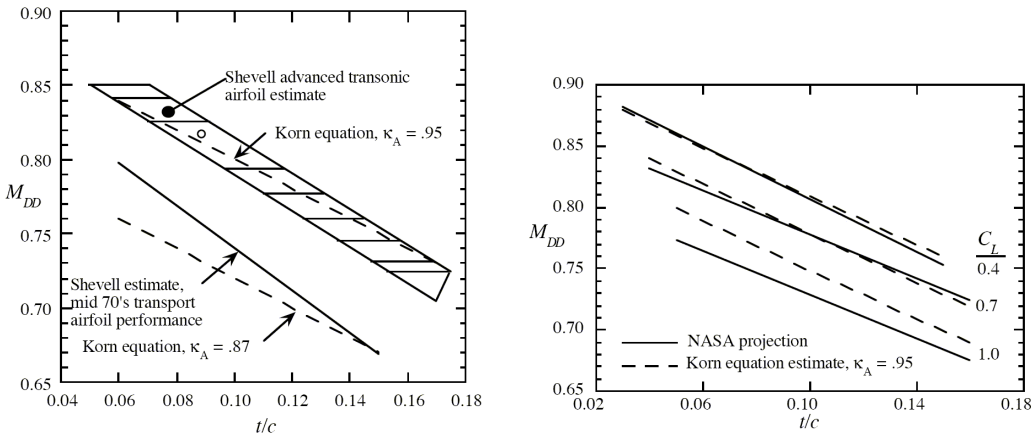

Figure 12: Transonic drag and thickness

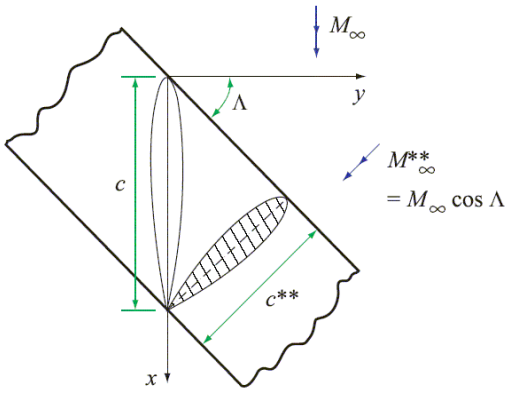

Figure 13: Sweep effects

where is the sweep angle. (Note that ESDU 90008 uses a double-star subscript to denote the equivalent 2D flow, ie M** rather than M2D).

Since for an infinite wing there can be no pressure gradients parallel to the leading edge, the pressure perturbations ($p - p_\infty$) are the same in the 2D and 3D cases (ie on the two sliced sections in figure 13). The local pressure coefficients (and hence also overall section lift coefficient) can therefore be linked.

$$\frac{p - p_\infty}{\frac{1}{2}\rho U^2} = \frac{(p - p_\infty)\cos^2(\Lambda)}{\frac{1}{2}\rho U^2 \cos^2(\Lambda)} = C_{p_{2D}} \cos^2(\Lambda) \tag{15}$$

Gives

$$C_P = C_{P_{2D}} \cos^2(\Lambda) \tag{16}$$

To obtain mappings for force coefficients we need to rewrite the 'swept' integrals in terms of the 'unswept' integrals; note that we are looking for the correct equivalence, not to resolve forces parallel and perpendicular to the leading edge.

Looking at C_L

$$C_L = \int C_p d\left(\frac{x}{c}\right) = \int C_{P_{2D}} \cos^2(\Lambda) d\left(\frac{x\cos(\Lambda)}{c\cos(\Lambda)}\right) \tag{17}$$

and remembering that

$$C_{L_{2D}} = \int C_{P_{2D}} d\left(\frac{x\cos(\Lambda)}{c\cos(\Lambda)}\right) \tag{18}$$

so

$$C_L = C_{L_{2D}} \cos^2(\Lambda) \tag{19}$$

The corresponding geometric transformations are

$$\frac{t}{c} = \frac{t}{c_{2D}} \cos(\Lambda) \tag{20}$$

$$\tan(\alpha)_{2D} = \frac{M_\infty \sin(\alpha)}{M_\infty \cos(\Lambda)} \tag{21}$$

Using small angle approximations for $\sin$ and $\tan$

$$\alpha = \alpha_{2D} \cos(\Lambda) \tag{22}$$

For drag, the drag coefficient on the perpendicular slice would be

$$C_{D_{2D}} = \int C_{P_{2D}} d\left(\frac{y}{c\cos(\Lambda)}\right) \tag{23}$$

$$C_D = \int C_p d\left(\frac{y}{c}\right) = \int C_{p_{2D}} \cos^3(\Lambda) d\left(\frac{y}{c\cos(\Lambda)}\right) \tag{24}$$

where the extra $\cos$ appears because y is the same on both slices, but c has been shortened (this is a somewhat unexpected detail!).

This means for pressure and wave drag

$$C_{D_p} = C_{D_{p_{2D}}} \cos^3(\Lambda) \tag{25}$$

$$C_{D_W} = C_{D_{W_{2D}}} \cos^3(\Lambda) \tag{26}$$

Thus the flow on a swept wing may be compared with the flow on an equivalent aerofoil which is: at a lower free-stream Mach number, thicker, and at a higher lift coefficient.

The beneficial effect of sweep is due to the fact that the first of these three factors generally easily outweighs the adverse effects of the last two. In particular, the appearance of shock waves, and their consequent adverse effects on the development of drag and separation, is progressively delayed as the sweep angle is increased.

These scaling transformations can also be seen in the empirical Korn equation used to relate drag rise Mach number to wing sweep, lift and thickness for transport aircraft.

For a wing we can now substitute these relations in to the Korn equation

$$M_{dd}\cos(\Lambda) + \frac{t}{c\cos(\Lambda)} + \frac{C_l}{10\cos^2(\Lambda)} \approx \kappa \tag{27}$$

It can be seen that each parameter has actually been transformed to its 2D equivalent, and then linearly combined to approximate their effect on the critical Mach number. Some accuracy is lost here owing to the infinite swept wing assumption, but the result is still useful.

Commonly the half-chord sweep angle is used, but you might also use the quarter-chord angle. Herein lies a restriction; the above working is for an untapered wing, where these angles are the same. Tapered wings can also be treated using a slightly more general analysis.

2.4.1 Estimating κ

It would be useful if there were a neat way to find κ for any aerofoil. This is a tricky thing to do, and in the past experimentation might have been used. Experiments, however, can be expensive - but what is 'expensive'? I learned this myself for transonics only recently. Expensive is £40,000 per day of testing (2012/13 ARA Bedford quote for use of their main transonic tunnel). This is not even for a flight Reynolds number, which may be achieved with a cryogenic tunnel such as the European Transonic Windtunnel (ETW) in Cologne, or the National Transonic Facility (NASA). I don't have any quotes for these, but I know my research budget is unlikely to stretch that far!

So it is understandable why people are interested in CFD; almost anything other than solid gold is cheaper than a day of testing in a high-end windtunnel. During your group design project you may want to know κ and CFD offers you a cheaper way forward, at the expense of lower accuracy.

The value of M_{dd} is often taken as the Mach number for which $\frac{\partial C_D}{\partial M} = 0.1$. So, if there was a tool that could return C_d, you could repeatedly find

$$\frac{\partial C_D}{\partial M} = \frac{C_D(M+\delta) - C_D(M-\delta)}{2\delta} + O(\delta^2) \tag{28}$$

which is a central finite difference approximation to the derivative.

The simplest tool you have at your disposal (although it is not simple!) is a program called VGK - 'viscous Garabedian Korn'. Garabedian and Korn worked the Courant institute (together with the previously mentioned Morawetz) and devised a method for numerical solution of the full potential equation in section 1.5.4. VGK is available from ESDU and was originally created at RAE Farnborough based on the methods of Garabedian and Korn. To get a value of κ it is only necessary to run the program in inviscid mode.

How does it work? This is a long story best left to the CFD course, but a summary is in order. The boundary layer components are similar to the ones you will see later in the course. The inviscid solution method takes an initial guess for the solution and discretises the full potential equation using finite differences to arrive at a set of algebraic equations. These are nonlinear, but are then linearised and solved to provide an update or 'delta' to the guessed solution. The process repeats until the guesses cease changing. There are many other details to consider, but the technique is similar to full CFD on the Euler or Navier-Stokes equations. Indeed, the origins of CFD lie in numerical methods for the full potential equation.

2.4.2 VGK

Let's consider operating VGK. Initially we start with the aerofoil coordinates in the VGK input format; be careful to avoid tabs in the input file. You can download the 0012 input file from *BlackBoard*. When prompted, specify a Mach number above zero (confusingly, the default value is zero, which cannot be used) and accept the remaining defaults, then save the set-up file (you can simply load this next time rather than setting the case up again from scratch).

M	$C_{D_{VGK}}$	$C_{D_{Lock}}$	$\frac{\partial C_D}{\partial M}$
0.7400	-0.0009	0.0018	N/A
0.7500	-0.0009	0.0026	N/A
0.7600	-0.0007	0.0037	N/A
0.7700	0.0001	0.0052	0.1200 (for M=0.775)
0.7800	0.0013	0.0070	0.1800
0.7900	0.0037	0.0093	0.2850
0.8000	0.0070	0.0121	0.3700
0.8100	0.0111	0.0155	0.4500
0.8200	0.0160	0.0195	0.5600
0.8300	0.0223	0.0244	0.6500
0.8400	0.0290	0.0300	0.7300
0.8500	0.0369	0.0366	0.8000
0.8600	0.0450	0.0442	0.8700
0.8700	0.0543	0.0529	0.9350
0.8800	0.0637	0.0629	0.9300
0.8900	0.0729	0.0742	0.9400
0.9000	0.0825	0.0870	0.9400
0.9100	0.0917	0.1013	0.7400
0.9200	0.0973	0.1174	N/A

Table 1: VGK results for NACA 0012 (note - negative C_D values are a numerical artefact, M_{crit} offset by 0.1 in Lock's relation)

Table 1 shows C_D (from integration of surface pressures) as a function of M at zero incidence. M_{DD} appears close to 0.775, giving a κ of about 0.895 ($= 0.775 + 0.0 + 0.12$). For a transonic aerofoil, this would be expected to be somewhat higher. Note that a κ of one corresponds to an aerofoil of zero thickness with an M_{DD} equal to the speed of sound at zero lift, which would be impossible in practice.

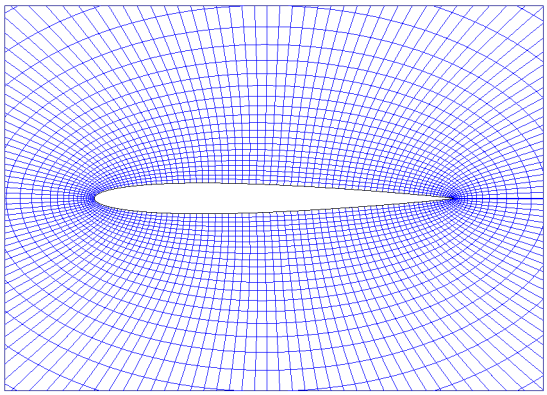

Figure 14: VGK NACA 0012 Mesh

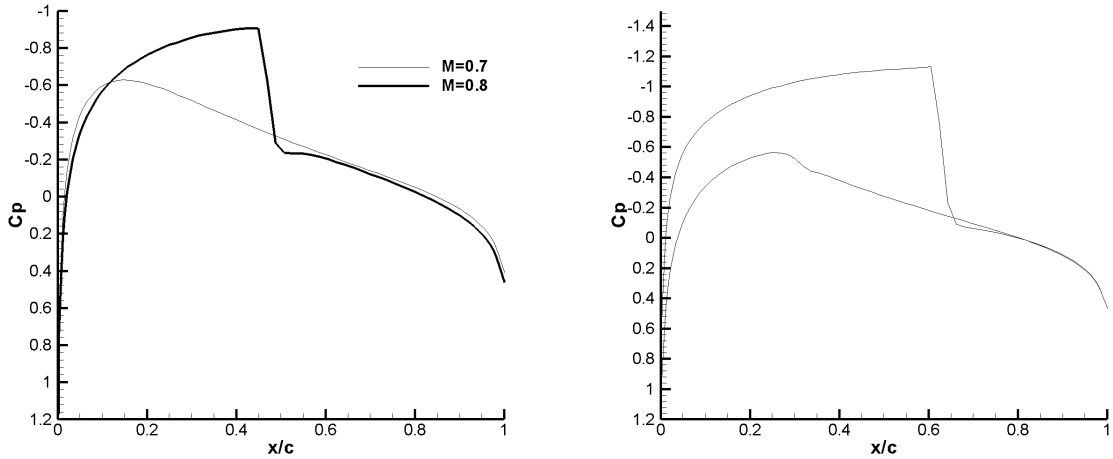

(a) M=0.7 and 0.8, $\alpha = 0^o$

(b) M=0.8, $\alpha = 1.25^o$

Figure 15: Transonic C_p plots for NACA 0012

3 Compressibility Considerations

Key points: *Göthert's Rule and its application to incompressible results, and the effect of sweep on range*

3.1 Göthert's Rule

The Prandtl-Glauert compressibility correction you met last year is not applicable in the same way to three-dimensional flows; you cannot simply take a three-dimensional result for C_L or C_M and scale it by $\frac{1}{\sqrt{1-M_\infty^2}}$.

The correct procedure is as follows:[4]

1. Take the geometry and scale y and z by $\sqrt{1-M_\infty^2}$ (so the aircraft gets shorter in z and reduces in span, but x is unchanged). The angle of attack must also be scaled by $\sqrt{1-M_\infty^2}$, because the z direction is being scaled
2. Perform the incompressible calculation on this geometry. Reference areas are now for the scaled (incompressible) geometry, so for example you would scale the reference area input for the geometry file for a tool like AVL
3. Take any coefficient of interest - C_p, C_L or C_M and multiply by $\frac{1}{1-M_\infty^2}$ to arrive at the compressible coefficient. The reference area, if you need it, is once again the original reference area of the compressible wing

You may be puzzling as to why the 2D approach is no longer suitable. This boils down to the fact that in 3D scaling the span influences the position of the tip vortices, so that the compressibility scaling has an influence that depends on the aspect ratio. In 2D aspect ratio is effectively infinite, but in 3D this influence is important. For wings of aspect ratio < 1, compressibility actually makes very little difference to the lift and moment properties.

To understand this, consider the following working (note: this mathematics is primarily for information, however the ideas behind the scaling must be understood. So, check you understand it, but do not memorise it. You may be asked a question regarding it but you will not be asked to produce it from memory)

$$(1-M_\infty^2)\frac{\partial^2\phi}{\partial x_c^2}+\frac{\partial^2\phi}{\partial y_c^2}+\frac{\partial^2\phi}{\partial z_c^2}=0 \tag{29}$$

let

$$\beta=\sqrt{1-M_\infty^2} \tag{30}$$

$$x_c=x_{ic} \tag{31}$$

$$\beta y_c=y_{ic} \tag{32}$$

$$\beta z_c=z_{ic} \tag{33}$$

$$\frac{\partial\phi}{\partial x_c}=\frac{\partial\phi}{\partial x_{ic}}\frac{\partial x_{ic}}{\partial x_c}+\frac{\partial\phi}{\partial y_{ic}}\frac{\partial y_{ic}}{\partial x_c}+\frac{\partial\phi}{\partial z_{ic}}\frac{\partial z_{ic}}{\partial x_c}=\frac{\partial\phi}{\partial x_{ic}} \tag{34}$$

$$\frac{\partial \phi}{\partial y_c} = \frac{\partial \phi}{\partial x_{ic}}\frac{\partial x_{ic}}{\partial y_c} + \frac{\partial \phi}{\partial y_{ic}}\frac{\partial y_{ic}}{\partial y_c} + \frac{\partial \phi}{\partial z_{ic}}\frac{\partial z_{ic}}{\partial y_c} = \frac{\partial \phi}{\partial y_{ic}}\beta \tag{35}$$

$$\frac{\partial \phi}{\partial z_c} = \frac{\partial \phi}{\partial x_{ic}}\frac{\partial x_{ic}}{\partial z_c} + \frac{\partial \phi}{\partial y_{ic}}\frac{\partial y_{ic}}{\partial z_c} + \frac{\partial \phi}{\partial z_{ic}}\frac{\partial z_{ic}}{\partial z_c} = \frac{\partial \phi}{\partial z_{ic}}\beta \tag{36}$$

$$\frac{\partial \phi_{x_c}}{\partial x_c} = \frac{\partial \phi_{x_c}}{\partial x_{ic}}\frac{\partial x_{ic}}{\partial x_c} + \frac{\partial \phi_{x_c}}{\partial y_{ic}}\frac{\partial y_{ic}}{\partial x_c} + \frac{\partial \phi_{x_c}}{\partial z_{ic}}\frac{\partial z_{ic}}{\partial x_c} = \frac{\partial^2 \phi}{\partial x_{ic}^2} \tag{37}$$

$$\frac{\partial \phi_{y_c}}{\partial y_c} = \frac{\partial \phi_{y_c}}{\partial x_{ic}}\frac{\partial x_{ic}}{\partial y_c} + \frac{\partial \phi_{y_c}}{\partial y_{ic}}\frac{\partial y_{ic}}{\partial y_c} + \frac{\partial \phi_{y_c}}{\partial z_{ic}}\frac{\partial z_{ic}}{\partial z_c} = \frac{\partial \phi_{y_c}}{\partial y_{ic}}\beta = \frac{\partial^2 \phi}{\partial y_{ic}^2}\beta^2 \tag{38}$$

$$\frac{\partial \phi_{z_c}}{\partial z_c} = \frac{\partial \phi_{z_c}}{\partial x_{ic}}\frac{\partial x_{ic}}{\partial z_c} + \frac{\partial \phi_{z_c}}{\partial y_{ic}}\frac{\partial y_{ic}}{\partial z_c} + \frac{\partial \phi_{z_c}}{\partial z_{ic}}\frac{\partial z_{ic}}{\partial z_c} = \frac{\partial \phi_{z_c}}{\partial z_{ic}}\beta = \frac{\partial^2 \phi}{\partial z_{ic}^2}\beta^2 \tag{39}$$

Substituting in gives

$$\beta^2\frac{\partial^2 \phi}{\partial x_{ic}^2} + \beta^2\frac{\partial^2 \phi}{\partial y_{ic}^2} + \beta^2\frac{\partial^2 \phi}{\partial z_{ic}^2} = 0 \tag{40}$$

$$\frac{\partial^2 \phi}{\partial x_{ic}^2} + \frac{\partial^2 \phi}{\partial y_{ic}^2} + \frac{\partial^2 \phi}{\partial z_{ic}^2} = 0 \tag{41}$$

Which is an incompressible problem. Notice nothing has been done to the velocity potential.

Consider the gradients $\frac{dy_c}{dx_c}$ and $\frac{dy_{ic}}{dx_{ic}}$. Since we have contracted in y we should expect $\frac{dy_c}{dx_c} = \frac{1}{\beta}\frac{dy_{ic}}{dx_{ic}}$, ie the same scaling applied to y. This gradient could also represent the gradient of a streamline, so streamline gradients should obey a similar rule.

However, this is not guaranteed, because we are dealing with the small perturbation potential equation, which is independent of V_∞ (it doesn't appear in the equation we are trying to solve). We need to know if any scaling should be applied to V_∞, as this influences C_p and thereby the other coefficients. We already know that $v'_c = \beta v'_{ic}$ from $\frac{\partial \phi}{\partial y_c} = \frac{\partial \phi}{\partial y_{ic}}\beta$ above, where v' is perturbation velocity in y.

To work this out consider

$$\frac{dy_c}{dx_c} = \frac{1}{\beta}\beta\frac{dy_c}{dx_c} = \frac{1}{\beta}\frac{dy_{ic}}{dx_{ic}} = \frac{1}{\beta}\frac{v'_{ic}}{u_{\infty_{ic}}} = \frac{1}{\beta^2}\frac{v'_c}{u_{\infty_{ic}}} = \frac{v'_c}{u_{\infty_c}} \tag{42}$$

So

$$\beta^2 u_{\infty_{ic}} = u_{\infty_c} \tag{43}$$

which was far from obvious.

We also know (since x and ϕ were unchanged)

$$u'_c = u'_{ic} \tag{44}$$

so since $C_p = -2\frac{u'_c}{u_{\infty c}} = -2\frac{u'_{ic}}{\beta^2 u_{\infty_{ic}}}$ (derived in aero 2 last year) we can conclude that the correct scaling for the lift and moment coefficients is $\frac{1}{\beta^2}$ (drag discussed later). †

†The careful amongst you will notice this is not what is commonly presented in textbooks or on the www (where the 2D case is almost always given). Most 2D workings link the compressible and incompressible flows around the same shape, whereas here we are linking them around different shapes. This is why an extra β appears. If we wished the objects to be the same we would need to scale back up by $\frac{1}{\beta}$ in the y direction, which would cancel a β again in the C_p scaling, and return us to two-dimensional Prandtl-Glauert; the two methods are equivalent. On a historical note, there are in fact three different[5] interpretations of the PG scaling, but Göthert's rule (also known as the streamline analogy) is the most commonly quoted and applied interpretation at high subsonic speed.

Conventionally we refer to the 3D 'version' as 'Göthert's Rule' (Göthert was a WW2-era German aerodynamicist, and the translation acquired by NACA popularised the method in the USA).

If you use the Mach number scaling in a potential flow tool like AVL, it is applying Göthert's Rule, not the Prandtl-Glauert rule as such (although Prandtl and Glauert would have been aware of the 3D variant, so often it is still attributed to them).

A further question often arises regarding induced drag. This is slightly more tricky, because it depends on an integral of $C_p \sin(\theta_c)$ rather than just C_p. Equation (42) tells us that $\frac{dy_c}{dx_c} = \frac{1}{\beta}\beta\frac{dy_c}{dx_c} = \frac{1}{\beta}\frac{dy_{ic}}{dx_{ic}}$ ($\approx \sin(\theta_c)$), which is approximately equal to θ_c, as the angles are small. This means that the induced drag coefficient found from the scaled geometry should be divided by β^3, not just β^2. This has an interesting effect as it means that the relationship between compressible induced drag and compressible lift is exactly the same as the relationship between incompressible induced drag and incompressible lift; this can be shown by taking the induced drag of an elliptically loaded wing at incompresible speed, scaling the aspect ratio, dividing by β^3 and then writing in terms of the compressible lift coefficient. The β terms cancel, ie

$$C_{d_{ic}} = \frac{1}{\beta^3}\frac{C_{l_{ic}}^2}{\pi\beta AR} = \frac{1}{\beta^3}\frac{\beta^4 C_{l_c}^2}{\pi\beta AR} = \frac{C_{l_c}^2}{\pi AR} \tag{45}$$

Of course, this simplification is not much use for vortex lattice work. Once you have successfully found the compressible lift, you might just as well get the compressible induced drag by dividing the incompressible induced drag by β^3. The idea is most useful where analytical results are being used.

A tool like AVL automatically applies this correction to the induced drag once you set the Mach number. As an instructive exercise you can confirm the behaviour by inputting scaled wings and comparing to results found when using the Mach number option in the code.

3.1.1 Göthert's Rule - why does it matter?

We care because Göthert's Rule means that wings of low aspect ratio see much less of a compressibility effect. For high aspect ratio wings, which are approximately 2D, it makes little difference. However, for missile fins, or tailplanes, which are much more 'stubby', you will get the wrong answer using Prandtl-Glauert in 3D.

The more frustrating aspect is that the correspondance between 3D incompressible and 3D compressible flow has been lost. The compressible velocity potential is not a simple function of the incompressible potential, as it was in 2D. This means we cannot take an incompressible 3D result and 'make it' compressible, but we can perform an incompressible calculation to find a compressible result. That incompressible calculation, however, is specific to that Mach number and cannot be used to find values at other Mach numbers.

If all this is too much for you, look at figure 16. On the left is the compressibile geometry, on the right is the incompressible geometry we need to solve for. Once we know the coefficients for the incompressible case, we divide by β^2 (for lift/moment) or β^3 (induced drag) and we have our compressible answers. That's all there is to it, but remember that $\alpha_{ic} = \beta\alpha_c$ also, which is easy to forget. If you use AVL, you can apply the rule automatically by altering the Mach number, which is a very useful feature if you wish to avoid doing all the coordinate scalings manually.

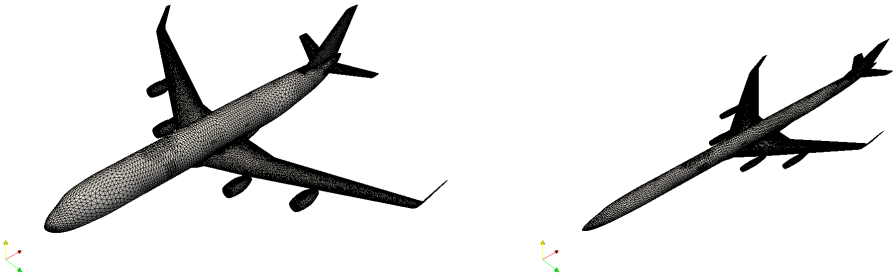

(a) Original shape - compressible flow (b) Transformed shape - incompressible flow

Figure 16: Compressibility transformation

3.1.2 Finite Wing Example

Following an example by Göthert, the lift coefficient of a finite rectangular wing may be approximately described by (this is not derived but only quoted here)

$$C_{L_\alpha} = \frac{5.65}{1 + \frac{1.8}{A_R}} \tag{46}$$

Adjusting this according to Göthert's Rule gives

$$C_{L_c} = \frac{1}{\beta^2} \frac{5.65}{1 + \frac{1.8}{\beta A_R}} \beta \alpha_c = \frac{5.65 A_R}{1.8 + \beta A_R} \alpha_c \tag{47}$$

The $\frac{1}{\beta^2}$ is the pressure coefficient (or lift coefficient scaling) dervied above. $A_{R_{ic}} = \beta A_R$ due to the spanwise scaling, and $\alpha_{ic} = \beta \alpha_c$

This gives

$$\frac{C_{L_c}}{C_{L_{ic}}} = \frac{1.8 + A_R}{1.8 + \beta A_R} \tag{48}$$

So for high aspect ratios the Prandtl-Glauert relation is recovered, but for low aspect ratios the lift coefficient is (in the limit of zero aspect ratio) independent of Mach number. One consequence of this is than the lift gradient of the wing increases more rapidly that the lift gradient of the tailplane as an aircraft increases Mach number.

3.1.3 Ellipse Example

The ratio $\frac{u'_{max}}{V_\infty} = \frac{t}{c}$ for an ellipse in potential flow (not proven here), where u'_{max} is the biggest increase in flow speed above freestream anywhere on the body. This result can be corrected for compressibility by

$$\frac{u'_{max_c}}{V_{\infty_c}} = \frac{1}{\beta^2} \beta \frac{t}{c} = \frac{1}{\beta} \frac{t}{c} \tag{49}$$

This is the original 2D scaling you met last year. Notice the effect of the scaling in y is to cancel a β as described, so the rules are actually the same.

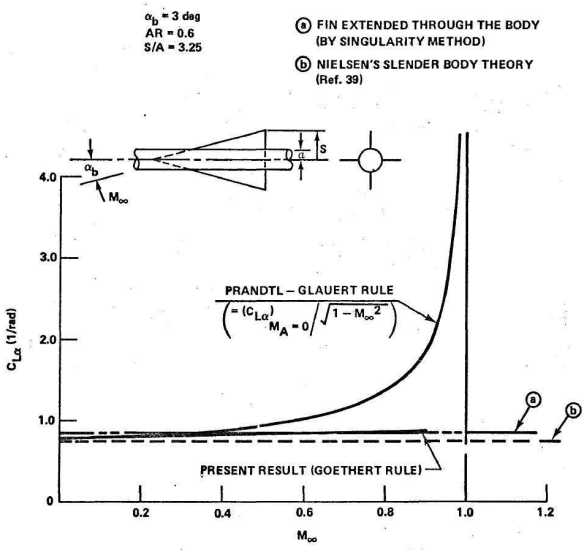

Figure 17: Comparison of Göthert and Prandtl-Gauert compressibility rules

3.1.4 Missile Fin Example

The graph in figure 3.1.4 compares the lift gradient for a low aspect ratio missile fin to the 2D Prandtl-Glauert scaling for a wing of aspect ratio 0.6. It is clear how poor a 2D scaling can be for a case like this (the 'correct' result is labelled line 'b').

3.2 Wing Sweep

Sweep is introduced to the wing design to reduce the adverse effects of compressibility (transonic and supersonic flows). Usually, sweep is chosen for high subsonic speed aeroplanes on the basis of transonic performance (increase critical Mach number). In the case of supersonic flight, sweep would be advantageous by positioning the entire wing within the Mach cone thus ensuring subsonic flow over the entire wing.

Sweep is not necessary for low speed flight (aeroplanes that fly up to M=0.6 usually are designed with no sweep); in fact, sweep can introduce a number of problems during low speed flight especially with stability and during high lift phases of the flight. Therefore, the final choice of sweep will have to take into account a number of factors affected by the sweep angle:

- High subsonic cruise: critical Mach Number
- Supersonic dash: subsonic or supersonic leading edges
- Low-speed performance: lift distribution, lift curve slope, maximum lift
- Low-speed stability: pitch-up, dihedral effect, cg location
- Radar cross-section: edge alignment
- Structural constraints: wing bending, wing spar, engine and undercarriage location

3.3 Effect of sweep on range

An interesting simplified analysis due to Küchemann gives some further insight into the effect of sweep angle on cruise performance.

For a family of conventional swept-wing aircraft with the same wing area S, and fuselage and tail-plane size the wing sweep Λ is varied according to the cruise speed to maintain the same Mach Number normal to the leading edge. From geometry, the cruise Mach Number and wing aspect ratio for each aircraft are then

$$M_{cruise} = \frac{M_0}{\cos(\Lambda)} \tag{50}$$

and

$$A_R = A_{R_0} \cos^2(\Lambda) \tag{51}$$

where the subscript 0 denotes the unswept member of the family. To a first order the wing structure may be taken to be the same for each aircraft, so that the overall weight W and wing loading W/S remain constant.

Before continuing, a brief reminder of the optimum lift/drag ratio.

$$\frac{C_L}{C_D} = \frac{C_L}{C_{D_0} + KC_L^2} \tag{52}$$

Differentiate and set the numerator to zero

$$C_{D_0} + KC_L^2 - 2KC_L^2 = 0 \tag{53}$$

$$C_L = \sqrt{\frac{C_{D_0}}{K}} \tag{54}$$

$$\frac{C_L}{C_{D\,max}} = \sqrt{\frac{C_{D_0}}{K}} \frac{1}{2C_{D_0}} = \frac{1}{2\sqrt{C_{D_0}K}} \tag{55}$$

If each aircraft cruises at the same proportion n of its maximum lift/drag ratio then

$$\left(\frac{L}{D}\right)_{cruise} = n\left(\frac{L}{D}\right)_{max} = n\frac{1}{2\sqrt{C_{D_0}K}} = \frac{n}{2}\sqrt{\frac{\pi A_R}{kC_{D_0}}} \tag{56}$$

Assuming that each aircraft is designed to the same aerodynamic standard, the induced drag factor k and the zero-lift drag coefficient C_{D_0} also remain constant. Cruise L/D is therefore proportional to $\sqrt{A_R}$, so that

$$\left(\frac{L}{D}\right) = \left(\frac{L}{D}\right)_0 \sqrt{\frac{A_R}{A_{R_0}}} = \left(\frac{L}{D}\right)_0 \cos(\Lambda) = \left(\frac{L}{D}\right)_0 \frac{M_0}{M} \tag{57}$$

and hence

$$M\frac{L}{D} = M\frac{M_0}{M}\left(\frac{L}{D}\right)_0 = M_0\left(\frac{L}{D}\right)_0 = constant \tag{58}$$

Since we are considering a family of aircraft with constant weight, and hence constant lift, then it follows that M/D is also constant - so that drag (and hence required thrust) only increases linearly with design Mach Number (rather than quadratically as would be the case for an individual member

of the family). Although a simplistic analysis, figure 18 shows that this captures the variation in cruise L/D of a realistic family of aircraft rather well.

The next step is to look at the effect on cruise performance - specifically on range. Recall the basic Breguet range equation:

$$R = \frac{V}{Sg}\frac{C_L}{C_D}\ln\left(\frac{W_1}{W_2}\right) = \frac{a_0}{Sg} = \left[M\frac{L}{D}\right]\ln\left(\frac{W_1}{W_2}\right) \tag{59}$$

For cruise above the tropopause (ie a height of 11km and above) temperature T and hence speed of sound a_0 are constant. Further, for turbojet engines the specific fuel consumption f at the design point is roughly constant, while the weight breakdown and hence start/finish weight ratio $\frac{W_1}{W_2}$ for the family of aircraft is also constant. The Breguet range R is then simply proportional to $\frac{ML}{D}$, and from the above analysis therefore constant for the family of aircraft considered.

In other words, the range of a family of aircraft is (to a first order) independent of sweep angle. **Sweep can therefore be considered primarily as a way of increasing cruise speed and hence reducing block time for a given range**, thereby achieving savings in terms of per-hour costs (eg crewing).

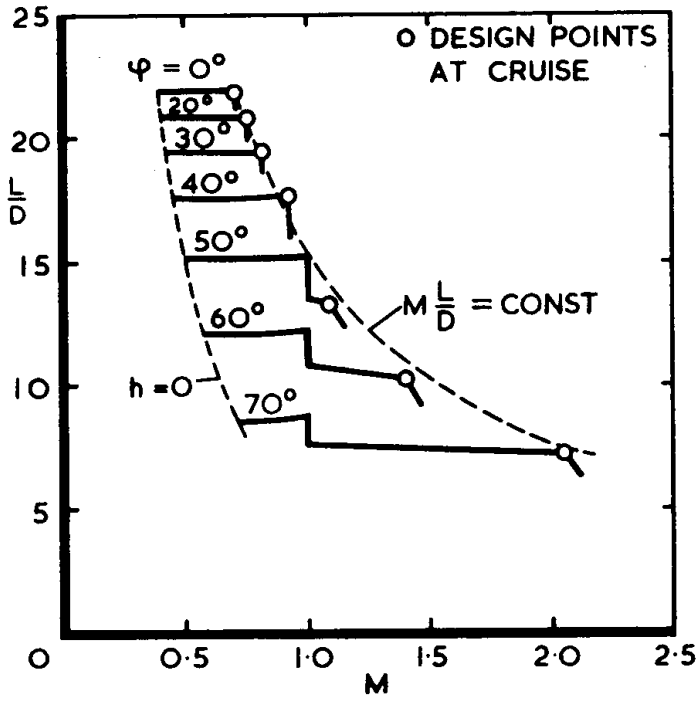

Figure 18: Lift/drag ratios for a family of swept-wing 150-seat transatlantic aircraft (ψ is sweep)

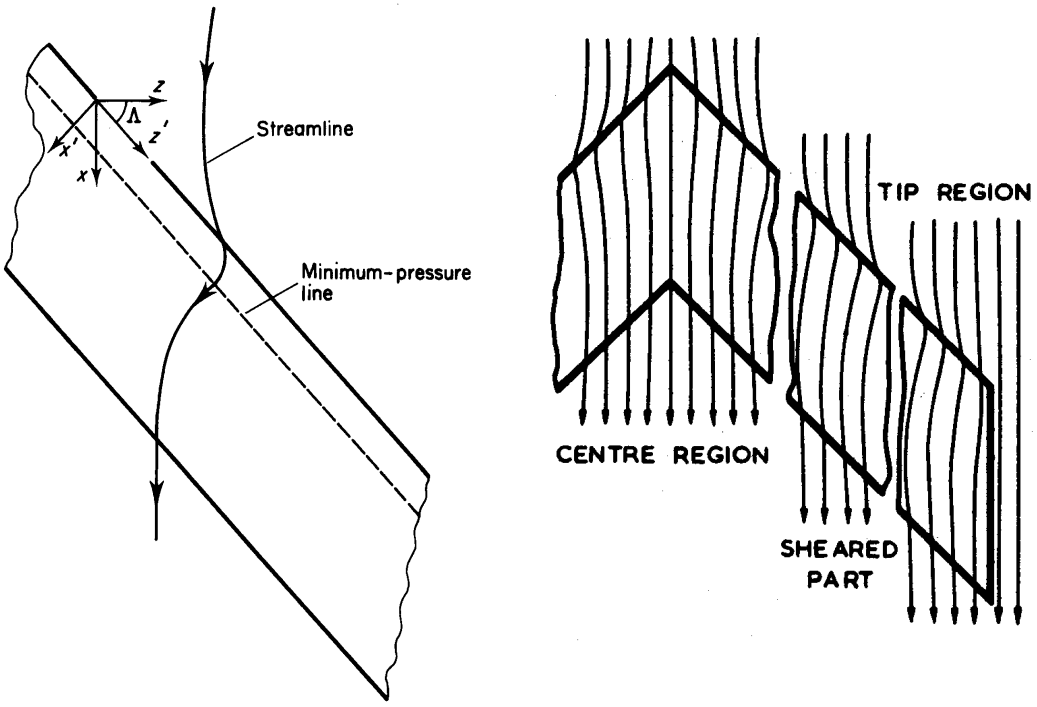

Figure 19: Cross-flow on infinite and finite sheared wings at zero incidence

3.4 Area Ruling in 3D

The area rule is concept you first met last year. Put simply, for sonic Mach numbers (ie M 1.0) the longitudinal distribution of the cross-sectional area of the complete aircraft (fuselage + wing + cockpit + stores + etc) should approximate to the minimum-drag Sears-Haack body (or at least vary **smoothly**). The resulting shapes give increases in critical Mach number, and reductions in transonic drag levels. Figures 20 and 19 show the interaction between spanwise streamline curvature and compressibility.

However, last year we did not mention how you might go about applying area ruling, which may be useful in your group design project in the future. A useful resource for computing cross-sectional area distributions for conceptual designs is `Sumo` (http://www.larosterna.com/sumo.html), and figure 21 shows two area distributions computed. The arrow points to a region near the tail for the T-tail configuration where there might be something to gain from repositioning of components, as the area slices indicate a brief rise in cross-sectional area which would likely raise compressibility drag. Note that the computation of wave drag available in `Sumo` is not suitable for transonic predictions.

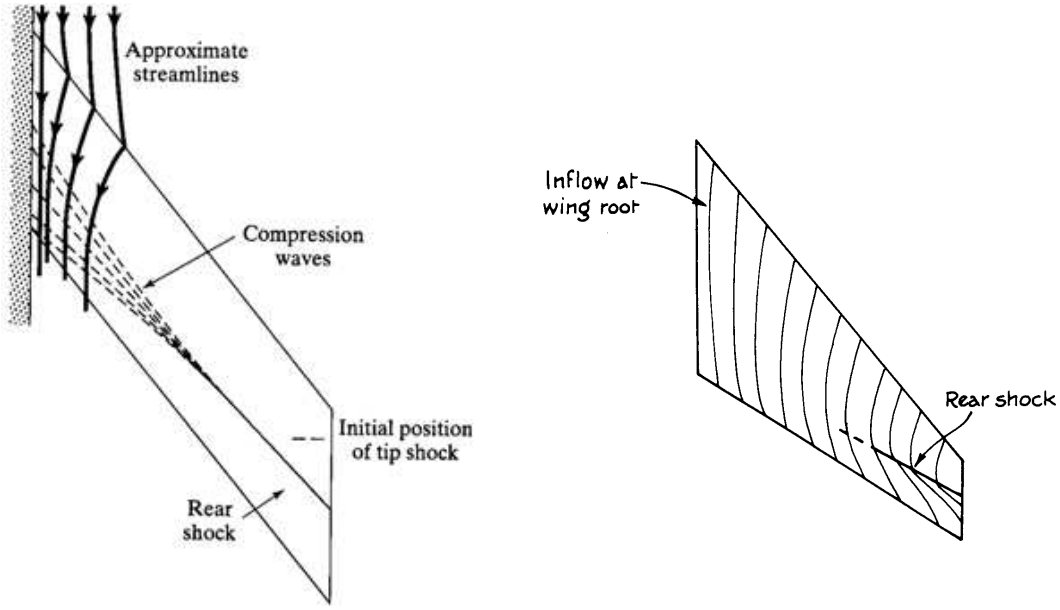

Figure 20: Outboard effect of flow constraint at wing root

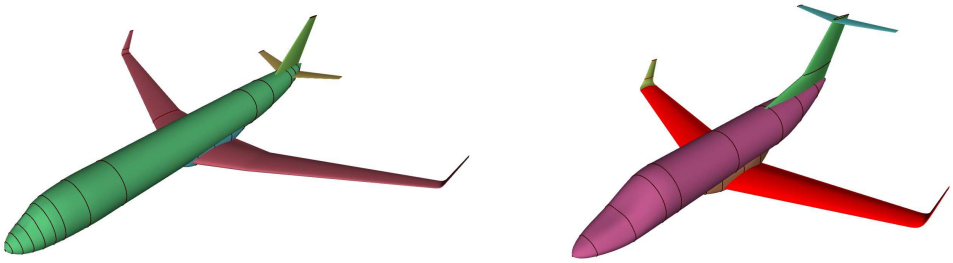

(a) Conventional

(b) T-tail

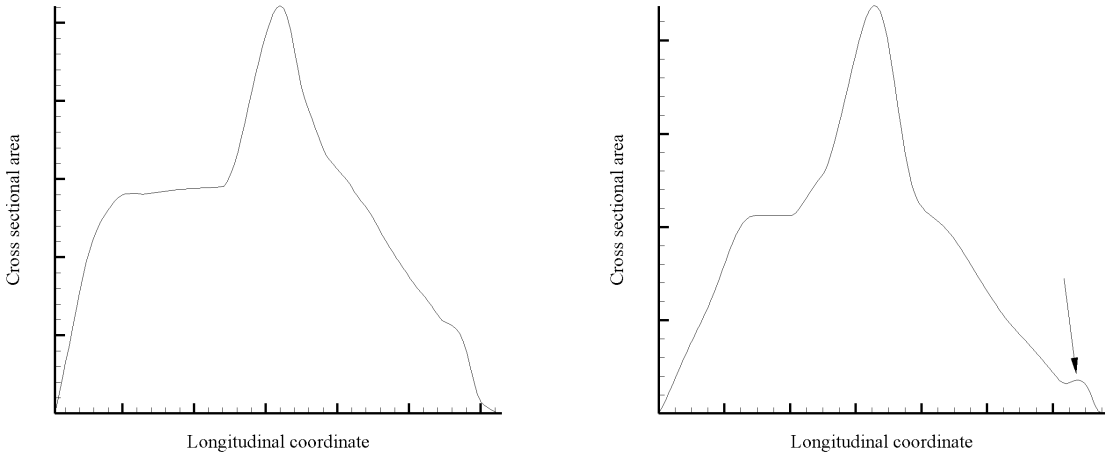

(c) Conventional - area

(d) T-tail - area

Figure 21: Perpendicular cross sectional area distributions for two aircraft

4 The Vortex Lattice Method

Key points: *Concept of vortex shedding, and revision of horsehoe vortex and lifting line models. Incorporation of lumped vortex thin aerofoil theory to form the Vortex Lattice method. Applications and Limitations of the Vortex Lattice Technique*

4.1 Introduction

We now turn to the vortex lattice method. It is in some ways similar to the panel method, and in fact is a bit simpler, but less accurate. It is very widely used in aerodynamics, particularly for wing analysis, as shall be discussed later. To begin, however, we shall revise some of the 3D wing theory you tackled last year.

4.2 Effect of Finite Span

The effect produced by a finite span wing is to reduce the suction near the tip, due to the span wise flow induced by the pressure differential between the high pressure lower surface and low pressure upper (figure 22). Vorticity is constantly being shed at the trailing edge, which rolls up out towards the tip forming a trailing edge vortex. This leads to two effects, a continuous alteration of lift along the span, and an induced drag caused by the effective downwash created.

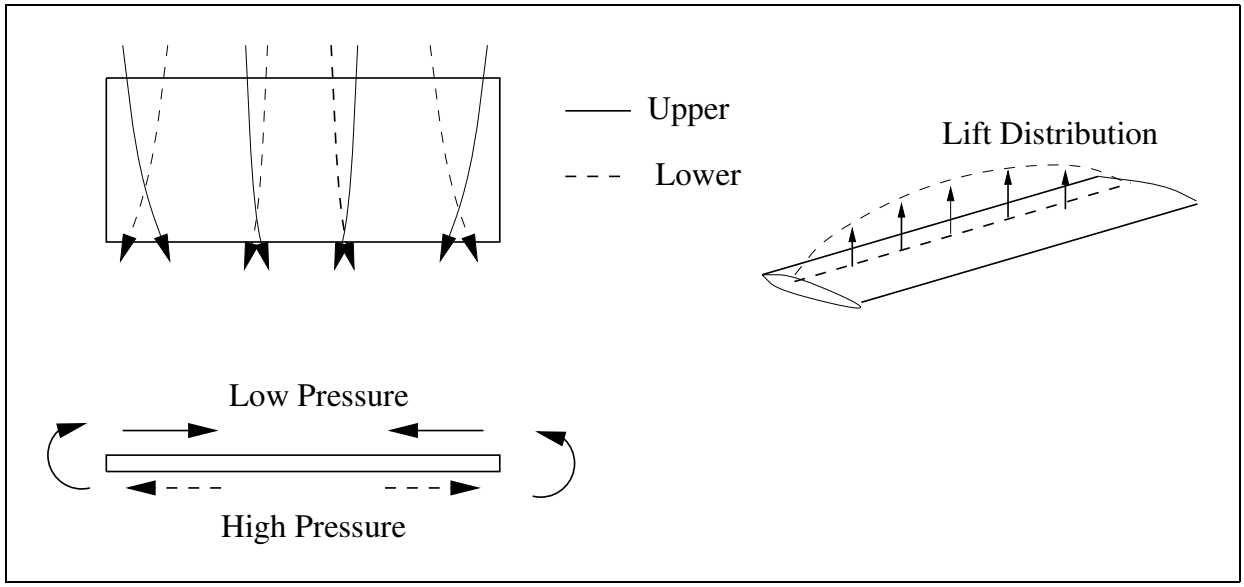

Figure 22: Thin Aerofoil Approximations

4.3 Models

The simplest model you used last year was the Horseshoe Vortex. This in essence represents the entire wing as a single vortex across the span, of a constant strength Γ. This vortex turns through 90 degrees at each tip (remember that the Helmholtz theorem states that a bound vortex cannot end in a

fluid), and extends downstream all the way back to the starting vortex, of equal and opposite strength Γ (figure 23). Whilst this is a simple and quick method, useful for early stage design calculations and investigation into the effects of coupled wings and ground effect, it is of limited accuracy, for as was explained in the section above, the lift reduces towards the tips (and in fact tends to zero), and hence so must the (local) vorticity.

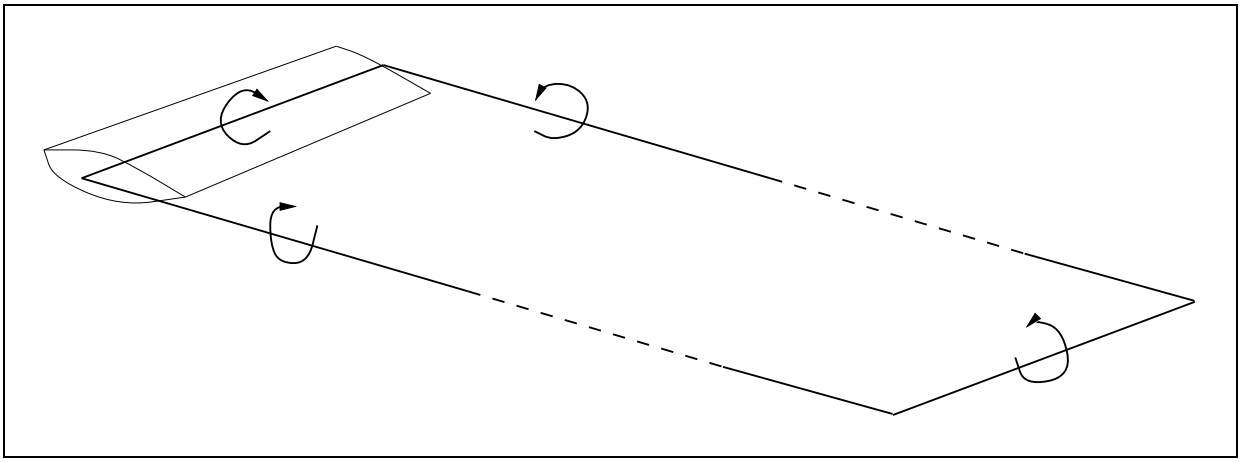

Figure 23: Horseshoe Vortex Model

An improvement was possible by splitting the vortex along the span into a large number of elemental vortices, each of a slightly different strength. This lead to *lifting line theory* (figure 24). The strength of the individual vorticies can be calculated either numerically, requiring that the spanwise vortex distribution be modelled as a series of small descrite step changes in circulation (representing the shedding of a tiny vortex into the wake), or as a continuous integral (and hence an analytical solution). Whilst the latter may seem more attractive initially, the suitability of the former to computational algorithms generally makes it more versatile and rapid. However, lifting line theory can be improved further by coupling it to the lumped vortex approximation of thin aerofoil theory.

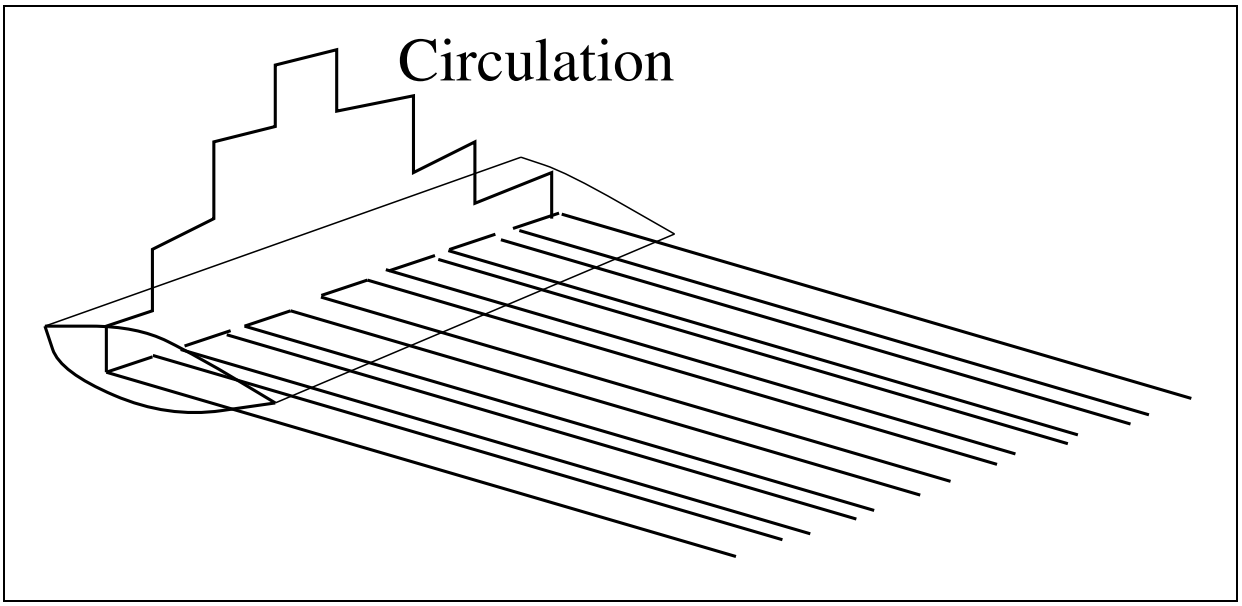

Figure 24: Lifting Line

4.4 The Vortex Lattice Method: Foundations

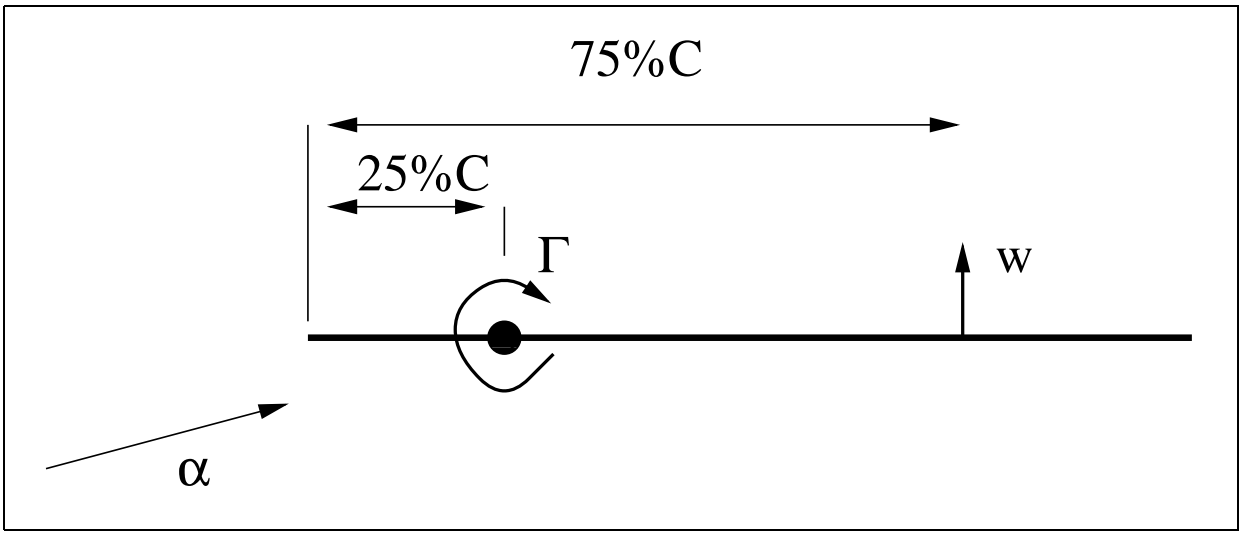

Figure 25: Lumped Vortex

As was discussed during the lectures on panel methods, the continuous chordwise integral expression for vorticity produced by thin aerofoil theory can be represented without too great a loss of accuracy by a single lumped vortex at 25% chord, with a control point imposed at k% chord. The velocity at the control point can then be expressed as a combination of that due to the vortex, of strength Γ, plus that due to the onflow velocity (U_∞) and incidence (α), as

$$\frac{-\Gamma}{2\pi(kc - c/4)} + U_\infty \sin\alpha = 0$$

Assuming small angles ($\sin\alpha \approx \alpha$), and that the Kutta theorem ($\Gamma = \pi\alpha c U_\infty$) is applied, we find

$$\frac{cU_\infty\alpha}{2(kc - c/4)} + U_\infty\alpha = 0$$

which is true *iff* $k = 75\%$. The same is true of a small section of the chord. This means that a wing may be broken down into a series of sections in the chorwise direction, each with a vortex placed at 25% of the panel chord, and a control point at 75%.

Combining this concept with the lifting line discussed earlier, we see that we can represent a wing as a series of panels (figure 26). Mathematically it is easier if these panels are collapsed onto the xy plane, as was the case with the camber line of thin aerofoil theory. Note, however, that this has the same implications, i.e. thickness effects are ignored, angles are assumed small, etc.

Once this is done, each panel is assigned a horseshoe vortex of strength $\Gamma_{i,j}$ at its 25% chord, with a control at 75%. The influence of the trailing arms of the horsehoe on the downwash at all the control points can then be calcuated from the *Biot-Savart Law*

$$w = \frac{\Gamma_{i.j}}{4\pi h}(\cos\alpha + \cos\beta)$$

which, as was the case with the panel method discussed in the last lecture, is defined entirely from the geometry of the model. As all the vortices effect all the panels we once again end up with a matrix of

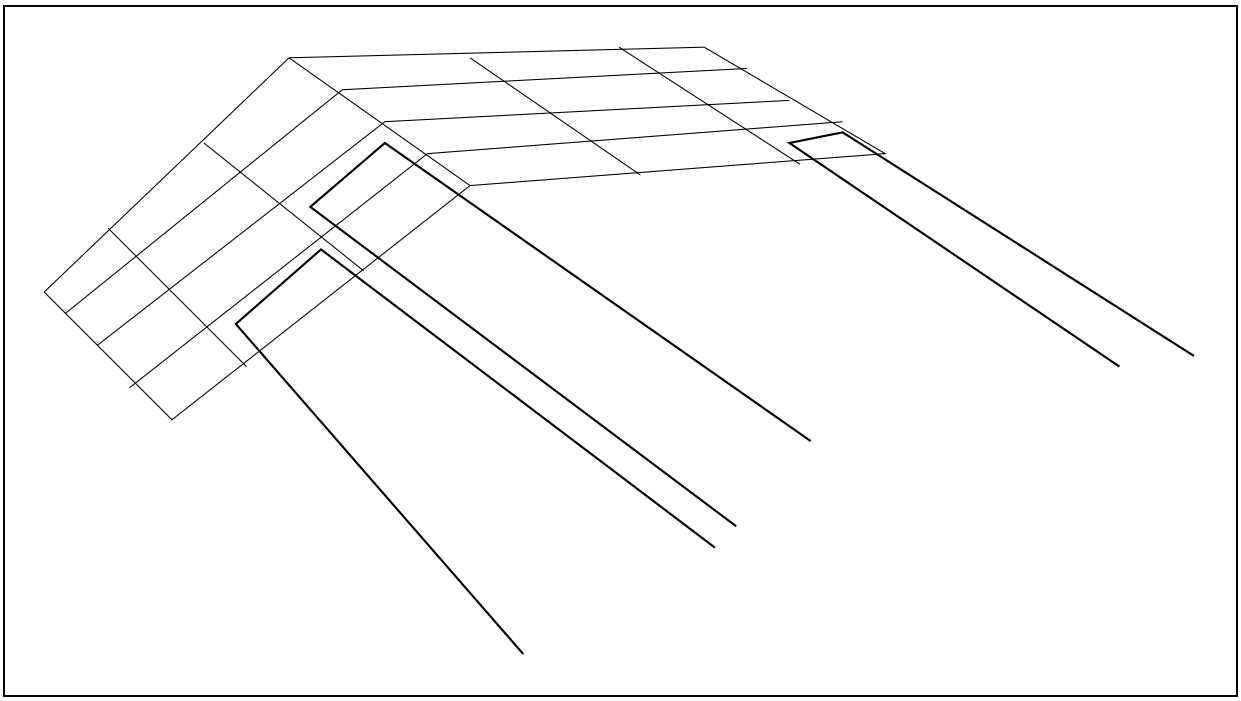

Figure 26: Vortex Lattice Representation of a Wing

the form

$$\begin{bmatrix} a_{1,1} & a_{1,2} & \dots & a_{1,npan} \\ a_{2,1} & a_{2,2} & & \\ \vdots & & & \\ a_{npan,1} & & & a_{npan,npan} \end{bmatrix} \begin{bmatrix} \Gamma_1 \\ \Gamma_2 \\ \vdots \\ \Gamma_{npan} \end{bmatrix} = -U_\infty \begin{bmatrix} \bar{n_1} \\ \bar{n_2} \\ \vdots \\ \bar{n_{npan}} \end{bmatrix}$$

Although in this case due to the fact we have flat panels, $\bar{n}_1 = \bar{n}_2 = ... = \bar{n}_{npan}$. This can be solved for the various Γ's in the same way as for σ in the panel method.

4.4.1 Calculating Lift

Unlike the panel method where lift, drag and moment must be calculated from integration of surface pressures and normals, use of the vortex lattice approach allows calculation of drag and lift from

$$D = \sum_{1}^{npan} \rho \Delta y_i w_i \Gamma_i$$

$$L = \sum_{1}^{npan} \rho \Delta y_i U_\infty \Gamma_i$$

$$M = \sum_{1}^{npan} \rho \Delta y_i U_\infty \Gamma_i (x_i - x_{ref})$$

$$C_D = \sum_{1}^{npan} \frac{2\Delta y_i w_i \Gamma_i}{U_\infty^2 S_{ref}}$$

$$C_L = \sum_{1}^{npan} \frac{2\Delta y_i \Gamma_i}{U_\infty S_{ref}}$$

$$C_M = \sum_{1}^{npan} \frac{2\Delta y_i \Gamma_i (x_i - x_{ref})}{U_\infty S_{ref} c}$$

where Δy, Γ, w, c, x_{ref} are panel spanwise extent, vortex strength, downwash, reference chord and moment arm respectively. S_{ref} is the reference area. Commonly in potential flow codes, $U_\infty = 1$ and $\rho = 1$ are used, because dimensionless coefficients do not depend on dimensional inputs.

4.5 Practical Implementation, Uses and Limitations

Whilst in theory a wing could be split into panels of any size and orientation, the method works best (most accurate results and/or faster solution) if the chordwise spacing is evenly distributed in terms of the local chord (i.e. if there are 4 panels, they extend from 0-25%, 25-50%, 50-75%, and 75-100% *local* chord across the entire wing), and that spacing is also even in the spanwise direction, except that a small gap (0.25% of cell width) is left at each tip (see figure 27). This also means that Δy becomes a constant, simplifying the equations for lift and drag above.

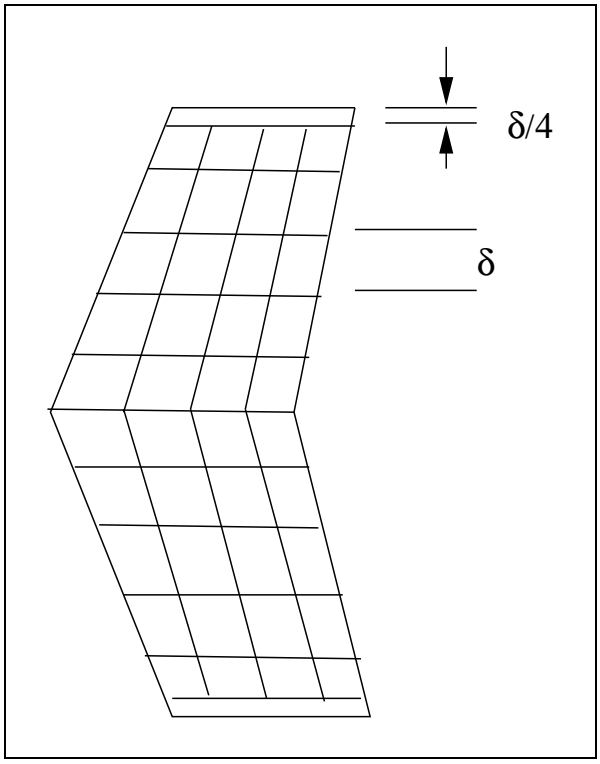

Figure 27: Tip Gap

The limitations of the vortex lattice method should be obvious; it is really a computerised version of thin aerofoil theory, and is subject to the same problems - thickness distributions are ignored, small angles and incidences are required, and inclusion of nacelles/bodies is difficult. However, it is a very widely used tool in the aerospace industry, for several reasons. It is simpler and more

rapid than panel methods, particularly for lifting bodies (i.e. wings), as no wake computation is required. Multi- element wings (flaps, slats) can be modelled fairly easily. By solution of the transonic small perturbation potential equations, rather than full potential (a bit more complex, but not too much), transonic solutions can be approximated, although there are problems with this (relating to non-linear aerodynamic effects such as shock waves). Perhaps most importantly, coupling of the vortex lattice solution to a structural analysis is fairly easy, as wings can often be represented as flat plates. Modal analysis then predicts linear displacement patterns, and combined with the (linear) vortex lattice method allows prediction of various aeroelastic effects, most importantly flutter. This practise is current industry state of the art, and can be accomplished through commercial FE solution packages such as NASTRAN and ZAERO.

4.6 Discrete Lifting Line/Weissinger Model

A particularly useful variant of the vortex lattice method exists that is commonly known as the Weissinger model/method. As initially proposed, the method is identical to the VLM, but with a single horseshoe vortex located at each spanwise station.

However, a useful modification can be made if the $\frac{3}{4}$ chord zero normal flow condition is replaced with a condition on the sectional lift coefficient. This is useful because it allows one to specify the lift curve gradient, which opens the door to a simplified 3D treatment of compressibility and nonlinear lift curves. Note that web searches for the 'Weissinger Model' usually return the vortex lattice variant, while the sectional lift variant is not often mentioned.

The idea works on the basis that

$$C_l = \frac{\rho V_\infty \Gamma}{\frac{1}{2}\rho V^2 c} = \frac{2\Gamma}{V_\infty c} = \frac{\partial C_l}{\partial \alpha}(\alpha_i - \alpha_0) \tag{60}$$

where the local angle of attack comes from the downwash (computed at $\frac{c_i}{4}$) from all horseshoe vortices

$$\alpha_i = tan^{-1}\left(\frac{w_i}{U_\infty}\right) \tag{61}$$

The utility of this method comes from the fact that C_l may be permitted to be any function of α, although a common choice that you will have seen from your 2^{nd} year work is $C_l = 2\pi\alpha$, or allowing for linear compressibility $C_l = \frac{2\pi\alpha}{\sqrt{1-M_\infty^2}}$. If equation (60) is solved at each spanwise station i together with $C_{l_i} = 2\pi\alpha_i$ then the problem may be written easily as a single linear system and solved with LU decomposition or similar.

However, at transonic speeds $C_l = \frac{2\pi\alpha}{\sqrt{1-M_\infty^2}}$ is deficient due to the nonlinearity of the normal shocks that form on the aerofoil. Instead, it is possible to perform a 2D CFD calculation for a range of angles of attack at a particular Mach number, to arrive at a relationship $C_l = f(\alpha)$, where f is an interpolation function (perhaps a polynomial fit) through the computed incidence points. This can capture some of the 2D nonlinearity, but needs to be adjusted to be reasonable for 3D.

One way to perform this adjustment is to couple the 3D Weissinger model to the 2D compressible data. However, $f(\alpha)$ is no longer a linear function, so the system cannot be written as a linear system and solved in a single step. Instead, it is possible to use an iteration of the type

$$C_{l_i}^{n+1} = C_{l_i}^n + k(C_l(\alpha_i^{n+1} - C_l(\alpha_i^n)) \tag{62}$$

So, the calculation proceeds as follows. First, all horseshoe vortices have zero strength, and the incidence at each station is only due to the freestream angle of attack. These sectional angles of attack give sectional lift coefficients via $C_l = f(\alpha)$. From the lift coefficients, equation (60) provides a new set of values for Γ_i. Now that the horseshoe vortices have an estimated strength, w_i and thus α_i can be recomputed, before proceeding to another estimate of C_{l_i}. The process continues until C_{l_i} does not change significantly between iterations, and providing that k in equation (62) is sufficiently small the iterates converge (if k is too large the process can be unstable and odd-even instability is seen in the Γ_i values).

This is a process that is suitable for your design project work. It is fast, but of course still somewhat limited, and perhaps best described as a '2.5D' method. It works reasonably because for high aspect ratio wings most of the compressible behaviour is 2D in nature, and not influenced by 3D effects (except through the trailing vortices altering the sectional angles of attack). For low aspect ratio wings two shocks can often merge into one near the tip, which is inherently a nonlinear 3D compressible effect. Despite this the method can still give surprisingly accurate results, although in general it is not suitable for low aspect ratio wings. Transport wings, conveniently, are almost invariably of high aspect ratios.

This technique is the same as that described in detail by Mason,[6] although it has probably been in common usage as long as the VLM itself. An incomplete implementation of this method is given in the coursework, which you may wish to use in future when complete. An unusual point is that the sectional 2D relationship is modified to account for compressibility but the 3D flowfield is not. This is an odd nuance, but not altogether unexpected given the hefty simplifications made, and by ignoring the chordwise direction we are implying that the aspect ratio is high.

You may wonder why we wish to use this method. The key idea is that once C_l is known along the span, the Korn equation (allowing for sweep) may be used to find the sectional drag divergence Mach numbers. These can give an estimate of the sectional critical Mach numbers, which in turn can be used in Lock's fourth power law (entirely empricial) to estimate the sectional wave drag coefficient C_{d_w}.

Although $\frac{\partial C_l}{\partial \alpha}$ is changed significantly by compressibility and nonlinear transonic effects, it remains roughly constant at a particular Mach number providing the incidence is fairly small. This means we can also linearise and solve a linear system to obtain our vortex strengths, rather than iterating.

$$\tan(\alpha_i) = \frac{V_\infty \sin(\alpha_\infty) + \sum_{j=1}^{j=N} a_{ij}\Gamma_j}{V_\infty \cos(\alpha_\infty)} \tag{63}$$

Assuming small velocity induced angles $\tan(\alpha_i) \approx \alpha_i$, and including an addition from the twist, gives

$$\alpha_i = \tan(\alpha_\infty) + \alpha_t + \frac{\sum_{j=1}^{j=N} a_{ij}\Gamma_j}{\cos(\alpha_\infty)} \tag{64}$$

Noting that

$$C_l = \frac{\rho V_\infty \Gamma}{\frac{1}{2}\rho V^2 c} = \frac{2\Gamma}{V_\infty c} \tag{65}$$

For convenience we can set $V_\infty = 1$ with no loss of generality.

$$\frac{\partial C_l}{\partial \alpha}\left(\tan(\alpha_\infty) + \alpha_t - \alpha_0 + \frac{\sum_{j=1}^{j=N} a_{ij}\Gamma_j}{\cos(\alpha_\infty)}\right) = \frac{2\Gamma_i}{c} \tag{66}$$

$$\left(a_{ii} - \frac{2\cos(\alpha_\infty)}{\frac{\partial C_l}{\partial \alpha}c}\right)\Gamma_i + \sum_{j=1, j\neq i}^{j=N} a_{ij}\Gamma_j = \cos(\alpha_\infty)(\alpha_0 - \alpha_t) - \sin(\alpha_\infty) \tag{67}$$

Which is a linear system for the vector of unknowns Γ_i to Γ_N. Although we have assumed α_i is small, we did not do the same for α_∞ as this was not algebraically necessary. This is of little relevance as the model is only applicable for small angles of attack.

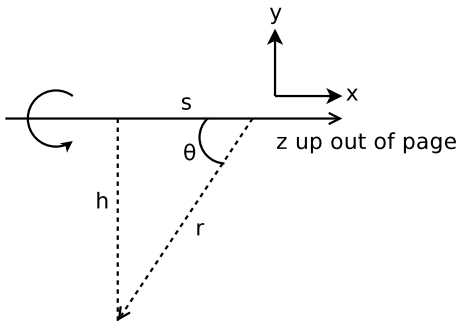

Figure 28: Vortex filament

4.7 Biot-Savart Integration

We need to know the a_{ij} influence coefficients. These are the z velocity components from the Biot-Savart integration

$$\mathbf{V} = \frac{\Gamma}{4\pi}\int \frac{\mathbf{ds}\times\mathbf{r}}{|\mathbf{r}|^3} \tag{68}$$

Why is the Biot-Savart law of this form?

A cross product gives a vector perpendicular to the other two vectors. So, the velocity is perpendicular the line element and the vector from the point in question to the line element. That part is simple and means that the velocity produced goes 'round and round' the vortex element. The area of a sphere is $4\pi r^2$ and we would like the area times the strength to remain fixed for any distance to the line segment, so this appears on the denominator (remember the $\frac{1}{2\pi r}$ factor in 2D). Finally, the vector $\mathbf{r}$ has a length, so we must divide by the length of $\mathbf{r}$ again to remove this unwanted effect.

Introduce

$$h = r\sin(\theta) \tag{69}$$

$$s = \frac{h}{\tan(\theta)} \tag{70}$$

$$ds = -\frac{h}{\sin^2(\theta)}d\theta \tag{71}$$

$$\mathbf{ds}\times\mathbf{r} = \begin{pmatrix} \frac{-h}{\sin^2(\theta)}d\theta \\ 0 \\ 0 \end{pmatrix} \times \begin{pmatrix} -s \\ -h \\ 0 \end{pmatrix} = \begin{pmatrix} 0 \\ 0 \\ \frac{h^2}{\sin^2(\theta)}d\theta \end{pmatrix} \tag{72}$$

Integral becomes

$$V_z = \frac{\Gamma}{4\pi}\int \frac{h^2}{\sin^2(\theta)}\frac{\sin^3(\theta)}{h^3}d\theta = \frac{\Gamma}{4\pi h}\int \sin(\theta)d\theta \tag{73}$$

$$V_z = \frac{\Gamma}{4\pi h}(\cos(\theta_A) - \cos(\theta_B)) \tag{74}$$

Checking sign conventions, $\cos(\pi) - \cos(0) = -2$, so as drawn the vortex would produce a downwards velocity, which is correct.

5 The Panel Method

Key points: *Limitations of Joukowski and thin aerofoil theory, concept of distributed source and influence coefficient, stages of a panel method, applications and limitations*

5.1 Introduction

We have now completed the section of the course dealing with viscous flows. We have also considered the interaction between inviscid and viscous solution processes through 'coupling' of a joukowski aerofoil solution method to an integral boundary layer calculation. This has allowed us to gain some understanding of the generic considerations required for such design and analysis techniques, however, the inviscid solution method itself (the Joukowski transformation) is not widely used, for several reasons. As was noted both earlier this year and last, Joukowski aerofoils are not much use practically (due to a zero thickness at the trailing edge, which cannot be easily manufactured). As an analysis method it lacks generality; an aerofoil shape is produced as a result of the flow analysis, rather than a flowfield about a given aerofoil being produced. Most importantly, this technique cannot be applied in three dimensions. It is also true that the thin aerofoil theory you were taught last year is not widely used, although for different reasons.

Whilst both the above methods have historical significance, and are useful teaching aids, it is equally important that you have some understanding of more current, practical tools. Over the next 4 weeks we are therefore going to study two methods that have been developed more recently, depend heavily on computational power, but are far more flexible in capability and hence used by many different parts of industry for various design jobs. We will, however, have to be somewhat more superficial in our treatment, due to the increased complexity of the techniques. These methods are called *panel methods* (which we shall consider for the next two weeks), and *vortex lattice* methods. Before discussing the panel method itself, however, we shall briefly revise thin aerofoil theory and the Joukowski transformation, and in particular their limitations.

5.2 Thin Aerofoil Theory

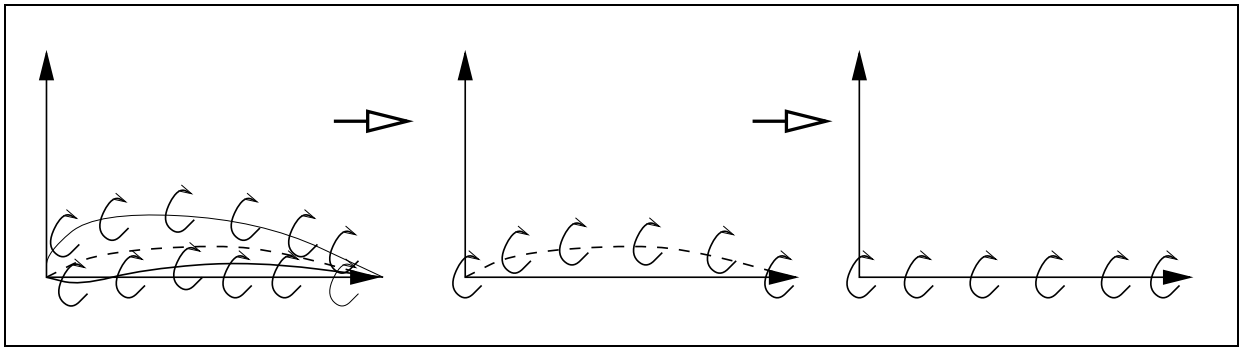

Figure 29: Thin Aerofoil Approximations

Last year you were introduced to thin aerofoil theory. Essentially, the aerofoil is represented as a single vortex sheet, situated on the mean camber line. As small camber is assumed, this vortex sheet

is then moved to the chord line (figure 29), and equations derived that allowed an expression for the vortex distribution to be related to the onset velocity, incidence, and camber, *viz*

$$\frac{1}{2\pi}\int_0^c \frac{\gamma(\xi)d\xi}{x-\xi} = V_\infty\Big(\alpha - \frac{dz}{dx}\Big) \tag{75}$$

which then could be solved either for zero camber ($\frac{dz}{dx} = 0$), or including this term, using geometric transformations and functions ($\sin, \cos$,etc.). A simpler, single element method with the vortex located at the 25% chord with a control point at 75% was also discussed, although this is somewhat less accurate. The details of the solution techniques will not be examined upon this year, although you may well find a brief review helpful in understanding the assumptions and limitations discussed below:

First, note that equation (75) does not have any terms dependent on the thickness distribution (i.e. surface shape). This means that only very thin aerofoils are reasonably approximated. Secondly, inherent in this method is the assumption that all angles are small, i.e. that incidence is low, and further the gradients of the surface/camber line are small. Again whilst this is reasonable in some cases, it essentially rules out the method for fat aerofoils, and more importantly any truly three dimensional shapes such as cars and complete aircraft, or multi element aerofoils, such as slat-wing-flap combinations. The solution accuracy near stagnation points is also poor, due singularity problems.

5.3 Joukoswki Transformations

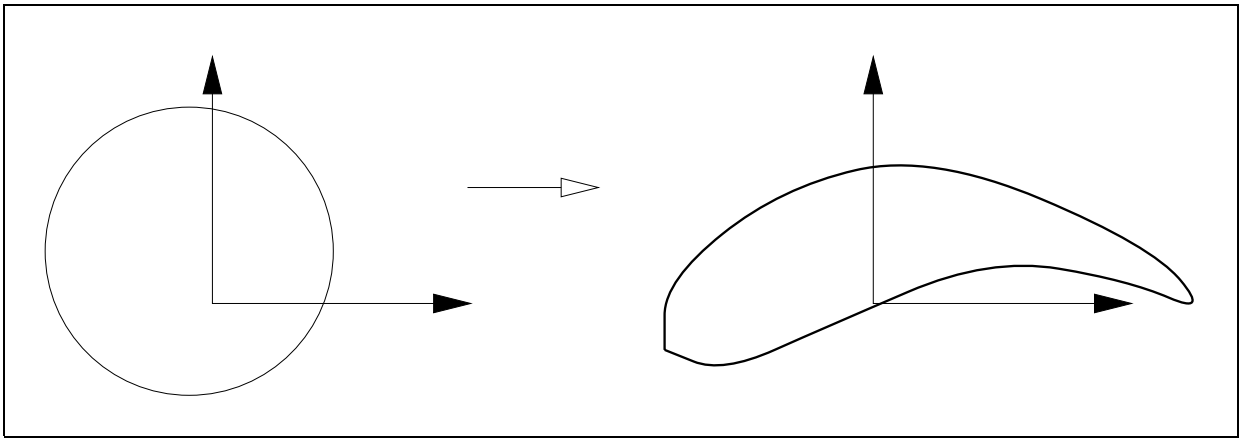

Figure 30: Joukowski Transformation

The Joukowski transformation and associated aerofoils discussed earlier this year do have the significant advantage that the solution is exact, and not limited to thin aerofoils. However, the aerofoil shapes produced are generally impractical, particularly due to their thin, cusped trailing edges that make manufacturing difficult, and storage of flaps etc., very difficult. The method also has the disadvantage of being inverse, in that the aerofoil shape is a product of the solution process, and hence it cannot answer the question 'what forces does this aerofoil/shape produce?', for an arbitrary input shape. Perhaps most importantly, it is strictly limited to 2D problems, as conformal mappings do not exist in higher dimensions.

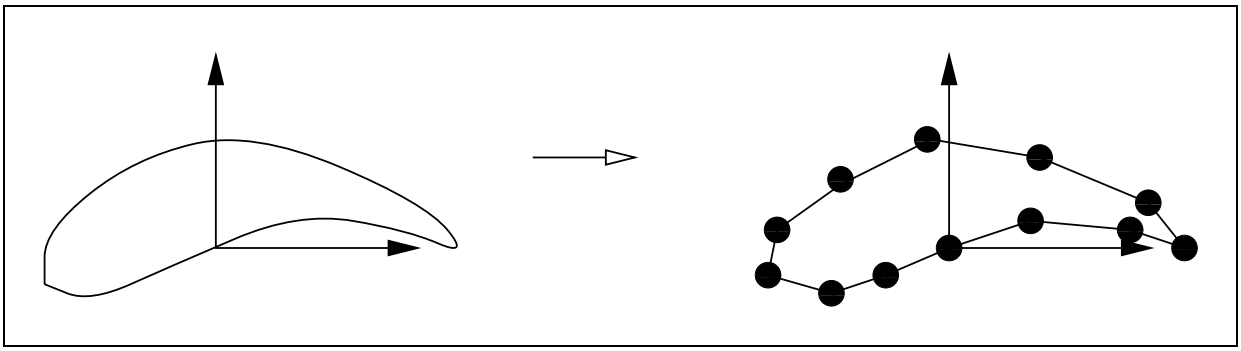

Figure 31: Panel Method, 2D

5.4 Panel Methods

In the late 1960's, a method was developed which made use of the rapid increases in computational power and speed to provide for the first time a method that had the capability to analyse flows around realistic geometries, and in many ways marked the birth of modern computational analysis. Although not generally classed as a full CFD technique, it shares many similarities including surface meshes and numerical solution, although the surrounding flow is not meshed.

Panel methods utilise linear solutions of the potential function ϕ, and hence are limited to subsonic, (strictly incompressible, although compressibility corrections such as the Prandtl - Glauert compressibility correction can be applied to allow velocities up to M_{crit}, where supersonic flow first occurs), inviscid flow. Solutions produced by the panel method can then of course be coupled to a boundary layer solver, as you did with the Joukowski transformation. They are, however, a far more rapid solution method than alternative (more flexible) CFD techniques, whilst being considerably more accurate than hand calculations. As such they are still widely used in 'state of the art' versions, particularly where speeds are low (landing configurations, land vehicles), e.g. NEWPAN, used extensively in formula one design, and developed while its author was here at the University of Bristol.

5.5 The Method

As mentioned, complex potentials and and transformations do not exist in three dimensions, and in fact there are *n*o analytical solutions here. We therefore have to resort to an approximate (numerical) procedure, based on what we know of the solution of LaPlace's equation ($\nabla^2\phi = 0$). This means essentially we have to make use of a large number of 'fundamental' solutions (the sources, sinks, vortices and doublets you were taught about last year), and using the fact that these solutions are linear, add them together to get the flow we want. Whilst any of the above can be used to make a panel method (we'll return to this later), we'll just consider sources, historically the first to be used and probably the easiest to understand.

The equation of a source is

$$\phi_S = \frac{\Lambda}{4\pi}\frac{1}{r}$$

in 3d, and

$$\phi_S = \frac{\Lambda}{2\pi}\ln r$$

in 2 (the form you met it in last year). Any combination of sources and sinks (and doublets, etc.)

satisfies LaPlaces equation, but discrete (lumpy) sources, etc., are awkward if placed on the surface of a body (due to the presence of singularities in the flow which make the physics a bit odd, black holes aside).

The way around this problem is to 'smear out' the sources on each panel area ΔS. If we label the distributed source strength σ, then

$$\Lambda = \sigma \Delta S$$

At a point P above the surface, assuming that σ is constant on each panel, the total potential induced, ϕ_P, is the sum of the contributions from all the elemental areas dS

$$\phi_P = \sum \frac{\sigma \Delta S}{4\pi} \frac{1}{r_P}$$

where r_P varies from element to element (see figure 32). Making the elemental area to tend to zero,

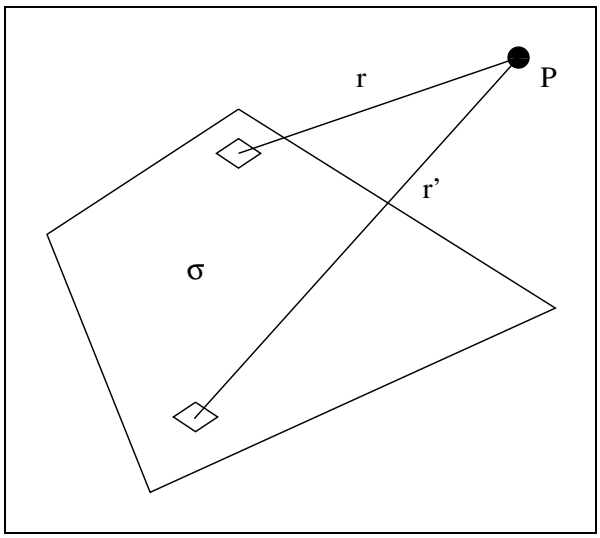

Figure 32: Influence of ΔS on P

we get

$$\phi_P(\Delta S) = \frac{\sigma}{4\pi} \iint_{\Delta S} \frac{dS}{r_P}$$

This equation can be calculated analytically for any flat panel shape and point P, although this can involve complicated and tedious mathematics, and hence we will not go through it here. The solution of this equation is called the *influence coefficient* (in this case *source influence coefficient* as we used sources, other fundamental solutions can also produce these coefficients) for the potential.

As well as analytical results for the potential induced by a (flat, constant source strength) panel, we can work out (by differentiation of the potential) the velocity induced by the source panel giving the *v*elocity influence coefficient.

In particular we can deduce the velocity normal to other parts of the body (i.e. at all the other panels. For instance the effect of the 'ith' panel on the normal velocity at the centre of panel 'j' is represented by

$$Un_{j,i} = a_{j,i}\sigma_i$$

where σ_i is the source strength on panel i, and $a_{j,i}$ is the velocity influence coefficient of panel 'i' on 'j'. This being the case, we can work out the total normal velocity at panel j by summing all the

contributions of every other panel (remember this is only possible because of linearity), i.e.

$$Un_j = \sum_{i=1}^{i=n} a_{j,i}\sigma_i$$

Assuming we have a solid surface, we obviously want this to be equal to zero, i.e. (not forgetting the contribution of the onset flow, as the panel may be at any orientation!)

$$Un_j + U_\infty.\bar{n_j} = 0$$

where $\bar{n_j}$ is the unit normal vector to panel j. This can be expressed as the summation

$$\sum_{1}^{n} a_{j,i}\sigma_i + U_\infty.\bar{n}_j = 0$$

In this equation, the only unknown is σ_i, as all the terms are either calculable from the known geometry ($a_{j,i}, \bar{n_j}$) or specified in advance (U_∞).

Rearranging a little gives

$$\sum_{1}^{n} a_{j,i}\sigma_i = -U_\infty.\bar{n}_j$$

and of course we also have

$$\sum_{1}^{n} a_{j-1,i}\sigma_i = -U_\infty.\bar{n}_{j-1}$$

etc.

So, assuming we have $npan$ panels, we have $npan$ unknown sources of strength σ_i. But we have also $npan$ equations like those above, so we can rewrite all this into matrix form:

$$\begin{bmatrix} a_{1,1} & a_{1,2} & \dots & a_{1,npan} \\ a_{2,1} & a_{2,2} & & \\ \vdots & & & \\ a_{npan,1} & & & a_{npan,npan} \end{bmatrix} \begin{bmatrix} \sigma_1 \\ \sigma_2 \\ \vdots \\ \sigma_{npan} \end{bmatrix} = -U_\infty \begin{bmatrix} \bar{n_1} \\ \bar{n_2} \\ \vdots \\ \bar{n_{npan}} \end{bmatrix}$$

which in English is

$$InfluenceMatrix \times SourceStrengths = -OnsetFlow \times NormalComponents$$

The influence matrix has $npan^2$ entries, non of which are zero. It is generally not symmetric, and combined these two factors mean that there are few efficient solution methods. As the number of panels for a typical aerodynamic configuration can easily run into the thousands (remember that each panel is flat, and hence large numbers of small ones are needed to give a realistic model of curved/doubly curved vehicle surfaces), this presents a large computational problem.

For instance, Gaussian elimination, a matrix solution method with which you should be familiar, requires approximately $\frac{1}{3}npan^3$ operations to invert the matrix. This then is not practical for large problems, as it takes too long (say ≈ 80 % of total solutions time, equivalent to several hours on a Cray). Instead of this, iterative techniques are used, and this is one of the areas which distinguish

between different versions of the method, clever use of computational algorithms can give one type a speed or stability advantage over its competitors.

Simply put, the equation

$$[\mathbf{A}].\bar{\sigma} = -U_\infty \bar{n}$$

is solved by guessing an initial solution for $\bar{\sigma}$, then generating an error vector $\bar{E}_1$:

$$\bar{E}_1 = -U_\infty \bar{n} - [\mathbf{A}].\bar{\sigma}$$

This is used to generate a second guess,

$$\bar{\sigma_2} = \bar{\sigma_1} + f(\bar{E}_1)$$

and so on, until $\bar{E}$ is as small as required. For a 'good' iterative method, only about 10 iterations will be needed, so we have 10 matrix multiplications, i.e. $\approx 10npan^2$ operations, which is $\ll \frac{1}{3}npan^3$ if npan is of order 1000.

Once the vector $\bar{\sigma}$ has been calculated, we can use tangential velocity influence coefficients (which again depend only on geometry, which is known) to get surface speeds, and from these we can use Bernoulli's equation to calculate the pressures (remember we are dealing with inviscid, incompressible flow).

In summary, the four stages of a panel method are:

1. Descritisation of body surface into panels and calculation of panel geometries
2. Calculation of panel influence functions and storage in influence matrix
3. Solution of influence matrix for strength of panel singularities
4. Calculation of surface velocities, thence pressures, from panel singularity strengths

5.6 Wakes

The above is accurate for a two dimensional aerofoil. However, a three dimensional wing is followed by a trailing edge wake, which rolls up to form trailing edge vortices. How this is allowed for is another one of the 'black arts' which varies from panel method to method. The basic solution method involves creating a series of flat wake panels behind the wing, which do not represent a physical surface, but a shear surface. However, the panels are included in the matrix solution, and hence are effected, and effect, the pressure distribution around the body. The positions of these panels are then 'relaxed', and a solution for the wing that allows lift generation is (hopefully) obtained. This process is shown graphically in figure 33.

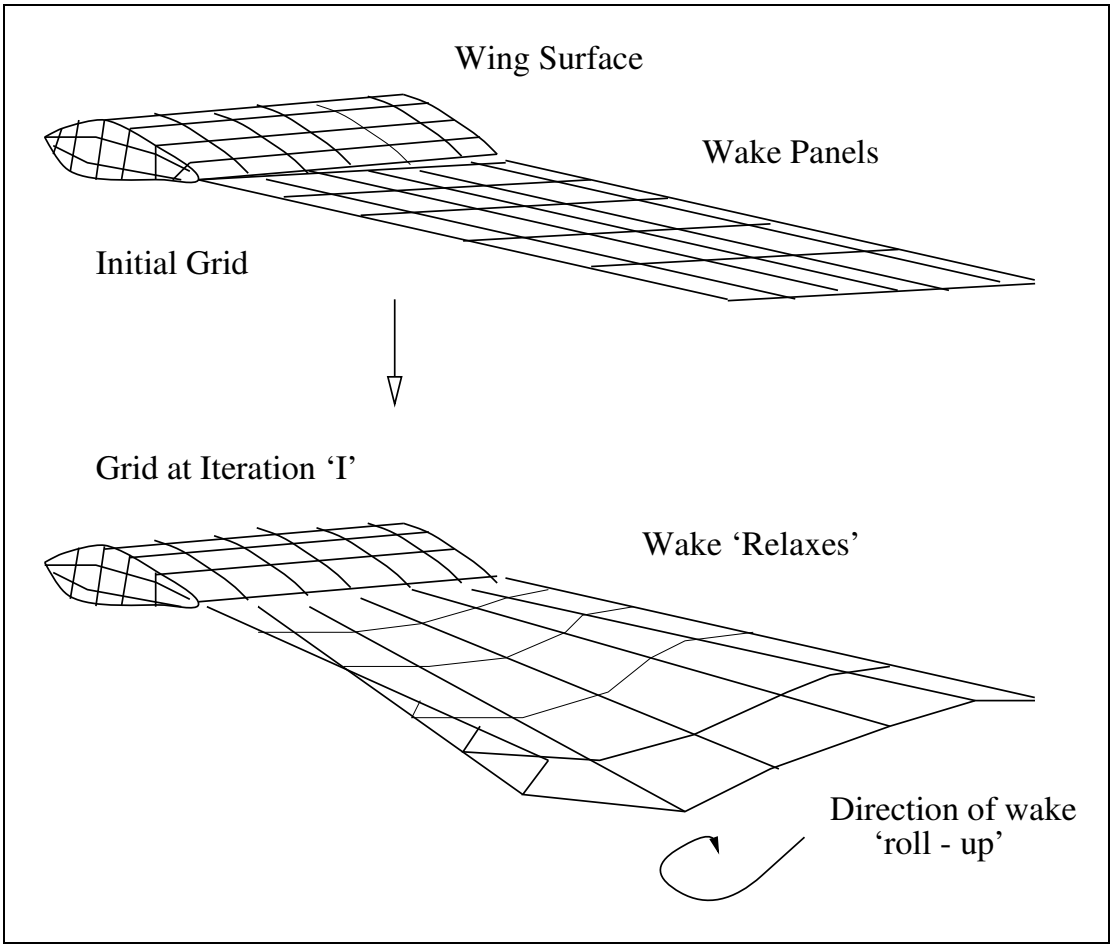

Figure 33: Wake Relaxtion

6 Complex Potential

Key points: *Revision of inviscid, irrotational, incompressible flow concepts, stream function and potential function and the Laplace equation. Discussion of complex numbers and potential functions, concept of holomorppic (analytic) functions, and the Cauchy-Riemann conditions*

6.1 Introduction

Conformal mapping and the concept of complex potential is a powerful mathematical tool that allows the calculation of the flows around realistic aerofoil shapes to be computed through relatively simple manipulation of the flow about a circle, with or without circulation (it should be pointed out at this point that conformal mapping is a much broader mathematical technique used in many subjects; however the bit we shall be concerned with is of particular aerodynamic importance). This lecture will describe the basics of complex potential, and discuss the limitations on the functions that can be used. To begin, however, we shall revise a little of what you learnt in the second year. The two sections may seem to be little related at first, but hopefully all will become clear at the end. We shall consider only two-dimensional flows, for reasons which shall become apparent.

6.2 Revision of Important 2nd Year Concepts

Last year, the Navier-Stokes equations which govern the flow of fluids such as air were discussed. While generally insoluble analytically, simplifications are possible if certain assumptions are allowed. These include some or all of:

- Inviscid Flow: The flow past a body may be considered to behave as an inviscid fluid *iff* (if and only if) the *effects* of viscosity (not necessarily the viscosity itself), are small enough to be negligible. At high Reynolds numbers (the ratio between inertial and viscous forces in a flow) typical of flows of aeronautical interest (e.g. about aircraft), this may be considered to be the case about streamlined (non-bluff) shapes for the majority of the flow, outside of thin attached boundary layers. This allows all viscous terms to be ignored, reducing the NS equations to the Euler Equations.

- Steady Flows: The effect of dynamic interactions between the structure and aerodynamic flows are of interest in the field of aeroelastics and manoeuvre analysis, but for the majority of the flight envelope of a typical aircraft (e.g. cruise) may be ignored. If this is the case, time derivatives are zero.

- Irrotational Flow. The *vorticity* of a flow is found by integrating the velocity around a closed contour (without a body in it) and dividing by the area. Its value is twice the rotational velocity of the fluid within the contour. In *inviscid* flows without a solid surface or shock waves, rotation can neither be created or destroyed, as the only forces acting on infinitesimal elements of the fluid (due to pressure) act through the centre of the fluid element, and hence cannot impart a torque. Generally, therefore, the vorticity in a fluid is always and remains zero. Such flows are considered *irrotational*. Vorticity is defined as:

$$\underline{\omega} = \underline{\nabla} \times \underline{U} = [\omega_x, \omega_y, \omega_z]^T$$

For two-dimensional flow to be irrotational $\omega_z = 0$, and so,

$$\frac{\partial v}{\partial x} = \frac{\partial u}{\partial y}$$

In such flows, and only such flows, the velocity potential ϕ exists, and is defined as

$$\frac{\partial \phi}{\partial x} = u; \qquad \frac{\partial \phi}{\partial y} = v$$

- Incompressible Flow: If the flow is low speed, the density of the flow changes much less than any other property, and hence all derivatives with respect to this variable may be ignored. This allows the introduction of a *stream function*, φ such that

$$\frac{\partial \phi}{\partial x} = \frac{\partial \varphi}{\partial y}$$
$$\frac{\partial \phi}{\partial y} = -\frac{\partial \varphi}{\partial x}$$

Lines of constant φ are the streamlines of the flow, and are at right angles to any lines of constant ϕ they cross at the point they intersect. It is easy to show that if the flow is irrotational and incompressible, Laplace's Equation

$$\frac{\partial^2 \phi}{\partial x^2} + \frac{\partial^2 \phi}{\partial y^2} = 0$$

is satisfied. This is important as solutions of this equation are linear, and hence complex flows may be modelled by adding together a series of solutions for simpler flows. The stream function also satisfies Laplace, i.e.

$$\frac{\partial^2 \varphi}{\partial x^2} + \frac{\partial^2 \varphi}{\partial y^2} = 0$$

6.3 Complex Functions

We define the imaginary number i as $\sqrt{-1}$. Obviously, therefore, $i^2 = -1$, and also $i^{-1} = -i$. A complex coordinate Z is defined as $Z = x+iy$, and is just another way of describing a point in the x, y plane, now called the *complex plane*. Such a point (x, y) may also be described in polar coordinates (r, θ) such that

$$x = r\cos\theta; \qquad y = r\sin\theta$$

i.e.

$$Z = x + iy = r\cos\theta + ir\sin\theta = r(cos\theta + i\sin\theta) = re^{i\theta}$$

where the last result comes from de Moivre's theorem. The expression $Z = re^{i\theta}$ is called the *polar form* of the complex coordinate.

Now consider a 'potential function' of Z, written in the form

$$\Phi = W(x + iy) = W(Z)$$

where $W(Z)$ is only a function of Z, e.g.

$$W(Z) = Z^3$$

or

$$W(Z) = Z - Z^2$$

The function $W(Z)$ will itself be complex, and hence may be described as

$$W(Z) = f(x, y) + ig(x, y)$$

for instance in the case of $W(Z) = Z^3$,

$$\begin{aligned} W(Z) &= (x + iy)(x + iy)(x + iy) \\ &= (x + iy)(x^2 - y^2 + 2ixy) \\ &= x^3 - xy^2 + 2ix^2y + iyx^2 - iy^3 - 2xy^2 \end{aligned}$$

and hence

$$\begin{aligned} f(x, y) &= x^3 - 3xy^2 \\ g(x, y) &= 3x^2y - y^3 \end{aligned}$$

If we consider two dimensional, inviscid, irrotational, incompressible and steady flows, as discussed in the previous section, the flow field is described by Laplace's equation. Hence, it would be useful if the function $W(Z)$ was itself a solution of this equation. If we differentiate it w.r.t x and y:

$$\frac{\partial W(Z)}{\partial x} = \frac{\partial W}{\partial Z}\frac{\partial Z}{\partial x}$$

As we defined $W(Z)$ to a function of Z and Z only

$$\frac{\partial W}{\partial Z} = \frac{dW}{dZ}$$

and

$$\frac{\partial Z}{\partial x} = \frac{\partial (x + iy)}{\partial x} = 1$$

So

$$\frac{\partial W(Z)}{\partial x} = \frac{dW}{dZ}$$

and hence

$$\frac{\partial^2 W(Z)}{\partial x^2} = \frac{\partial}{\partial x}\frac{dW}{dZ} = \frac{\partial Z}{\partial x}\frac{\partial}{\partial Z}\frac{dW}{dZ} = \frac{d^2W}{dZ^2}$$

For y derivatives,

$$\frac{\partial W(Z)}{\partial y} = \frac{\partial W}{\partial Z}\frac{\partial Z}{\partial y} = \frac{dW}{dZ}\frac{\partial (x + iy)}{\partial y} = i\frac{dW}{dZ}$$

And hence

$$\frac{\partial^2 W(Z)}{\partial y^2} = \frac{\partial}{\partial y} i\frac{dW}{dZ} = \frac{\partial Z}{\partial y}\frac{\partial}{\partial Z} i\frac{dW}{dZ} = i^2\frac{d^2W}{dZ^2} = -\frac{d^2W}{dZ^2}$$

Finally

$$\frac{\partial^2 W(Z)}{\partial x^2} + \frac{\partial^2 W(Z)}{\partial y^2} = \frac{d^2W}{dZ^2} - \frac{d^2W}{dZ^2} = 0$$

which is what we wanted.

However, there are some limitations on what functions we may use. Most importantly, we require that the derivative $\frac{dW(Z)}{dZ}$, formally defined as

$$\frac{dW(Z)}{dZ} = \lim_{\Delta Z \to 0} \frac{W(Z+\Delta Z) - W(Z)}{\Delta Z}$$

where $(Z + \Delta Z) = ((x + \Delta x) + i(y + \Delta y))$, tends to the same result regardless of the order in which we take Δx and Δy.

If we consider the limit where $\Delta x \to 0$ whilst $\Delta y = 0$, and remember as discussed above

$$W(Z) = f(x, y) + ig(x, y)$$

where f and g are themselves real, we have

$$\begin{aligned}\frac{dW(Z)}{dZ} &= \lim_{\Delta x \to 0} \frac{f(x+\Delta x, y) + ig(x+\Delta x, y) - f(x,y) - ig(x,y)}{\Delta x} = \lim_{\Delta x \to 0} \frac{\Delta f + i\Delta g}{\Delta x} \\ &= \lim_{\Delta x \to 0} \frac{\Delta f}{\Delta x} + i \lim_{\Delta x \to 0} \frac{\Delta g}{\Delta x} = \quad \frac{\partial f}{\partial x} + i\frac{\partial g}{\partial x}\end{aligned}$$

Next, take $\Delta y \to 0$ whilst $\Delta x = 0$:

$$\begin{aligned}\frac{dW(Z)}{dZ} &= \lim_{\Delta y \to 0} \frac{f(x, y+\Delta y) + ig(x, y+\Delta y) - f(x,y) - ig(x,y)}{\Delta y} = \lim_{\Delta y \to 0} \frac{\Delta f + i\Delta g}{i\Delta y} \\ &= \lim_{\Delta y \to 0} -i\frac{\Delta f}{\Delta y} + \lim_{\Delta y \to 0} \frac{\Delta g}{\Delta y} = \quad -i\frac{\partial f}{\partial y} + \frac{\partial g}{\partial y}\end{aligned}$$

The only way these two expressions can be identical is if both real and imaginary parts are identical, i.e.

$$\begin{aligned}\frac{\partial f}{\partial x} &= \frac{\partial g}{\partial y} \\ \frac{\partial f}{\partial y} &= -\frac{\partial g}{\partial x}\end{aligned}$$

These are the **Cauchy-Riemann conditions**. A function satisfying these conditions as well as being single-valued (only one Z at each point in (x, y) plane) and bounded (i.e. not infinite) in some region of the x, y (or equivalent Z) plane is called a *regular* function. The terms *holomorphic* and *analytic* are also used in some textbooks.

The question then naturally arises as to what these functions may be. Referring back to the section revising last years work, we have the equations for potential and stream function

$$\begin{aligned}\frac{\partial \phi}{\partial x} &= \frac{\partial \varphi}{\partial y} \\ \frac{\partial \phi}{\partial y} &= -\frac{\partial \varphi}{\partial x}\end{aligned}$$

and hence we may write

$$W(Z) = \phi(x, y) + i\varphi(x, y)$$

and hopefully the point of all the previous mathematics becomes clear. It is also worth noting here (we will come back to this) that if we have $W(Z) = \phi(x, y) + i\varphi(x, y)$ then

$$\frac{\partial W(Z)}{\partial Z} = \frac{\partial \phi}{\partial x} + i\frac{\partial \varphi}{\partial x} = \frac{\partial \varphi}{\partial y} - i\frac{\partial \phi}{\partial y} = u - iv$$

6.3.1 Exercise for Next Lecture:

Prove that if the flow is irrotational and incompressible, the potential and stream functions obey Laplace's equation, as stated on page 5.

7 Complex Potential Examples

Key points: *Complex number representation of simple potential flow (source, sink, vortex, doublet), complex representation of lifting/non lifting flow about a circle*

7.1 Introduction

Last lecture introduced the concept of complex potential, and showed that it provides an alternative method for analysing a flow field where the potential function is valid, and Laplace's equation is satisfied (i.e. inviscid, irrotational, incompressible steady flows). This lecture we shall look at some of the elements of potential flows introduced last year, and how they appear in complex potential form. This will provide us with the tools we need for *conformal mapping*, which allows us to move from simple flows to more complex aerofoil type flows with relative ease. We shall proceed in an inverse manner, i.e. the correct function to give the desired flow will be given, and demonstrated to have the required properties.

7.2 Basic Solutions

Uniform Onset Flow:
Consider the complex function

$$W(Z) = Ue^{-i\alpha}Z$$

where $e^{-i\alpha} = \cos\alpha - i\sin\alpha$ by de Moivre's theorem. Expanding this we see that

$$W(Z) = U(\cos\alpha - i\sin\alpha)(x + iy)$$

and hence it obvious that the function is single-valued (U and α are constants, and hence for every value of $Z(x, y)$ there is one, and only one value of $W(Z)$). This can be represented as a sum of ϕ and $i\varphi$, by expanding to real and imaginary parts:

$$\begin{aligned} W(Z) &= U(\cos\alpha - i\sin\alpha)(x + iy) \\ &= U(x\cos\alpha - ix\sin\alpha) + Ui(y\cos\alpha - iy\sin\alpha) \\ &= U(x\cos\alpha + y\sin\alpha) + iU(y\cos\alpha - x\sin\alpha) \end{aligned}$$

so

$$\begin{aligned} \phi &= U(x\cos\alpha + y\sin\alpha) \\ \varphi &= U(y\cos\alpha - x\sin\alpha) \end{aligned}$$

Taking the derivative of the potential function to get derivatives (the stream function could also be used):

$$\begin{aligned} \frac{\partial\phi}{\partial x} &= u = U\cos\alpha \\ \frac{\partial\phi}{\partial y} &= v = U\sin\alpha \end{aligned}$$

and hence this gives a uniform flow velocity of magnitude U and angle to the x axis of α.

We noted last lecture that the velocities may also be expressed as $\frac{dW(Z)}{dZ} = u - iv$, which in this case is

$$\frac{dW(Z)}{dZ} = \frac{dUe^{-i\alpha}Z}{dZ} = Ue^{-i\alpha} = U\cos\alpha - iU\sin\alpha$$

and hence we can verify by inspection that these results are indeed the same.

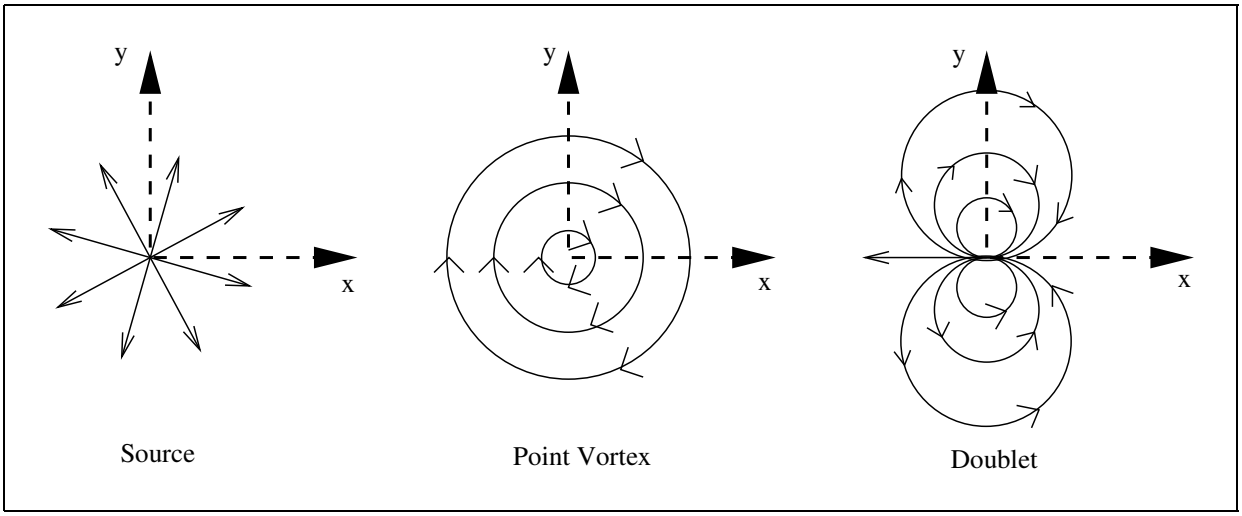

Figure 34: *Simple Incompressible Flow Solutions*

Source:
The complex potential function for a source is

$$W(Z) = \frac{\Lambda}{2\pi}\ln(Z)$$

where Λ is the strength (flow rate). A negative value gives a sink. The flow relating to this function may be verified in the following manner; taking the derivative of $W(Z)$ with respect to Z to get velocities gives

$$\frac{dW(Z)}{dZ} = u - iv = \frac{\Lambda}{2\pi Z} = \frac{\Lambda}{2\pi(x+iy)}$$
$$= \frac{\Lambda(x-iy)}{2\pi(x+iy)(x-iy)} = \frac{\Lambda(x-iy)}{2\pi(x^2+y^2)}$$

but $x^2 + y^2 = r^2$, and so

$$u = \frac{\Lambda x}{2\pi r^2}, \qquad v = \frac{\Lambda y}{2\pi r^2}$$

Alternatively, in polar coordinates,

$$W(Z) = \frac{\Lambda}{2\pi}\ln(Z)$$
$$Z = x + iy = r\cos\theta + ir\sin\theta = r(\cos\theta + i\sin\theta)$$

and by deMoivres $\cos\theta + i\sin\theta = e^{i\theta}$, hence

$$Z = re^{i\theta}$$
$$\ln(Z) = \ln(r) + i\theta$$
$$W(Z) = \frac{\Lambda}{2\pi}\ln(r) + i\frac{\Lambda\theta}{2\pi}$$

This means that

$$\phi = \frac{\Lambda}{2\pi}\ln(r), \qquad \varphi = \frac{\Lambda\theta}{2\pi}$$

which are the potential and stream functions identified as a source in your lectures last year (note that streamlines are lines of constant θ, i.e. radial lines).

Point Vortex:
The function

$$W(Z) = \frac{-\Gamma}{2\pi i}\ln(Z)$$

is similar to a source (given that Λ and $-\Gamma$ are constants, which could theoretically have the same value). However, the presence of i on the denominator means that (using polar coordinates)

$$W(Z) = \phi + i\varphi = \frac{-\Gamma}{2\pi i}\Big(\ln(r) + i\theta\Big)$$

and so

$$\phi = -\frac{\Gamma\theta}{2\pi}, \qquad \varphi = \frac{\Gamma}{2\pi}\ln(r)$$

which are the potential and stream functions of a vortex you met last year. Note that streamlines have constant radius, i.e. are circular about the origin, and hence are at right angles to the streamlines of the source where they cross. This follows logically from the fact that the equations for source and vortex differ only in the latter having i as a multiplier (actually $1/i = -i$, due to sign conventions), given that in the complex plane the vector 1 is at right angles to i.

Doublet:
For a doublet we have the complex potential

$$\begin{aligned} W(Z) = \phi + i\varphi &= \frac{\kappa}{\pi Z} \\ &= \frac{\kappa}{\pi(x+iy)}\frac{x-iy}{x-iy} \\ &= \frac{\kappa(x-iy)}{\pi(x^2+y^2)} \end{aligned}$$

which gives

$$\phi = \frac{\kappa x}{\pi r^2}, \qquad \varphi = -\frac{\kappa y}{\pi r^2}$$

and using the fact that

$$\cos\theta = \frac{x}{r}, \qquad \sin\theta = \frac{y}{r}$$

may also be expressed as

$$\phi = \frac{\kappa\cos\theta}{\pi r}, \qquad \varphi = -\frac{\kappa\sin\theta}{\pi r}$$

which as expected are the potential and stream functions for a doublet you met last year, for a doublet with its axis pointing right to left, as shown in the RHS of figure 34. More generally, if we define α_d as the angle of the doublet, measured anti-clockwise from the direction of the x axis, then the equation of the potential flow is given by:

$$W(Z) = -\frac{\kappa e^{i\alpha_d}}{\pi Z}$$

Note that in the above example, α_d is 180 degrees, or π radians, and because

$$e^{i\alpha} = \cos(\alpha) + i\sin(\alpha)$$

and due to the periodicity of sine and cosine functions

$$\cos(\pi + \alpha) = -\cos(\alpha); \qquad \sin(\pi + \alpha) = -\sin(\alpha)$$

we have

$$e^{i(\pi+\alpha)} = -e^{i\alpha}$$

and hence

$$W(Z) = -\frac{\kappa e^{i\pi}}{\pi Z} = \frac{\kappa e^{i0}}{\pi Z} = \frac{\kappa}{\pi Z}$$

as above.

7.3 Flow About a Circle

We now have the 'tool kit' of solutions for incompressible flow that you were introduced to last year, but with a different method of expressing them. As before, more complex flows can be created by summing the simpler components, as the solutions all obey Laplace's equation, and are therefore linear. For instance, consider a uniform flow, left to right, with a doublet pointing into the flow. Adding together the two potential components we have

$$\begin{aligned} W(Z) &= UZe^{-i\alpha} - \frac{\kappa e^{i(\pi+\alpha)}}{\pi Z} = \phi + i\varphi \\ W(Z) &= UZe^{0i} + \frac{\kappa e^{0i}}{\pi Z} = \phi + i\varphi \\ &= U(x + iy) + \frac{\kappa(x - iy)}{\pi(x^2 + y^2)} \end{aligned}$$

Note that the inclusion of α will not be important here, but will become of important when we deal with a lifting case. Streamlines ($\varphi =$ const.) can be found from

$$\varphi = Uy - \frac{\kappa y}{\pi r^2} = Uy\Big(1 - \frac{\kappa}{U\pi r^2}\Big)$$

Obviously if $y = 0$, φ is constant and equal to 0. Alternatively, the inside of the bracket may be zero, which gives

$$U\pi r^2 = \kappa \quad \Rightarrow \quad r^2 = \frac{\kappa}{\pi U}$$

which is the equation of a circle about the origin, with a radius R of

$$R = \sqrt{\frac{\kappa}{\pi U}}$$

This equation may also be used in reverse to calculate the strength of source required to produce a specified R, i.e.

$$\kappa = \pi U R^2$$

Note that there is also a quick trick in section 21.6 to get the doublet strength using complex potential, and you may want to look at it when you're more familiar with complex potential.

Now, substituting this into our equation for $W(Z)$ we get

$$W(Z) = UZ + \frac{UR^2}{Z}$$

$$\boxed{W(Z) = U\Big(Z + \frac{R^2}{Z}\Big)}$$

This equation is of fundamental importance in aerodynamics, and we will be using it again in the future.

Turning to the velocity field, differentiating $W(Z)$ w.r.t. Z we get

$$\frac{dW(Z)}{dZ} = U\Big(1 - \frac{R^2}{Z^2}\Big) = u - iv$$

At the lowest and highest points of the circle, $Z = -iR$ which produces

$$\frac{dW(Z)}{dZ} = U\Big(1 - \frac{R^2}{(\pm iR)^2}\Big) = U(1+1)$$

and hence the horizontal velocity u is equal to $2U$, and v is zero. At the leading and trailing edges, $Z = \pm R$, and so

$$\frac{dW(Z)}{dZ} = U\Big(1 - \frac{R^2}{(\pm R)^2}\Big) = 0$$

i.e. the stagnation points.

To turn this zero lift flow into a lifting one, we add a vortex, stength Γ, so that

$$W(Z) = U\Big(Z + \frac{R^2}{Z}\Big) + \frac{-\Gamma}{2\pi i}\ln(Z)$$

Calculating the velocities as before

$$\frac{dW(Z)}{dZ} = U\Big(1 - \frac{R^2}{Z^2}\Big) - \frac{\Gamma}{2\pi i Z} = u - iv$$

This is zero when

$$U\Big(1 - \frac{R^2}{Z^2}\Big) - \frac{\Gamma}{2\pi i Z} = 0 = Z^2 - \frac{\Gamma}{2U\pi i}Z - R^2$$

i.e. a quadratic in Z. For any non-zero value of Γ, the solution will be complex, and hence the stagnation points are moved off the x axis, though they remain on the circle as shown below.

7.3.1 Defining the Lift-Curve Slope Using the Vortex Strength

From the Kutta-Joukowski theorem (met last year), we know that lift and circulation (vorticity) are related, by

$$Lift = \rho U \Gamma$$

In order to calculate Γ, we rotate the onset flow through an angle α (see figure 35). We now have

$$W(Z) = U\Big(e^{-i\alpha}Z + \frac{e^{i\alpha}R^2}{Z}\Big) - \frac{\Gamma}{2\pi i}\ln(Z)$$

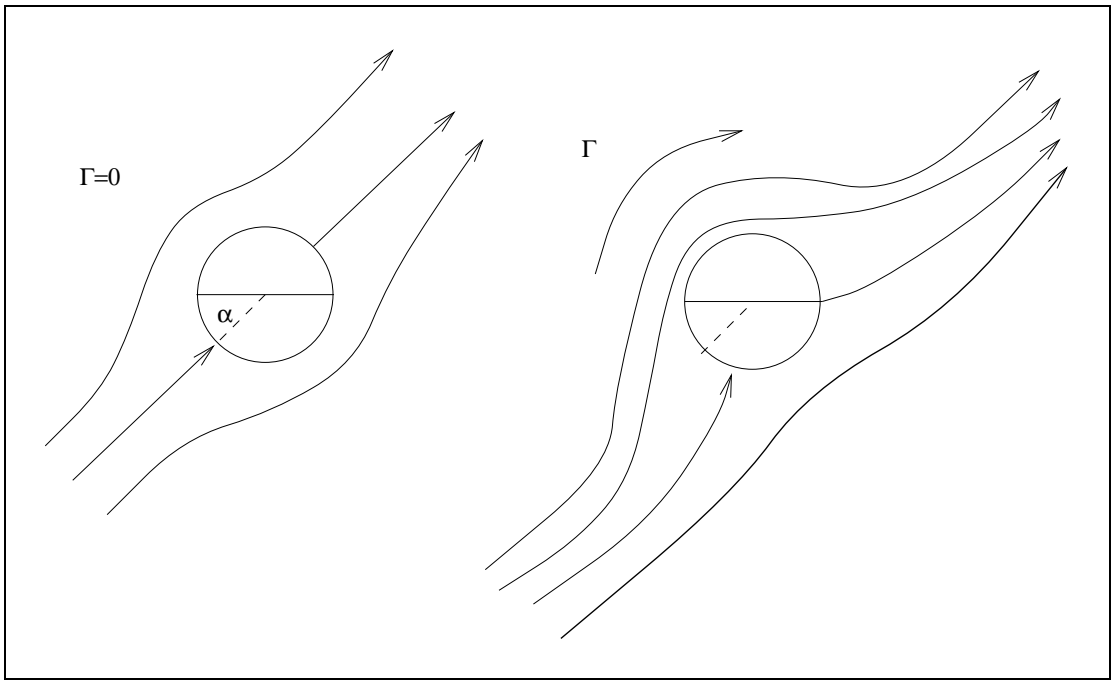

Figure 35: *Effect of α and Γ on Flow about a Circle*

Fixing the trailing edge at $\theta = 0$, i.e. $iy = 0$ gives us a condition to specify. The velocities are now

$$\frac{dW(Z)}{dZ} = U\Big(e^{-i\alpha} - e^{i\alpha}\frac{R^2}{Z^2}\Big) - \frac{\Gamma}{2\pi i Z}$$

or, writing Z in polar coordinates

$$\frac{dW(Z)}{dZ} = U\Big(e^{-i\alpha} - e^{i\alpha}\frac{R^2}{r^2 e^{2i\theta}}\Big) - \frac{\Gamma}{2\pi i r e^{i\theta}}$$

$$\frac{dW(Z)}{dZ} = U\Big(\cos\alpha - i\sin\alpha - \frac{R^2}{r^2}(\cos\alpha + i\sin\alpha)(\cos 2\theta - i\sin 2\theta)\Big) + \frac{\Gamma i}{2\pi r}(\cos\theta - i\sin\theta)$$

$$\frac{dW(Z)}{dZ} = U\cos\alpha - U\frac{R^2}{r^2}\cos 2\theta\cos\alpha - U\frac{R^2}{r^2}\sin 2\theta\sin\alpha + \frac{\Gamma}{2\pi r}\sin\theta$$
$$+i\Big(-U\sin\alpha + U\frac{R^2}{r^2}\sin 2\theta\cos\alpha - U\frac{R^2}{r^2}\cos 2\theta\sin\alpha + \frac{\Gamma}{2\pi r}\cos\theta\Big)$$

As at a stagnation point both u and v are zero, on the circle $r = R$ this gives

$$U\cos\alpha - U\frac{R^2}{R^2}\cos 2\theta\cos\alpha - U\frac{R^2}{R^2}\sin 2\theta\sin\alpha + \frac{\Gamma}{2\pi R}\sin\theta = 0$$
$$-U\sin\alpha + U\frac{R^2}{R^2}\sin 2\theta\cos\alpha - U\frac{R^2}{R^2}\cos 2\theta\sin\alpha + \frac{\Gamma}{2\pi R}\cos\theta = 0$$

However, at the trailing edge we know that $\theta = 0$ (because we specified it so), and hence the term involving Γ in the first equation is zero regardless of Γ. Using the second gives

$$-U\sin\alpha - U\sin\alpha + \frac{\Gamma}{2\pi R}\cos\theta = 0$$

and as $\theta = 0$ we have

$$2U\sin\alpha = \frac{\Gamma}{2\pi R}$$
$$\Gamma = U\sin\alpha 4\pi R$$

or alternatively

$$\alpha = sin^{-1}\Big(\frac{\Gamma}{4U\pi R}\Big)$$

We can now give lift coefficient assuming small α (where $\sin\alpha \to \alpha$) as

$$C_L = \frac{Lift}{\frac{1}{2}\rho U^2 S} = \frac{\rho U(U\alpha 4\pi R)}{\frac{1}{2}\rho U^2 S}$$

But for a circle $S = 2R$ per unit span, and the chord of the resulting flat plate aerofoil under the Joukowsky transformation is 4R (to be shown), so

$$\begin{aligned} C_L &= \frac{4\rho U^2 R\alpha\pi}{\frac{1}{2}4\rho U^2 R} \\ &= 2\pi\alpha \end{aligned}$$

which gives lift curve slope for a 2D flat plate

$$\boxed{\frac{dC_L}{d\alpha} = 2\pi}$$

This is a pretty long winded approach, and the algebra can actually be cut down a lot. A reminder of the complex potential we're using

$$\frac{dW}{dZ} = U\left(e^{-j\alpha} - \frac{R^2 e^{j\alpha}}{Z^2}\right) - \frac{\Gamma}{2\pi j Z}$$

sticking firmly to complex notation gives at the trailing edge (where both real and imaginary velocities need to vanish, as this is to be a stagnation point)

$$0 = Ue^{-j\alpha}R^2 e^{2j\theta} - \frac{\Gamma}{2\pi j}Re^{j\theta} - UR^2 e^{j\alpha}$$

then $\theta = 0$ (trailing edge)so these exponentials are unity.

$$\frac{\Gamma}{2\pi j}R = Ue^{-j\alpha}R^2 - UR^2 e^{j\alpha} = UR^2(\cos(\alpha) - j\sin(\alpha) - \cos(\alpha) - j\sin(\alpha)) = -UR^2 2j\sin(\alpha)$$

$$\Gamma = 4\pi UR\sin(\alpha)$$

$$C_L = \frac{\rho U 4\pi UR\sin(\alpha)}{\frac{1}{2}\rho U^2 4R} \approx 2\pi\alpha$$

Hence 2π gradient.

So far, all we have done is demonstrated an alternative method for generating the potential flow solutions you had last year, and you may be wondering what the point was. The answer is that the complex plane may be transformed through a process called 'conformal mapping', and hence the solution of flow around a circle can be used to provide the velocity (and hence pressure) distributions around much more aerofoil-like shapes. This is what we shall move on to next lecture.

7.3.2 Solution to last lecture's Question

Demonstrate that if the flow is irrotational and incompressible, the potential and stream functions satisfy the Laplace Equation.
Potential function first:

$$\frac{\partial^2\phi}{\partial x^2}+\frac{\partial^2\phi}{\partial y^2}=\frac{\partial}{\partial x}\Big(\frac{\partial\phi}{\partial x}\Big)+\frac{\partial}{\partial y}\Big(\frac{\partial\phi}{\partial y}\Big)=\frac{\partial}{\partial x}\Big(\frac{\partial\varphi}{\partial y}\Big)+\frac{\partial}{\partial y}\Big(-\frac{\partial\varphi}{\partial x}\Big)$$

We can swap the order of differentiation, and thus

$$\frac{\partial}{\partial x}\Big(\frac{\partial\varphi}{\partial y}\Big)+\frac{\partial}{\partial y}\Big(-\frac{\partial\varphi}{\partial x}\Big)=\frac{\partial^2\varphi}{\partial x\partial y}-\frac{\partial^2\varphi}{\partial x\partial y}=0$$

which was what we wanted to prove. For the stream function, the process is very similar

$$\frac{\partial^2\varphi}{\partial x^2}+\frac{\partial^2\varphi}{\partial y^2}=\frac{\partial}{\partial x}\Big(\frac{\partial\varphi}{\partial x}\Big)+\frac{\partial}{\partial y}\Big(\frac{\partial\varphi}{\partial y}\Big)=\frac{\partial}{\partial x}\Big(-\frac{\partial\phi}{\partial y}\Big)+\frac{\partial}{\partial y}\Big(\frac{\partial\phi}{\partial x}\Big)=-\frac{\partial^2\varphi}{\partial x\partial y}+\frac{\partial^2\varphi}{\partial x\partial y}=0$$

7.3.3 Exercise for Next Lecture:

Show that the velocity around a circle, given by

$$\frac{dW(Z)}{dZ}=U\Big(1-\frac{R^2}{Z^2}\Big)=u-iv$$

can be used to prove the result given last year that the magnitude of the tangential velocity around a non-lifting cylinder in a uniform onflow U, assuming incompressible, irrotational, and inviscid flow is $Vel=2U\sin\theta$.

8 Conformal Mapping

Key points: *Definition and purpose of conformal mapping, preservation of intersection angles, Joukowski Transformation, mapping the circle to itself, a line and an ellipse, and symmetric aerofoils*

8.1 Introduction

The purpose of conformal mapping is to perform an operation that allows the relatively simple solution for flow about a circle we calculated last lecture to be used to generate the flow about an aerofoil. We wish to map the Z plane (coordinates (x, iy)) to another plane we shall call the ζ plane (coordinates $(\xi, i\eta)$)

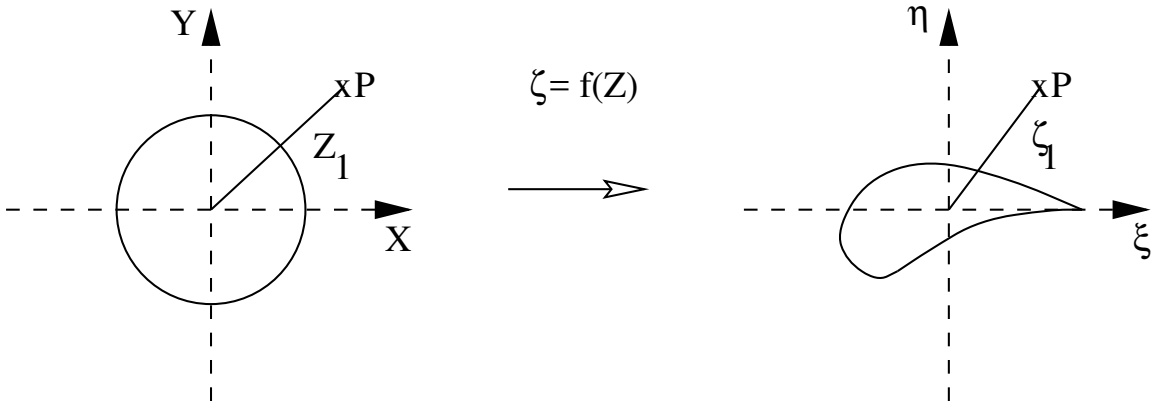

In the Z plane we have the flow about a circle described as

$$W(Z) = U\Big(Z + \frac{R^2}{Z}\Big)$$

The transformation maps the exterior of one shape in the Z plane to the exterior of a different shape in the ζ plane. Hence this transformation may be expressed as

$$\zeta = f(Z) \tag{76}$$

or

$$\zeta(\xi + i\eta) = f(Z(x + iy))$$

We can use simple shapes in the initial complex plane (e.g. a circle plus vortex), and map these to an aerofoil shape. The mapping must be unique (i.e. a one-to-one correspondence between points in the two planes), as unique transformations in both directions must be possible.

8.1.1 Basic Principles

Consider the line Δs in the Z plane between Z_1 and Z_2 in the Z plane, and its corresponding transformed line $\Delta\sigma$ between ζ_1 and ζ_2 in the ζ (figure 18.1.1). Approximating the line joining them as a straight line, and remembering that $e^{i\theta} = \cos\theta + i\sin\theta$, and $\Delta x = \Delta s\cos\theta$, etc., we have

$$\Delta Z = \Delta s e^{i\theta}, \qquad \Delta\zeta = \Delta\sigma e^{i\omega}$$

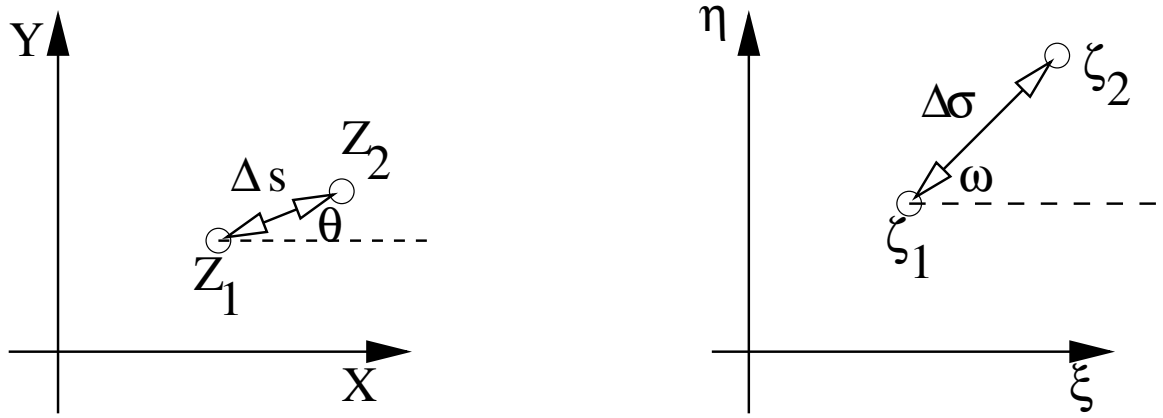

Figure 36: *Transformation Between Planes*

From equation (76):

$$\frac{d\zeta}{dZ} = \frac{df(Z)}{dZ}$$

i.e.

$$d\zeta = \frac{df(Z)}{dZ} dZ$$

and as

$$\frac{df(Z)}{dZ} = \lim_{\Delta Z \to 0} \frac{\Delta\zeta}{\Delta Z} = \frac{\Delta\sigma}{\Delta s} e^{i(\omega-\theta)}$$

and hence in the limit of very small gaps between (Z_1, Z_2) (where any curve joining the points tends to a straight line), we see that the transformation $f'(Z)$ represents a scaling ($\frac{d\sigma}{ds}$), and a rotation $\omega - \theta$. This has the important consequence that lines intersecting at an angle β at any point P in the Z plane also intersect each other at the same angle β in the ζ plane, as both lines are rotated by the same amount.

8.2 The Joukowsky Transformation

Consider a circle in the Z plane centred at the origin. We can map this to the ζ plane using

$$\boxed{\zeta = Z + \frac{b^2}{Z}}$$

where b is some constant. This is the **Joukowsky transformation**, sometimes spelt Zhukovsky, and also called the Kutta-Joukowsky transformation.

As

$$Z = re^{i\theta} = r\cos\theta + ir\sin\theta$$

and on the surface of the circle $r = R$ we can calculate the (x, y) coordinates of the surface in the Z plane as

$$x = R\cos\theta, \qquad y = R\sin\theta$$

Transforming to the ζ plane:

$$\begin{aligned}\zeta = \xi + i\eta = Z + \frac{b^2}{Z} &= Re^{i\theta} + \frac{b^2}{Re^{i\theta}} = Re^{i\theta} + \frac{b^2}{R}e^{-i\theta} \\ &= R\cos\theta + Ri\sin\theta + \frac{b^2}{R}\big(\cos\theta - i\sin\theta\big) \\ \Rightarrow \xi = \big(R + \frac{b^2}{R}\big)\cos\theta, &\qquad \eta = \Big(R - \frac{b^2}{R}\Big)\sin\theta\end{aligned}$$

If $b = 0$ then the mapping is unity, i.e. points in the Z plane transform to identical points in the ζ plane (as should be obvious from the definition of the transformation), and

$$\xi = R\cos\theta, \qquad \eta = R\sin\theta$$

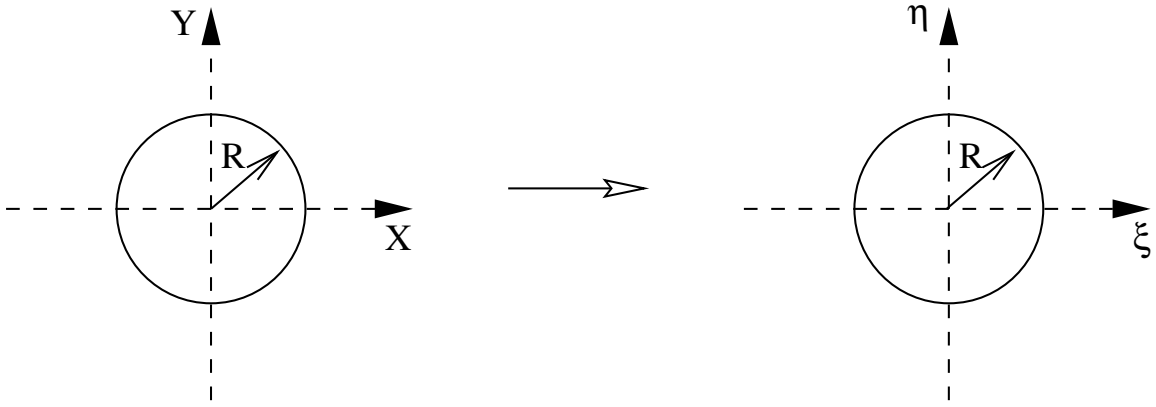

If $b = R$, then the mapping collapses the imaginary dimension (as $R - \frac{b^2}{R} = 0$), and stretches x by a factor of two. Hence in the ζ plane we have a line:

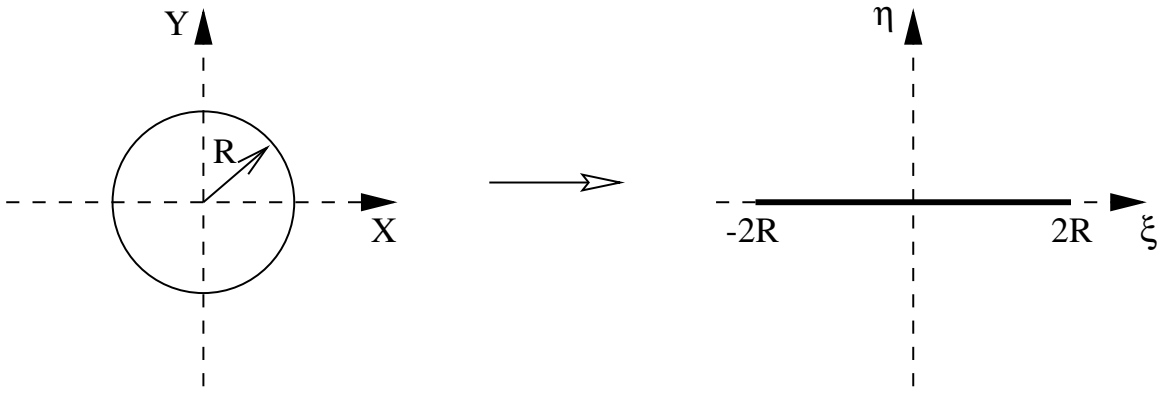

and if $0 \leq b \leq R$ we have an ellipse which crosses the ξ axis as $\pm(R+\frac{b^2}{R})$, and the η axis at $\pm(R-\frac{b^2}{R})$, and

$$\begin{aligned}\xi &= \Big(R + \frac{b^2}{R}\Big)\cos\theta \\ \eta &= \Big(R - \frac{b^2}{R}\Big)\sin\theta\end{aligned}$$

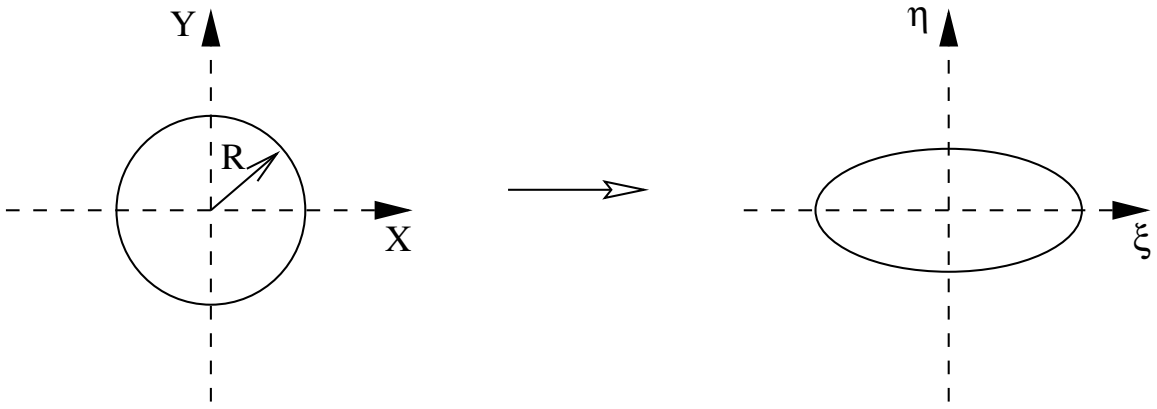

Next, we can move the centre of the circle a distance $-d$ along the x axis. We now have

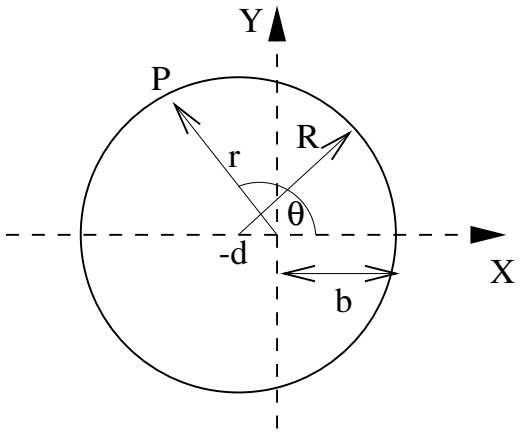

The radius of the circle is still R, but now we define b as the distance between the origin of the circle and where the circle crosses the x axis at positive x, which gives us

$$b = R - d, \qquad \text{or} \qquad R = b + d$$

The equation of the circle is no longer given by $Z = Re^{i\theta}$, but $Z = re^{i\theta}$, where r is a variable dependent on θ:

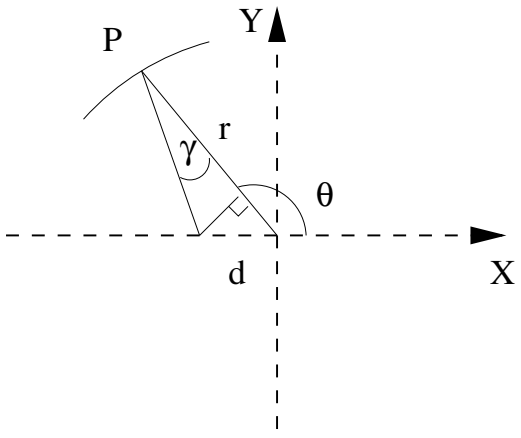

i.e.

$$r = -d\cos\theta + R\cos\gamma$$

Now d is small, γ is also small, and hence $\cos\gamma \to 1$, allowing us to write

$$r = -d\cos\theta + R = -d\cos\theta + b + d$$

dividing through by b, replacing d/b with a single variable e gives us

$$\frac{r}{b} = 1 + e - e\cos\theta$$

i.e.

$$\frac{b}{r} = (1 + e - e\cos\theta)^{-1} = (1 + e(1 - \cos\theta))^{-1}$$

The binomial expansion of this expression is

$$(1 + e(1 - \cos\theta))^{-1} \approx 1 - e(1 - \cos\theta) + \frac{e^2}{2}(1 - \cos\theta)^2 + ...$$

Neglecting higher order terms as negligible (as $e \ll 1$) we arrive at

$$\frac{b}{r} = 1 - e + e\cos\theta$$

We now have expressions for r/b and b/r which we can substitute into the Joukowski transformation:

$$\begin{aligned}
\zeta = \xi + i\eta = Z + \frac{b^2}{Z} &= re^{i\theta} + \frac{b^2}{re^{i\theta}} \\
&= r(\cos\theta + i\sin\theta) + \frac{b^2}{r}(\cos\theta - i\sin\theta) \\
&= b\Big(\frac{r}{b} + \frac{b}{r}\Big)\cos\theta + ib\Big(\frac{r}{b} - \frac{b}{r}\Big)\sin\theta \\
\Rightarrow \zeta = \xi + i\eta &= 2b\cos\theta + i2be(1 - \cos\theta)\sin\theta
\end{aligned}$$

Hence the coordinates in the ζ plane are

$$\xi = 2b\cos\theta, \qquad \eta = 2be(1 - \cos\theta)\sin\theta$$

This shape extends from $-2b$ to $+2b$ on the ξ axis, and is symmetrical about the ξ axis, as the η coordinate is dependent on $(1 - \cos\theta)$, which is always positive, and $\sin\theta$, which has rotational symmetry about $\theta = \pi$ (i.e. η for any θ between π and 2π is equal and opposite to the value of η for $2\pi - \theta$). Differentiating η with respect to θ gives

$$\begin{aligned}
\frac{d\eta}{d\theta} &= 2be\big((1 - \cos\theta)\cos\theta + \sin\theta\sin\theta\big) \\
&= 2be\big(\cos\theta - \cos^2\theta + \sin^2\theta\big) \\
&= 2be(\cos\theta - \cos^2\theta + (-\cos^2\theta + 1)\big) \\
&= -2\cos^2\theta + \cos\theta + 1 \\
&= (2\cos\theta + 1)(-\cos\theta + 1)
\end{aligned}$$

This means that the surface gradient is zero when $\theta = 0$ and $\theta = \frac{2\pi}{3}$. The former means that the trailing edge is sharp (which affects the practicalities of Joukowski aerofoils, and will be dealt with

later). The second angle determines the position of maximum thickness, and substitution into the equation for ξ gives

$$\xi = 2b\cos\left(\frac{2\pi}{3}\right) = -b$$

and

$$\eta = 2be\Big(1 - \cos\big(\frac{2\pi}{3}\big)\Big)\sin\big(\frac{2\pi}{3}\big) = 2be\big(1 + \frac{1}{2}\big)\sqrt{\frac{3}{4}} = be\frac{3}{2}\sqrt{3}$$

Hence the thickness to chord ratio is

$$\frac{t}{c} = \frac{2be\frac{3}{2}\sqrt{3}}{4b} \approx 1.3e$$

Using all this information, it should be apparent that what we we end up with is a symmetrical aerofoil shape.

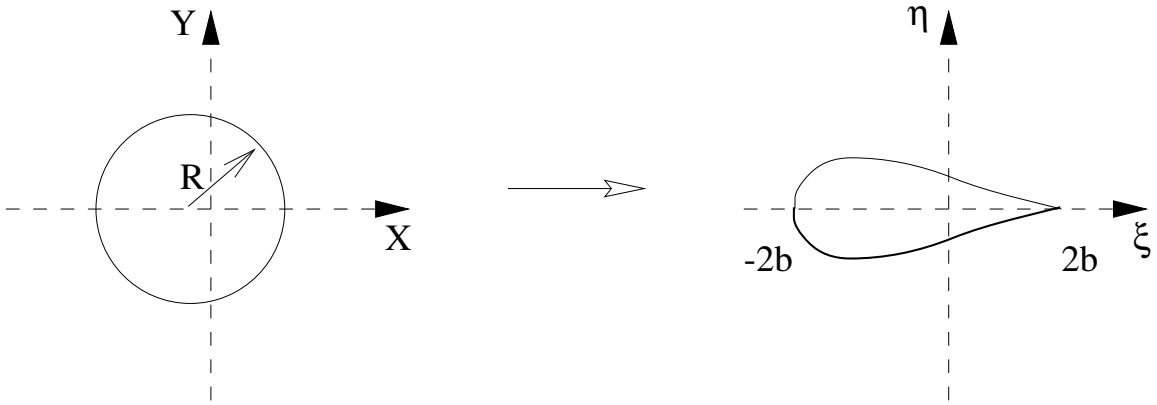

We have now managed to create a shape that looks like the more familiar (and useful) aerofoil. Next lecture, we shall move on to demonstrate how camber can be produced, and make use of velocity transformations to allow pressure distributions to be calculated.

8.2.1 Solution to last lecture's Question

The flow around a circle on the circumference radius R in uniform onset flow U is found from

$$\frac{dW(Z)}{dZ} = U\left(1 - \frac{R^2}{Z^2}\right) = u - iv$$

Which leads to

$$\begin{aligned} u - iv &= U\Big(1 - \frac{R^2}{(Re^{i\theta})^2}\Big) \\ &= U\big(1 - e^{-2i\theta}\big) \\ &= U\big(1 - (\cos 2\theta - i\sin 2\theta)\big) \\ &= U\big(1 - \cos^2\theta + \sin^2\theta - 2i\sin\theta\cos\theta\big) \end{aligned}$$

from $\sin^2\theta + \cos^2\theta = 1$, we get

$$u = 2U\sin^2\theta, \qquad v = 2U\sin\theta\cos\theta$$

the magnitude of the flow velocity, V, is thus

$$\begin{aligned} V &= \sqrt{u^2 + v^2} \\ &= \sqrt{4U^2 \sin^4\theta + 4U^2 \sin^2\theta \cos^2\theta} \\ &= \sqrt{(2U \sin\theta)^2(\sin^2\theta + \cos^2\theta)} \\ &= 2U \sin\theta\sqrt{1} \\ &= 2U \sin\theta \end{aligned}$$

which was the result we required.

8.2.2 Exercise for Next Lecture:

Calculate the surface coordinates for ten degree intervals of the symmetric Joukowski aerofoil produced when $d = 0.02$, and $R = 0.27$ (it is suggested that this is done in excel or a similar spreadsheet to avoid reptitive calculations).

9 Cambered Aerofoils and Velocity Transformations

Key points: *Creation of camber by moving the circle, velocity transformation, circulation effect on stagnation point*

9.1 Adding Camber

Last lecture we created a symmetrical aerofoil shape by displacing a circle in the Z plane an amount $-d$ in the x direction, and then applying the Joukowsky transformation. This lecture, we shall begin by considering the same circle, displaced by a vector $(-d, ih)$:

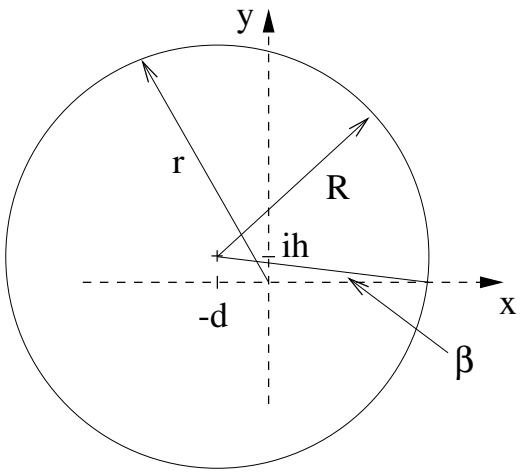

where

$$h = R\sin\beta = (b+d)\sin\beta$$

Since d and β are small, we can say $b + d \to b$ and $\sin\beta \to \beta$ and so

$$h \approx b\beta$$

As before the complex coordinate of the circle edge is described by $Z = re^{i\theta}$, where r is dependent on θ (see below)

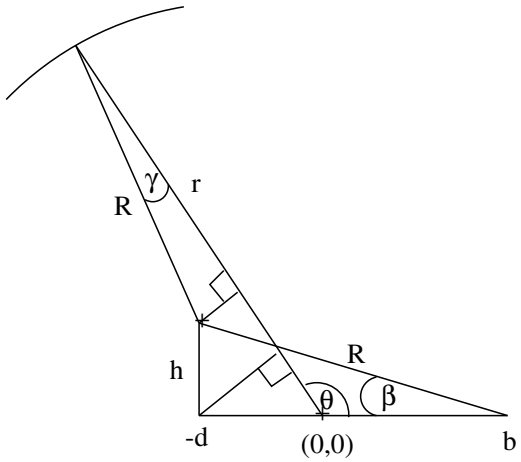

and hence we can express r as

$$r = R\cos\gamma + h\sin\theta - d\cos\theta$$

As before, $\cos\gamma \to 1$, and b is defined by the intersection of the circle with the x axis, i.e.

$$R = b + d$$

and so

$$r = b + d + b\beta\sin\theta - d\cos\theta$$

Again, we substitute in e $(= \frac{d}{b})$

$$\frac{r}{b} = 1 + e - e\cos\theta + \beta\sin\theta$$

binomial expansion results in

$$\frac{b}{r} = 1 - e + e\cos\theta - \beta\sin\theta$$

Substituting these into the transformation again

$$\begin{aligned}
\zeta = \xi + i\eta = Z + \frac{b^2}{Z} &= re^{i\theta} + \frac{b^2}{re^{i\theta}} \\
&= r(\cos\theta + i\sin\theta) + \frac{b^2}{r}(\cos\theta - i\sin\theta) \\
&= b\left(\frac{r}{b} + \frac{b}{r}\right)\cos\theta + ib\left(\frac{r}{b} - \frac{b}{r}\right)\sin\theta \\
\Rightarrow \zeta = \xi + i\eta &= 2b\cos\theta + i2b(e - e\cos\theta + \beta\sin\theta)\sin\theta \\
\Rightarrow \xi = 2b\cos\theta, &\qquad \eta = 2be(1 - \cos\theta)\sin\theta + 2b\beta\sin^2\theta
\end{aligned}$$

i.e. identical exprerssion for ξ and η as for the earlier symmetrical expression, except that there is an extra term $2b\beta sin^2\theta$ added to the latter. As this is always positive, it has the effect of adding a camber to the aerofoil. Hence the circle radius R is transformed into a cambered aerofoil, again chord $4b$. It again may be shown that the maximum thickness still occurs at $\theta = 2\pi/3$ and the maximum t/c is still $\approx 1.3e$.

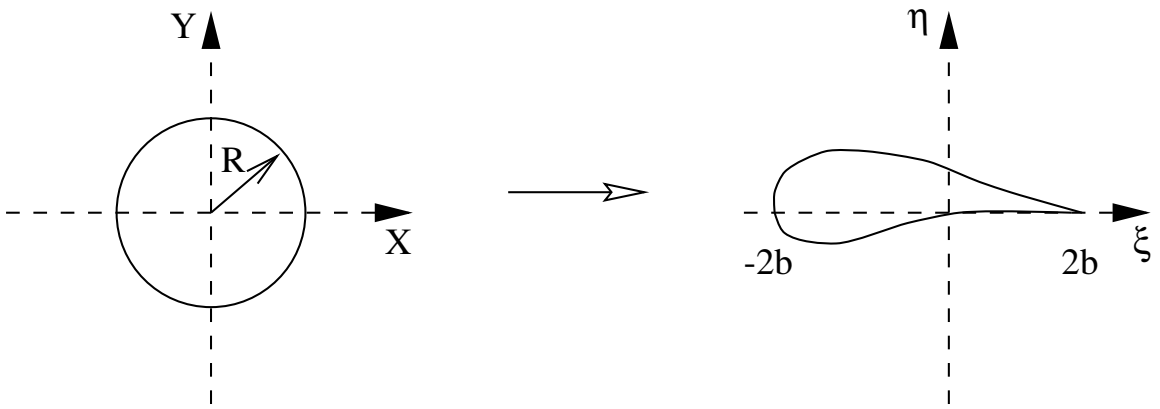

9.2 Velocity Calculations

Having mapped the shape of a circle to an aerofoil, the next step is to determine the velocity (and hence pressure) distribution around the surface in the ζ plane. Initially consider uniform flow around a circle in the Z plane:

$$W(Z) = U\left(Z + \frac{R^2}{Z}\right), \qquad q_Z = \frac{dW(Z)}{dZ} = u - iv$$

In the ζ plane we have

$$W(\zeta) = U\left(\zeta + \frac{R^2}{\zeta}\right), \qquad q_\zeta = \frac{dW(\zeta)}{d\zeta} = \bar{u} - i\bar{v}$$

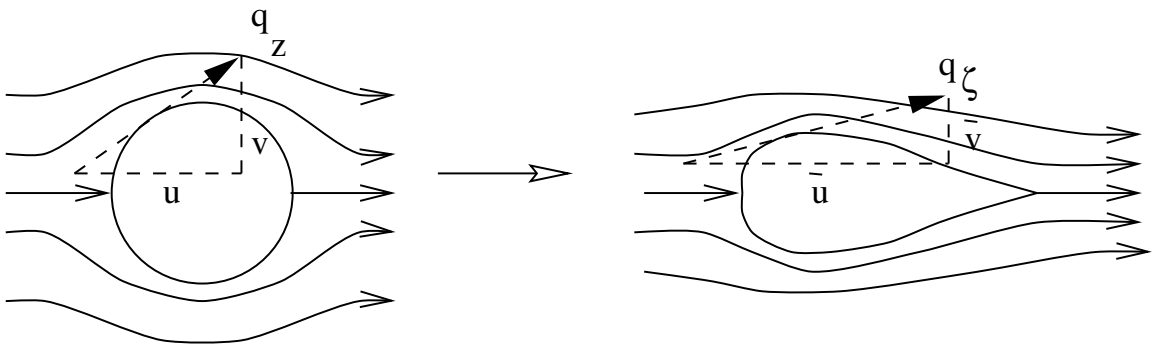

There is a scaling between these two planes, as discussed at the beginning of the last lecture. We need to know what this scaling is to determine the velocities in the ζ plane, i.e. we need

$$\left|\frac{\text{Velocity in } \zeta \text{ plane}}{\text{Velocity in } Z \text{ plane}}\right|$$

Hence, we use

$$\frac{\left|\frac{dW}{d\zeta}\right|}{\left|\frac{dW}{dZ}\right|} = \left|\frac{dZ}{d\zeta}\right|$$

$$\zeta = Z + \frac{b^2}{Z} \Rightarrow \frac{d\zeta}{dZ} = 1 - \frac{b^2}{Z^2} = 1 - \frac{b^2}{r^2}e^{-i2\theta} = 1 - \frac{b^2}{r^2}\big(\cos 2\theta - i\sin 2\theta\big)$$

Using Pythagoras' Hypothesis on the real and imaginary components gives

$$\left|\frac{d\zeta}{dZ}\right| = \left((1 - \frac{b^2}{r^2}\cos 2\theta)^2 + \frac{b^4}{r^4}\sin^2 2\theta\right)^{\frac{1}{2}} = \left(1 - \frac{2b^2}{r^2}\cos 2\theta + \frac{b^4}{r^4}\cos^2 2\theta + \frac{b^4}{r^4}\sin^2 2\theta\right)^{\frac{1}{2}}$$

$$\Rightarrow \left|\frac{dZ}{d\zeta}\right| = \left(1 - \frac{2b^2}{r^2}\cos 2\theta + \frac{b^4}{r^4}\right)^{-\frac{1}{2}}$$

This means that the scaling factor is not constant, but dependent on the position of the point in the Z plane, i.e.

$$\left|\frac{dZ}{d\zeta}\right| = f(r,\theta) = f(x,y)$$

Returning now to the transformations we calculated earlier, for a symmetric aerofoil we begin with a circle radius R in a uniform onflow U, centred at $(-d, 0)$,

$$W(Z) = U\Big(Z + \frac{R^2}{Z}\Big)$$

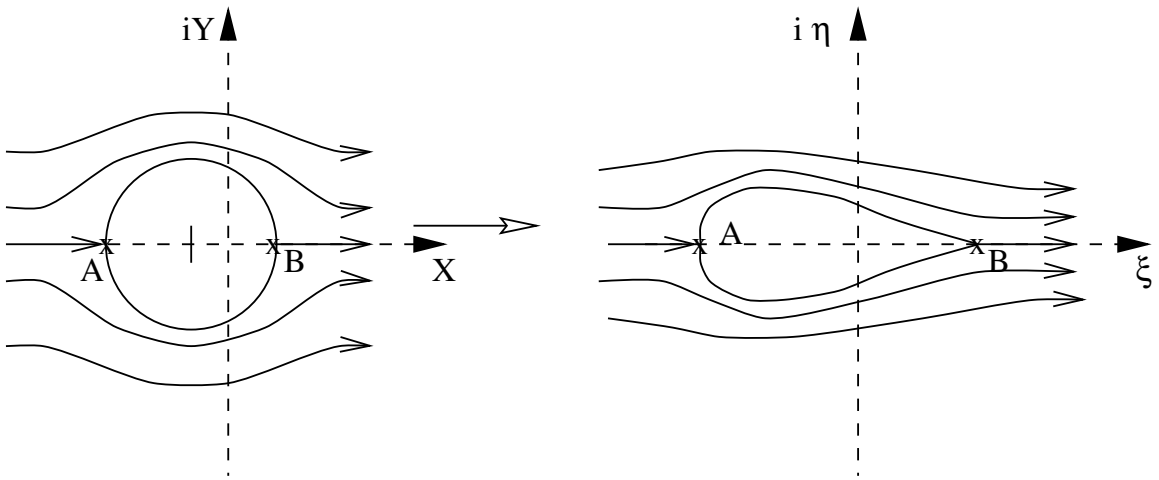

We then turn the flow through an angle α, and shift the circle origin. The onflow and doublet must be rotated (remember that the angle of the doublet is really $\pi + \alpha$, as explained in the handout on complex potential examples), hence

$$W(Z) = U\Big(e^{-i\alpha}Z + \frac{R^2 e^{i\alpha}}{Z}\Big)$$

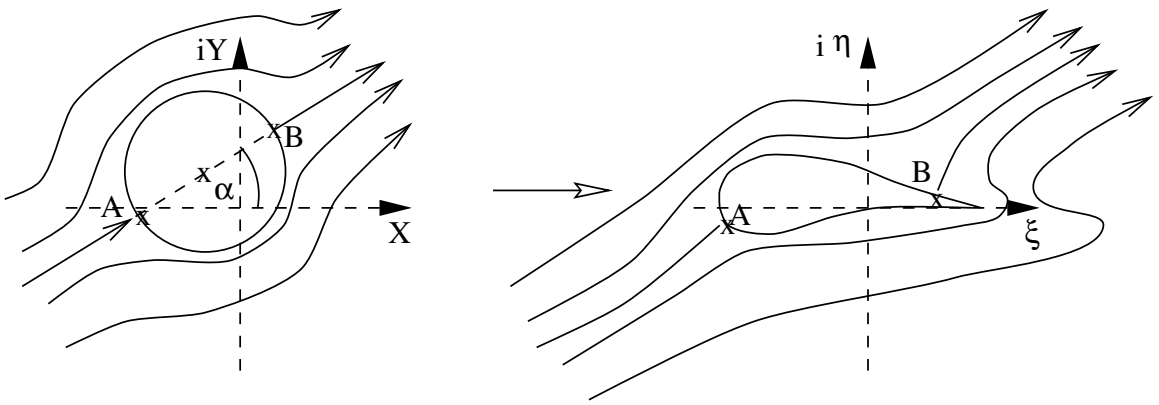

This is the situation with no circulation and hence no lift. If we add in a vortex to move the rear stagnation point to the trailing edge of the aerofoil (i.e. $y = 0$) in the Z plane, we get

$$W(Z) = U\Big(e^{-i\alpha}Z + \frac{R^2 e^{i\alpha}}{Z}\Big) - \frac{\Gamma}{2\pi i}\ln(Z)$$

It is important to realise that the velocity at any point on the circumference of the circle is unchanged by the translation of the centre of the circle from $(0, 0)$ to $(-d, h)$. This is because the flow about

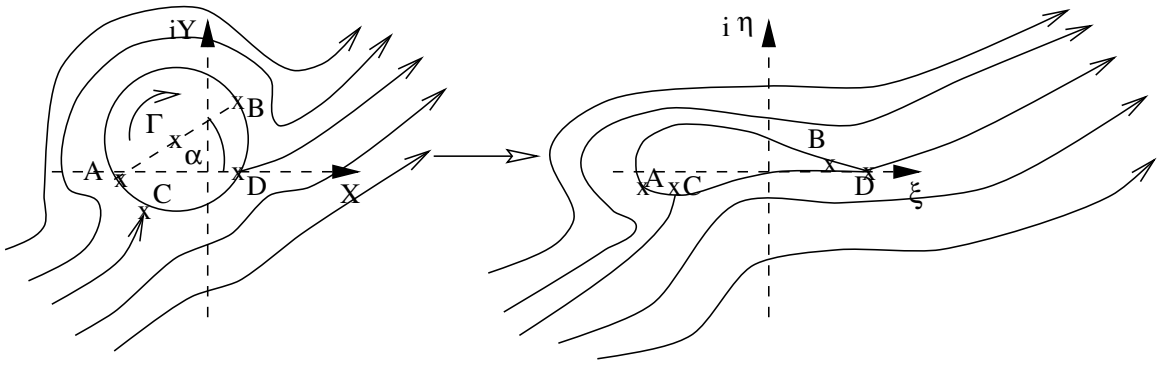

a circle is the same, regardless of where we choose to put our (arbitrary) origin. In other words, we can solve for the circumferential velocity about a circle at the origin (with or without incidence, and with or without circulation), and then slide this solution to any other place in the (x, y) plane without altering the flowfield, *relative to the centre of the circle*. This being the case, we can solve for the velocity about the circle by using standard solution methods (below), as long as all angles are measured from the intersection of the centre of the circle and the horizontal plane. In order to differentiate this angle from θ, measured from the intersection of the origin and the horizontal plane, we shall label it Θ.

9.2.1 Circumferential velocity from complex potential

What is the fastest way to extract the circumferential velocity on the circle using complex potential? Let's address this by returning to the velocity

$$\frac{dW}{dZ} = U\left(e^{-j\alpha} - \frac{R^2 e^{j\alpha}}{Z^2}\right) - \frac{\Gamma}{2\pi j Z} \tag{77}$$

$$\frac{dW}{dZ} = U\left(e^{-j\alpha} - \frac{R^2 e^{j\alpha}}{r^2} e^{-2j\theta}\right) - \frac{\Gamma}{2\pi j r} e^{-j\theta} \tag{78}$$

There is a very useful result that $\overline{A}B = \mathbf{a}\cdot\mathbf{b} + |\mathbf{a}\times\mathbf{b}|\, j$ which allows dot products to be written as a complex multiplication, where $\mathbf{a} = (A_{real}, A_{imag}, 0)^T$ and $\mathbf{b} = (B_{real}, B_{imag}, 0)^T$. This can be seen from

$$\overline{A}B = (A_{real} - A_{imag}j)(B_{real} + B_{imag}j) = \tag{79}$$

$$A_{real}B_{real} + A_{imag}B_{imag} + (A_{real}B_{imag} - A_{imag}B_{real})j \tag{80}$$

$$\mathbf{a}\cdot\mathbf{b} + |\mathbf{a}\times\mathbf{b}|\, j = \begin{bmatrix} A_{real} \\ A_{imag} \\ 0 \end{bmatrix} \cdot \begin{bmatrix} B_{real} \\ B_{imag} \\ 0 \end{bmatrix} + \left| \begin{bmatrix} A_{real} \\ A_{imag} \\ 0 \end{bmatrix} \times \begin{bmatrix} B_{real} \\ B_{imag} \\ 0 \end{bmatrix} \right| j \tag{81}$$

$$= A_{real}B_{real} + A_{imag}B_{imag} + (A_{real}B_{imag} - A_{imag}B_{real})j \tag{82}$$

The derivative of the complex potential is $u - jv$, which is the conjugate of $u + jv$. So, since we already have the conjugate, we just need to multiply by $je^{j\theta}$ (which is a vector that is anti-clockwise tangential to the surface of the circle)

$$\frac{dW}{dZ} j e^{j\theta} = U\left(j e^{j\theta - j\alpha} - j\frac{R^2}{r^2} e^{j\alpha - j\theta}\right) - \frac{\Gamma}{2\pi r} \tag{83}$$

taking the real part to give (note that the complex part, which would be the radial velocity, is $j\cos(\theta-\alpha) - j\cos(\alpha-\theta) = 0$ when $r = R$, as would be hoped)

$$v_{tangential} = U\left(-\sin(\theta-\alpha) - \frac{R^2}{r^2}\sin(\theta-\alpha)\right) - \frac{\Gamma}{2\pi r} \tag{84}$$

note a minus depending on which way we consider to be positive (clockwise or anticlockwise). The above is anticlockwise positive; you can get clockwise positive by looking for the component along $-je^{j\theta}$.

$\theta - \alpha$ is the angle relative to the freestream direction. Labelling this Θ_f, and renaming $v_{tangential}$ as q_{circle} to avoid confusion allows us to express the equation for the velocity on the surface of the circle as

$$q_{circle} = -2U\sin\Theta_f - \frac{\Gamma}{2\pi R}$$

where we have take advantage of the fact that on the circle, $r = R$. Also, remember Θ_f is measured from the right hand side of the doublet axis, not the real axis.

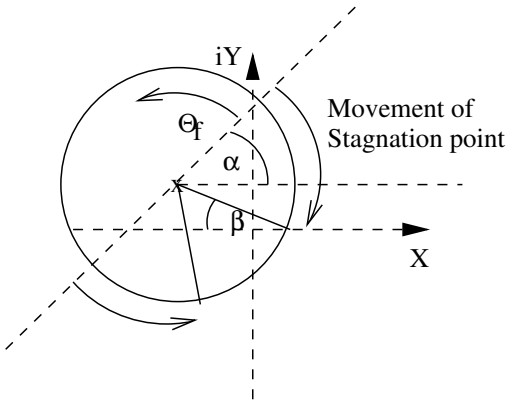

We have also shown

$$\Gamma = 4\pi RU\sin\Theta_s$$

where again parallel onflow was assumed and equal and opposite movement of the stagnation points (through an angle Θ_s) occurred. Transferring this to the coordinate system and onflow angles chosen here (see figure above), we get

$$\Gamma = 4\pi UR\sin(\alpha+\beta)$$

which gives the velocity at any point on the circle (assuming the circulation required to give perfect trailing edge stagnation) as

$$\begin{aligned} q_{circle} &= -2U\sin\Theta_f - 2U\sin(\alpha+\beta) \\ &= -2U\big(\sin\Theta_f + \sin(\alpha+\beta)\big) \end{aligned}$$

The aerofoil profile depends on d and h, and if d is below a certain level, the trailing edge is not sharp but slightly rounded. In this case (and in most real viscous cases) the stagnation point will not be exactly at the trailing edge, and the flow is not perfectly tangential to both surfaces. Hence, the above equation is written more generally as

$$q_{circle} = -2U\big(\sin\Theta_f + k\sin(\alpha+\beta)\big)$$

where k is less than one, i.e. the full Joukowsky circulation is not produced. Only the circumferential velocity need be considered, as we already know the radial velocity will be zero as the circle is a solid surface - this must also be the case in the ζ plane, as both surfaces are a streamline.

We now have the velocity in the Z plane. What we want, however, is to know what it is in the ζ plane. Only the absolute value is required, as we are really only interested in pressures, i.e.

$$C_P = 1 - \left(\frac{q}{U}\right)^2$$

Reminder:

$$C_P = \frac{P - P_\infty}{\frac{1}{2}\rho_\infty U_\infty^2}$$

but for incompressible

$$P_\infty + \frac{1}{2}\rho_\infty U_\infty^2 = P + \frac{1}{2}\rho_\infty q^2$$

$$\Rightarrow \frac{P_\infty}{\frac{1}{2}\rho_\infty U_\infty^2} + 1 = \frac{P}{\frac{1}{2}\rho_\infty U_\infty^2} + \frac{\frac{1}{2}\rho_\infty q^2}{\frac{1}{2}\rho_\infty U_\infty^2}$$

or (U_∞ is U here)

$$C_P = 1 - \frac{q^2}{U^2}$$

We demonstrated last lecture that angles are preserved through conformal mapping, hence because the circumferential velocity q_{circle} is parallel to the local surface, the transformed component of this velocity, $q_{aerofoil}$ will also be parallel to the local surface in the ζ plane. As there can be no flow through a solid surface, this is all the velocity there is, allowing us to use it in the above equation to calculate pressure coefficient.

To find $q_{aerofoil}$ we return to the definition of the Joukowsky transformation:

$$\zeta = Z + \frac{b^2}{Z}$$

$$\xi + i\eta = x + iy + \frac{b^2}{x + iy} = x + iy + \frac{b^2(x - iy)}{x^2 + y^2}$$

$$\Rightarrow \xi = x\left(1 + \frac{b^2}{x^2 + y^2}\right), \qquad \eta = y\left(1 - \frac{b^2}{x^2 + y^2}\right)$$

So, x, y at any point around the circle is required

Hence

$$x = R\cos\Theta - d, \qquad y = R\sin\Theta + R\sin\beta$$

as before we assume $R = b + d$ (as β is small), and so

$$x = (b + d)\cos\Theta - d, \qquad y = (b + d)\sin\Theta + (b + d)\sin\beta$$

which means for any value of Θ from 0 to 2π we have the coordinates of the circle edge. These are then put into the above equations to give the coordinates in the transformed plane (ξ, η).

The velocity at any point in the Z plane is also known. For the uniform freestream at an angle α to the x-axis flowing about a circle with circulation, we have

$$q_{circle} = -2U\big(\sin\Theta_f + k\sin(\alpha + \beta)\big)$$

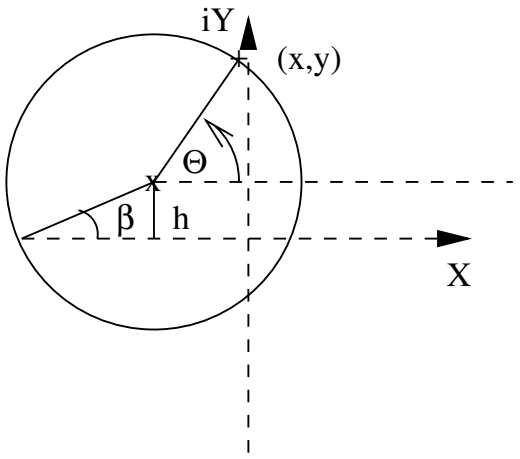

where Θ_f is measured from the freestream direction. The velocity at the solid surface in the transformed plane is then

$$q_{aerofoil} = q_{circle}\left|\frac{dZ}{d\zeta}\right|$$

The scaling factor is best evaluated in Cartesian coordinates (these are already calculated above)

$$\begin{aligned}\frac{d\zeta}{dZ} &= 1 - \frac{b^2}{Z^2} = 1 - \frac{b^2}{x^2 - y^2 + 2ixy} \\ &= 1 - \frac{b^2(x^2 - y^2 - 2ixy)}{(x^2 - y^2 + 2ixy)(x^2 - y^2 - 2ixy)} \\ &= 1 - \frac{b^2(x^2 - y^2)}{(x^2 + y^2)^2} + i\frac{2b^2xy}{(x^2 + y^2)^2} = S_r + iS_i\end{aligned}$$

where $S_r(x, y)$ is the real component of the scaling, and $S_i(x, y)$ is the imaginary component. Thus

$$\left|\frac{d\zeta}{dZ}\right| = \sqrt{S_R^2 + S_i^2}$$

The aerofoil surface velocity is then

$$\begin{aligned}q_{aerofoil} &= q_{circle}\left|\frac{dZ}{d\zeta}\right| = \frac{q_{circle}}{U\sqrt{S_R^2 + S_i^2}} \\ \frac{q_{aerofoil}}{U} &= \frac{-2(\sin\Theta_f + k\sin(\alpha + \beta))}{\sqrt{S_R^2 + S_i^2}} \\ \frac{q_{aerofoil}}{U} &= \frac{-2(\sin(\Theta - \alpha) + k\sin(\alpha + \beta))}{\sqrt{S_R^2 + S_i^2}}\end{aligned}$$

This can then be used to give the surface pressure coefficient directly,

$$C_P = 1 - \left(\frac{q_{aerofoil}}{U}\right)^2$$

which in turn can be integrated to give lift, drag (zero by d'Alembert), and pitching moment coefficients.

The required quantities are therefore

b	Input as quarter of desired final chord
d	Horizontal Offset
h	Vertical Offset
α	Incidence
k	Fraction of Joukowsky circulation

9.2.2 Limitations, Uses, and Alternatives to the Joukowsky Transformation

The Joukowsky transformation has been used for aerofoil design since the early years of last century. Unlike the lifting line and potential methods introduced to you last year, it is in principle exact (given that the assumptions of inviscid, irrotational and incompressible flow hold true), even at stagnation points and the leading/trailing edges. However, it is an *indirect* method, in that the aerofoil shape is produced by the analysis process, rather than being specified *a priori*. It also produces zero thickness at the trailing edge, which makes manufacturing Joukowsky aerofoils impractical. Having said that, the process is still used to generate exact solutions against which numerically based point source/panel methods can be checked (you will be introduced to the latter later in the course). The problem of the thin trailing edge may be removed by the use of an alternative transformation, known as the *Karman-trefftz* transformation

$$\left(\frac{Z+2b}{Z-2b}\right) = \left(\frac{\zeta+b}{\zeta-b}\right)^n$$

which results in a finite angle at the trailing edge (this will not be proven, you can check it yourself if you are interested).

10 Introduction To Boundary Layer Theory

Key Points: *Concept of thin boundary layers, Laminar, Turbulent and Transitional flows, thin layer assumptions and their effects*

10.1 What is A Boundary Layer?

About a hundred years ago, the field of fluid dynamics was split into two apparently unconnected disciplines. Hydrodynamics dealt with inviscid fluid flows, usually irrotational and incompressible, slipping freely past immersed bodies. Away from the surfaces of such bodies, the methods appeared to give good results, but it predicted that no drag forces should exist, and could only account for lift through circulation, which it could not explain. Hydraulics, on the other hand, was necessary and effective for analysis involving fluids in pipes and other related areas (including ship design), but was largely empirical and lacked theoretical justification. In 1904, however, Prandtl linked these two groups by a concept called *Boundary Layer Theory*.

The essential points of the theory were:

- However small viscosity may be, it cannot be ignored, particularly near solid surfaces. Here the velocity of the flow must change from zero at the wall (due to the no-slip condition) to the free stream velocity in a short distance. This means that the velocity gradient $\frac{\partial U}{\partial y}$, where U is the fluid velocity and the y direction is normal to the surface, is large. As the shear stress in a Newtonian Fluid is given by
$$\tau = \mu \frac{\partial U}{\partial y}$$
in turn the resultant (frictional) force acting on a body is significant.
- The ratio of inertial to viscous forces (defined by the Reynolds Number $Re = \frac{UL}{\nu}$, where L is some representative length and ν is the kinematic viscosity, $\frac{\mu}{\rho}$) is of critical importance in boundary layer behaviour. For Reynolds numbers greater than about 10^5, the regions next to the body where the shear stresses are important are thin, and become thinner as Re increases. As Re values associated with real world applications such as around aircraft are typically at least 10^5, and often much greater, this result means that the theory has considerable use.
- The relative thinness of these boundary layers means that the Navier Stokes Equations governing the flow may be simplified.
- Outside the boundary layers the classical methods involving inviscid flows apply, as the effects of viscosity are much reduced.

Therefore the flow past a body such as a wing may be thought of as consisting of two regions (figure 37), an inviscid outer flow, and an inner boundary layer (which extends downstream of the body to form a *wake*) which contains all the effects of viscosity, such as skin friction, and generation of vorticity. The boundary layer has two principle effects on the forces calculated by inviscid analysis; it alters the apparent shape of the body, resulting in altered pressure distributions and hence lift force and introduces *Boundary Layer Pressure Drag* (a component of *Form Drag*), and the shearing of

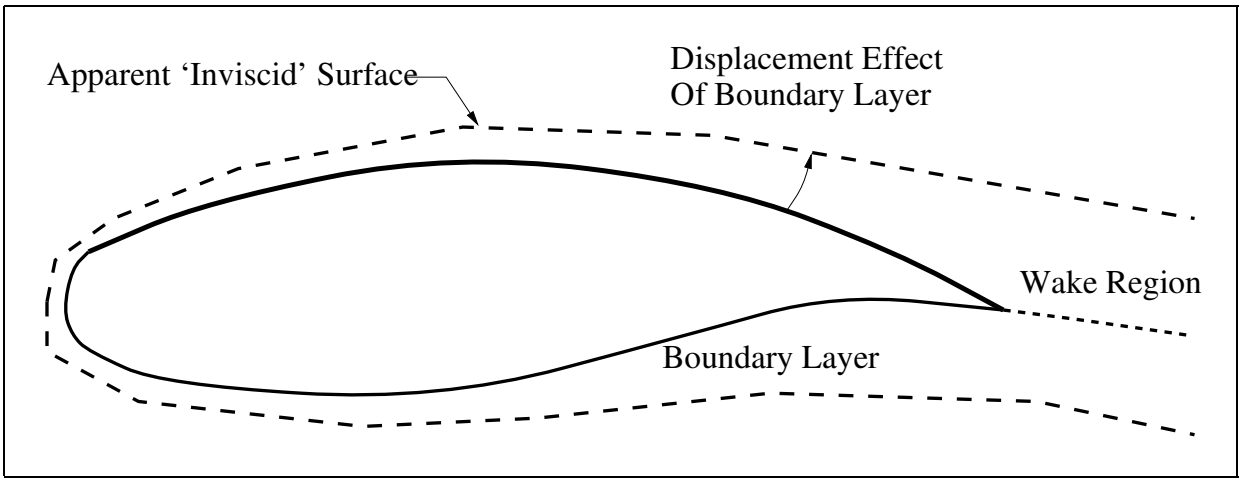

Figure 37: *Boundary Layer Effect on Inviscid Flows (greatly exaggerated)*

the flow at the surface directly produces a drag force, called *Skin-Friction Drag*. These effects are generally small, but are very significant if the boundary layer separates.

The boundary layer thickness, δ, is defined as the distance from the wall at which the velocity in the boundary layer, u, is equal to that in the 'inviscid' flow external to the layer, u_e. In theory, the two values are only exactly identical at an infinite distance from the surface, and hence for a practical reasons δ is actually related to some finite ratio of u/u_e, e.g. the point where the velocity is 99% that of the external flow (strictly, this would be denoted $\delta_{0.99}$).

10.2 Laminar, Transition, and Turbulent Flows

The flow within a boundary layer or wake may be categorised as being *laminar*, *transitional*, or *turbulent*. Laminar flows are characterised by a layering of the flow (hence the name), in which higher speed particles slide smoothly over lower speed ones. The molecular dissipation is sufficiently strong that any perturbations in the velocities in the flow are rapidly damped out. In turbulent flow, however, this is not the case, and fluctuations in velocity become much larger. The flow is characterised by the presence of 'turbulent eddies' of various sizes, which cause the mixing of fluids from various layers and hence velocities. This means that the velocity profile through most of the layer is more uniform, which in turn results in a higher velocity gradient (and hence shear stress and friction) at the wall. Typical velocity profiles for these two flow types are shown in figure 38.

Transitional flows, as the name implies, arise between regions of laminar and turbulent flows. The mechanisms involved in transition are complex, and only partially understood. Transitional regions are characterised by intermittency. This means that rather than a gradual change between laminar and turbulent flows, where the fluctuations in velocity slowly increase, the flow in a transitional region is either laminar or turbulent, but varies in time between the two. Obviously, as one moves further into the transition region, the percentage of time in any given interval for which the flow may be characterised as turbulent increases, until at the end of the transition zone, the flow is always in a turbulent state. Generally, a flow begins as laminar but, as the Reynolds number increases, passes through transition and then becomes turbulent. We shall be spending this and the next four lectures concentrating on methods for analysis of laminar boundary layers. Transition and turbulence shall be dealt with in the following five lecture block.

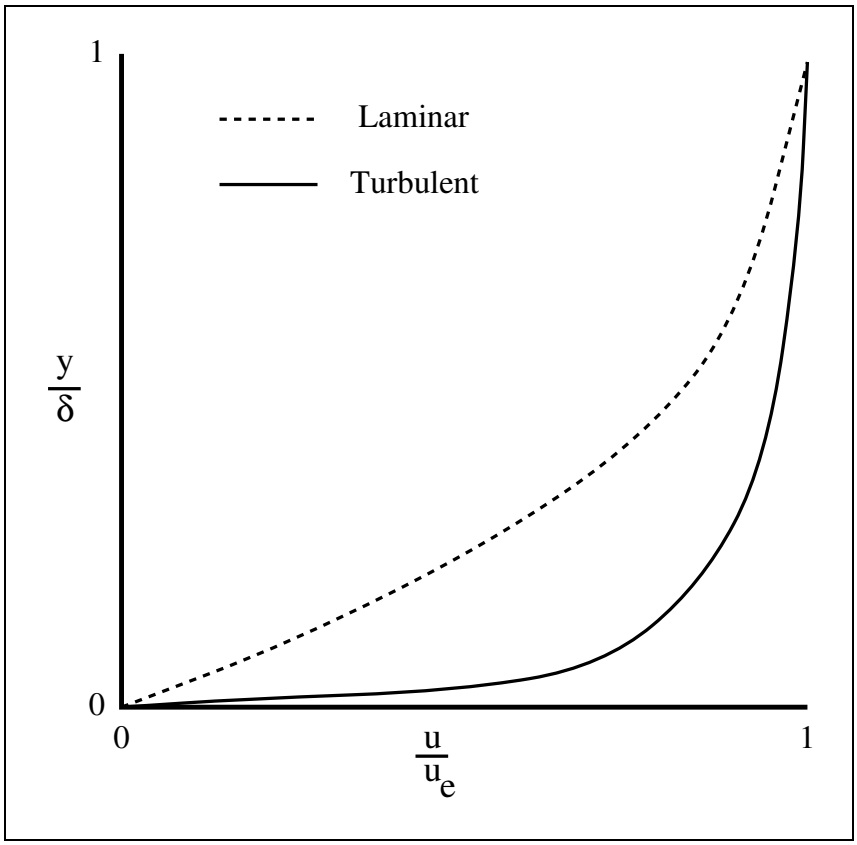

Figure 38: *Typical Velocity Profiles*

10.3 The Thin Layer Equations

As mentioned in the introduction, the boundary layer concept allows reduction of the complex Navier-Stokes Equations. Derivation of the Navier Stokes Equations will not be attempted here, as it is a long and mathematically complex process which it is not really necessary to understand to make use of the result. *However*, such a derivation is available in many text books dealing with viscous flows, and it is suggested that you at least read through the process at some point, particularly if you have any doubts about the origin or legitimacy of the equations used in the rest of this handout.

Before applying the specific thin boundary layer assumptions, we shall make some assumptions about the flow with which we are dealing, to reduce the complexity of the initial more general equations. This is done to reduce not only the complexity of the equations, but also that of the methods we will be investigating in later lectures. However, we shall at various points return to a more complete description of the flow to understand the implications of, among other things, compressibility and heat transfer, which we shall initially ignore.

The assumptions we shall start from are: that the flow is two dimensional, steady, and incompressible. The latter assumption means that one of the usual variables, ρ is now constant (and as a consequence μ and ν are also constant), and hence one of the equations may be dropped. In fact, this assumption effectively de-couples the energy equation, and unless heat transfer is to be considered, it no longer needs to be solved, greatly simplifying the solution process. Finally, we ignore the presence of body forces within the boundary layer itself (the surface is a boundary of the layer, and hence the forces generated there may be treated via boundary conditions). Given these assumptions, the equations that govern the flow of a perfect, Newtonian gas are:

Continuity

$$\frac{\partial u}{\partial x} + \frac{\partial v}{\partial y} = 0 \tag{85}$$

x-momentum

$$u\frac{\partial u}{\partial x} + v\frac{\partial u}{\partial y} = -\frac{1}{\rho}\frac{\partial p}{\partial x} + \nu\left(\frac{\partial^2 u}{\partial x^2} + \frac{\partial^2 u}{\partial y^2}\right) \tag{86}$$

y-momentum

$$u\frac{\partial v}{\partial x} + v\frac{\partial v}{\partial y} = -\frac{1}{\rho}\frac{\partial p}{\partial y} + \nu\left(\frac{\partial^2 v}{\partial x^2} + \frac{\partial^2 v}{\partial y^2}\right) \tag{87}$$

Even these apparently simple equations are too complex to be solved analytically in all but a very few special cases. To keep things as simple as possible initially, we shall restrict ourselves to two dimensional flow along a flat plate with x parallel, and y normal to the plate, and examine the implications of the thin layer assumption on these equations.

We define a thickness δ_u through which velocity gradients are large enough to make viscosity significant, but outside of which the flow may be considered inviscid. If the Reynolds number is large, this layer will be thin compared to any surface extension (i.e. $\delta/c \ll 1$), and hence in the boundary layer

$$\frac{\partial}{\partial y} \gg \frac{\partial}{\partial x}$$

This means that the change in a variable occurs much more rapidly through a boundary layer than along it. At first sight this would appear to suggest that the first term in the continuity equation may be neglected. However, the second term is a derivative of v, and as the flow is primarily parallel,

$$\frac{v}{u_e} = O\left(\frac{\delta_u}{c}\right) \ll 1$$

where u_e is the flow velocity outside the boundary layer, $O()$ means order of, and c is the local chord (see figure 39). This means that the first term expresses a small change in a large number, and the second a larger change, but in a small number. Hence the two terms can be seen to be of roughly the same magnitude. In fact, this result is required, for if either of the terms could be neglected, the other would also be equal to zero, and we could have no velocity gradients anywhere in the flow. This means that the continuity equation cannot be simplified from its form expressed in Equation (1)

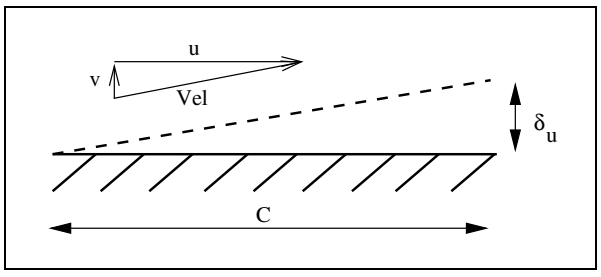

Figure 39: *Length and Velocity Scales*

Turning to the momentum equations, as $\frac{\partial}{\partial x}$ is small, all terms involving $\frac{\partial}{\partial x^2}$ may be neglected, giving the x momentum as

$$u\frac{\partial u}{\partial x} + v\frac{\partial u}{\partial y} = -\frac{1}{\rho}\frac{\partial p}{\partial x} + \nu\frac{\partial^2 u}{\partial y^2} \tag{88}$$

The y momentum equation has four terms involving derivatives of v, which as already discussed is small. Hence all second derivatives may be neglected, reducing the right hand side to just the pressure term. On the left, the first term is the small derivative of a small number, and may thus be neglected, and whilst the second derivative is non-negligible (see the discussion on the continuity equation), it is multiplied by a small number (v) and may be ignored. In effect then, the y-momentum equation becomes just

$$\frac{1}{\rho}\frac{\partial p}{\partial y} \approx 0$$

which tells us that the pressure is approximately constant through a boundary layer. This is important, as this allows the pressure imposed by an inviscid analysis of the flow to be applied to the boundary layer, and indeed give surface pressures.

If pressure is constant through the boundary layer, there is no longer any need to solve the y-momentum equation, and the flow is described completely by Equations (1) and (4). However, before moving on to solution methods, we shall perform dimensional analysis on the x-momentum equation to derive an important result. Dimensional analysis may be thought of as a method by which representative values for the variables are used to derive approximate results; details are not provided, but a 'feel' for the relative sizes and importance of various terms can be attained.

If we take U_1, ρ_1, c, and μ_1 to be representative values of the velocity, density, chord, and viscosity in the boundary layer, then the largest term on the LHS of equation (88) is of order $\frac{U_1^2}{c}$. If we consider for now flows where there are no pressure gradients in the x direction (e.g. over a flat plate), then $\frac{\partial p}{\partial x} = 0$ and hence the RHS of the equation is dominated by a term of the order of $\frac{\mu_1 U_1}{\rho_1 \delta_u^2}$. Inverting and equating these gives

$$\frac{c}{U_1^2} \approx \frac{\rho_1 \delta_u^2}{\mu_1 U_1} \tag{89}$$

$$\Rightarrow \frac{\mu_1}{\rho_1 U_1 c} \approx \frac{\delta_u^2}{c^2} \tag{90}$$

which in turn results in $\frac{\delta_u}{c} = O(Re^{-\frac{1}{2}})$, implying that the boundary layer grows at a rate proportional to the inverse of the root of the Reynolds number in a zero pressure gradient environment. This is an important result which we shall return to in later lectures.

10.3.1 Compressible flow

The boundary layer assumptions have more of an impact on the governing equations if less initial assumptions are made. Considering for instance unsteady compressible flow, (i.e. only applying the assumption of two dimensional flow) we have the following thin layer equations

$$\frac{\partial \rho}{\partial t} + \frac{\partial \rho u}{\partial x} + \frac{\partial \rho v}{\partial y} = 0$$

$$\rho\Big(\frac{\partial u}{\partial t} + u\frac{\partial u}{\partial x} + v\frac{\partial u}{\partial y}\Big) = -\frac{\partial p}{\partial x} + \frac{\partial}{\partial y}\Big(\mu\frac{\partial u}{\partial y}\Big)$$

$$\rho\Big[\frac{\partial}{\partial t}(c_pT) + u\frac{\partial}{\partial x}(c_pT) + v\frac{\partial}{\partial y}(c_pT)\Big] - \Big(\frac{\partial p}{\partial t} + u\frac{\partial p}{\partial x}\Big) = \frac{\partial}{\partial y}\Big(k\frac{\partial T}{\partial y}\Big) + \mu\Big(\frac{\partial u}{\partial y}\Big)^2$$

The energy equation must be retained for compressible flow as the temperature and velocity fields are coupled. In fact, dimensional analysis shows that the thermal boundary layer thickness, δ_T may be

related to the momentum layer via

$$\frac{\delta_u}{\delta_T} = O\Big(\frac{\mu_1 c_p}{k_1}\Big)^{\frac{1}{2}} = O(\sigma_1^{\frac{1}{2}})$$

where σ is the Prandtl number, and is equal to $\frac{\mu c_p}{k}$. If the Prandtl number is unity, therefore, the thermal and momentum boundary layers are the same size. Air typically has a Prandtl number of about 0.7, and is essentially independent of T away from points of phase change.

Again it is stressed that whilst we shall be dealing mainly with methods for analysis of incompressible flows, this is primarily due to the simplifications this produces, and it should always be borne in mind that what we do for such flows can also be done for compressible ones, though with some restrictions and with a good deal more computational effort. We shall from time to time examine these issues in more detail.

10.3.2 Curved Surfaces

So far, we have been assuming that the flow is over a flat plate. However, real aerodynamic surfaces (such as aerofoils) tend to be curved. We use a body fitting coordinate system (i.e. x along the surface, y normal to it). Then if the local radius of curvature of the wall is R, there must be a pressure gradient normal to the wall which produces the centripetal acceleration. Imagine a rectangular element measuring Δx by Δy, with a pressure on the lower edge of p and on the upper edge of $p + \frac{\partial p}{\partial y}\Delta y$, so

$$\left(p + \frac{\partial p}{\partial y}\Delta y - p\right)\Delta x = \Delta x \Delta y \frac{\rho u^2}{R}$$

giving

$$\frac{\partial p}{\partial y} = \frac{\rho u^2}{R}$$

This means there will be a pressure change through the boundary layer Δp of order $\frac{\rho U_1^2 \delta_u}{R}$, which may be neglected if $\frac{\delta_u}{R} \ll 1$, i.e. for curvatures where the radius is much larger than the boundary layer thickness. As boundary layers are so thin, this applies to the majority of aerodynamically useful shapes, although care must be taken in some cases.

10.3.3 Question for next lecture

Using the thin layer assumptions and the continuity equation, show that the two dimensional, unsteady, compressible version of the x momentum equation:

$$\frac{\partial \rho u}{\partial t} + \frac{\partial \rho u^2}{\partial x} + \frac{\partial \rho u v}{\partial y} = -\frac{\partial p}{\partial x} + \frac{\partial}{\partial x}\Big(\mu\Big(\frac{\partial u}{\partial x} + \frac{\partial u}{\partial x} - \frac{2}{3}\Big(\frac{\partial u}{\partial x} + \frac{\partial v}{\partial y}\Big)\Big)\Big) + \frac{\partial}{\partial y}\Big(\mu\Big(\frac{\partial u}{\partial y} + \frac{\partial v}{\partial x}\Big)\Big)$$

reduces too

$$\rho\Big(\frac{\partial u}{\partial t} + u\frac{\partial u}{\partial x} + v\frac{\partial u}{\partial y}\Big) = -\frac{\partial p}{\partial x} + \frac{\partial}{\partial y}\Big(\mu\frac{\partial u}{\partial y}\Big)$$

11 Boundary Layer Integral Equations

Key points: *Concept of Integral methods, displacement and momentum thickness. Derivation and use of the Momentum Integral Equation*

11.1 Introduction

Last lecture we showed that the equations that govern the motion of the flow within thin and attached boundary layers for two dimensional, steady, incompressible flow are

$$\frac{\partial u}{\partial x} + \frac{\partial v}{\partial y} = 0 \tag{91}$$

$$u\frac{\partial u}{\partial x} + v\frac{\partial u}{\partial y} = -\frac{1}{\rho}\frac{dp}{dx} + \nu\frac{\partial^2 u}{\partial y^2} \tag{92}$$

These equations may be solved directly using a numerical approach on a discrete set of grid points, and indeed this is a common approach made feasible by todays high powered computers. However, before the advent of such machines, solution of the boundary layer equations was performed through analytical integration of the equations. Whilst this class of techniques is somewhat restricted in its range of applicability by some necessary assumptions about the flow under investigation, it gives valuable insight into the physical behaviour of the flows, and hence we shall be spending the next few lectures investigating these so-called *integral methods*. Indeed, due to their rapid application, and relation to physical parameters, such methods are still in widespread use in more simple aerodynamic analysis packages, and hence are not just of historical interest. This lecture, we shall begin the process by deriving expressions useful for characterising boundary layer properties, (the displacement and momentum thicknesses), and finally examine the Momentum Integral Equation (MIE), the solution of which comprises the central focus of integral methods.

11.1.1 Boundary Conditions, and Displacement and Momentum Thickness

If we consider once more steady flow over a flat plate with x in the primary flow direction, and y perpendicular to it, then when $y = 0$ (i.e. at the surface), due to the no slip condition $u, v = 0$. If we denote the freestream conditions external to the boundary layer (which may depend on x) with a subscript e, then from Eqn. 92, at the wall

$$\mu\Big(\frac{\partial^2 u}{\partial y^2}\Big)_{wall} = \frac{dp}{dx} = -\rho_e u_e \frac{du_e}{dx}$$

with the term on the far right being derived from application of Eqn. 92 to the external flow, remembering that viscosity there is zero, that the flow is over a flat plate and hence $v_e = 0$ and assuming that p is solely a function of x. This means that if there is no external pressure gradient,

$$\Big(\frac{\partial^2 u}{\partial y^2}\Big)_{wall} = 0$$

At the outer edge of the boundary layer, we wish the properties to be identical to those of the freestream, i.e.

$$u = u_e, \qquad \rho = \rho_e, \qquad \partial u/\partial y = \partial^2 u/\partial y^2 = ... = 0, \text{etc., at } y = \delta_u$$

Technically, this can only truly be the case if δ_u is an infinite distance from the wall. However, if we take a more reasonable definition, for instance where the velocity is 99.5% that of the freestream, we find that $\delta/c \approx 5/Re^{\frac{1}{2}}$ (remember we derived the $Re^{-\frac{1}{2}}$ rule last lecture). For a typical aircraft with a trailing edge Re of 10^6 say, this means that $\delta/c \approx 0.005$, and hence this represents a very thin layer.

Although δ itself is a bit ambiguous, and depends on the specified u/u_e, other measurements of boundary layer thickness that have physical significance can be defined much more accurately. First, the *displacement thickness*, δ^* is defined as

$$\delta^* = \int_0^h \Big(1 - \frac{\rho u}{\rho_e u_e}\Big) dy$$

where h is any value a small amount greater than δ_u. If the equation above is multiplied on both sides by $\rho_e u_e$, it should be obvious that this gives the deficit in mass flow past the surface caused by the presence of the boundary layer (compared to that which would be the case for a purely inviscid flow). This defect causes a movement of fluid out into the main flow. Outside of the boundary layer therefore, the flow is exactly equivalent to an inviscid flow about the body with its surface displaced by δ^*.

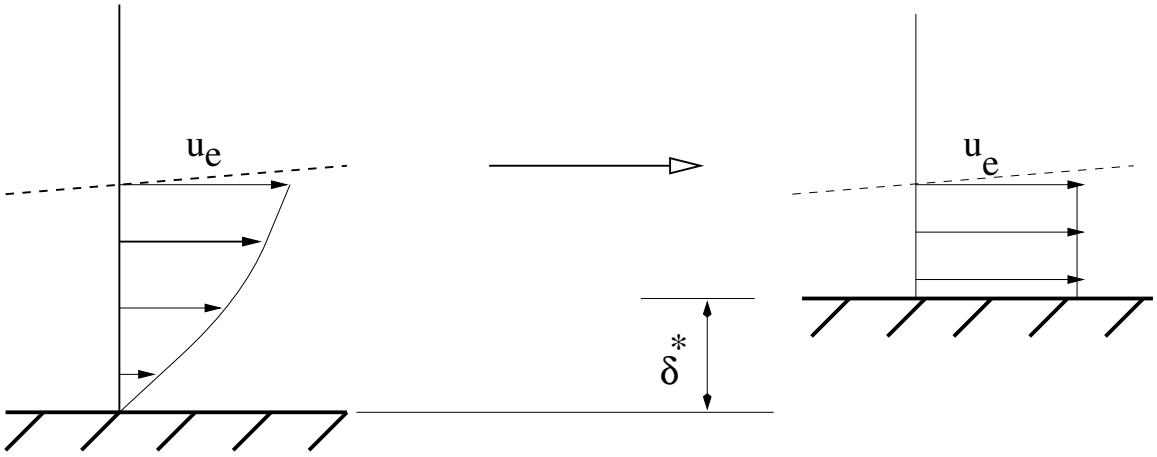

Momentum thickness is defined as

$$\theta = \int_0^h \frac{\rho u}{\rho_e u_e}\left(1 - \frac{u}{u_e}\right) dy$$

From this we can see that $\rho_e u_e^2 \theta$ is the deficit in streamwise momentum transport with a boundary layer compared to that for inviscid flow. As a change in momentum produces a force, this relates to the drag of the body, both frictional and pressure.

In the form written above, these values are applicable to both compressible and incompressible flows. However, as we are dealing with incompressible flow, $\rho_e = \rho$, and hence all we require is some form of expression for u/u_e, to calculate δ^* and θ, which in turn give a rapid method for calculation of pseudo surface displacement and drag, without requiring detail of the inner flow to be explicitly calculated. Before we move on to examining methods for determining u/u_e, however, we shall derive the *Momentum Integral Equation*, which allows us to calculate the drag of a body to a reasonable level of accuracy, once δ^* and θ are known. It is this property (the drag) which we are of course most interested in.

11.2 The Momentum Integral Equation

Consider the control volume ABCD shown in figure below. The mass flow entering the volume must

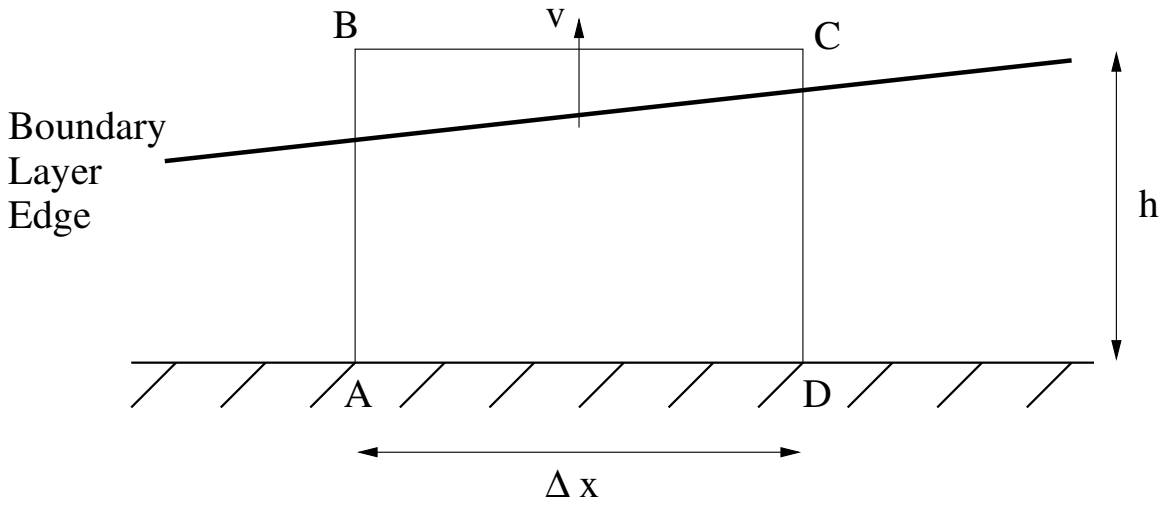

equal that flowing out. Inflow across face AB is

$$\dot{m}_{AB} = \int_0^h \rho u dy \Big|_{\text{at AB}}$$

Outflow across CD is

$$\dot{m}_{CD} = \int_0^h \rho u dy \Big|_{\text{at CD}}$$

and outflow across BC is $\rho_e v_h \Delta x$ (we assume Δx is sufficiently small that there is no variation in v_h along its length). This therefore means that

$$\int_0^h \rho u dy \Big|_{\text{at AB}} - \int_0^h \rho u dy \Big|_{\text{at CD}} = \rho_e v_h \Delta x \tag{93}$$

or

$$\rho_e v_h = \frac{\int_0^h \rho u dy\big|_{\text{at AB}} - \int_0^h \rho u dy\big|_{\text{at CD}}}{\Delta x}$$

As $\Delta x \to 0$, higher terms in Δx may be neglected, and the above tends to

$$\rho_e v_h = -\frac{d}{dx}\Big(\int_0^h \rho u dy \Big)$$

Next, consider *x-momentum:* Rate of momentum in across AB is

$$\dot{xmom}_{AB} = \int_0^h \rho u^2 dy \Big|_{\text{at AB}}$$

Rate out across CD

$$\dot{xmom}_{CD} = \int_0^h \rho u^2 dy \Big|_{\text{at CD}}$$

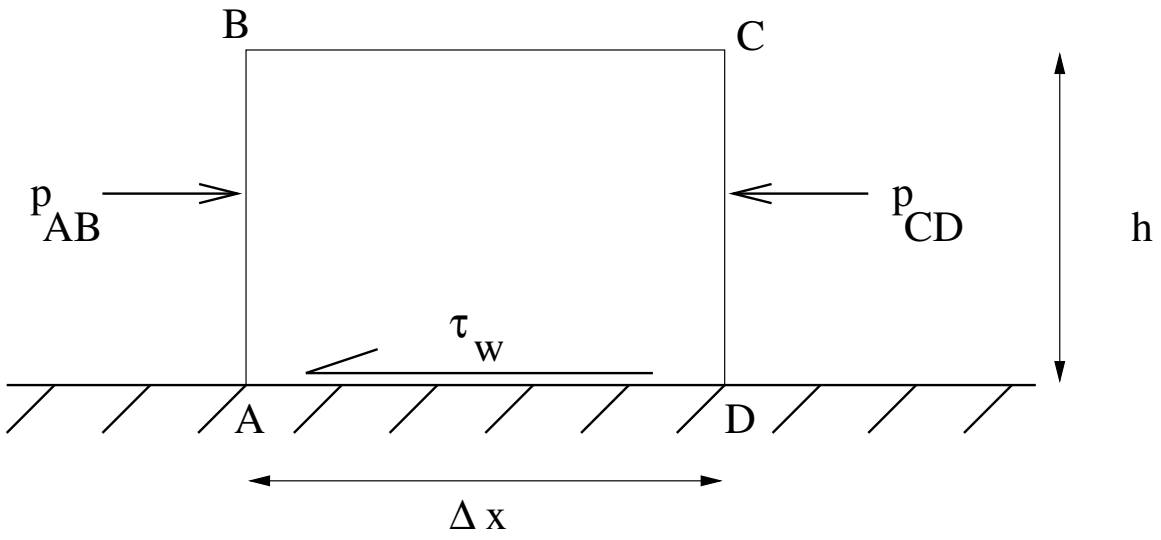

and rate out through face BC is $\rho_e u_e v_h \Delta x$. Summing all these to give a rate of production of x momentum gives

$$\int_0^h \rho u^2 dy\bigg|_{\text{at AB}} - \int_0^h \rho u^2 dy\bigg|_{\text{at CD}} - \rho_e u_e v_h \Delta x \tag{94}$$

This must be balanced by the forces acting on the control volume (see above, where τ_w is the wall shear stress). The net force in the x direction is thus

$$p_{AB}h - p_{CD}h - \tau_w \Delta x \tag{95}$$

and so as the sum of equations 94 and 95 must be zero, we may finally write

$$-\int_0^h \rho u^2 dy\bigg|_{\text{at AB}} + \int_0^h \rho u^2 dy\bigg|_{\text{at CD}} + \rho_e u_e v_h \Delta x = -(p_{CD} - p_{AB})h - \tau_w \Delta x$$

Substituting Eqn. 93 for $\rho_e v_h \Delta x$, then dividing through by Δx and allowing it to tend to zero gives

$$\frac{d}{dx}\left(\int_0^h \rho u^2 dy\right) - u_e \frac{d}{dx}\left(\int_0^h \rho u dy\right) = -h\frac{dp}{dx} - \tau_w$$

which is the momentum integral equation. We can express this in a more useful form by using the expressions for δ^* and θ as follows:-

From Eqn. 92 for the external, inviscid, steady one dimensional flow we have

$$-\frac{dp}{dx} = \rho_e u_e \frac{du_e}{d_x}$$

and so the above equation may be written (where an integration by parts has also been performed)

$$\frac{d}{dx}\left[\int_0^h \rho u(u-u_e)dy\right] + \frac{du_e}{dx}\left[\int_0^h \rho u dy\right] = h\rho_e u_e \frac{du_e}{dx} - \tau_w$$

$$\Rightarrow \frac{d}{dx}\left[\int_0^h \rho u(u_e-u)dy\right] + \frac{du_e}{dx}\left[\int_0^h (\rho_e u_e - \rho u)dy\right] = \tau_w$$

$$\Rightarrow \frac{d}{dx}(\rho_e u_e^2 \theta) + \frac{du_e}{dx}\rho_e u_e \delta^* = \tau_w$$

If we denote the ratio δ^*/θ as H, known as the *shape factor*, we may then write

$$\frac{d\theta}{dx} + \frac{\theta}{u_e}\frac{du_e}{dx}(H+2) + \frac{\theta}{\rho_e}\frac{d\rho_e}{dx} = \frac{\tau_w}{\rho_e u_e^2}$$

Which is the most commonly used form on the MIE. If we may assume incompressible flow, the all derivatives with respect to ρ and ρ_e are zero, and hence

$$\frac{d\theta}{dx} + \frac{\theta}{u_e}\frac{du_e}{dx}(H+2) = \frac{\tau_w}{\rho_e u_e^2}$$

Note: Sometimes the above are expressed in terms of a *local skin friction coefficient*, c_f, defined as

$$c_f = \frac{\tau_w}{\frac{1}{2}\rho_e u_e^2}$$

rendering the compressible and incompressible MIE equations as

$$\frac{d\theta}{dx} + \frac{\theta}{u_e}\frac{du_e}{dx}(H+2) + \frac{\theta}{\rho_e}\frac{d\rho_e}{dx} = \frac{c_f}{2}$$
$$\frac{d\theta}{dx} + \frac{\theta}{u_e}\frac{du_e}{dx}(H+2) = \frac{c_f}{2}$$

Before progressing further, it should be noted that other integral equations may be derived, and are sometimes needed for heat transfer problems. The most common are the *kinetic energy integral equation* and the *total energy equation*. The method of derivation is similar.

11.3 Use of the MIE

Worked Example: Calculate the drag coefficient of a flat plate at zero incidence with steady flow on one side only, length 1 metre, in a sea level flow at 40 m/s. Assume incompressible, laminar flow, and a linear velocity profile within the boundary layer.

As the flow is incompressible, and at zero incidence, all derivatives w.r.t ρ and p (and hence u_e disappear), and the MIE becomes

$$\frac{d\theta}{dx} = \frac{c_f}{2} = \frac{\tau_{wall}}{\rho u_e^2} \tag{96}$$

The velocity profile is linear, equal to 0 at the wall, and u_e at $y = \delta$, hence

$$\frac{u}{u_e} = \frac{y}{\delta}$$

Substituting this into the equations for δ^* and θ gives

$$\delta^* = \int_0^\delta \left(1 - \frac{u}{u_e}\right)dy = \int_0^\delta \left(1 - \frac{y}{\delta}\right)dy = \left[y - \frac{y^2}{2\delta}\right]_0^\delta = \delta - \frac{\delta}{2} = \frac{\delta}{2}$$
$$\theta = \int_0^\delta \frac{u}{u_e}\left(1 - \frac{u}{u_e}\right)dy = \int_0^\delta \frac{y}{\delta}\left(1 - \frac{y}{\delta}\right)dy = \left[\frac{y^2}{2\delta} - \frac{y^3}{3\delta^2}\right]_0^\delta = \frac{\delta}{2} - \frac{\delta}{3} = \frac{\delta}{6}$$

Also

$$\tau_{wall} = \mu \frac{\partial u}{\partial y}$$

and as

$$u = \frac{y}{\delta} u_e \Rightarrow \frac{\partial u}{\partial y} = \frac{u_e}{\delta}$$

substitution into Eqn. 96 gives

$$\frac{d\theta}{dx} = \frac{\mu u_e}{\delta \rho_e u_e^2} \Rightarrow \frac{d\theta}{d\delta}\frac{d\delta}{dx} = \frac{\nu}{\delta u_e} \Rightarrow \frac{1}{6}\frac{d\delta}{dx} = \frac{\nu}{\delta u_e} \Rightarrow \delta d\delta = \frac{6\nu}{u_e} dx$$

Integrating (and ignoring constants of integration as $\delta = 0$ when $x = 0$):

$$\delta^2 = \frac{12\nu x}{u_e} \Rightarrow \frac{\delta}{x} = \sqrt{\frac{12\nu}{x u_e}} = \sqrt{12} Re^{-\frac{1}{2}}$$

This result means that

$$\frac{\delta^*}{x} = \frac{1}{2}\frac{\delta}{x} = 1.732 Re^{-\frac{1}{2}}, \qquad \frac{\theta}{x} = \frac{1}{6}\frac{\delta}{x} = 0.557 Re^{-\frac{1}{2}}, \qquad \text{and} \qquad H = 3.0$$

and

$$c_f = \frac{2\tau_{wall}}{\rho_e u_e^2} = \frac{2\nu}{u_e \delta} = \frac{2\nu}{\sqrt{12} Re^{-\frac{1}{2}} x u_e} = \frac{2}{\sqrt{12}} \frac{Re^{\frac{1}{2}}}{Re} = \frac{\theta}{x} = 0.577 Re^{-\frac{1}{2}}$$

Now, only this friction force acts on the plate, so

$$C_D = C_F = \frac{1}{c}\int_0^c c_f dx = \frac{0.577}{c}\int_0^c \sqrt{\frac{\nu}{u_e x}} dx = \frac{0.577}{c}\Big[2\sqrt{\frac{x\nu}{u_e}}\Big]_0^c = \frac{1.155}{c}\sqrt{\frac{\nu c}{u_e}} = 1.155 Re_c^{-\frac{1}{2}}$$

From the information in the question, we have u_e = 40, $x_e = 1$, and we know $\nu = 1.461 * 10^{-5}$ at sea level (given in first set of lecture notes, would be given in an exam), so

$$Re_c = \frac{40 * 1}{1.461 * 10^{-5}} = 2.738 * 10^6$$

so

$$\mathbf{C_D = 0.00070}$$

(or a drag force of 0.68 Newtons per metre span).

This result was derived assuming a linear approximation to the velocity profile through the flow. However, we know this is a relatively poor approximation, as, for instance $\frac{\partial u}{\partial y} \neq 0$ at $y = \delta$. Next lecture we will look at more accurate profiles, and see how these affect the results.

11.3.1 Solution to last lecture's question

Using the thin layer assumptions and the continuity equation, show that the two dimensional, unsteady, compressible version of the x momentum equation:

$$\frac{\partial \rho u}{\partial t} + \frac{\partial \rho u^2}{\partial x} + \frac{\partial \rho u v}{\partial y} = -\frac{\partial p}{\partial x} + \frac{\partial}{\partial x}\Big(\mu\Big(\frac{\partial u}{\partial x} + \frac{\partial u}{\partial x} - \frac{2}{3}\Big(\frac{\partial u}{\partial x} + \frac{\partial v}{\partial y}\Big)\Big)\Big) + \frac{\partial}{\partial y}\Big(\mu\Big(\frac{\partial u}{\partial y} + \frac{\partial v}{\partial x}\Big)\Big)$$

reduces too

$$\rho\Big(\frac{\partial u}{\partial t}+u\frac{\partial u}{\partial x}+v\frac{\partial u}{\partial y}\Big)=-\frac{\partial p}{\partial x}+\frac{\partial}{\partial y}\Big(\mu\frac{\partial u}{\partial y}\Big)$$

Answer: The continuity equation in compressible flow is given in the handout as

$$\frac{\partial \rho}{\partial t}+\frac{\partial \rho u}{\partial x}+\frac{\partial \rho v}{\partial y}=0 \tag{97}$$

First considering the left hand side;

$$LHS=\frac{\partial \rho u}{\partial t}+\frac{\partial \rho u^2}{\partial x}+\frac{\partial \rho uv}{\partial y}=u\frac{\partial \rho}{\partial t}+\rho\frac{\partial u}{\partial t}+u\frac{\partial \rho u}{\partial x}+\rho u\frac{\partial u}{\partial x}+u\frac{\partial \rho v}{\partial y}+\rho v\frac{\partial u}{\partial y}$$

collecting terms we get

$$LHS=u\bigg(\frac{\partial \rho}{\partial t}+\frac{\partial \rho u}{\partial x}+\frac{\partial \rho v}{\partial y}\bigg)+\rho\bigg(\frac{\partial u}{\partial t}+u\frac{\partial u}{\partial x}+v\frac{\partial u}{\partial y}\bigg)$$

where the inside of the brackets is zero from Eqn 97, and the second term is what we wanted.

Turning to the RHS, thin layer theory means we can assume that all $\frac{\partial}{\partial x}$ are small, and hence we neglect all terms involving $\frac{\partial^2}{\partial x^2}$ as negligable, this immediately reduces the eqn. to

$$RHS=-\frac{\partial p}{\partial x}+\frac{\partial(-\frac{2}{3}\mu\frac{\partial v}{\partial y})}{\partial x}+\frac{\partial}{\partial y}\Big(\mu(\frac{\partial u}{\partial y}+\frac{\partial v}{\partial x})\Big)$$

However, we know from consideration of the flow pattern, and the definition of the axis system that v, the normal flow velocity is small, and does not vary much in the x direction. Hence the second derivatives with respect to this variable may be ignored, and hence we have

$$\rho\Big(\frac{\partial u}{\partial t}+u\frac{\partial u}{\partial x}+v\frac{\partial u}{\partial y}\Big)=-\frac{\partial p}{\partial x}+\frac{\partial}{\partial y}\Big(\mu\frac{\partial u}{\partial y}\Big)$$

as required.

11.3.2 Exercise for next lecture:

Show explicitly that

$$\frac{d}{dx}(\rho_e u_e^2\theta)+\frac{du_e}{dx}\rho_e u_e\delta^*=\tau_w$$

may be expressed as

$$\frac{d\theta}{dx}+\frac{\theta}{u_e}\frac{du_e}{dx}(H+2)+\frac{\theta}{\rho_e}\frac{d\rho_e}{dx}=\frac{\tau_w}{\rho_e u_e^2}$$

where $H=\delta^*/\theta$

12 Simple Solutions for Laminar Boundary Layers

Key points: *Derivation of the Blasius Solution and comparison with linear, concept of similar solutions and the Falkner-Skan Equation.*

12.1 Blasius Solution

At the end of the last lecture we calculated the drag of a flat plate in incompressible, steady, laminar flow assuming that the velocity profile was linear. As mentioned, however, we know that a linear profile cannot be the correct one, due to discontinuities in velocity gradient at the boundary layer edge. We shall begin this lecture by deriving the exact solution for such flows.

If we have incompressible flow and no incidence (and hence no external velocity or pressure gradient), the boundary layer equations become

$$\frac{\partial u}{\partial x} + \frac{\partial v}{\partial y} = 0 \tag{98}$$

$$u\frac{\partial u}{\partial x} + v\frac{\partial u}{\partial y} = \nu\frac{\partial^2 u}{\partial y^2} \tag{99}$$

with boundary conditions $u, v = 0$ at the wall, and $u = u_e$ at an infinite distance from the plate.

The lack of gradients in the external flow in the x direction means that similarity of velocity profiles may be assumed, as there is no mechanism to introduce any changes. In other words, the variation of velocity within the boundary layer, u/u_e, is independent of x, except in that the thickness of the layer changes. Hence if we use a coordinate system based on η, where $\eta = y/\phi(x)$, we will have constant values for u/u_e at constant η, provided we make the correct choice for the function $\phi(x)$. Here, $\phi(x)$ represents the boundary layer thickness. We know from dimensional considerations (lecture 6) that the thickness of the boundary layer varies with $x/Re_x^{\frac{1}{2}}$, and hence we may consider

$$\eta = \text{const.}\frac{y}{x}\left(\frac{u_e x}{\nu}\right)^{\frac{1}{2}} = \frac{y}{2}\left(\frac{u_e}{\nu x}\right)^{\frac{1}{2}}$$

where the constant is chosen as $\frac{1}{2}$ purely for numerical convenience in that which follows.

As we have incompressible flow, it follows from the continuity equation that there exists a stream function φ such that

$$u = \frac{\partial \varphi}{\partial y}, \qquad v = -\frac{\partial \varphi}{\partial x}$$

and this fact means we can replace the two equations involving u and v for one involving φ. The following is chosen for the stream function:

$$\varphi = (u_e x \nu)^{\frac{1}{2}}.F(\eta)$$

In order to determine what this function F is, we note that

$$u = \frac{\partial \varphi}{\partial \eta}\frac{\partial \eta}{\partial y} = (u_e x\nu)^{\frac{1}{2}}\frac{F'}{2}\left(\frac{u_e}{\nu x}\right)^{\frac{1}{2}} = \frac{u_e F'}{2}$$

where $'$ represents differentiation w.r.t η. Similarly,

$$v = -\frac{\partial \varphi}{\partial x} = \frac{1}{2}\Big(\frac{u_e \nu}{x}\Big)^{\frac{1}{2}}(F'\eta - F)$$

From these we can further deduce that

$$\frac{\partial u}{\partial x} = -\frac{u_e}{2}F''\frac{y}{4x}\Big(\frac{u_e}{\nu x}\Big)^{\frac{1}{2}}, \quad \frac{\partial u}{\partial y} = u_e\frac{F''}{4}\Big(\frac{u_e}{\nu x}\Big)^{\frac{1}{2}}, \quad \frac{\partial^2 u}{\partial y^2} = \frac{u_e^2 F'''}{8\nu x}$$

Substituting all this in to Eqn 99 gives

$$-\frac{u_e F'}{2}\left(\frac{u_e}{2}F''\frac{y}{4x}\Big(\frac{u_e}{\nu x}\Big)^{\frac{1}{2}}\right) + \frac{1}{2}\Big(\frac{u_e\nu}{x}\Big)^{\frac{1}{2}}(F'\eta - F)\left(u_e\frac{F''}{4}\Big(\frac{u_e}{\nu x}\Big)^{\frac{1}{2}}\right) = \nu\left(\frac{u_e^2 F'''}{8\nu x}\right)$$

$$\Rightarrow -\frac{y}{2}\Big(\frac{u_e}{\nu x}\Big)^{\frac{1}{2}}\Big(\frac{F'F''u_e^2}{8x}\Big) + \frac{\eta u_e^2}{8x}F'F'' - \frac{u_e^2}{8x}FF'' = \frac{u_e^2 F'''}{8x}$$

$$\Rightarrow -\frac{\eta F'F''u_e^2}{8x} + \frac{\eta F'F''u_e^2}{8x} = \frac{u_e^2 F'''}{8x} + \frac{u_e^2 FF''}{8x}$$

or, dividing through by the common factor $\frac{u_e^2}{8x}$,

$$FF'' + F''' = 0$$

with boundary conditions $F = 0, F' = 0$ at $\eta = 0$, and $F' = 2$ at $\eta = \infty$. This non-linear equation cannot be solved analytically, but can be done so numerically. The first successful attempt was made by Blasius in 1908, and the equation is named after him. However, since then the method has been refined, and modern computers make the solution relatively trivial. Table 2 gives the profile, which may be considered to be an exact solution to the flat plate problem.

It is found that $F''(0) = 1.328$, and since $\tau_{wall} = \mu(\frac{\partial u}{\partial y})_{wall} = \frac{1}{4}\mu u_e(\frac{u_e}{\nu x})^{\frac{1}{2}}F''(0)$, it follows that the local skin friction c_f is

$$c_f = 2\frac{\tau_{wall}}{\rho u_e^2} = \frac{1}{2}\Big(\frac{\nu}{u_e x}\Big)^{\frac{1}{2}}F''(0) = \frac{0.664}{Re_x^{\frac{1}{2}}}$$

and similarly, using the relations derived last lecture,

$$C_f = 1.328Re_c^{-\frac{1}{2}}, \qquad , \frac{\delta^*}{x} = 1.721Re_x^{-\frac{1}{2}}, \qquad \frac{\theta}{x} = 0.664Re_x^{-\frac{1}{2}}$$

It should be noted that the values for these properties calculated last lecture using a linear profile are not that different, and hence for some situations even such a crude approximation as a linear velocity profile can give useful figures.

12.2 Similar Solutions, Incompressible Flow

Having found an exact solution for the flow over a flat plate, the question naturally arises as to whether solutions for the flow over more complex surfaces using the same approach are possible. The answer to this is yes, but only for a limited number of types of flow. These flows are characterised by possessing similar profiles, i.e. as for the flat plate problem, the velocity profile u/u_e is the same all through the flow, as long as the normal distance is scaled with the boundary layer thickness. The most useful of these special cases is when $u_e = \text{const.}x^n$.

$\eta = \frac{1}{2}y\left(\frac{u_e}{\nu x}\right)^{\frac{1}{2}}$	F	$\frac{1}{2}F'(=\frac{u}{u_e})$
0.0	0.0	0.0
0.1	0.0066	0.0664
0.2	0.0266	0.1328
0.3	0.0597	0.1989
0.4	0.1061	0.2647
0.5	0.1656	0.3298
0.6	0.2380	0.3938
0.8	0.4203	0.5168
1.0	0.6500	0.6298
1.2	0.9223	0.7290
1.4	1.2310	0.8112
1.6	1.5691	0.8761
1.8	1.9295	0.9233
2.0	2.3058	0.9555
2.5	3.2833	0.9916
3.0	4.2976	0.9990
3.5	5.2793	0.9999
4.0	6.2792	1.0000

Table 2: *The Blasius Profile*

As before, we have incompressible, steady flow, and hence the only difference between the equations of motion for this case as opposed to that of the flat plate is the inclusion of the pressure term in the x direction.

$$\frac{\partial u}{\partial x} + \frac{\partial v}{\partial y} = 0 \tag{100}$$

$$u\frac{\partial u}{\partial x} + v\frac{\partial u}{\partial y} = -\frac{1}{\rho}\frac{dp}{dx} + \nu\frac{\partial^2 u}{\partial y^2} \tag{101}$$

However, in the flow just outside the boundary layer, by our definition we may ignore the viscous terms, and hence we have

$$u_e\frac{\partial u_e}{\partial x} = -\frac{1}{\rho_e}\frac{\partial p}{\partial x}$$

Because the flow is incompressible, $\rho = \rho_e$, which allows to rewrite the momentum equation as

$$u\frac{\partial u}{\partial x} + v\frac{\partial u}{\partial y} = u_e\frac{\partial u_e}{\partial x} + \nu\frac{\partial^2 u}{\partial y^2}$$

We may then write

$$u_e = u_0(x/L)^n$$

where u_0 and L are a reference velocity and length respectively, and if we use the same definition of η as before we get

$$\eta = \frac{y}{2}\left(\frac{u_e}{\nu x}\right)^{\frac{1}{2}} = \frac{y}{2}\left(\frac{u_0}{\nu}\right)^{\frac{1}{2}}\left(\frac{x^{\frac{n-1}{2}}}{L^{\frac{m}{2}}}\right)$$

and as before

$$\varphi = (u_e \nu x)^{\frac{1}{2}} F(\eta) = (u_0 \nu)^{\frac{1}{2}} \left(\frac{x^{\frac{n+1}{2}} F(\eta)}{L^{\frac{n}{2}}} \right)$$

and by differentiation

$$u = \frac{\partial \varphi}{\partial y} = \frac{u_e}{2} F'(\eta)$$

By a similar process to that for flat plate flows, the stream function may be differentiated and substituted for the velocities and their differentials in the momentum equation. After some algebraic manipulation, we find that the equation requiring solution is

$$F''' + (n+1)FF'' - 2n(F')^2 + 8n = 0$$

with boundary conditions $F = F' + 0$ at $\eta = 0$, and $F' = 2$ at $\eta = \infty$. The solution of this equation is simplified somewhat by introducing a new variable ξ such that

$$\xi = \eta\big(2(n+1)\big)^{\frac{1}{2}} = y\big(\frac{1}{2}(n+1)\frac{u_e}{\nu x}\big)^{\frac{1}{2}}$$

and thus

$$f(\xi) = \big(\frac{1}{2}(n+1)\big)^{\frac{1}{2}} F(\eta)$$

so that $u/u_e = f'(\xi)$. This allows the equation to be solved to be written as

$$f''' + ff'' + \frac{2n}{n+1}(1 - (f')^2) = 0$$

with boundary conditions $f = f' = 0$ at $\xi = 0$, and $f' = 1$ at $\xi = \infty$, and now $'$ represents differentiation with respect to ξ. This equation is often refered to as the *Falkner-Skan* equation, and as with the Blasius solution must be solved numerically. Solutions with $n > 0$ represent accelerating flows, and hence favourable pressure gradients. For these flows, there is a unique solution for each n. If $n < 0$, the flow is decelerating (adverse pressure gradient), and an infinite number of solutions exist. However, only one of these has an exponential approach to the far field boundary condition, and as all the $n > 0$ solutions have this property, it is argued that this is the correct solution.

The numerical solution of this equation (which shall not be attempted) gives rise to a family of solutions which in the region $-0.05 < n < 0.5$ may be expressed approximately as

$$c_f = 1.28(n + 0.1)^{0.58} Re_x^{-\frac{1}{2}}$$
$$\frac{\delta^*}{x} = 0.71(n + 0.15)^{-0.47} Re_x^{-\frac{1}{2}}$$
$$\frac{\theta}{x} = 0.33(n + 0.22)^{-0.46} Re_x^{-\frac{1}{2}}$$
$$H = \frac{\delta^*}{\theta}$$

although it should be emphasised that these are fairly crude curve fits intended merely to allow us to do some numerical examples with rapidity. These curves are shown with some exact solutions to the Falkner-Skan Equations in figure 40.

Some important results produced by the actual equations (not the curve fits) are: if n equals 0, the Blasius solution is recovered exactly, as would be hoped, and if $n = -0.0904$, the local skin friction coefficient is zero, which implies separation.

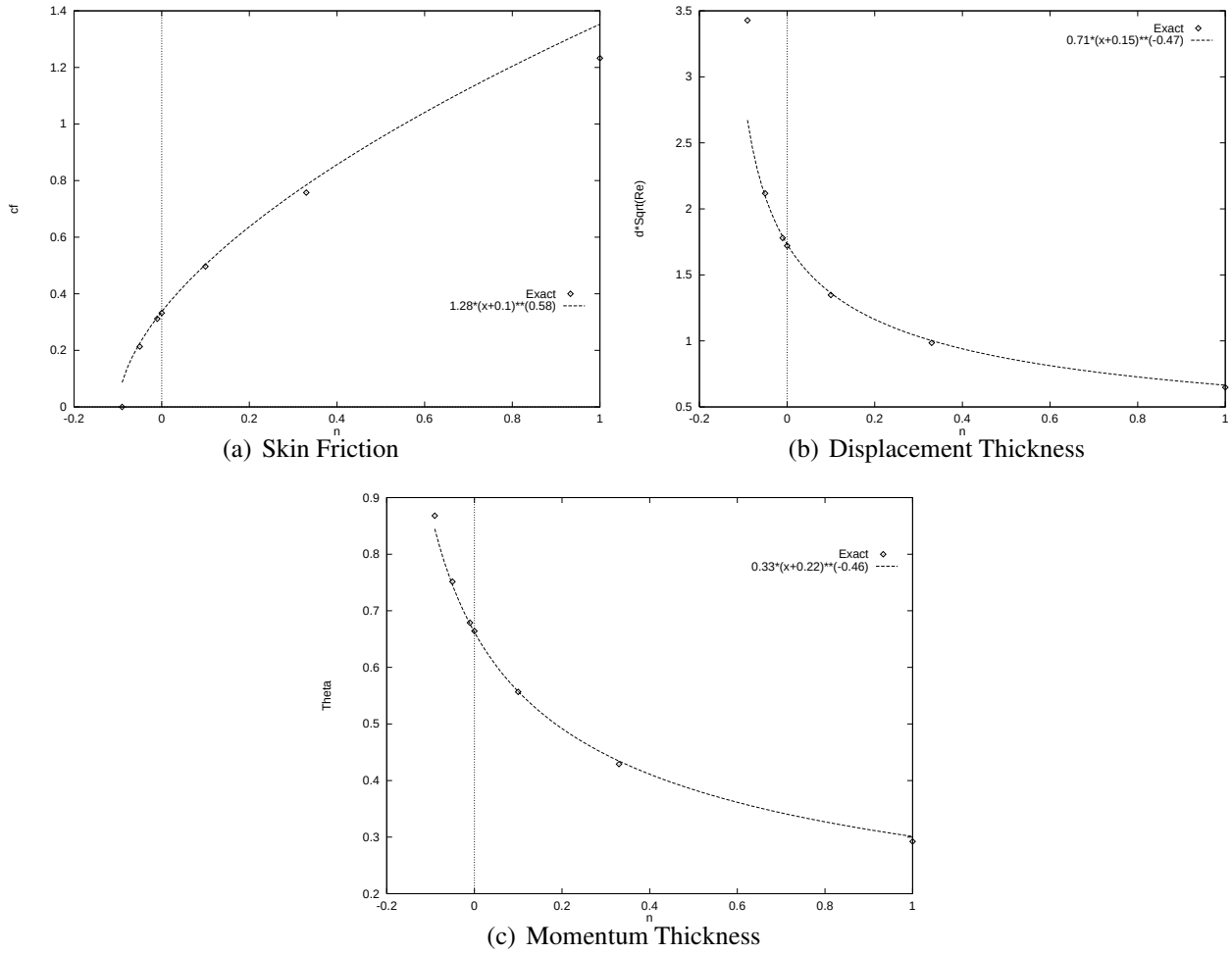

(a) Skin Friction (b) Displacement Thickness

(c) Momentum Thickness

Figure 40: *Effect of n on Boundary Layer Properties with the Falkner-Skan Transformation*

The usefulness of these results may be understood when the fact that the inviscid flow past a wedge of semi angle $\pi\beta/2$ at zero incidence is given by

$$u_e = \text{const.}x^{\beta/(2-\beta)} = \text{const.}x^n$$

where x is the distance from the nose is considered. In particular the case where β = 1 (i.e. a blunt nose) gives rise to the equation $u_e = \text{const.}x$, and hence allows the flow in the vicinity of a stagnation point to be calculated. There are other combinations of u_0 and n which are identifiable with flows of practical interest, but these are the most important.

12.3 Compressible Flows

In the preceding sections much use has been made of the fact that in incompressible flow the momentum and energy equations are independent, and hence only the momentum equation was generally considered (it should be noted at this point that a similar process can be used to derive temperature profiles from the energy equations to allow heat transfer problems to be investigated independent of the momentum equation, but these are more complex and generally of less use in aerodynamics, and have been ignored). In compressible flow, however, this is no longer the case, and hence both momentum and energy equations need be considered together.

Unfortunately, this of course increases the complexity of the mathematics involved, and we will not be going into it in this course. However, you need to be aware of how compressible flows may be analysed, usually by the principle of similar solutions, which requires identification of a mathematical transformation which allows a compressible boundary layer to be modelled as a *similar* incompressible one. The most commonly used method is the *Stewartson-Illingworth* transformation. Unfortunately, such methods are only strictly accurate in the case where either the Prandtl number, $\sigma, = 1$ (remember $\sigma_{air} \approx 0.7$), or $\rho\mu = \text{const}$. Fortunately, the dependence on σ is small, especially near 1, and hence such methods may be used to derive useful results.

12.3.1 Solution to last lecture's question

Show explicitly that

$$\frac{d}{dx}(\rho_e u_e^2 \theta) + \frac{du_e}{dx}\rho_e u_e \delta^* = \tau_w$$

may be expressed as

$$\frac{d\theta}{dx} + \frac{\theta}{u_e}\frac{du_e}{dx}(H+2) + \frac{\theta}{\rho_e}\frac{d\rho_e}{dx} = \frac{\tau_w}{\rho_e u_e^2}$$

where $H = \delta^*/\theta$

Answer Differentiating using the chain rule gives

$$\rho_e u_e^2 \frac{d\theta}{dx} + \rho_e \theta \frac{du_e^2}{dx} + u_e^2 \theta \frac{d\rho_e}{dx} + \rho_e u_e \delta^* \frac{du_e}{dx} = \tau_w$$

dividing through by $\rho_e u_e^2$, and noting that

$$\frac{du_e^2}{dx} = 2u_e \frac{du_e}{dx}$$

gives

$$\frac{d\theta}{dx} + \frac{2\theta}{u_e}\frac{du_e}{dx} + \frac{\theta}{\rho_e}\frac{d\rho_e}{dx} + \frac{\delta^*}{u_e}\frac{du_e}{dx} = \frac{\tau_w}{\rho_e u_e^2}$$

Gathering terms:

$$\frac{d\theta}{dx} + (\frac{2\theta}{u_e} + \frac{\delta^*}{u_e})\frac{du_e}{dx} + \frac{\theta}{\rho_e}\frac{d\rho_e}{dx} = \frac{\tau_w}{\rho_e u_e^2}$$

and finally as $H = \delta^*/\theta$, we have

$$\frac{d\theta}{dx} + \frac{\theta}{u_e}\frac{du_e}{dx}(H+2) + \frac{\theta}{\rho_e}\frac{d\rho_e}{dx} = \frac{\tau_w}{\rho_e u_e^2}$$

$Q.E.D.$

12.3.2 Question for next lecture

A wedge, semi-angle 20^0, is immersed in an incompressible flow with $\rho = 1.225Kg/m^3$ and $\mu = 1.8 * 10{-}5Kg/(ms)$, and a free stream velocity of $50m/s$. Using the approximation to the Falkner Skan equations given in this handout, calculate the displacement and momentum thicknesses 50cm downstream of the apex (measured along the surface of the wedge). Assume that the flow in this region is described exactly by

$$u_e = 2U_\infty x^n$$

where n is as defined above.

13 Application of Integral Methods

Key points: *Range of applicability of exact solutions. Thwaites method and uni-parametric assumption. Applicability of empirical methods. Stagnation point calculations*

13.1 Introduction

In the last handout we looked at exact solutions to the boundary layer equations (all be they numerically derived). However, whilst valuable as test cases for other methods, they are only applicable to a relatively small number of flowfields (i.e. those over flat plates, and about wedges). In order to allow the analysis of more complex shapes that do not conform to these restrictions on external velocity distributions, etc., only two alternative approaches are possible. One way is to solve the boundary layer equations numerically on finite volume grids through CFD analysis. This requires, however, very small grids and complex and time consuming methods for solving coupled equations. Even though modern computers are becoming ever more powerful, this still comprises a significant effort in most cases. Alternatively, the integral equations and properties we derived three lectures ago may be used to give approximate answers in much shorter time scales. The results produced by such methods are often surprisingly accurate, as they involve empirical quantities derived from a large numbers of experiments. The most widely used method in incompressible flow analysis is Thwaites method.

13.2 Thwaites Method

Thwaites method is applicable for incompressible, laminar boundary layers with and without pressure gradients. It introduces two dimensionless parameters l and m

$$l = \frac{\theta}{u_e}\Big(\frac{\partial u}{\partial y}\Big)_{wall} = \frac{\theta \tau_{wall}}{u_e \mu}, \qquad m = \frac{\theta^2}{u_e}\Big(\frac{\partial^2 u}{\partial y^2}\Big)_{wall}$$

The equations of motion in the boundary layer to be solved (from the derivation lecture) are

$$\frac{\partial u}{\partial x} + \frac{\partial v}{\partial y} = 0 \tag{102}$$

$$\frac{\partial u}{\partial t} + u\frac{\partial u}{\partial x} + v\frac{\partial u}{\partial y} = -\frac{1}{\rho}\frac{dp}{dx} + \nu\frac{\partial^2 u}{\partial y^2} \tag{103}$$

We know that at the wall, u and v are zero, hence for a steady flow (time derivatives are zero), from equation 103 we have

$$0 = -\frac{1}{\rho}\frac{dp}{dx} + \nu\frac{\partial^2 u}{\partial y^2}_{wall}$$

However, in the flow just outside the boundary layer, by our definition we may ignore the viscous terms, and hence we have

$$\frac{\partial u_e}{\partial t} + u_e\frac{\partial u_e}{\partial x} = -\frac{1}{\rho_e}\frac{dp}{dx}$$

and again assuming steady flows and substituting for the pressure derivative results in

$$\nu\frac{\partial^2 u}{\partial y^2}_{wall} = -u_e\frac{du_e}{dx}$$

(note this only true for incompressible flow where by definition $\rho_e = \rho_{wall}$). This being the case we may write

$$m = \frac{\theta^2}{u_e}\Big(\frac{\partial^2 u}{\partial y^2}\Big)_{wall} = \frac{\theta^2\nu}{u_e\nu}\Big(\frac{\partial^2 u}{\partial y^2}\Big)_{wall} = \frac{\theta^2(-u_e)}{u_e\nu}\Big(\frac{du_e}{dx}\Big) = -\frac{\theta^2}{\nu}\Big(\frac{du_e}{dx}\Big)$$

Examining these equations for l and m, we see that l is dependent on $\left(\frac{\partial u}{\partial y}\right)_{wall}$, the frictional stress at the wall, and m is dependent on the external velocity gradient. We then make the assumption that the velocity profiles are uni-parametric. When we examined the flow over a flat plate, it was supposed that the velocity profiles within the boundary layer were essentially the same everywhere, except that they scaled as the thickness of the boundary layer grew, i.e. the velocity at 20% of the boundary layer thickness was the same everywhere, it was merely the physical location of the point of 20% thickness that moved as the layer grew. We made this assumption principally because there was no reason to suppose it was *not* true, due to the fact that the external velocity, pressure, and density were the same everywhere, and hence there was no method by which disturbances to the boundary layer could be introduced to alter its velocity profile. In this case, we are allowing a velocity gradient in the external flow, and hence the shape of the velocity profile will depend on other parameters, as changes in the external velocity (and more importantly the *gradient* of that change) do introduce a method for profile distortion. However, we are assuming that there remains a family of curves which depend on only *one* other parameter, which in this case is m. Comparison with more accurate methods demonstrate that this is a reasonable assumption for favourable pressure gradients ($\frac{dp}{dx} < 0$), but less so for adverse ones.

The MIE derived in handout 11 is

$$\frac{d\theta}{dx} + \frac{\theta}{u_e}\frac{du_e}{dx}(H+2) = \frac{\tau_{wall}}{\rho u_e^2}$$

Multiplying through by θu_e, and introducing the parameters m and l:

$$\begin{aligned}
\theta u_e\frac{d\theta}{dx} + \theta^2\frac{du_e}{dx}(H+2) &= \frac{\theta\tau_{wall}}{\rho u_e} \\
\theta u_e\frac{d\theta}{dx} - \nu m(H+2) &= \frac{\mu}{\rho}l \\
u_e\frac{1}{2}\frac{d\theta^2}{dx} &= \nu l + \nu m(H+2) \\
u_e\frac{d\theta^2}{dx} &= 2\nu\big(m(H+2)+l\big)
\end{aligned}$$

which can be written

$$u_e\frac{d\theta^2}{dx} = \nu L(m) \qquad \text{where} \qquad L(m) = 2\big(m(H+2)+l\big)$$

By making use of a number of known exact and approximate solutions covering a wide range of pressure distributions, Thwaites defined this function as

$$L(m) = 0.45 + 6m$$

This may seem to some to be a bit of a fudge, but in fact semi empirical methods such as this often result in methods of good accuracy and wide ranging applicability, and such is the case here. The

usefulness of such methods depend on the accuracy of the underlying assumptions (in this case the uni-parametric nature of the boundary layer profile). However, if accurate, it allows the reduction of a wide range of data from varied experimental situations to a relatively simple equation such as the one above, that never the less accurately describes the flow behaviour in many cases (as noted previously, the method is more accurate in the case of favourable pressure gradients).

Using this definition of $L(m)$ results in the MIE reducing to

$$\begin{aligned} u_e\frac{d(\theta^2)}{dx} &= 0.45\nu - 6\theta^2\frac{du_e}{dx} \\ u_e\frac{d(\theta^2)}{dx} + 6\theta^2\frac{du_e}{dx} &= 0.45\nu \\ u_e^6\frac{d(\theta^2)}{dx} + 6u_e^5\theta^2\frac{du_e}{dx} &= 0.45u_e^5\nu \\ \frac{d}{dx}\left(u_e^6\theta^2\right) &= 0.45\nu u_e^5 \end{aligned}$$

This may be integrated from a sharp leading edge, where $\theta = 0, x = 0$, or from a stagnation point where $u_e = 0$, which in both cases removes the constants of integration and results in

$$\theta_{x1}^2 = 0.45\frac{\nu}{u_e^6}\int_0^{x1} u_e^5 dx$$

which is a relatively simple equation to solve numerically.

At a forward stagnation point on a bluff body (e.g. an aerofoil), there will be a finite initial thickness of θ (and also δ, as the flow will slow from freestream to zero velocity in a short, but finite, thickness, and hence a boundary layer forms immediately). To calculate this, we remember that last lecture we noted during the derivation of the Falkner-Skan equation that the flow near a stagnation point may be described as

$$u_e = Kx$$

where K is some constant (which may be found from the inviscid analysis results). Substituting this into the above equation results in

$$\begin{aligned} \theta_{x1}^2 &= 0.45\frac{\nu}{u_e^6}\int_0^{x1} u_e^5 dx \\ \Rightarrow \theta_{x1}^2 &= 0.45\frac{\nu}{K^6x^6}\left[\frac{1}{6}K^5x^6\right]_0^{x1} \\ \Rightarrow \theta_{x1}^2 &= \frac{0.45}{6}\frac{\nu}{K} \end{aligned}$$

i.e. the momentum thickness is constant in the region very near stagnation, and has a thickness that may be determined from freestream kinetic viscosity and a velocity gradient determined from inviscid flow.

13.2.1 Using Thwaites Method

Thwaites method may used in the following way (it is re-iterated at this point that the method is *only* applicable to two dimensional, incompressible, steady flows). First, an inviscid solution of the flow

m	l	H	m	l	H
-0.25	0.500	2.00	0.040	0.153	2.81
-0.20	0.463	2.07	0.048	0.138	2.87
-0.14	0.404	2.18	0.056	0.122	2.94
-0.12	0.382	2.23	0.060	0.113	2.99
-0.10	0.359	2.28	0.064	0.104	3.04
-0.08	0.333	2.34	0.068	0.095	3.09
-0.064	0.313	2.39	0.072	0.085	3.15
-0.048	0.291	2.44	0.076	0.072	3.22
-0.032	0.268	2.49	0.080	0.056	3.30
-0.016	0.244	2.55	0.084	0.038	3.39
0.0	0.220	2.61	0.086	0.027	3.44
0.016	0.195	2.67	0.088	0.015	3.49
0.032	0.168	2.75	0.090	0.0	3.55

Table 3: *Thwaites Parameters*

about the body is used to derive values for u_e at as many points as are deemed required about the aerofoil. θ^2 may then be calculated directly at all these points (assuming known ν, which is of course constant in incompressible flow). However, the two properties we really need to know are H, as this will allow us to calculate the displacement thickness δ^*, and l, as this gives us τ_{wall}. (Note that due to the MIE these are dependent on each other, and hence in theory one may be used to calculate the other). The relationship of these properties to m have been calculated using a range of exact solutions (most notably by Curle and Skan), and are given in table 3. Alternatively we may use Cebeci and Bradshaws formulae:

$$l(n) = \begin{cases} 0.22 - 1.57m - 1.8m^2 & \text{for } -0.1 < m < 0.0 \\ 0.22 - 1.402m - \frac{0.018m}{0.107-m} & \text{for } 0.0 < m < 0.1 \end{cases}$$

$$H(n) = \begin{cases} 2.61 + 3.75m + 5.24m^2 & \text{for } -0.1 < m < 0.0 \\ 2.088 + \frac{0.0731}{0.14-m} & \text{for } 0.0 < m < 0.1 \end{cases}$$

13.2.2 Numeric Example

Consider the flow along a flat plate with a mildly favourable pressure distribution at sea level (i.e. $\nu = 1.461 * 10^{-5}$) such that the external velocity is

$$u_e = 30(1 + 0.2x)$$

within the range $0 \leq x \leq 1$. Using say 5 control points at $x = 0, 0.2, 0.4, 0.6, 0.8$, and 1.0, we may derive the following values:

From these values, and as

$$\frac{du_e}{dx} = \frac{d}{dx}\big(30(1 + 0.2x)\big) = 6$$

we may go on to calculate

If we take, for instance, the final column, and compare it with the Blasius solution derived last week $\delta^*/x = 1.721Re^{-\frac{1}{2}}$, using the flow at the trailing edge gives us $Re_{te} = \frac{1.225*36*1.0}{1.789*10^{-5}} = 2.465 * 10^6$ and

x	u_e	u_e^5	$\sum_0^x u_e^5 \Delta x$	U_e^6	θ^2
0.0	30	$24.3 * 10^6$	0	$729 * 10^6$	0.0
0.2	31.2	$29.56 * 10^6$	$5.386 * 10^6$	$0.922 * 10^9$	$3.839 * 10^{-8}$
0.4	32.4	$35.70 * 10^6$	$11.91 * 10^6$	$1.157 * 10^9$	$6.769 * 10^{-8}$
0.6	33.6	$42.82 * 10^6$	$19.76 * 10^6$	$1.439 * 10^9$	$9.029 * 10^{-8}$
0.8	34.8	$51.38 * 10^6$	$29.18 * 10^6$	$1.776 * 10^9$	$1.080 * 10^{-7}$
1.0	36.0	$60.47 * 10^6$	$40.36 * 10^6$	$2.177 * 10^9$	$1.219 * 10^{-7}$

Table 4: *Calculation of* θ^2

x	θ	$m(= -\frac{\theta^2}{\nu}\frac{du_e}{dx})$	l	$\tau_{wall}(= \frac{lu_e\mu}{\theta})$	H	δ^*
0.0	0.0	0	0.220	na	2.61	0.0
0.2	$1.959 * 10^{-4}$	-0.016	0.244	0.695	2.55	$5.00 * 10^{-4}$
0.4	$2.602 * 10^{-4}$	-0.028	0.262	0.584	2.51	$6.53 * 10^{-4}$
0.6	$3.005 * 10^{-4}$	-0.037	0.275	0.550	2.47	$7.42 * 10^{-4}$
0.8	$3.286 * 10^{-4}$	-0.044	0.285	0.540	2.45	$8.05 * 10^{-4}$
1.0	$3.491 * 10^{-4}$	-0.050	0.294	0.542	2.43	$8.48 * 10^{-4}$

Table 5: *Calculation of Other Parameters*

hence $\delta^* = 10.96 * 10^{-4}$, which is similar, although slightly larger than the value calculated here. In fact, for a constant velocity profile, the difference between Thwaites method and the exact Blasuis solution is only about 1%, and the majority of the difference here is due to the velocity gradient, and associated favourable pressure gradient retarding its growth.

Before moving on to compressible flows, it is worth noting at this point that other more complex methods do exist for incompressible flows, which are of particular use for adverse pressure gradients and near separated flows. These are based on using results from both the MIE and the similar Kinetic Energy Integral Equation, and the most accurate of these approximate methods is probably that due to Head, which allows a two parameter model of the velocity profile, as opposed to the one parameter method of Thwaite.

13.3 Compressible flows

As usual, the mathematics involved in the derivation and application of compressible methods is too complex to be gone into any detail here. There are several methods for dealing with compressible flows (e.g. Cohen and Reshotko, Luxton and Young), but generally these are based upon the Stewartson-Illingworth transformation, and as was noted previously this means they require assumptions of a unit Prandtl number, or constant $\rho\mu$. Whilst still of some use, they are more complex, and hence the benefit of applying such methods compared to finite difference (CFD) techniques (which do not require the previous assumptions) is less. It should also be remembered that incompressible assumption in a boundary layer is broader in application than for inviscid flow, as the velocity is greatly retarded in a large part of it.

13.3.1 Solution to last weeks Question

A wedge, semi-angle 20^0, is immersed in an incompressible flow with $\rho = 1.225Kg/m^3$ and $\mu = 1.8 * 10{-}5Kg/(ms)$, and a free stream velocity of $50m/s$. Using the approximation to the Falkner Skan equations given in this handout, calculate the displacement and momentum thicknesses 50cm downstream of the apex (measured along the surface of the wedge).

Answer The semi-angle of the wedge is 20^0, or $0.349R$. Hence

$$\beta = \frac{2 \times 0.349}{\pi} = 0.22$$

This means that

$$n = \frac{\beta}{2 - \beta} = 0.125$$

At $50cm$ from the nose, the Reynolds number is given by

$$Re_x = \frac{\rho u_e x}{\mu} = \frac{1.225 \times 2 \times 50 \times 0.5^{0.125} \times 0.5}{1.8 \times 10^{-5}} = 3.12 \times 10^6$$

Hence

$$\begin{aligned} \delta^* &= 0.5\Big(0.71(0.125 + 0.15)^{-0.47}(3.12 \times 10^6)^{-\frac{1}{2}}\Big) \\ &= 0.369mm \\ \theta &= 0.5\Big(0.33(0.125 + 0.22)^{-0.46}(3.12 \times 10^6)^{-\frac{1}{2}}\Big) \\ &= 0.152mm \end{aligned}$$

14 Squire Young Method for Aerofoil Drag Prediction

14.1 Introduction

Thwaites method, and other similar techniques, allow the development of the boundary layer around an aerofoil to be calculated. From this, integration of the local skin friction coefficient will allow an estimate of the skin friction drag, but the effect of displacement thickness on the pressure distribution, and hence the impact of profile drag, is more difficult to estimate directly. In order to get around this problem, Squire and Young developed a method which allows an estimate of the total drag of the aerofoil due to the presence of the boundary layer to be estimated directly. This is the subject of this weeks lecture.

14.2 Control Volume Analysis

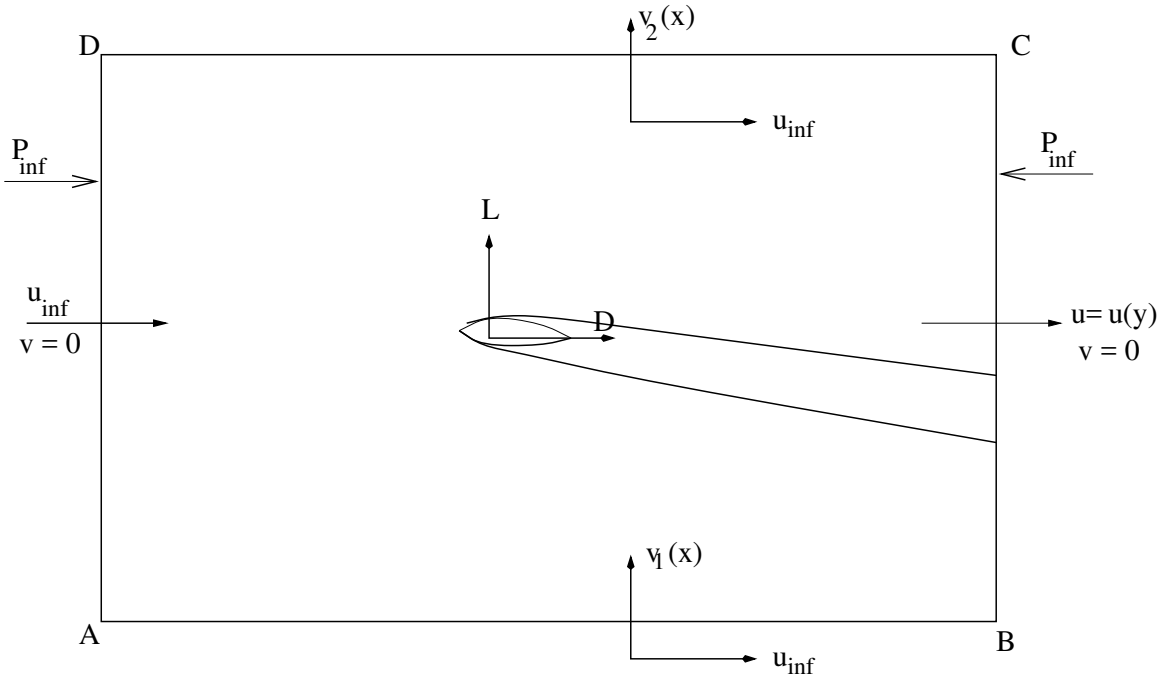

Consider a control volume around an aerofoil as shown above. Assuming incompressible flow, from conservation of mass we have

$$\int_A^B V_1(x)dx - \int_B^C U(y)dy - \int_D^C V_2(x)dx + \int_A^D U_\infty dy = 0 \tag{104}$$

Also, as no forces act at the boundaries (pressure terms cancel), any momentum imbalance must be equal and opposite to the force acting on the aerofoil. In the x direction, the force acting on the aerofoil is the drag, and hence

$$\int_A^D \rho_\infty U_\infty^2 dy + \int_A^B \rho_\infty U_\infty V_1(x)dx - \int_D^C \rho_\infty U_\infty V_2(x)dx - \int_B^C \rho_\infty U^2(y)dy = Drag \tag{105}$$

But as ρ_∞, U_∞ are constants,

$$\int_A^B \rho_\infty U_\infty V_1(x)dx - \int_D^C \rho_\infty U_\infty V_2(x)dx = \rho_\infty U_\infty \left[\int_A^B V_1(x)dx - \int_D^C V_2(x)dx \right]$$

and from Equation (104)

$$= \rho_\infty U_\infty \left[\int_B^C U(y)dy - \int_A^D U_\infty dy \right]$$

Substituting this for the middle two terms of Equation (105) gives a momentum loss of

$$\begin{aligned} Drag &= \int_A^D \rho_\infty U_\infty^2 dy + \rho_\infty U_\infty \int_B^C U(y)dy - \rho_\infty U_\infty \int_A^D U_\infty dy - \int_B^C \rho_\infty U^2(y)dy \\ &= \rho_\infty U_\infty \int_B^C U(y)dy - \int_B^C \rho_\infty U^2(y)dy \\ &= \rho_\infty U_\infty^2 \int_B^C \frac{U(y)}{U_\infty}\left(1 - \frac{U(y)}{U_\infty}\right)dy = \rho_\infty U_\infty^2 \theta_\infty \end{aligned}$$

and hence

$$Drag = \rho_\infty U_\infty^2 \theta_\infty = C_D \frac{1}{2} \rho_\infty U_\infty^2 c \qquad \text{(per unit span)} \tag{106}$$

$$\Rightarrow C_D = \frac{2\theta_\infty}{c} \tag{107}$$

This result means that if we can predict how θ varies in the wake, and thus obtain θ_∞, we can predict the aerofoil drag.

14.3 Flow in the Wake

As there is no solid surface in the wake, there can be no skin friction, which means that the MIE is

$$\frac{d\theta}{dx} + (H+2)\frac{\theta}{u_e}\frac{du_e}{dx} = 0$$

Inviscid analysis of the aerofoil will provide u_e at the trailing edge, and the boundary layer integral properties may be found by simply summing the values on the upper and lower surfaces

$$\begin{aligned} \theta_{t.e.} &= \theta_{upper} + \theta_{lower} \\ \delta^*_{t.e.} &= \delta^*_{upper} + \delta^*_{lower} \\ H_{t.e.} &= \frac{\delta^*_{t.e.}}{\theta_{t.e.}} \end{aligned}$$

Far downstream, $u_e \to U_\infty$ and $\theta \to \theta_\infty$. We also need to know H_∞ in order to solve the momentum integral equation.

Consider the velocity distribution in the wake:

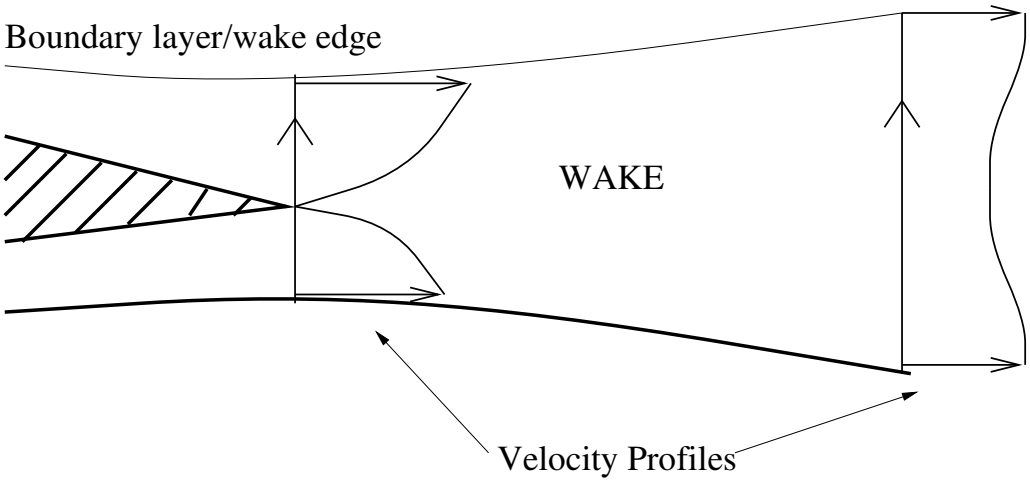

Near the aerofoil, the wake has a large velocity reduction in the centre (due to the no slip condition at the tip of the t.e., which demands that the velocity there be zero). Far downstream, the viscosity in the wake region has produced mixing, which causes the wake to widen (due to entrainment of the outer inviscid flow), but the deficit is reduced (due to the mixing of the lower speed flow with neighbouring higher speed flows).

It has been experimentally verified that far from the aerofoil, the wake velocity profile may be approximated as

$$U(y) \approx u_e\left(1 - \frac{U_{deficit}}{u_e}\cos^2\left(\frac{\pi y}{2\delta}\right)\right)$$

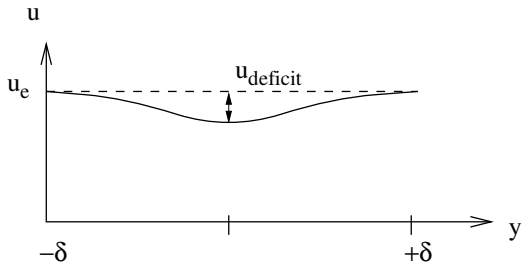

So the integral quantities in the wake are

$$\delta^* = \int_{-\delta}^{\delta} 1 - \left(1 - \frac{u_{deficit}}{u_e}\cos^2\left(\frac{\pi y}{2\delta}\right)\right)dy$$

$$\Rightarrow \delta^* = \frac{u_{deficit}}{u_e}\int_{-\delta}^{\delta}\cos^2\left(\frac{\pi y}{2\delta}\right)dy$$

but

$$\int_{-\delta}^{\delta}\cos^2\left(\frac{\pi y}{2\delta}\right)dy = \text{const.}$$

$$\Rightarrow \delta^* = \frac{u_{deficit}}{u_e} \times \text{const.}$$

Turning to the momentum thickness, we have

$$\theta = \int_{-\delta}^{\delta} \frac{u(y)}{u_e}\left(1 - \frac{u(y)}{u_e}\right)dy = \frac{u_{deficit}}{u_e}\int_{-\delta}^{\delta} \cos^2\left(\frac{\pi y}{2\delta}\right)\left(1 - \frac{u_{deficit}}{u_e}\cos^2\left(\frac{\pi y}{2\delta}\right)\right)dy$$

$$\theta = \frac{u_{deficit}}{u_e}\int_{-\delta}^{\delta} \cos^2\left(\frac{\pi y}{2\delta}\right)dy - \left(\frac{u_{deficit}}{u_e}\right)^2\int_{-\delta}^{\delta} \cos^4\left(\frac{\pi y}{2\delta}\right)dy$$

$$\Rightarrow \theta = \frac{u_{deficit}}{u_e} \times \text{const.} - \left(\frac{u_{deficit}}{u_e}\right)^2 \times \text{different const.}$$

As already mentioned, the further downstream we travel, the more the wake spreads and mixes, and hence $\frac{u_{deficit}}{u_e}$ reduces. As this is the case, $\left(\frac{u_{deficit}}{u_e}\right)^2$ must become very small, and may be neglected. This means that

$$\theta \to \delta^*$$

which in turn implies

$$H_\infty = 1.0$$

We now have values for the trailing edge H and farfield value. However, to integrate the MIE we need to know how H varies between these two. The simplest approximation is to assume that the variation is linear, i.e.

$$H_{average} = \frac{1}{2}(H_{t.e.} + H\infty) = \frac{1}{2}(H_{t.e.} + 1) \tag{108}$$

This allows the momentum integral equation to be integrated to produce θ_∞:

$$\frac{d\theta}{dx} + (H_{average} + 2)\frac{\theta}{u_e}\frac{du_e}{dx} = 0$$

Integrating form the t.e. to ∞:

$$\int_{t.e.}^{\infty} \frac{d\theta}{\theta} = -(H_{average} + 2)\int_{t.e.}^{\infty} \frac{du_e}{u_e}$$

$$[\ln(\theta)]_{t.e.}^{\infty} = -(H_{average} + 2)[\ln(u_e)]_{t.e.}^{\infty}$$

$$\ln(\theta_\infty) - \ln(\theta_{t.e.}) = -(H_{average} + 2)\Big(\ln(u_\infty) - \ln(u_{t.e.})\Big)$$

$$\ln\left(\frac{\theta_\infty}{\theta_{t.e.}}\right) = -(H_{average} + 2)\ln\left(\frac{u_\infty}{u_{t.e.}}\right)$$

Taking the exponent of both sides gives

$$\left(\frac{\theta_\infty}{\theta_{t.e.}}\right) = \left(\frac{u_\infty}{u_{t.e.}}\right)^{-(H_{average}+2)}$$

but from Equation (108)

$$H_{average} + 2 = 2 + \frac{1}{2}H_{t.e.} + \frac{1}{2} = \frac{5 + H_{t.e.}}{2}$$

which implies that

$$\theta_\infty = \theta_{t.e.}\left(\frac{u_{t.e.}}{u_\infty}\right)^{\left(\frac{H_{t.e.}+5}{2}\right)}$$

Substituting this into Equation (107) finally results in

$$C_D = \frac{2\theta_\infty}{c} = \frac{2\theta_{t.e.}}{c}\left(\frac{u_{t.e.}}{u_\infty}\right)^{\left(\frac{H_{t.e.}+5}{2}\right)}$$

which gives us the important result that the drag coefficient of the aerofoil may be computed using only the quantities at the trailing edge.

In conclusion therefore, we now have methods available that allow direct calculation of the drag of an aerofoil, including both skin friction and that due to displacement thickness, directly from the inviscid flow solution. The Squire Young method does depend upon an assumption of linear H in the wake, but this has been demonstrated to be of good accuracy for most aerofoil shapes provided that the incidence is reasonably small (and of course there is no separation). Finally, it should be noted that the method depends only on the values for momentum thickness and velocity at the trailing edge, and makes no assumptions about the velocity profiles. The method is therefore just as applicable to turbulent boundary layers as to laminar.

15 Turbulent Boundary Layers

Key points: *Concept of a turbulent eddy, time averaging and time scales of turbulence. The turbulent flow thin layer equations, and the concept of turbulent viscosity. The structure of a turbulent boundary layer, and the idea of intermittency at the edge.*

15.1 Introduction

Turbulence remains the most complex, least understood phenomena facing aerodynamic analysis. It is characterised by the presence of rapid fluctuations of flow properties, even under steady macroscopic conditions. This means, for example, that an aerofoil of fixed geometry immersed in a flow that is uniform in space and time at upstream farfield will still be subjected to considerable variation in flow properties with time at any given point on the surface due to the presence of these fluctuations, known as eddies.

These eddies vary in size and composition, but fortunately tend to form cohesive structures, known as vortex filaments. This means that a turbulent flow may be thought of as a collection of parcels of flow being transmitted downstream. Analysing the behaviour of each little packet individually is impossible, but a time averaging approach does provide useful results. Whilst at first this may seem a little strange, it should be remembered that our approach to analysis of any fluid is similar. In reality a fluid is a collection of individual molecules, but there is no need to calculate the motion of each and every one, instead an average motion may be used. This forms the basis of the continuum assumption.

Laminar boundary layers become turbulent through a process known as transition, which we shall discuss in more detail in a later lecture. For now, however, it is enough to know that the process is highly Reynolds number dependent (the higher the Re the more likely transition is), but it is also significantly affected by such things as surface roughness, disturbances in the outer flow, and pressure gradients. The principle effect of transition is the change in behaviour of the flow in response to a small disturbances; in a laminar flow they are rapidly damped by the action of molecular viscosity, whilst in a turbulent flow the disturbances grow.

15.2 Time Scales and Time Averages of Turbulent Flows

Despite the complexity of the detail of the motion in a turbulent boundary layer, it is possible to use statistical analysis methods to produce useful results. In general, the knowledge of the exact behaviour at any location is not necessary for an aerodynamicist, what is of importance is macroscopic properties like lift and drag. While these values will vary over very short time periods, over any reasonably sensible time scale, an average value will prove sufficient. As the time scales related to both cruise and manoeuvring flight are far greater than the time scales of turbulence, such approximations produce accurate results.

Consider the velocity profile in a boundary layer. You were introduced to a ‘typical’ turbulent velocity profile in the first handout dealing with boundary layers, where it was noted that due to the mixing process, the velocity profile was more uniform (or ‘fuller’) than an equivalent laminar one. However, implicit in such a profile is this concept of time averaging; in reality a turbulent boundary layer velocity profile at a particular point in space will be constantly changing. Only by averaging over a

reasonable period of time, do we end up with a profile which may be characterised via appropriate equations (see fig. 41). Once this is done, however, we may use this time averaged profile in the equations for δ^*, θ, and the MIE as we did previously with laminar boundary layers.

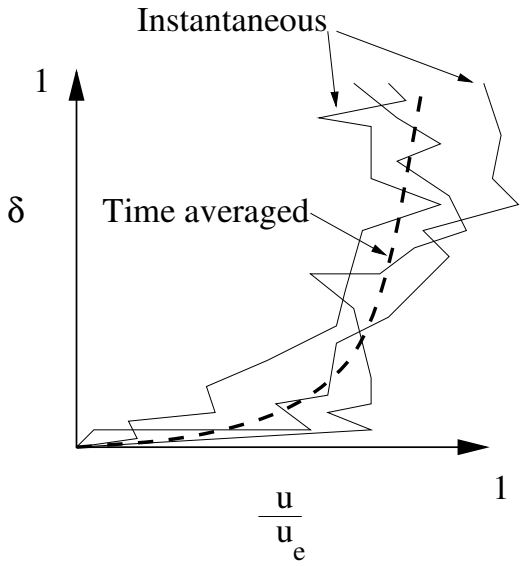

Figure 41: Velocity Profiles in a Turbulent Boundary Layer (Exaggerated)

15.3 The Turbulent Boundary Layer Equations

As we have oft noted, laminar boundary layers are governed by two equations, the continuity and x momentum equations

$$\frac{\partial u}{\partial x} + \frac{\partial v}{\partial y} = 0$$
$$u\frac{\partial u}{\partial x} + v\frac{\partial u}{\partial y} = -\frac{1}{\rho}\frac{dp}{dx} + \nu\frac{\partial^2 u}{\partial y^2}$$

Implicit is the assumption that u, v etc. are not functions of time (this is the definition of a steady flow, one of the assumptions used to derive these equations). However, in a turbulent layer, even if the overall flow is steady, u, v are still varying in time to a some small extent (see fig 42), and hence

$$u = \hat{u} + u'; \qquad v = \hat{v} + v'$$

etc., where for example $\hat{u}$ is the average value found from

$$\hat{u} = \frac{1}{2T}\int_{t-T}^{t+T} u.dt \tag{109}$$

where the time interval $2T$ is much greater than the period of fluctuation of u, and u' is the fluctuating component of velocity about this mean.

Putting these into the continuity equation gives

$$\frac{\partial u}{\partial x} + \frac{\partial v}{\partial y} = \frac{\partial \hat{u} + u'}{\partial x} + \frac{\partial \hat{v} + v'}{\partial y} = 0$$

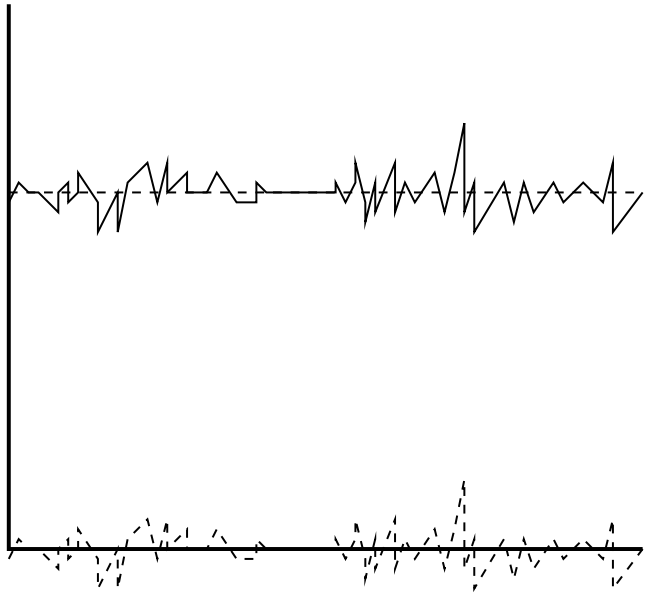

Figure 42: Flow Variable Time History in a Turbulent Flow

taking the time average (denoted by an overline) of this gives

$$\overline{\frac{\partial \hat{u} + u'}{\partial x}} + \overline{\frac{\partial \hat{v} + v'}{\partial y}} = 0$$
$$\Rightarrow \overline{\frac{\partial \hat{u}}{\partial x}} + \overline{\frac{\partial u'}{\partial x}} + \overline{\frac{\partial \hat{v}}{\partial y}} + \overline{\frac{\partial v'}{\partial y}} = 0$$

If q is some variable, then $\overline{\hat{q}}$ (the time average of a time average) is just the time average $\hat{q}$, as this is by definition constant in time. Similarly the time average of $\frac{\partial \hat{q}}{\partial x}$ is just $\frac{\partial \hat{q}}{\partial x}$ as this gradient is also constant in time. Secondly, the time average of a fluctuating component (e.g. q') is by definition 0, as can be seen from Eqn. 109, and hence the derivative of the time average of q' is also zero. This means we may express the above as

$$\frac{\partial \hat{u}}{\partial x} + \frac{\partial \hat{v}}{\partial y} = 0$$

and we see we have the same equation for continuity that we had in laminar flows, as long as we only deal with the time averaged velocities.

The x momentum equation given previously is in *non-conservative* form, but here it is easier to deal with the *conservative form*

$$\frac{\partial u^2}{\partial x} + \frac{\partial uv}{\partial y} = -\frac{1}{\rho}\frac{dp}{dx} + \nu\frac{\partial^2 u}{\partial y^2}$$

(consult handout 'Boundary Layer Integral Equations' if you are not sure why these are equivalent). Now, again considering some quantity q, then

$$\frac{\partial q^2}{\partial x} = \frac{\partial(\hat{q} + q')^2}{\partial x} = \frac{\partial(\hat{q}^2 + 2\hat{q}q' + q'^2)}{\partial x}$$
$$= \frac{\partial \hat{q}^2}{\partial x} + 2\frac{\partial \hat{q}q'}{\partial x} + \frac{\partial q'^2}{\partial x} = \frac{\partial \hat{q}^2}{\partial x} + 2\hat{q}\frac{\partial q'}{\partial x} + 2q'\frac{\partial \hat{q}}{\partial x} + \frac{\partial q'^2}{\partial x}$$

When time averaged, all of the parts of the form q' or its derivative become zero, as do those of this form but multiplied by an already averaged (and therefore constant) quantity, and we get

$$\overline{\frac{\partial q^2}{\partial x}} = \frac{\partial \hat{q}^2}{\partial x} + 0 + 0 + \overline{\frac{\partial q'^2}{\partial x}} = \frac{\partial \hat{q}^2}{\partial x} + \overline{\frac{\partial q'^2}{\partial x}}$$

Substituting for u, v, p in the x-momentum equation and time averaging gives

$$\frac{\partial \hat{u}^2}{\partial x} + \overline{\frac{\partial u'^2}{\partial x}} + \overline{\frac{\partial (\hat{u}+u')(\hat{v}+v')}{\partial y}} = -\frac{1}{\rho}\overline{\left(\frac{d\hat{p}}{dx} + \frac{dp'}{dx}\right)} + \nu\overline{\frac{\partial}{\partial y}\left(\frac{\partial(\hat{u}+u')}{\partial y}\right)}$$

$$\Rightarrow \frac{\partial \hat{u}^2}{\partial x} + \overline{\frac{\partial u'^2}{\partial x}} + \overline{\frac{\partial \hat{u}\hat{v}}{\partial y}} + \overline{\frac{\partial u'\hat{v}}{\partial y}} + \overline{\frac{\partial v'\hat{u}}{\partial y}} + \overline{\frac{\partial u'v'}{\partial y}} = -\frac{1}{\rho}\overline{\left(\frac{d\hat{p}}{dx} + \frac{dp'}{dx}\right)} + \nu\overline{\frac{\partial}{\partial y}\left(\frac{\partial \hat{u}}{\partial y} + \frac{\partial u'}{\partial y}\right)}$$

Again, when time averaged, all of the parts of the form q' or its derivative become zero (and hence all terms and derivatives of the form $\hat{q}p'$ are also zero by the chain rule), and we get

$$\frac{\partial \hat{u}^2}{\partial x} + \overline{\frac{\partial u'^2}{\partial x}} + \frac{\partial \hat{u}\hat{v}}{\partial y} + 0 + 0 + \overline{\frac{\partial u'v'}{\partial y}} = -\frac{1}{\rho}\left(\frac{d\hat{p}}{dx} + 0\right) + \nu\frac{\partial}{\partial y}\left(\frac{\partial \hat{u}}{\partial y} + 0\right)$$

$$\Rightarrow \frac{\partial \hat{u}^2}{\partial x} + \frac{\partial \hat{u}\hat{v}}{\partial y} = -\frac{1}{\rho}\frac{d\hat{p}}{dx} + \nu\frac{\partial^2 \hat{u}}{\partial y^2} - \left(\overline{\frac{\partial u'^2}{\partial x}} + \overline{\frac{\partial u'v'}{\partial y}}\right)$$

Or, multiplying by ρ and collecting terms,

$$\rho\left(\frac{\partial \hat{u}^2}{\partial x} + \frac{\partial \hat{u}\hat{v}}{\partial y}\right) = -\frac{d\hat{p}}{dx} + \frac{\partial}{\partial y}\left(\mu\frac{\partial u}{\partial y} - \rho\overline{u'v'}\right) - \rho\overline{\frac{\partial u'^2}{\partial x}}$$

This is essentially the same x momentum equation as for laminar flow (again noting that we are dealing here with average not instantaneous values), but with two extra terms on the right hand side. As these are both of the form of a constant times a velocity derivative, they are known as *Reynolds stresses* or *turbulent shear stresses*. In a general three dimensional turbulent flow there are nine, corresponding to the usual shear stress tensor (i.e. $\tau_{xx}, \tau_{xy}, \tau_{xz}$, etc.). The reason we have only two is due to the prior application of the boundary layer assumptions, and the fact that we only consider one momentum equation. In compressible flows, the density also has a fluctuating component ρ', and things become even more complex, with a further 20+ terms in the three momentum equations. It is thus easy to see why compressible turbulent flows in particular are poorly understood.

Returning to the simplified equation above, we can appeal to the thin layer assumption once again, and state that as

$$\frac{\partial}{\partial y} >> \frac{\partial}{\partial x}$$

the first of these stresses dominates the latter, which we neglect. But what about this quantity $-\rho u'v'$?

Consider first a parcel of fluid moving from some level y in the boundary layer towards the surface (i.e. v is negative). Flow higher up in the boundary layer has a higher velocity than that below, and hence this parcel has a higher u than the flow it moves into. This means that u' is positive, and hence so is $-\rho u'v'$. A similar argument can be made in reverse to show that if v is positive, the parcel of flow is moving into a region of higher u, and hence u' is negative, and once again $-\rho u'v'$ is positive. This means that this stress is always positive, and may become significant if the fluctuations are large. Noting that it is given by the product of density and two velocity fluctuations, this term can

be expressed as an x-momentum flux, and through the equivalence of momemtum change and force, this may in turn be expressed as a shear stress.

Remembering that $\mu\frac{\partial u}{\partial y}$ is the expression for the molecular induced viscosity associated with laminar boundary layers, now denoted τ_l, it is logical to label $-\rho\overline{u'v'}$ as the turbulent viscosity τ_t. Boussinesq hypothesised in 1877 that this viscosity could be linearly related to the derivative of velocity in the same way as the molecular viscosity, i.e.

$$\tau_t = -\rho\overline{u'v'} = \mu_t\frac{\partial u}{\partial y}$$

where μ_t is the *eddy viscosity coefficient*. This concept is of fundamental importance, particularly with respect to turbulence modelling.

15.4 The Structure of a Turbulent Boundary Layer

Before discussing the structure of a turbulent boundary layer, we need to introduce two further parameters:
Friction Velocity The friction velocity, u_t, is related to the wall friction, and is defined as

$$u_t = \sqrt{\frac{\tau_w}{\rho}}$$

Wall Units Dimensions normal to the wall in turbulent boundary are often expressed in terms of 'wall units' (y^+), a non dimensional number given by

$$y^+ = \frac{yu_t}{\nu}$$

which is in fact a Reynolds number based on u_t and the distance from the wall.

Very close to the wall, the no-slip condition means that not only must the mean velocity be zero at the wall, but also the fluctuating components $u'v'$ are too. This means that the turbulent viscosity ($-\rho u'v'$) tends to zero, and the flow behaves in a laminar fashion. For this reason the innermost region is known as the *viscous sub-layer*. It is extremely thin, generally less than one hundredth of the total boundary layer thickness, or about 10 wall units. In this region, the mean velocity varies in an almost exactly linear fashion with distance from the wall, and hence the shear stress is assumed constant and equal to the wall shear stress, τ_{wall}, i.e.

$$\tau_{wall} = \mu\frac{\partial u}{\partial y}$$

This means that

$$u = \frac{\tau_{wall}y}{\mu}$$
$$\Rightarrow \frac{u}{u_t} = \frac{\tau_{wall}y}{\mu u_t} = \frac{\rho u_t^2 y}{\mu u_t} = \frac{u_t y}{\nu} = y^+$$

Outside the viscous sub-layer, the behaviour of the flow is dominated by the turbulent eddies, and hence the turbulent shear stresses dominate the viscous stress. The *inner layer*, extends to about 40% of the thickness of the boundary layer, and is a region containing a wide range of eddy frequencies and sizes. Outside of this is the outer layer, which is in many ways similar except that the edge of boundary layer, itself time variant, lies somewhere in this region. The instantaneous edge of the boundary layer may range from 0.4 to 1.2 of the average value, and hence the outer layer is characterised by *intermittency*. This means that at any given (x, y) location that lies within this outer boundary layer region, the flow will at times be laminar, and at times turbulent. The nearer the wall, the more time in a given interval will be spent in a turbulent regime, and vice-versa. This intermittency is generally modelled using the *The Klebanoff Intermittency Function*, the details of which are beyond the scope of this course.

15.4.1 Exercise for Next Week:

Sketch 'typical' velocity profiles for a turbulent and equivalent laminar boundary layers. What is the principle reason for the difference in shape?

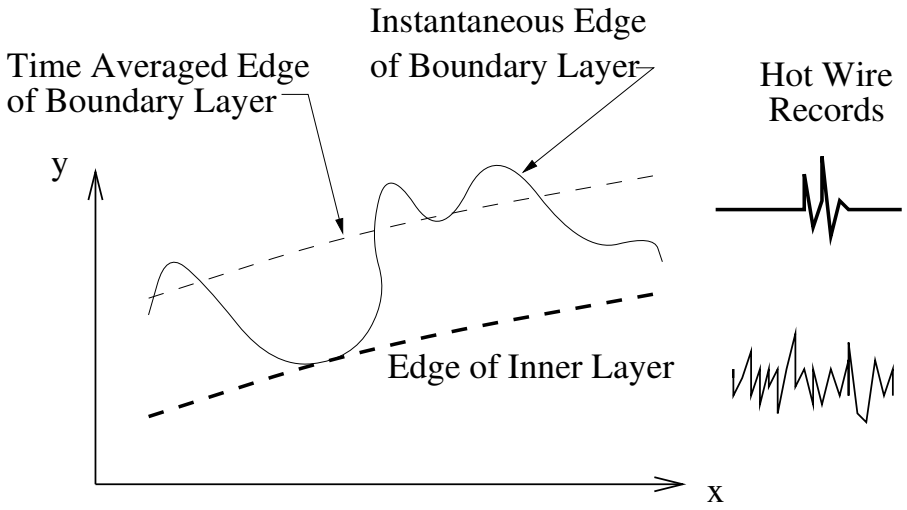
Instantaneous Edge
of Boundary Layer
Time Averaged Edge
of Boundary Layer
Hot Wire
Records
y
Edge of Inner Layer
x

16 Integral Methods for Turbulent Boundary Layers

Key points: *Power law profiles, use of the MIE, Entrainment and Lag*

16.1 Introduction

Last week we derived the turbulent thin layer equations, and discussed the form and structure of a turbulent boundary layer in general terms. However, an idea of what the general structure is is not enough to allow us to predict drag or other flow properties. As was the case for laminar boundary layers, what is needed is some method for determining the effect of the boundary layer in a quantitative fashion. Again, this problem may be tackled in one of two ways; either finite differencing and computational methods, or approximate and empirical methods to generate rapid but less accurate/general results. As was the case for laminar layers, we shall concentrate on the latter approach, as it is historically important, and provides useful results in a short time.

16.2 Power Law Methods

The simplest method for analysis of the turbulent boundary layer is to approximate the velocity profile through a boundary layer as some function of η and only η (recall that $\eta = y/\delta$)). As with the Blasius profile in laminar layers, this carries with it the assumption that the velocity profile is unaffected by any streamwise gradients, and hence is unchanged in that direction except for a linear scaling with boundary layer depth. This implies that the method is most applicable to flows with no velocity or pressure gradients (e.g. over a flat plate - note also that the power law profiles discussed below were derived from data for pipe flows, which once fully developed are independent of streamwise location).

Empirical data suggests that for such flows, a good approximation to a turbulent profile is given by

$$\frac{u}{u_e} = \eta^{\frac{1}{n}}$$

where n depends upon Re. For $5\times10^5 < Re < 10^7$, $n = 7$ provides a good fit, whilst for $10^6 < Re < 10^8$, $n = 9$ is the preferred value. Unlike the Blasius profile however, this fit is entirely empirical, and has no formal theoretical justification.

Using this profile, and recalling that the definition of displacement thickness is independent of flow type if time averaged velocities are used

$$\delta^* = \int_0^\delta \left(1 - \frac{\rho u}{\rho_e u_e}\right) dy$$

As we have incompressible flow, $\rho = \rho_e$, and further

$$\eta = \frac{y}{\delta} \Rightarrow \frac{d\eta}{dy} = \frac{1}{\delta} \Rightarrow dy = \delta d\eta$$

we can write this as

$$\delta^* = \delta \int_0^1 1 - \frac{u}{u_e} d\eta \tag{110}$$

$$\Rightarrow \frac{\delta^*}{\delta} = \int_0^1 1 - \eta^{\frac{1}{n}} d\eta = \left[\eta - \frac{n}{n+1}\eta^{\frac{n+1}{n}}\right]_0^1 = \left(1 - \frac{n}{n+1}\right) \tag{111}$$

Similarly, θ in incompressible flow is given by

$$\theta = \int_0^\delta \frac{u}{u_e}\left(1 - \frac{u}{u_e}\right)dy \tag{112}$$

$$\Rightarrow \frac{\theta}{\delta} = \int_0^1 \eta^{\frac{1}{n}} - \eta^{\frac{2}{n}} d\eta = \left[\frac{n}{n+1}\eta^{\frac{n+1}{n}} - \frac{n}{n+2}\eta^{\frac{n+2}{n}}\right]_0^1 \tag{113}$$

$$\Rightarrow \frac{\theta}{\delta} = \frac{n}{n+1} - \frac{n}{n+2} = \frac{n}{(n+1)(n+2)} \tag{114}$$

However, the local skin friction coefficient, c_f, is given by

$$c_f = \frac{\tau_{wall}}{\frac{1}{2}\rho u_e^2}$$

but

$$\tau_{wall} = \mu\frac{\partial u}{\partial y} = \mu\frac{\partial u}{\partial \eta}\frac{\partial \eta}{\partial y} = \frac{\mu}{\delta}u_e\frac{1}{n}\eta^{\frac{1-n}{n}} = \frac{\mu u_e}{n\delta}\frac{1}{\eta^{\frac{n-1}{n}}}$$

and hence for any value of n greater than 1, this tends to infinity as η tends to zero, i.e. infinite skin friction at the surface! Obviously, this is due to the limited accuracy of the assumed profile rather than being a real effect, and hence we use an empirical result derived from pipe flow data called the Blasius Correction:

$$c_f = \frac{0.0468}{Re_\delta^{0.25}} \text{for n = 7}, \qquad c_f = \frac{0.0290}{Re_\delta^{0.2}} \text{for n = 9} \tag{115}$$

The derivation of the MIE is also independent of any assumption about the laminar or turbulent nature of the flow, and hence may be used to derive expressions for the displacement and momentum thickness. As shown previously, for the case of uniform external flow (i.e. $\frac{du_e}{dx} = 0$), the MIE becomes

$$\frac{d\theta}{dx} = \frac{c_f}{2}$$

Assuming for now that $n = 7$, we substitute for c_f

$$2\frac{d\theta}{dx} = \frac{0.0468\nu_e^{0.25}}{u_e^{0.25}\delta^{0.25}}$$

Substituting $n = 7$ into Equation (114) gives $\delta = 10.29\theta$ and hence

$$2\frac{d\theta}{dx} = \frac{0.0261\nu_e^{0.25}}{u_e^{0.25}\theta^{0.25}}$$

$$\Rightarrow 2\theta^{0.25}d\theta = \frac{0.0261\nu_e^{0.25}}{u_e^{0.25}}dx$$

$$\Rightarrow 1.6\theta^{1.25} = \frac{0.0261\nu_e^{0.25}}{u_e^{0.25}}x$$

Dividing through by 1.6, and raising both sides to the power of 0.8,

$$\theta = \frac{0.0372\nu_e^{0.2}}{u_e^{0.2}}\frac{x}{x^{0.2}}$$

$$\Rightarrow \frac{\theta}{x} = \frac{0.0372}{Re_x^{0.2}}$$

and using the relationships derived earlier results in

$$\frac{\delta}{x} = \frac{0.383}{Re_x^{0.2}}, \qquad \frac{\delta^*}{x} = \frac{0.0479}{Re_x^{0.2}}, \qquad c_f = \frac{0.0595}{Re_x^{0.2}}, \qquad C_F = \frac{0.074}{R_c^{0.2}}$$

Following through with a similar process for $n = 9$ gives

$$\frac{\delta}{x} = \frac{0.27}{Re_x^{\frac{1}{6}}}, \qquad \frac{\theta}{x} = \frac{0.023}{Re_x^{\frac{1}{6}}}, \qquad \frac{\delta^*}{x} = \frac{0.027}{Re_x^{\frac{1}{6}}}, \qquad c_f = \frac{0.0075}{Re_x^{\frac{1}{6}}}, \qquad C_F = \frac{0.045}{R_c^{\frac{1}{6}}}$$

Note that these results imply that the boundary layer in a turbulent flow grows proportional to $\approx x^{0.8}$ as opposed to $x^{0.5}$ for laminar flows, and hence at an Re of say 10^6, the trailing edge thickness on an aerofoil is about 0.024 chord, as opposed to about 0.005 for laminar.

16.3 Worked Example

16.3.1 Q:

An aircraft flies at a speed of 100 m/s at an altitude of 10000 m, where $\rho = 0.4135, \mu = 1.458 \times 10^{-5}$. Roughness at the leading edge of the wing causes immediate transition to occur, replacing originally laminar flow over the whole chord. By modelling the wing (span $10m$, chord $2m$) as an equivalent flat plate, calculate a rough estimate of the increase in drag.

16.3.2 Ans:

The Reynolds number at the trailing edge is

$$Re_c = \frac{\rho * U * c}{\mu} = \frac{0.4135 * 100 * 2}{1.458 \times 10^{-5}} = 5.67 \times 10^6$$

Assuming a flat plate and laminar flow, we may use the Blasius solution

$$C_F = 1.328 Re_c^{-\frac{1}{2}} = 0.558 \times 10^{-3}$$

Allowing for both sides of the plate, and integrating the skin friction force across the span (note that as a flat plate is assumed this is the only force that acts in the x direction) gives

$$\text{Drag} = \frac{1}{2}\rho U^2 * 10 * 2 * 2 * 0.558 \times 10^{-3} = 46.1N$$

However, if the entire flow is turbulent, we approximate with a power law velocity profile, using in this case $n = 7$ as $Re < 10^7$. In this case

$$C_F = \frac{0.074}{R_c^{0.2}} = 3.3 \times 10^{-3}$$

and hence

$$\text{Drag} = \frac{1}{2}\rho U^2 * 10 * 2 * 2 * 3.3 \times 10^{-3} = 272.8N$$

and hence the drag has increased by 226.7 Newtons, or 492 %. *Note that whilst our simplifying assumptions mean that this is a significant underestimation of the drag in both cases, the ratio of turbulent to laminar cases is much more realistic.*

16.4 More Complex Geometries

Whilst the power law profile is really only applicable to zero streamwise gradient flows, it may be used to calculate aerofoil flows if some loss of accuracy is tolerable. If this is the case, we use the MIE in the form

$$\frac{d\theta}{dx} + \frac{\theta}{u_e}\frac{du_e}{dx}(H+2) = \frac{c_f}{2}$$

and selecting the appropriate value of c_f from Equation (115), both of which are of the form $c_f = K_\delta Re_\delta^{-\frac{2}{n+1}}$, gives

$$\frac{d\theta}{dx} + \frac{\theta}{u_e}\frac{du_e}{dx}(H+2) = \frac{K_\theta}{2Re_\theta^{\frac{2}{n+1}}}$$

where K_θ is a different constant dependent on K_δ and n (as $\theta \propto \delta$ for given n). Then

$$\theta^{\frac{2}{n+1}}\frac{d\theta}{dx} + \theta^{\frac{n+3}{n+1}}\frac{1}{u_e}\frac{du_e}{dx}(H+2) = \frac{K_\theta}{2}\left(\frac{u_e}{\nu}\right)^{-\frac{2}{n+1}}$$

Multiplying both sides by $u_e\phi = u_e^{\frac{(H+2)(n+3)}{n+1}}$ and integration by parts we get

$$\frac{d}{dx}\left(\frac{n+1}{n+3}\theta^{(n+3)/(n+1)}u_e^\phi\right) = \frac{K_\theta}{2}\left(\frac{u_e}{\nu}\right)^{-\frac{2}{n+1}}u_e^\phi$$

where $\phi = \frac{(H+2)(n+3)}{n+1}$. Integrating with respect to x produces

$$(\theta^{\frac{n+3}{n+1}}u_e^\phi)_x - (\theta^{\frac{n+3}{n+1}}u_e^\phi)_t = \frac{n+3}{n+1}\frac{K_\theta}{2}\int_{x_t}^{x} u_e^\phi\left(\frac{u_e}{\nu}\right)^{-\frac{2}{n+1}}dx \tag{116}$$

where subscript t denotes the point of transition, which we shall deal with next week.

Equation (116) is similar in form to Thwaites method for laminar flows, and may be integrated in the same way using u_e, ν calculated using an inviscid analysis (provided incidence and thickness are small), except that there is one extra unknown in the equation, being H. However, as this appears in ϕ on both sides, it is reasonable to assume that θ is relatively insensitive to H. A constant value may therefore be used, generally 1.4. This, however, further reduces the accuracy of the method.

16.5 More Sophisticated Methods

As mentioned previously, power law methods have dubious theoretical justification with regard to their application to flows with gradients in the external flow. To overcome this, more sophisticated methods have been created. The two main concepts involved are *entrainment*, and *lag*.

16.5.1 Heads Entrainment Method

One of the major deficiencies in the above method is that it requires an assumption of constant H. In fact this is a variable, and is effected by the external flow field. If we could provide some equation for H, then the method would be more accurate, and also allow some direct influence of the external flow on the solution variables. After some early attempts at empirical models, Head proposed the

entrainment method, generally considered to be the most reliable of this group. An *entrainment velocity* E is introduced, which represents the rate at which the volume flow rate in the boundary layer is increasing (i.e. the boundary layer is increasing in thickness, hence there is more flow within the boundary layer. This extra flow must be coming into the boundary layer through the edge, with an average velocity $E(x)$ (see below) The volume flow rate $Q(x)$ at a point x is

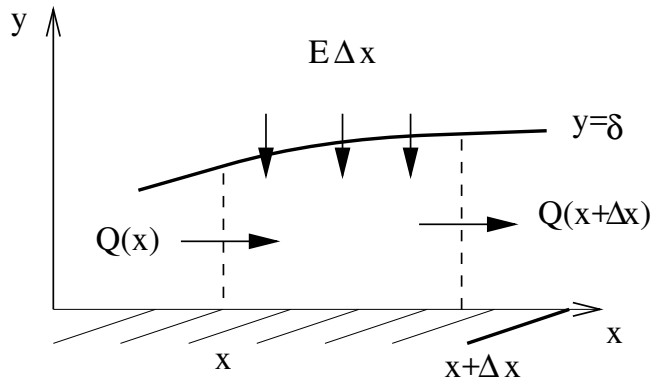

$$Q(x) = \int_0^{\delta(x)} u dy$$

and E is

$$E = \frac{dQ}{dx}$$

As

$$\delta^* = \int_0^{\delta} \Big(1 - \frac{u}{u_e}\Big) dy$$

substitution gives us

$$\delta^* = \delta - \frac{Q}{u_e}$$

and further

$$E = \frac{d}{dx} u_e(\delta - \delta^*) = \frac{d}{dx}(u_e \theta H_1)$$

where

$$H_1 \equiv \frac{\delta - \delta^*}{\theta}$$

It is then assumed that the flow is uni-parametric in H_1 (*c.f.* the Falkner-Skan relationships for laminar flows) i.e. $\frac{E}{u_e}\big(H_1\big), H\big(H_1\big)$. Empirical relationships for these functions, and c_f, combined with the MIE give four equations for four unknowns (θ, H, H_1, and c_f), and hence may be solved simultaneously in a streamwise manner to calculate boundary layer properties.

16.5.2 Greens Method and the Lag Equation

Despite being an improvement on previous methods, Head's technique was found to have two important failings: implicit in the method is the assumption that the local turbulence structure is determined solely from the mean local conditions, and the lag between changes in the external flow structure and the local turbulence was not taken into account (i.e. it is assumed that the changes in the external flow, due to pressure etc., transmit immediately through the whole layer, which in reality is not the

case). This meant that the method had limited accuracy in flows with high gradients. This lead to the development of *lag entrainment equations* which in essence provide a way in which this time lag can be accounted for. The widest used of these methods is that of Green, which has also been extended to compressible flows. However, the lag equation is solved through the modelling of both turbulent kinetic and transport equations, and is thus considerably more complicated than the methods described above.

16.5.3 Solution to last weeks Question

Sketch 'typical' velocity profiles for a turbulent and equivalent laminar boundary layers. What is the principle reason for the difference in shape?

Answer

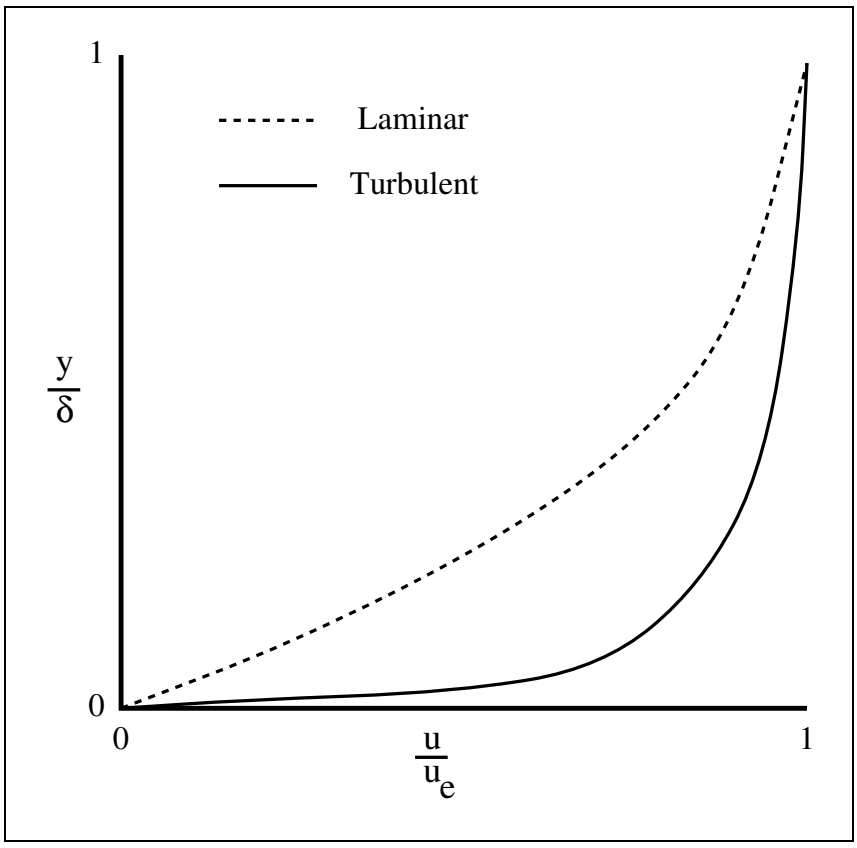

The principle reason for the difference in shape is the higher mixing induced by the presence of turbulent eddies. This means that the velocity is more uniform over most of the boundary layer, but this in turn means that the velocity gradient near the wall is higher, resulting in higher wall stress.

16.5.4 Question for Next Week

Assuming that a power law profile is accurate, show that

$$H = 1.29 \text{ when } n = 7, \qquad , H = 1.22 \text{ when } n = 9$$

17 Boundary Layer Transition

Key points: *Overview of the process of transition, the uncertainty in its modelling, and methods which can be used. Three dimensional transition*

17.1 Introduction

The last two lectures have described the properties of the turbulent boundary layer, and discussed methods to model their effects. However, it has been stated several times that boundary layers nearly always begin as laminar, and turn turbulent some distance downstream. This lecture shall consider the process by which this happens, known as *transition*.

Transition in a boundary layer is a complex process, dependent on a variety of parameters, and is still not totally understood. This means that we shall treat the subject in a moderately brief and superficial way, as always focusing on the issues of most relevance to the practising aerodynamicist; i.e. reducing the problem to something simple enough that can be readily used for wing design, yet still give good enough answers. This is of course somewhat subjective, dependent on the term 'good enough', and will be largely empirical.

17.2 Development of Transition

Transition modelling involves the analysis of the propagation of infinitesimal wave-like disturbances in the flow. At all times, tiny disturbances are being introduced into the boundary layer, from noise and vibration, and any non-uniformities in the external flow or surface. In laminar flows, these infinitesimal disturbances are damped by viscous action. However, as Reynolds number increases (remember Reynolds number is the ratio of the inertial to viscous forces), the overall effectiveness of this damping decreases, and eventually at a certain critical Reynolds number, these disturbances are no longer damped and the flow begins the process of transition. The details of the relative stability of these *Tollmien -Schlicting* waves, as they are known, may be calculated mathematically, and shown to be a function of their frequency, and external pressure gradients (adverse gradients significantly increase the likelihood of their propagation, whilst favourable gradients have the opposite effect, and may even reverse the transition process, causing re-laminarisation of turbulent layers).

Once these waves have developed, they move downstream. Even the smallest unevenness in the flow will cause differential movement of these (initially two dimensional) waves, and loops will form in the wave front. Eventually they become so contorted that a *turbulent spot* is formed. This marks the point at which the transition regime begins (the Tollmein Schlichting waves, although the ultimate cause of transition, are essentially laminar flow phenomena). Downstream of the spot, a 'packet' of turbulent flow spreads out into a roughly triangular lump which moves downstream. At other places along the wave front, more turbulent spots form, produce turbulence, and then disappear again. This dynamic process introduces *intermittency* to the flow, which means that in this region the flow at a point is sometimes laminar, and sometimes fully turbulent. This is similar in concept to the outer region of a turbulent boundary layer as discussed two weeks ago, but the intermittency is governed by different functions.

The further downstream we move, the more spots form, and hence the greater the region of turbu-

lent flow, until eventually there are so many regions of turbulence merging into each other, that the whole flow may be considered turbulent, and transition is complete. This process is demonstrated graphically in figure 43.

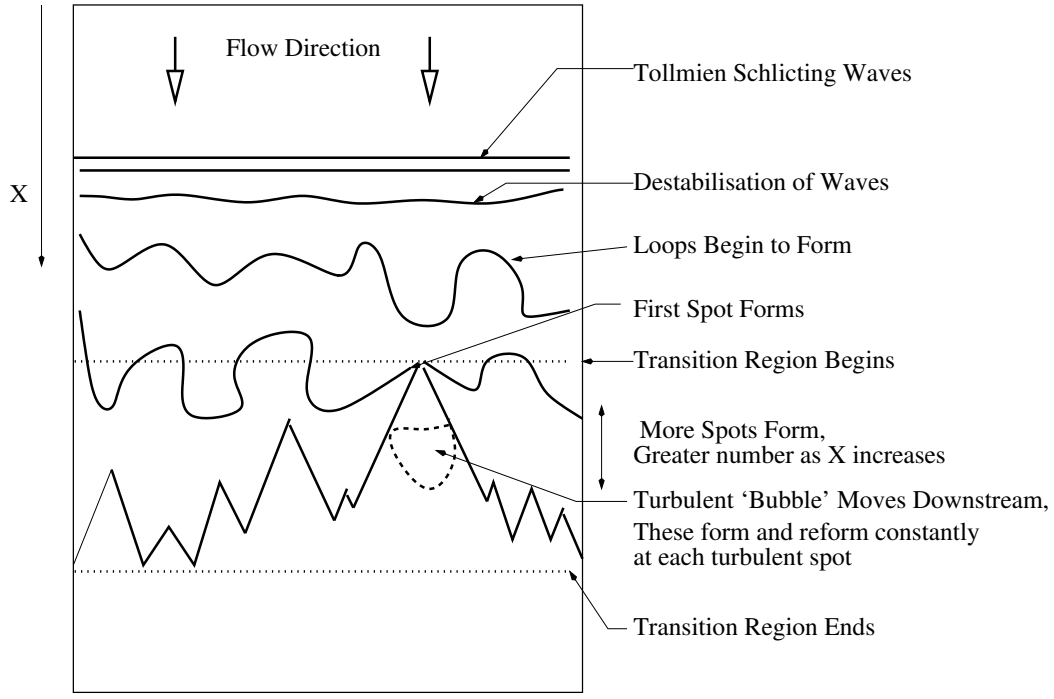

Figure 43: *Transition Region at some instantaneous time* t

Other factors may effect the transition process such as surface roughness, the turbulence level in the external flow, and heat transfer and mass flow through the surface. The first two effectively bypass the laminar stages of transition by causing direct formation of turbulent spots, and hence reduce the Reynolds number of transition. Suction and wall cooling essentially remove mass and energy respectively from the boundary layer, causing it to behave as if it were at a lower Reynolds number and hence delaying transition. Finally noise and streamwise curvature also can cause alteration in transition behaviour, concave stream-wise curvature being destabilising (due to the formation of so called 'Gortler vortices').

For a simple flat plate, It can be demonstrated that transition is impossible below a critical value of $Re_x = 1.41 \times 10^5$, but will inevitably have occurred by $Re_x = 3.2 \times 10^6$. Surface roughness can alter the range of transition from this latter value for a smooth plate, to about 3×10^5 (i.e. a reduction by a factor of 10) for a rough one. As with most of the other factors however, surface roughness has a non-linear effect on transition; for any given flow there is a minimum roughness below which no effect is produced, and a maximum above which no further reduction in Re_{crit} occurs. This range is determined largely empirically.

17.2.1 Modelling Transition

Given that transition is such a complex process, the question naturally arises as to how we shall be able to incorporate it into our drag prediction methods. The honest answer to this is 'not very well'. However, we can make some assumptions of varying applicability which allow some approximation

to the process to be made.

First, we shall assume that the whole of the transition process, from the formation of the first spot to the point where the whole layer is turbulent occurs at a single point (line in 3D). This avoids the problem of mathematically modelling the intermittency during transition, and is actually a pretty good approximation for the high Reynolds number flows that we shall typically be dealing with. We can then use the fact that the boundary layer is continuous at transition to calculate a pseudo fully turbulent boundary layer from some point x_s which has the same momentum thickness at the transition point as the laminar boundary layer calculated from the aerofoil nose (see below). As we have shown previously, if the Squire Young method is used to predict the total drag, this is dependent only on the momentum thickness at the trailing edge, not on the total distribution over the wing.

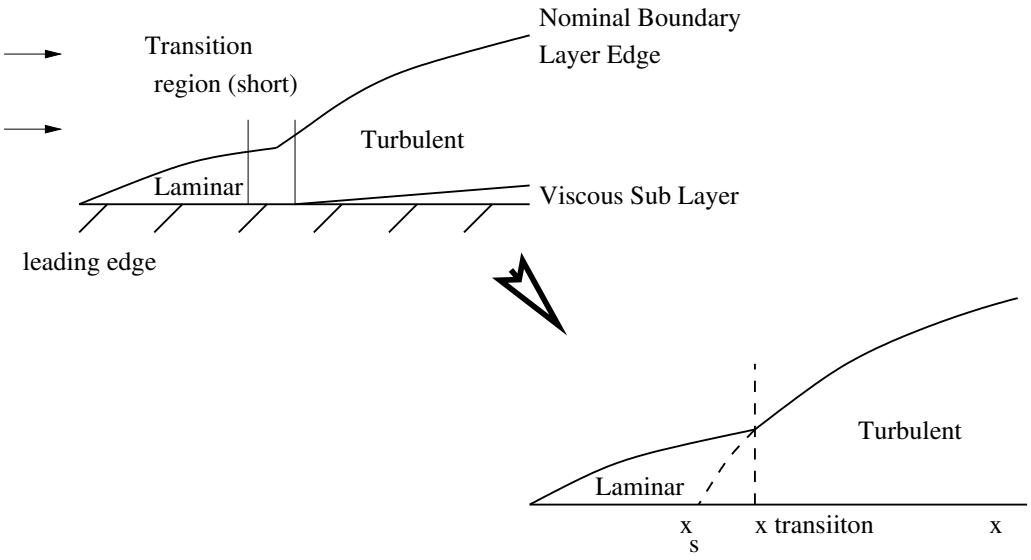

This then leaves the problem of locating the point of transition itself. There are several ways in which this can be done, the simplest (and most common, particularly in CFD and other numerical schemes) is to simply define a critical Reynolds number, below which laminar flow is assumed, and above which the flow is turbulent. A common choice for this is $Re_{crit} = 5 \times 10^5$ based on streamwise length. Alternatively, knowledge of the physical behaviour of such flows may be used, for instance laminar flows are very sensitive to pressure gradients, and hence cannot remain laminar for any significant distance downstream of the widest point of an aerofoil (where pressure gradient sign changes).

More mathematical methods exist, generally based on curve fits to empirical results. For instance Michel has shown for an aerofoil type transition the formula

$$Re_\theta = 1.174\left(1 + \frac{22400}{Re_x}\right)Re_x^{0.46}$$

may be used to determine the point of transition. This formula does to some extent include the effect of pressure gradient (as the growth of Re_θ relative to Re_x is greater in adverse pressure gradients), but does not include effects of roughness, etc., and hence should be used with caution and only for similar bodies to those for which it was derived (which fortunately for us was aerofoils). Unfortunately, what all this really comes down to is that when dealing with transition, there is no substitute for experience and an understanding of which effects are important, which you can only develop with practise and time.

17.3 Other Transition Processes

17.3.1 Transition Bubbles

Laminar boundary layers cannot withstand even moderately adverse pressure gradients, and readily separate in this case. The adverse pressure gradient and separation causes transition to occur. The

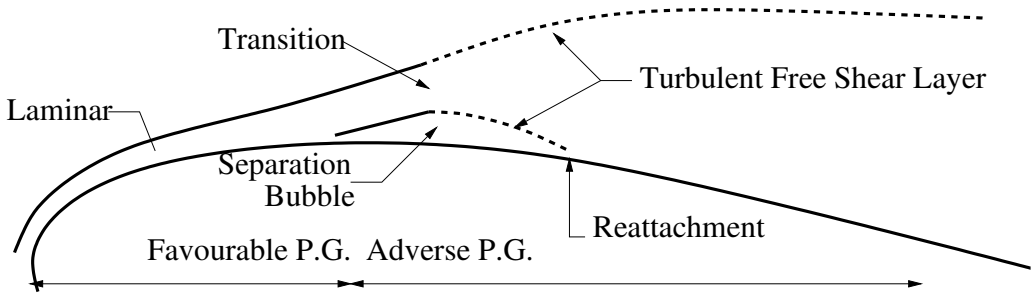

rapid thickening of the turbulent boundary layer causes reattachement - and so a separation bubble is formed. Very little can be done about this process (which obviously becomes more likely as incidence and hence pressure gradients increase) apart from modifying the aerofoil profile to increase the region of favourable pressure gradient and move the separation aft.

17.3.2 Three Dimensional Effects

Tollmien-Schlicting waves and transition bubbles are essentially two dimensional effects. On swept wings there will be a velocity component parallel to the leading edge, and this can create three dimensional effects.

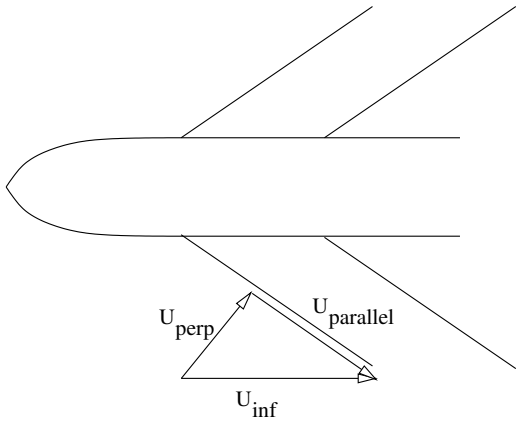

17.3.2.1 Crossflow Instability Near the leading edge of a wing the perpendicular velocity over the wing changes rapidly from zero at the stagnation point to a maximum at the widest part of the aerofoil, whilst the parallel velocity remains largely constant. This causes a large change in the external velocity vector, causing inflection within the boundary layer, which in turn leads to instability and transition. The magnitude of this effect can be reduced by reducing the flow acceleration over the leading edge, i.e. reducing $\frac{\partial U_{perp}}{\partial s}$. Unfortunately, there is another, potentially more catastrophic 3-D transition mechanism:

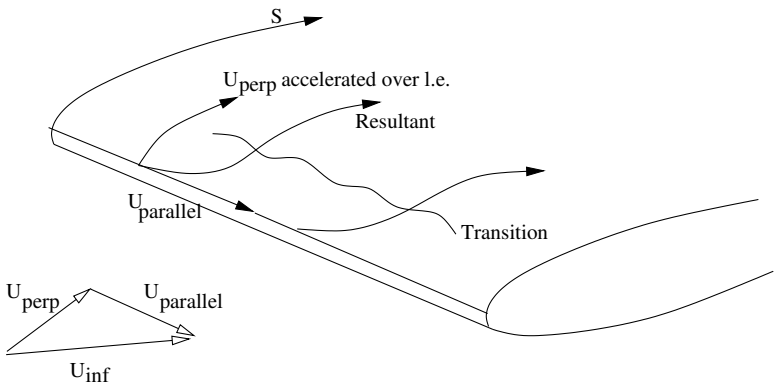

17.3.2.2 Attachment Line Transition The boundary layer grows along the attachment line (the line made up of all the stagnation points), and may become turbulent here. The attachment line

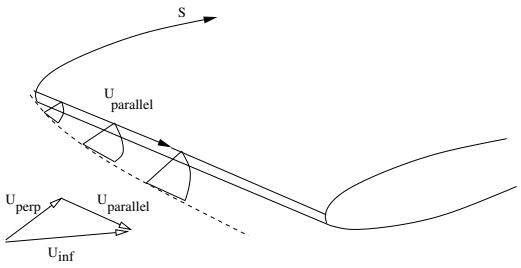

boundary layer thickness is proportional to $\left(\frac{\nu}{\frac{\partial U_{perp}}{\partial s}}\right)^{\frac{1}{2}}$. If we can use this to construct a Reynolds number based on the thickness of the attachment line boundary layer and $U_{parallel}$

$$Re_{a.l.} = \frac{U_{parallel}}{\nu}\left(\frac{\nu}{\frac{\partial U_{perp}}{\partial s}}\right)^{\frac{1}{2}}$$

it is found that

$$Re_{a.l.} > 800 \Rightarrow \text{Transition}$$

If the attachment line becomes turbulent then the whole wing will have a turbulent boundary layer, increasing overall drag considerably. There are three possible methods to alleviate this problem:

1. Reduce $U_{parallel}$, i.e. Reduce the sweep
2. Reduce attachment line boundary layer thickness by increasing $\frac{\partial U_{perp}}{\partial s}$
3. Use suction at the leading edge

All three have consequences for other design decisions (wing sweep is often chosen because of compressible flow considerations, the second increases the likelihood of crossflow instability, and the last requires piping, power, etc.).

17.3.3 Solution to last weeks Question

Assuming that a power law profile is accurate, show that

$$H = 1.29 \text{ when } n = 7, \qquad H = 1.22 \text{ when } n = 9$$

Answer As

$$H = \frac{\delta^*}{\theta}$$

and as was shown in last weeks lecture

$$\frac{\delta^*}{\delta} = \frac{1}{n+1}, \quad \frac{\theta}{\delta} = \frac{n}{(n+1)(n+2)}$$

then

$$H = \frac{\delta^*}{\delta}\frac{\delta}{\theta} = \frac{1}{(n+1)}\frac{(n+1)(n+2)}{n} = \frac{n+2}{n}$$

Hence

$$\text{If } n = 7, \quad H = \frac{9}{7} = 1.29, \text{ and if } n = 9, \quad H = \frac{11}{9} = 1.22$$

17.3.4 Question for Next Week

Calculate the point of transition on a flat plate immersed in uniform flow ($U = 50m/s, \rho = 1.225, \mu = 1.79 \times 10^{-5}$), assuming transition occurs at a)$Re = 1.41 \times 10^5$, b) $Re = 3.2 \times 10^6$

18 Differential Methods

Key points: *Flowfield discritisation. Differential approximation by finite differences. Turbulence Modelling - Prandtle mixing length hypothesis, wide variety of methods*

18.1 Introduction

Thus far in the course, we have concentrated on integral techniques for boundary layers. These methods are relatively simple (in application if not derivation!), and although helped by the use of a computer, can be calculated by hand if necessary (they of course evolved at a time when computers did not exist). However, they are limited in applicability and accuracy, particularly with respect to truly three dimensional flows. As an alternative, so-called *differential* boundary layer solutions may be devised, and these are what we shall be discussing in this lecture.

Differential boundary layer solutions belong within a much wider group of methods, known as Computational Fluid Dynamics (CFD). This class of solution techniques have become more widespread in the last twenty to thirty years, due to the rapidly increasing computational power available. The area is the subject of an optional course some of you may already be studying, or wish to next year. However, differential boundary layer methods have two properties which are unique within this wider group. First, only a part of the flowfield (the boundary layer) is modelled, and the external flow must be solved using a separate technique (this may be CFD based, but need not be. The Joukowski method already examined, and the panel and vortex lattice methods to be introduced towards the end of the course can also be 'coupled' to a boundary layer solution method). Second, the nature of the thin layer equations (parabolic, rather than elliptic) means that even in subsonic flows, the flow at a streamwise point is independent of any developments downstream. This means that the boundary layer may be solved by 'space-marching', i.e. solving the flow at point x, then $x + \Delta x$, and so on, without having to allow for the solution at $x + \Delta x$ to effect that at x. This is not generally the case for CFD solutions (however, we have already used this property in the development of integral methods, where solution is based on a streamwise stepping method).

18.2 Formulation of the Problem

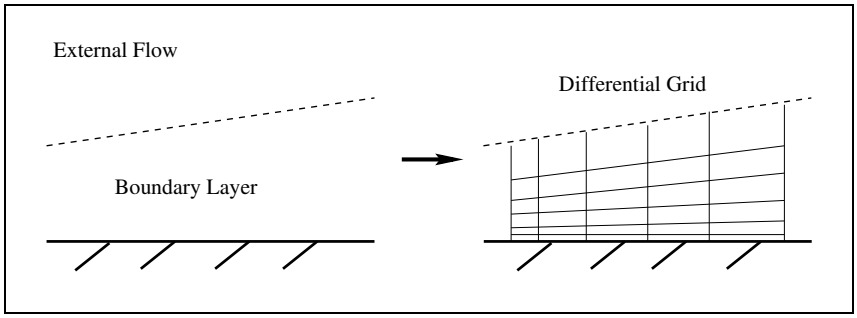

Figure 44: *Differential Grids for Boundary Layers*

Differential techniques solve the boundary layer by breaking it down into a large number of small cells (figure 44). The thin layer equations are then expressed in a form known as *finite-difference*

equations, which in simple terms means that the partial differentials are expressed as the difference between neighbouring values, i.e. between two neighbouring cells i, j and i, j (see figure 45),

$$\frac{\partial u}{\partial x} \approx \frac{\Delta u}{\Delta x} = \frac{u_{i+1} - u_i}{x_{i+1} - x_i}$$

(This is a slight simplification, for more details you will have to take the CPA course, but for our purposes this view is sufficient). Obviously, these approximations become more accurate the smaller the cells, and this is the reason for the much closer spacing of cells where gradients are high (i.e. near the wall) in figure 44.

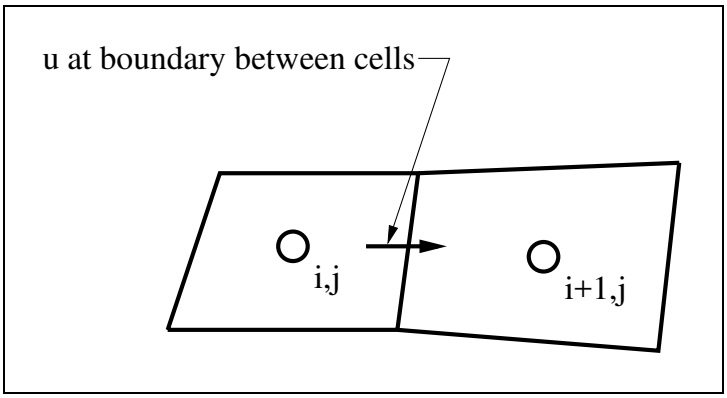

Figure 45: u *Between Cells*

18.3 Practical Application

As with integral methods, we assume we have a solution of the inviscid external flow available from some other solution process. This means we have velocity and pressure distributions around the object under analysis. The boundary layer itself is then split into a grid. There are a number of points to be considered at this stage.

First, the extent of the grid perpendicular to the surface must be defined. Whilst technically it should extend an infinite distance from the wall to ensure that the boundary condition $u(y) = u_e$ is met, this is obviously impractical. As the velocity u tends to u_e rapidly in the normal direction to the surface (this is key to the whole concept of a boundary layer), a more reasonable approximation is to extend the mesh to some distance y_{edge} where further increments in y have no effect on the solution within a specified tolerance. This distance need only be a little greater than δ, but as this property is itself a product of the solution, some trials may be required to ensure that the grid is sufficient in normal extent.

Next, the distribution of cells in the mesh is also important, as the majority of the change occurs near the surface, and hence small cells are needed there, whilst further out, less happens and hence small cells would waste computing time. Linear scaling is often used (where each cell out is n times larger than the cell nearer the wall, n generally being between 1 and 2), although exponential and other spacings are used (grid generation is a very complex topic, more information is contained in text books and in the CPA option). Having uneven spacing however does reduce the accuracy of differencing methods, and in order to avoid this grids are often transformed to a second plane in which spacing is even (figure 46). This increases the complexity of the equations, but improves accuracy.

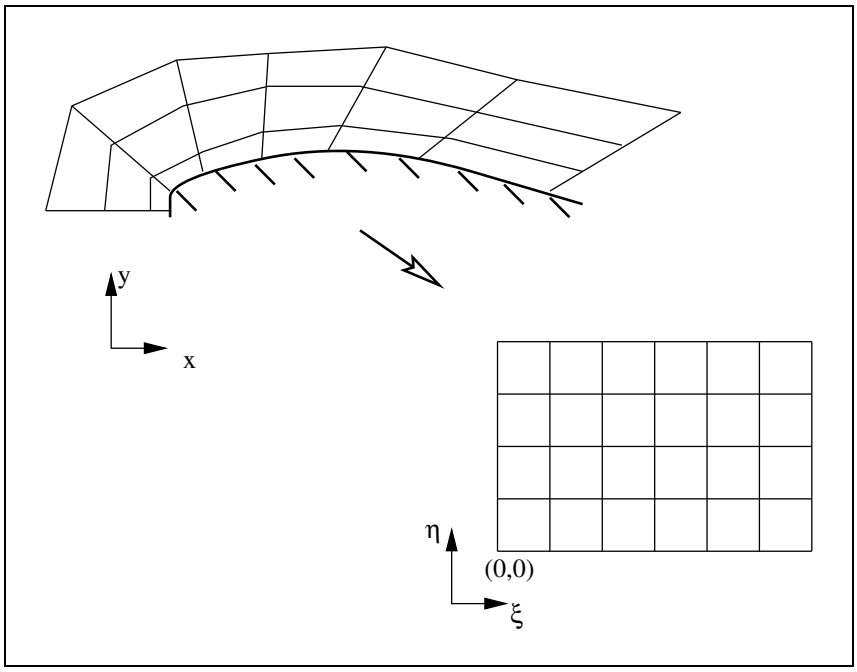

Figure 46: *Grid Transformations*

An initial velocity profile is then used to define conditions at the inflow boundary (i.e $\xi = 0$ in the figure above). For two-dimensional, steady, incompressible laminar flows with no heat transfer, the governing equations

$$\frac{\partial u}{\partial x} + \frac{\partial v}{\partial y} = 0 \tag{117}$$

$$u\frac{\partial u}{\partial x} + v\frac{\partial u}{\partial y} = -\frac{1}{\rho}\frac{dp}{dx} + \nu\frac{\partial u}{\partial y} \tag{118}$$

are then approximated using the differencing technique already discussed, and the solution sweeps downstream. If desired, integral properties such as θ may be calculated by numerical integration.

The advantages of such a method over say Thwaites technique, is that no assumptions of uni-parametric flow, or indeed any assumptions about the external flow are made, and hence the method is widely applicable. In many ways, this is conceptually a simpler method for the solution of such flows (no complex algebra and empirical relations are involved), it is only the shear number of calculations required (and some black arts involved in grid spacing, etc.) that make things more complex. This is especially true when some of the above assumptions (e.g. compressibility) are removed, as the nature of the solution method is unchanged, just the number of equations increases. However, as was the case for integral methods, turbulence considerably complicates the picture.

18.4 Turbulence Modelling

In most real applications, the majority of the boundary layer is turbulent, and some is transitional. In order to model such flows, we need some method of including the effects of the turbulent motion on the flow. The most common method is based on the *turbulent viscosity* concept introduced in the first lecture dealing with turbulent flows.

Remember that using time averaging and dimensional reasoning to retain only the most important influences of turbulence, the boundary layer streamwise momentum equation for incompressible flow becomes

$$\rho\left(\frac{\partial u^2}{\partial x}+\frac{\partial uv}{\partial y}\right)=-\frac{dp}{dx}+\frac{\partial}{\partial y}\left(\mu\frac{\partial u}{\partial y}-\rho\overline{u'v'}\right)$$

(flow quantities u, v etc. are assumed to represent time averaged quantities, i.e. $\bar{u}, \bar{v}$ etc.). Using the eddy viscosity concept, this becomes

$$\rho\left(\frac{\partial u^2}{\partial x}+\frac{\partial uv}{\partial y}\right)=-\frac{dp}{dx}+(\mu+\mu_t)\frac{\partial^2 u}{\partial y^2}$$

The problem is then reduced to one of modelling μ_t, the eddy viscosity, which unlike μ is not a fluid property, but varies from point to point in the flow. This is the realm of *turbulence modelling*, a large and still expanding area of current research.

The methods used to approach this problem can be split into a number of different categories depending on how many extra differential equations are used to help find the value of μ_t; hence there are zero, one, and two equation models. Further, the concept of eddy viscosity itself is an assumption, and greater realism can be produced by going back to the Reynolds stresses themselves, and deriving methods based on them. However, all these models eventually rest on empirical relationships, the more complex methods resting on more general empirisisms and thus generally being of greater applicability, although not necessarily of much greater accuracy.

For regions where the boundary layer assumption is fully justifiable (i.e. thin layers with no separations etc.), the simple zero equation models have been found to be generally reliable, and suffer little inferiority in terms of performance compared to more recent techniques.

18.4.1 Zero Equation Models

Zero equation models are based on Prandtl's mixing length hypothesis. In essence, an analogy is drawn between the mean free path of a molecule, and a mixing length in turbulent flow. Eddies are assumed to form, travel some typical distance unchanged, and then mix with the surrounding flow. Imagine that some eddy forms at a point y_1 with local velocity u_1, and then moves up through the boundary layer by this mixing length l_1. Assuming this length to be small, the time averaged velocity at this point u_2 is given by

$$u_2 \approx u_1 + l_1\frac{\partial u}{\partial y}$$

and hence the local velocity fluctuation caused by the dissipation of the eddy is

$$|u'| \approx |u_2 - u_1| = l_1\left|\frac{\partial u}{\partial y}\right|$$

If we then assume that v' is of the same order of magnitude, and considering the signs of u', v', we get

$$-\rho\overline{u'v'} \approx const.\rho l_1^2\left(\frac{\partial u}{\partial y}\right)\left|\frac{\partial u}{\partial y}\right|$$

Following the Boussinesq hypothesis we have

$$-\rho\overline{u'v'} = \tau_t = \mu_t\frac{\partial u}{\partial y}$$

and so we end up with

$$\mu_t = \rho l^2 \left| \frac{\partial u}{\partial y} \right|$$

where l is a new constant, proportional to l_1. Near the wall, but outside of the viscous sub-layer, the only logical length scale available is the distance from the wall, y, and hence it is hypothesised that

$$l = Ky$$

where K is the Karman constant (normally 0.4 or 0.41). This same result can be used to derive a closer approximation to the velocity profile in the inner layers, known as the Law of the Wall. This has been demonstrated to produce accurate results (for the inner region only) over a wide range of flows. Consult any text book on boundary layers for a full derivation of this profile if you are interested.

(*Note: you will not be expected to remember or use any of the formulae below in an exam, they are for completeness only*). This is valid in the inner layer outside of the viscous sub-layer. The latter may be taken into account via van Driest's formulation

$$l = Ky(1 - e^{\frac{-y+}{A_0}})$$

where A_0 is an empirical value generally between 24 to 26, and given for instance by Cebbeci and Smith as

$$A_0 = 26\left(1 - 11.8\frac{\nu u_e}{u_t^3} i_e\right)^{-\frac{1}{2}}$$

The mixing length hypothesis does not hold for the outer layer, as the flow is sometimes turbulent, sometimes not. However, whilst it is turbulent it is a good approximation, and this intermittency can then be allowed for via other empirical relations, of which there are several (e.g. Cebbeci and Smith, Baldwin-Lomax). As an example, the Cebbeci-Smith formulation

$$\frac{\mu_t}{\rho} = 0.0168 u_e \delta^* \gamma_0$$

where γ_0 is

$$\gamma_0 = \frac{1}{2}\left(1 - \text{erf}\left[5\left(\frac{y}{\delta} - 0.78\right)\right]\right)$$

'erf' being the error function

$$\text{erf}\sigma = \frac{1}{\sqrt{2\pi}} \int_{-\sigma}^{\sigma} e^{-\frac{\sigma^2}{2}} d\sigma$$

The switch between the inner and outer law equations occurs when the two values are the same to ensure continuity.

18.5 Conclusions

As should be obvious even from the very brief treatment here, differential methods are generally extremely complex, and are much more difficult to implement than integral equivalents. There are many areas still to be explored, particularly with respect to turbulence modelling (this is covered in greater detail in the fourh year advanced option 'Turbulent Flow'). Further, the problem of transition

has not been discussed - essentially it is just as difficult a problem for differential as integral methods, and similar approximations (point transition at critial Reynolds numbers, etc.), are employed.

However, differential methods offer the possibility of finding solutions to flows to which integral methods cannot be applied, and hence are in widespread use. At present, the commonest methods used in industry are based on zero equation models with constant Re_{crit} transition, and hence are of limited complexity, but also with little theoretical justification. However, the increasing power of computers, and widespread use of CFD methods for inviscid flows, mean the use and complexity of such solution methods will only increase.

18.5.1 Solution to last weeks Question

Calculate the point of transition on a flat plate immersed in uniform flow ($U = 50m/s, \rho = 1.225, \mu = 1.79 \times 10^{-5}$), assuming transition occurs at a)$Re = 1.41 \times 10^5$, b) $Re = 3.2 \times 10^6$ **Answer**

$$Re_{crit} = \frac{\rho U x}{\mu} \Rightarrow x_{crit} = \frac{Re_{crit}\mu}{\rho U}$$

Hence for case a)

$$x_{crit} = \frac{1.41^5 * 1.79 \times 10^{-5}}{1.225 * 50} = 0.041m$$

and for case b

$$x_{crit} = \frac{3.2^6 * 1.79 \times 10^{-5}}{1.225 * 50} = 0.935m$$

18.5.2 Question for Next Week

List the advantages and disadvantages of differential boundary layer methods compared to integral ones.

19 Realistic Boundary Layers

Key points: *Consequences of adverse pressure gradients and separation, advantages of turbulent boundary layers in this situation. Effect of shock waves on boundary layers, and vice versa. Drag reduction techniques*

19.1 Introduction

So far, we have described how to model and analyse boundary layers under relatively mild external conditions. In other words, we have assumed that the external flow gradients are such that the boundary layer remains thin and attached to the surface. Although this is in most cases true for streamlined bodies at small incidence, the flows around aircraft can be much more complex, particularly for instance when manoeuvring, or at supersonic speeds. We shall begin this lecture by examining these issues, before turning to methods by which what we have learned about boundary layers may be used to reduce the drag they produce.

19.2 Separation

Adverse pressure gradients cause a retardation of the velocity profile within the boundary layer, as in effect some of the kinetic energy in the layer must be converted into pressure in order to maintain force balance.This reduces the velocity gradient near the wall (see below). Eventually the retardation is sufficient that a reverse flow exists at the surface, and the flow has separated. This causes a significant change in the behaviour of the boundary layer; it becomes unsteady (on a macroscopic scale, not just turbulent), three dimensional, highly curved, and of dimensions significant with respect to those of the body. In other words, it violates the thin layer assumptions, and hence the methods discussed previously cannot be used.

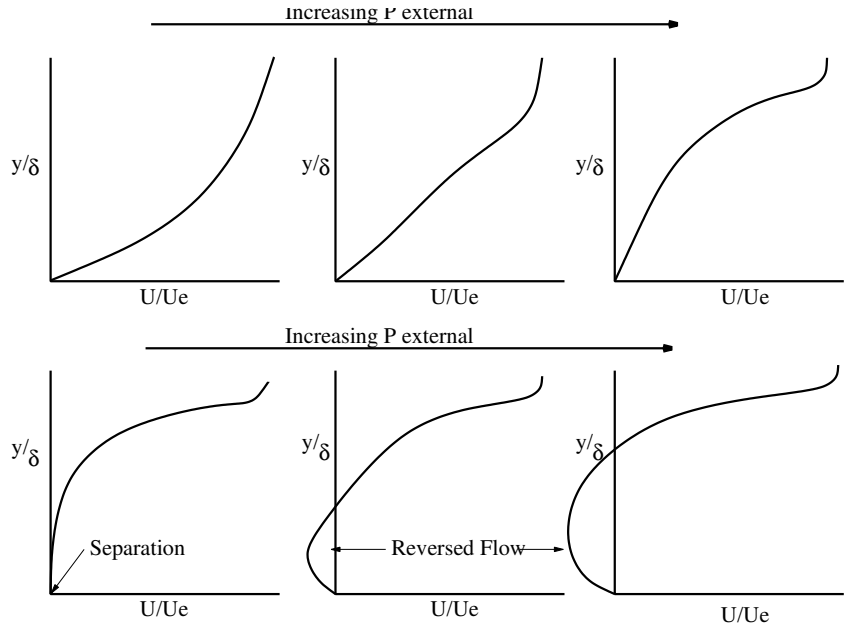

Figure 47: Velocity Profiles in an Adverse Pressure Gradient

At the separation point, the velocity gradient $\frac{\partial u}{\partial y}$ is zero, and this in turn results in the skin friction being zero. This might sound desirable, as skin friction drag is thus removed, but the impact on the remainder of the flowfield is very large due to the considerable amount of vorticity shed into the outer flow in the viscous region, and overall results in a significant increase in drag.

Where a boundary layer separates depends on a variety of factors, as well as the pressure gradient; for instance, a sharp expansion corner (i.e. a rearwards facing step) will always cause the flow to separate. Another significant factor is the nature of the boundary layer. As the fuller velocity profile of a turbulent boundary layer means that a greater retardation of the flow is required to cause zero velocity gradient at the surface, turbulent boundary layers are less prone to separation. This means it is sometimes desirable to encourage transition, despite the higher friction associated with turbulent layers, and this can influence wing design.

Predicting the point of separation is sometimes easy, for instance in the case of geometric triggers or shock wave interaction (assuming the shock wave location to be accurately predicted). However, in general it is a very difficult proposition for 'smooth' surfaces, e.g. aerofoils, as the location is *extremely* sensitive to upstream turbulence in the main flow and velocity gradients in general. This not only means that predicting the separation point is difficult, but also that the location is itself unsteady (even in what would otherwise be called a steady flow), moving back and forth as the turbulence in the external flow varies.

Generally, the methods described in this course cannot be applied to the problem of separation, integral methods in particular usually being inappropriate. The only reasonable way to approach the problem numerically is through full Navier-Stokes based CFD solutions, and even here the influence of the turbulence modelling on the predicted results is significant, and not properly understood. However, in some restricted cases, particularly the separation bubbles discussed in the transition lecture, where the separated region is not very extensive in either chord or normal directions, some integral methods may be applied, obviously with care and a healthy skepticism about the accuracy.

19.3 Shock Wave Interactions

In the course so far, we have considered predominantly the boundary layers formed in low speed, incompressible flows. Even though an incompressible assumption in boundary layer calculations may be applied to a greater range of freestream Mach numbers than for the majority of the flowfield, at high enough speeds compressibility effects do become important, and must be considered. A key example of this is shock wave - boundary layer interactions.

The cruise Mach number of many jet aircraft is sufficiently high that at least some part of the wing is in supersonic flow. If the flight Mach number of the aircraft is less than 1 (i.e. 'transonic' flight), this supersonic flow will terminate in a shock wave at some point before the trailing edge. Shock waves also form and interact with aircraft surfaces in many supersonic regimes, and of course in the exhaust system of jets and rockets.

In a truly inviscid flow, the shock wave would form a thin region extending all the way down to the wing surface. However, as at least some of the boundary layer is subsonic regardless of the external Mach number, a mechanism is provided that communicates the presence of the shock wave upstream. This causes the boundary layer to thicken ahead of the shock wave, turning the external flow, causing compression waves to form ahead of the nominal shock position, as below.

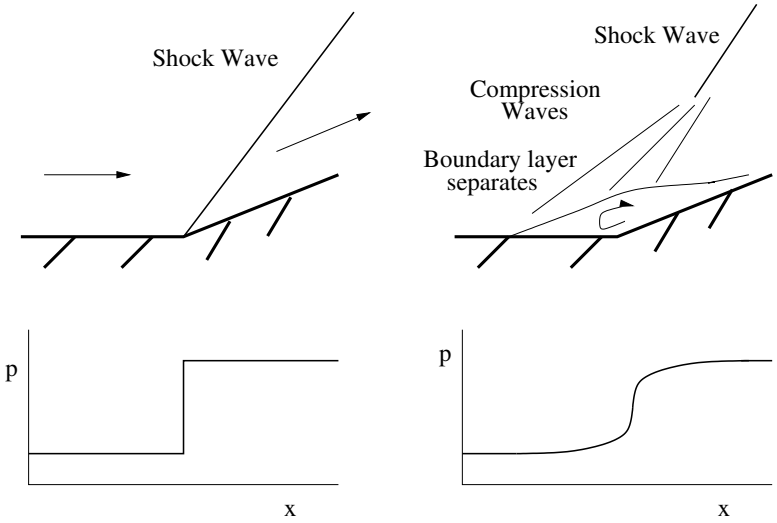

Figure 48: Flowfields and Surface Pressures (approximate) at a Compressive Corner

Under the shock itself, the pressure gradient is extremely adverse. This can lead to transition or separation locally, dependent on the local external Mach number and Reynolds numbers, as well as the condition (laminar or turbulent) of the boundary layer approaching the shock wave. Around convex surfaces, the further acceleration can lead to the formation of a multiple shock system.

If the local external Mach number is greater than about 1.3, the pressure rise associated with the shock wave is generally sufficient to cause separation of the boundary layer ahead of the shock wave, which causes significant compressive turning of the flow in a similar fashion to the flow past a supersonic wedge (the separated flow is low speed, and hence at a relatively high pressure). The sudden change in flow direction around this fluidic wedge causes the formation of an oblique shock ahead of the main shock wave, as you saw in the nozzle experiment lab last year, giving rise to a lambda (or system of lambda) shock wave(s). This causes significant differences between the behaviour of an 'inviscid' and 'viscous' flow in the primary external flow.

Finally it should be noted that the detailed behaviour of such interactions, particularly in three dimensional flows, is extremely complicated, poorly understood, and subject to considerable and ongoing research.

19.4 Drag Reduction through Boundary Layer Control

Boundary layer drag is a significant contributor to the overall aircraft drag. Managing the boundary layer in some way to reduce the amount of drag produced can therefore lead to an improvement in aircraft performance. We shall look at two ways this has been attempted, one of principally historic interest, and one that may yet prove effective.

19.4.1 Laminar Flow Aerofoils

The drag force produced by a boundary layer depends on the amount of laminar vs. turbulent flow; laminar boundary layers have lower skin friction and grow at a slower rate, and hence a greater extent of laminar flow reduces the drag. Towards the end of the second world war, so called *laminar flow* aerofoils were designed to maximise the extent of the laminar boundary layer. Used on aircraft like the Typhoon, Meteor, Mustang, etc., an increase in laminar flow is achieved by shifting the maximum thickness of the aerofoil as far towards the trailing edge as reasonably possible. As generally speaking

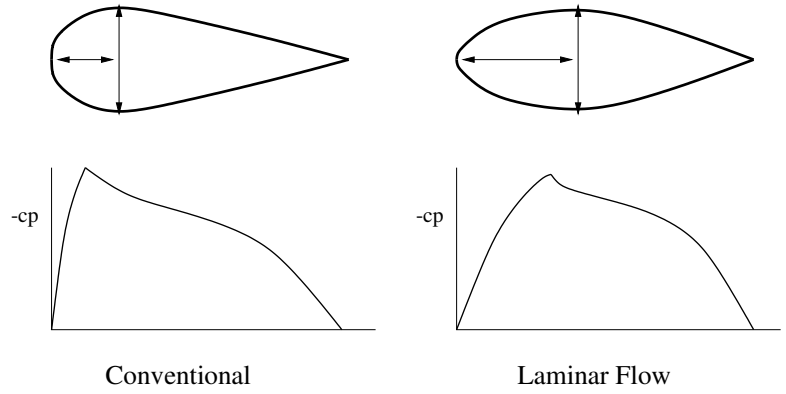

Figure 49: Shape and Pressure Distributions, Conventional and Laminar Flow Aerofoils

the switch from favourable to adverse pressure gradient occurs at some fraction of this widest point, this extends the amount of favourable gradient and hence laminar flow (figure 49). However, as incidence is altered, the location of the minimum pressure moves forward, (as it does on any aerofoil), but has a more dramatic effect on laminar flow aerofoils as the sharper, longer nose means the minimum pressure moves more rapidly with incidence. This is the reason for the 'drag bucket' in figure 50. These aerofoils are therefore only effective for wings which maintain a small range of incidences for the majority of flight. In reality, the problems are worse than this, as transition is highly dependent on roughness, and hence maintaining laminar flow in the face of debris in the atmosphere (dirt, flies, even rain drops) is difficult. Particularly with the advent of transonic cruise (where other considerations dominate), laminar flow aerofoils are generally no longer employed.

19.4.2 Boundary Layer Suction

Unlike the laminar flow concept, which is passive in nature, boundary layer suction is an active drag reduction measure, reliant on a secondary system to suck through a porous wall. This removes mass flow from the boundary layer, in effect 'fooling' it into behaving as if it were at a shorter distance form the leading edge. This process works on both turbulent and laminar boundary layers (in fact sufficient suction can re-laminarise a boundary layer). Unfortunately, power is of course required to maintain the pressure difference between the boundary layer and the suction device, and there is some concern that the amount of power saved by reducing the drag of the aircraft is *less* than the power required to suck the boundary layer. Opinion is divided on this issue, and the optimism and effort going into researching these methods ebbs and flows. Recently there appears to have a been a revival of interest after an extended period of neglect. Whether practical considerations (as with laminar flow aerofoils, such methods are especially sensitive to dirt, dust, etc clogging the suction system) can be overcome and an operational system developed remains to be seen.

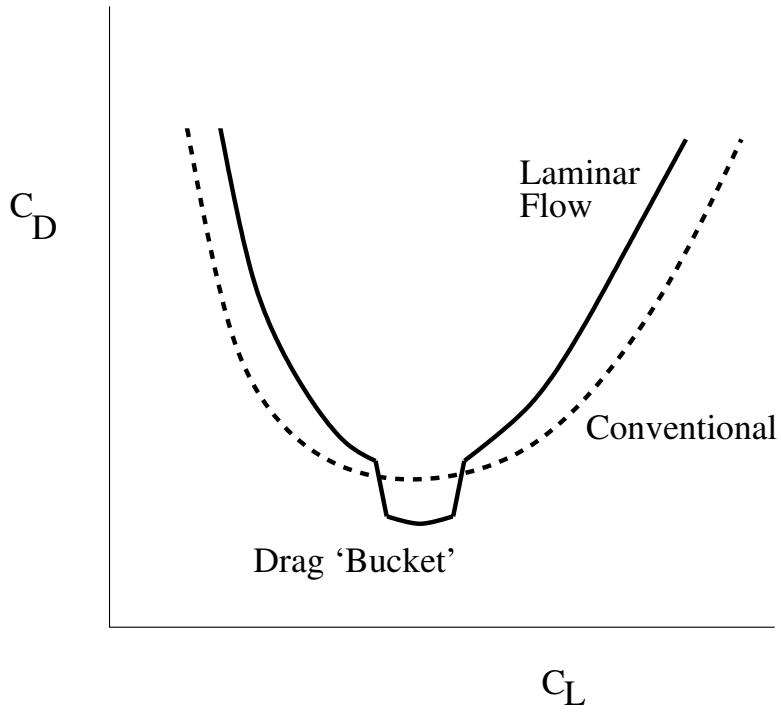

Figure 50: C_L vs C_D, Conventional and Laminar Flow aerofoils

19.4.3 Solution to last weeks Question

List the advantages and disadvantages of differential boundary layer methods compared to integral ones.

Answer
Advantages are: more general applicability, less assumptions about external flowfield, less complex derivations.

Disadvantages are: Requires lots and lots of calculations - must have high speed computers. Turbulence modelling often theoretically suspect, and may not always be generally applicable. Answer can depend on the grid used, this must be crefully designed and hence adds to solution process.

20 Solution Methods for Aerodynamics

Key points: *Multiplicity of methods available, differences between full field and coupled solution methods, variety of techniques and interchangeability of coupled partners, transpiration method and reasons for its use*

20.1 Introduction

In the last lecture of the course, we are going to consider what options are available to an aerodynamicist to solve any given aerodynamic problem. This shall be done in a general and superficial way, and cover all the methods we have already used, plus several other possibilities. However, you should consider that in reality, method selection will of course depend on what tools are actually available at a given company, the relative strengths and weaknesses of each, and what is considered usual practise. It is also true that all the methods outlined below are still evolving, and hence the relative strengths and weaknesses are not necessarily definitive, nor is the list of possibilities exhaustive. Never the less, the points made below are generally valid, and should prove to be a useful guide.

20.2 Full Field Viscous Modelling

The first possibility we shall discuss is the solution of the complete Navier Stokes Equations on a finite volume grid which encompasses the body in question. In practise, this means that we enclose a body within a grid in three dimensions, and then solve the exact equations through finite difference (or volume) equations (for more details see the CpA course). This may sound an attractive and straight forward option, but in reality there are several serious complications.

First, turbulence poses a massive problem; to model the tiny eddies accurately at the Reynolds numbers of aircraft (so called DNS, or Direct Numerical Simulation - see Turbulence course for a full explanation) is entirely impractical, as it would require thousands of years on even the most advanced computers. This being the case, *turbulence modelling* is used, this being a process similar to that discussed in the lecture on differential boundary layer models. This allows solution of the flow, but introduces a plethora of alternative methods (at the last estimate I am aware of, there were well over 100 types of turbulence model, and no prospect of the number diminishing), all of which have different strengths, applications, and most importantly empirical inputs. This often means that the typical user is unaware of all kinds of tweaks inherent in the code design, which in some cases may lead to inaccurate or inappropriate results. In other words, the range of flows to which a given code is applicable may not be apparent to the end user, and worse still the code will often be sufficiently robust that it will produce results that will not be obviously spurious, but *are* inaccurate. These may then be used without the errors being realised. Finally, grid generation is a complex but vitally important area which can be almost as computationally intensive as the solution itself, and many turbulence models are highly sensitive to grid density, and cell size and orthogonality.

That said, Navier Stokes solutions allow the whole flowfield to be solved in one step, be it a time consuming one, and allow the modelling of such features as separation and shock wave - boundary layer interaction. As such they are becoming more widely used, though often in the later stages of the design cycle, i.e. they are used to check the results produced by the simpler, quicker, but less accurate methods used in the initial design. As such they may be thought of as a much cheaper alternative to

wind-tunnel or flight testing.

20.3 Coupled Flowfield Methods

If a Navier Stokes simulation is either impractical or unnecessary, the flow field may be split into two regions, an inviscid majority and a viscous boundary layer. A variety of solution techniques are available for each, and any single inviscid solution method may be used to generate input for any of the boundary layer solvers - all that is passed from one to the other is a pressure and velocity distribution.

The primary techniques available for solution of a three dimensional inviscid flowfield are Euler CFD solvers, panel methods, or the vortex lattice method. these are supplemented by thin aerofoil and Joukowski methods for two dimensional flow. (There are also one or two generally less well used methods that are never the less highly suited to certain design problems, for instance the Method of Characteristics often used for rocket nozzle flowfield analysis, etc.)

- *Euler simulations* are similar to the Navier Stokes methods described above, except viscous effects are ignored. This not only means that the problem of turbulence modelling is avoided, but also that sparser grids may be used (velocity gradients near the wall are much lower), and hence less calculations are needed. Current solution times for a full aircraft configuration are in the order of hours, although this does heavily depend on the configuration. The principal advantage of these techniques is their ability to model non-linear effects such as shock waves accurately, and hence predict transonic flows.

- *Panel Methods* have already been discussed in some detail. A surface pressure distribution can be generated more rapidly than through solution of the Euler equations, but the technique is restricted to subsonic applications. The method is particularly suitable to modelling the flow about cars (especially Formula 1 designs), as well as modelling landing/take-off configurations of aircraft, and low speed aircraft in general (such as light commercial single seaters, etc.).

- The *Vortex Lattice* method has also already been discussed. Again, it is more rapid than the Euler simulation, due to the nature of the formulation it is well suited to wing analysis. However, although solutions at transonic speeds are possible, they are less accurate, and give much less detail (no shock waves, etc.).

- Thin Aerofoil and Joukowski Methods Being limited to two dimensions means these methods are not widely used these days (except as teaching aids).

Turning to the boundary layer, the two principal solution classes have been covered in this course, namely integral and differential methods. However, as discussed there are several different options available for the former, and the latter requires turbulence modelling, with all the variety of methods that entails. Each may therefore be subdivided into categories dependent on whether the flow may be assumed laminar (or not), whether compressibility effects are important (or not) and whether heat transfer is likely to be a significant factor (or not).

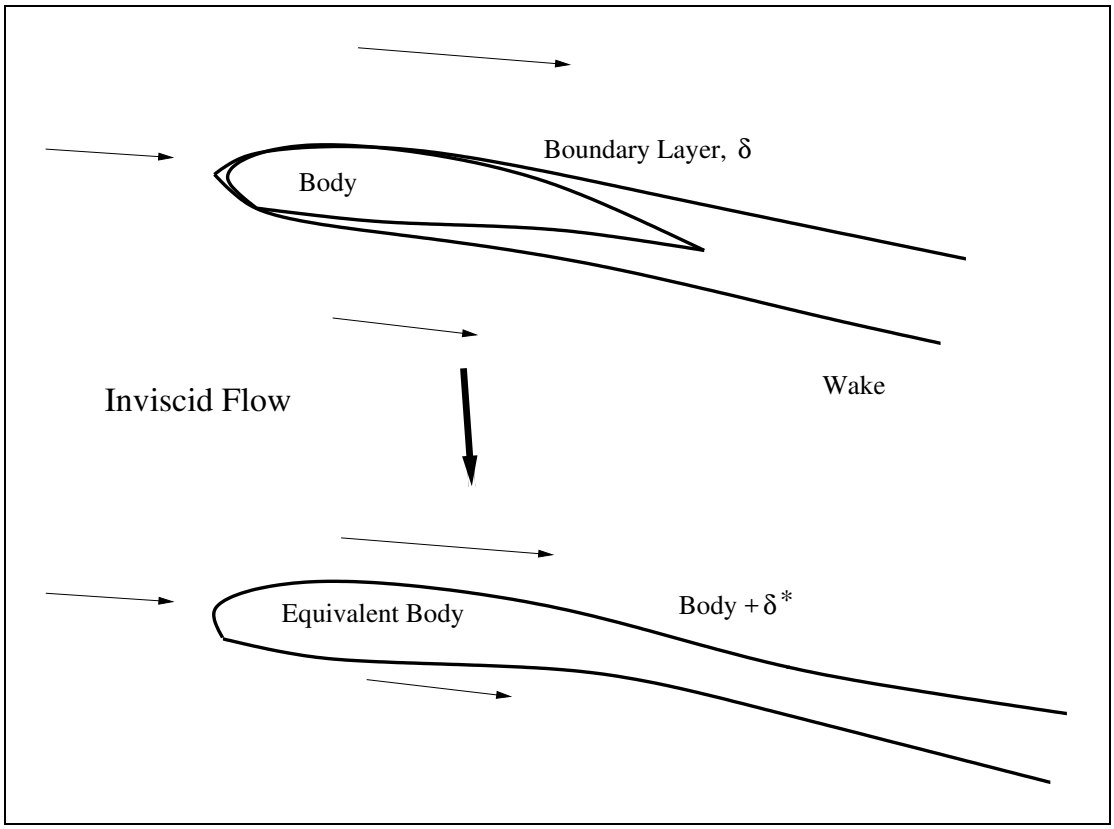

Figure 51: *Effect of Boundary Layer on Inviscid Flowfield*

20.3.1 Coupling

Once the appropriate pair of solution techniques, one inviscid, and one viscous, have been selected, there remains the problem of how to connect the two. In the course so far, we have generally applied the boundary layer solution as a one step correction to the forces produced by the inviscid solution. In many cases, such a method does produce good enough results. However, more accurate results can be produced if the solution provided by the boundary layer solver is used to improve that produced by the inviscid.

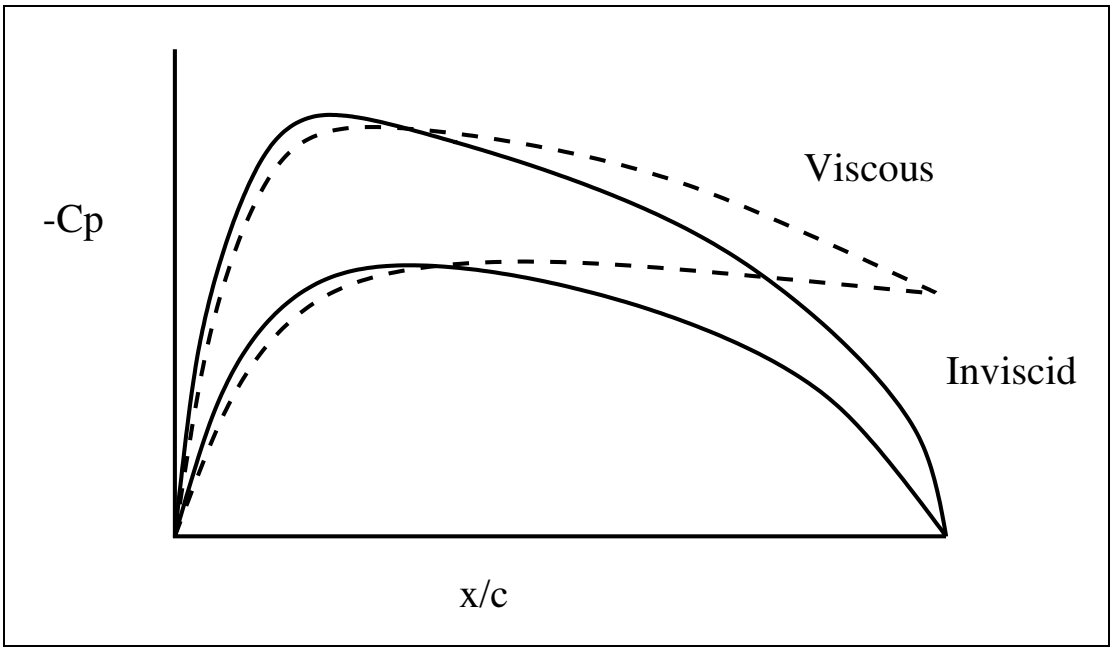

Figure 52: *Effect of Boundary Layer on Pressure Coefficient*

The inviscid analysis of an aerofoil should produce a stagnation point at the trailing edge, assuming sufficient circulation (this in fact is one of the criteria used to generate the Joukowski transformation). This in turn implies that the pressure coefficient, given by

$$c_p = 1 - \frac{p}{p_\infty}$$

is unity at this point, and therefore the velocity ratio $\frac{u}{u_\infty}$ used in the Squire Young method is zero. However, in reality the pressure does not quite recover to freestream here, due to the presence of the boundary layer distorting the extent of the inviscid flow. In effect, the shape the inviscid flow 'sees' is the shape plus the displacement thickness, and thus the displacement thickness in the wake causes the apparent shape to extend to infinity downstream, and hence stagnation never occurs (see figures 51 and 52). This means that the velocity $\frac{u}{u_\infty}$ is in fact non-zero.

This means that re-calculating the inviscid flowfield about the new effective shape, and then recreating the boundary layer from this new flowfield, will give a more accurate estimation for both drag and lift. As the pressure gradients ahead of the trailing edge are also effected, the boundary layer itself will be slightly different, and hence this process is often iterated a number of times.

The change in shape created by the boundary layer thickness may be allowed for in several ways, the simplest being known as the *transpiration* method. Rather than extend the body to be modelled indefinitely downstream, the same shape is used, but a *transpiration velocity* is introduced *through* the surface of the body, such that the vector sum of the surface velocity of the original solution and this transpiration velocity results in a flow tangential to the edge of the displacement thickness at the effective surface (figure 53). The pressures and velocities thus produced are the same as would be calculated for an inviscid solution about the displaced surface.

(As an aside, it should be mentioned that the code I gave you for calculating aerofoil lift and drag actually uses the values for pressure and velocity ratio from the penultimate point on the Joukowski transformation, where the velocity ratio is non-zero. This is the simplest, although least accurate, way of avoiding the difficulty introduced. That explained above is preferable, although more complex).

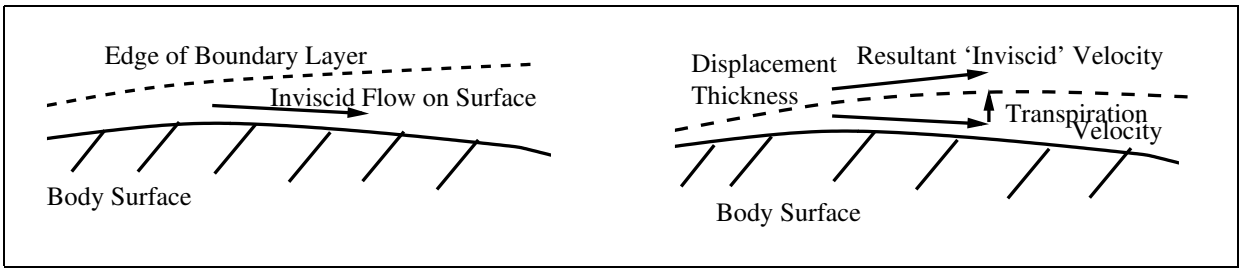

Figure 53: *Effect of Transpiration Velocity*

20.4 Conclusions

As you can see from the diversity of methods discussed here, the number of tools available to the aerodynamicist is considerable. Selection of a method appropriate for the task in hand is vital if the least amount of resources (including time) are to be expended in finding the required solution. You must decide the answers to a series of questions before making this decision, such as what types of flow fields dominate (e.g. inviscid, inviscid with boundary layers, or fully separated three dimensional turbulent flow), and what kind of data is needed at output (i.e. is it just lift and drag, or are detailed surface pressures and velocity distributions required?). Hopefully this course as a whole has given you some insight into how to answer these questions.

21 Revision of Potential Flow

This section is examinable unless otherwise indicated, but contains substantial parts from previous years.

21.1 Stream Function ψ

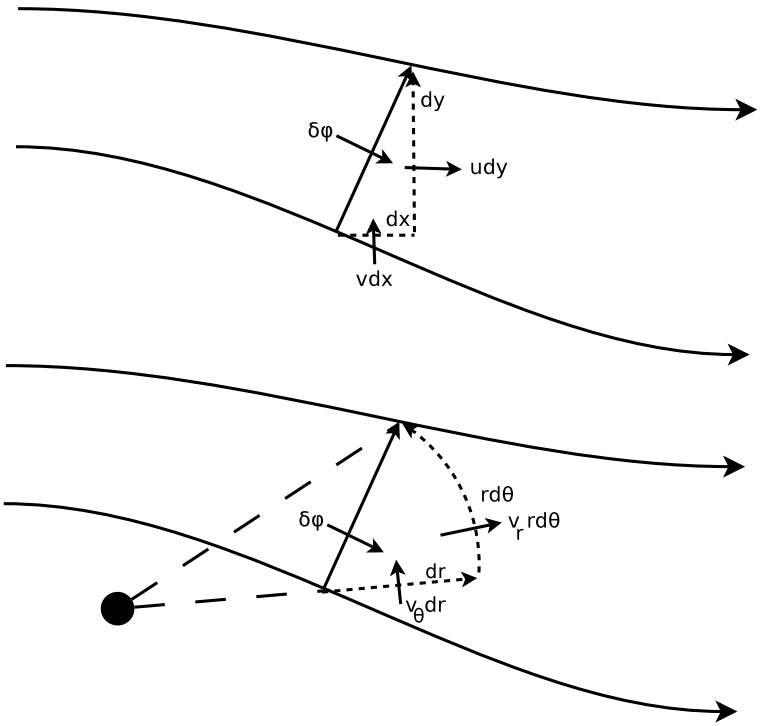

Figure 54: Streamfunction in cartesian and polar coordinates

ψ has a neat interpretation that permits an easy physical understanding. The change in stream function represents the volume flow rate between those two streamlines (along a streamline it remains constant by definition).

21.1.1 Cartesian

The volume flow rate $\delta\psi$ between the streamlines on which A and B lie is

$$\delta\psi = -v\Delta x + u\Delta y \tag{119}$$

This can be derived with a steady control volume from figure 54 so that $0 = \text{in} - \text{out}$.

Calculus tells us that a further result must also hold

$$\delta\psi = \frac{\partial\psi}{\partial x}\Delta x + \frac{\partial\psi}{\partial y}\Delta y \tag{120}$$

By comparison between the two results

$$u = \frac{\partial\psi}{\partial y} \tag{121}$$

$$v = -\frac{\partial \psi}{\partial x} \tag{122}$$

21.1.2 Polar

Volume flow in figure 54 tells us that

$$\delta\psi = -v_\theta \Delta r - rV_r \Delta(-\theta) = -v_\theta \Delta r + rv_r \Delta\theta \tag{123}$$

While calculus says that

$$\delta\psi = \frac{\partial \psi}{\partial r}\Delta r + \frac{\partial \psi}{\partial \theta}\Delta\theta \tag{124}$$

By comparison

$$v_r = \frac{1}{r}\frac{\partial \psi}{\partial \theta} \tag{125}$$

$$v_\theta = -\frac{\partial \psi}{\partial r} \tag{126}$$

21.2 Potential Function ϕ

ϕ has no particular physical meaning; it is simply a scalar, **defined so that its gradient is the velocity**. Linking the gradient to the velocity components is done through comparison to the vector-gradient change, as shown below.

21.2.1 Cartesian

$$\delta\phi = \frac{\partial \phi}{\partial x}\Delta x + \frac{\partial \phi}{\partial y}\Delta y = \nabla\phi \cdot \mathbf{ds} \tag{127}$$

Importantly, the right hand side equality it a vector statement and it is idependent of the coordinate system (cartesian, polar, spherical etc.)

$$\nabla\phi \cdot \mathbf{ds} = \nabla\phi \cdot \begin{pmatrix} dx \\ dy \end{pmatrix} = \begin{pmatrix} u \\ v \end{pmatrix} \cdot \begin{pmatrix} dx \\ dy \end{pmatrix} \tag{128}$$

This can only be true if

$$u = \frac{\partial \phi}{\partial x} \tag{129}$$

$$v = \frac{\partial \phi}{\partial y} \tag{130}$$

21.2.2 Polar

$$\delta\phi = \frac{\partial \phi}{\partial r}\Delta r + \frac{\partial \phi}{\partial \theta}\Delta\theta = \nabla\phi \cdot \mathbf{ds} \tag{131}$$

$$\nabla\phi \cdot \mathbf{ds} = \nabla\phi \cdot \begin{pmatrix} dr \\ rd\theta \end{pmatrix} = \begin{pmatrix} v_r \\ v_\theta \end{pmatrix} \cdot \begin{pmatrix} dr \\ rd\theta \end{pmatrix} \tag{132}$$

Notice the two components are rather different to the cartesian case. The vector statement can only be true if

$$v_r = \frac{\partial \phi}{\partial r} \tag{133}$$

$$v_\theta = \frac{1}{r}\frac{\partial \phi}{\partial \theta} \tag{134}$$

21.2.3 ϕ and ψ Comparison

Learning the following table may be useful:

$$\frac{\partial \phi}{\partial x} = u = \frac{\partial \psi}{\partial y} \tag{135}$$

$$\frac{\partial \phi}{\partial y} = v = -\frac{\partial \psi}{\partial x} \tag{136}$$

$$\frac{\partial \phi}{\partial r} = v_r = \frac{1}{r}\frac{\partial \psi}{\partial \theta} \tag{137}$$

$$\frac{1}{r}\frac{\partial \phi}{\partial \theta} = v_\theta = -\frac{\partial \psi}{\partial r} \tag{138}$$

The interesting symmtery is no coincidence.

21.3 Uniform Flow

$$u = U_\infty \cos(\alpha) = \frac{\partial \phi}{\partial x} = \frac{\partial \psi}{\partial y} \tag{139}$$

$$v = U_\infty \sin(\alpha) = \frac{\partial \phi}{\partial y} = -\frac{\partial \psi}{\partial x} \tag{140}$$

$$\phi = U_\infty x \cos(\alpha) + U_\infty y \sin(\alpha) \tag{141}$$

$$\psi = U_\infty y \cos(\alpha) - U_\infty x \sin(\alpha) \tag{142}$$

$$W = \phi + j\psi = U(x + jy)(\cos(\alpha) - j\sin(\alpha)) = U_\infty Z e^{-j\alpha} \tag{143}$$

21.4 Source/sink

$$2\pi r v_r = \Lambda \tag{144}$$

$$v_r = \frac{\Lambda}{2\pi r} = \frac{1}{r}\frac{\partial \psi}{\partial \theta} = \frac{\partial \phi}{\partial r} \tag{145}$$

$v_\theta = 0$ implies no integration function $f(r)$, just a constant of integration, which may be set to zero.

$$\phi = \frac{\Lambda}{2\pi}\ln(r) \tag{146}$$

$$\psi = \frac{\Lambda \theta}{2\pi} \tag{147}$$

Notice that

$$\ln(Z) = \ln(re^{j\theta}) = \ln(r) + \ln(e^{j\theta}) = \ln(r) + j\theta \tag{148}$$

So

$$W = \phi + j\psi = \frac{\Lambda}{2\pi}(\ln(r) + j\theta) = \frac{\Lambda}{2\pi}\ln(Z) \tag{149}$$

21.5 Vortex

$$2\pi r v_\theta = \Gamma \tag{150}$$

$$v_\theta = \frac{\Gamma}{2\pi r} = -\frac{\partial\psi}{\partial r} = \frac{1}{r}\frac{\partial\phi}{\partial\theta} \tag{151}$$

$v_r = 0$ implies no integration function $f(\theta)$, just a constant of integration, which may be set to zero.

$$\phi = \frac{\Gamma\theta}{2\pi} \tag{152}$$

$$\psi = -\frac{\Gamma}{2\pi}\ln(r) \tag{153}$$

Notice that

$$\ln(Z) = \ln(re^{j\theta}) = \ln(r) + \ln(e^{j\theta}) = \ln(r) + j\theta \tag{154}$$

So

$$W = \phi + j\psi = \frac{\Gamma}{2\pi}(\theta - j\ln(r)) = \frac{\Gamma}{2\pi j}(\theta j + \ln(r)) = \frac{\Gamma}{2\pi j}\ln(Z) \tag{155}$$

21.6 Doublet

A doublet is the limit of a source and sink of equal strength brought closer and closer together. This is not quite the same as a source on top of a sink, which would give zero flow and be of little use.

$$\psi = \frac{\Lambda\theta}{2\pi} = \frac{\Lambda\tan^{-1}\left(\frac{y}{x-a}\right)}{2\pi} \tag{156}$$

$$\psi = \frac{\Lambda\theta}{2\pi} = \Lambda\frac{\tan^{-1}\left(\frac{y}{x+a}\right) - \tan^{-1}\left(\frac{y}{x-a}\right)}{2\pi} \tag{157}$$

Making use of $A = \tan^{-1}\left(\frac{y}{x+a}\right)$ and $B = \tan^{-1}\left(\frac{y}{x-a}\right)$ with

$$\tan(A-B) = \frac{\tan(A) - \tan(B)}{1 + \tan(A)\tan(B)} \tag{158}$$

So

$$\tan(A-B) = \frac{\left(\frac{y}{x+a}\right) - \left(\frac{y}{x-a}\right)}{1 + \frac{y^2}{x^2-a^2}} = \frac{-2ya}{x^2+y^2-a^2} \tag{159}$$

$$(A-B) = \tan^{-1}\frac{-2ya}{x^2+y^2-a^2} \tag{160}$$

We know that a is approaching zero in the limit. So, we can use a small angle approximation for $\tan^{-1}$, but there is still a problem with Λa in the numerator. This cannot be allowed to be zero or

no flow will exist, so we specify that Λ becomes very big as a drops, such that Λa remains fixed at a value κ. We therefore have (noting that a^2 is very small and can be neglected)

$$\psi = \Lambda \frac{\tan^{-1}\left(\frac{-2ya}{x^2+y^2-a^2}\right)}{2\pi} \approx \Lambda \frac{\left(\frac{-2ya}{x^2+y^2-a^2}\right)}{2\pi} \approx \Lambda \frac{\left(\frac{-2ya}{x^2+y^2}\right)}{2\pi} \tag{161}$$

$$\psi = \frac{-\kappa y}{\pi(x^2+y^2)} = \frac{-\kappa y}{\pi r^2} = \frac{-\kappa r \sin(\theta)}{\pi r^2} = \frac{-\kappa \sin(\theta)}{\pi r} \tag{162}$$

$$\frac{\partial \psi}{\partial r} = \frac{\kappa \sin(\theta)}{\pi r^2} = -\frac{1}{r}\frac{\partial \phi}{\partial \theta} \tag{163}$$

$$\phi = \frac{\kappa \cos(\theta)}{\pi r} \tag{164}$$

So

$$W = \phi + j\psi = \frac{\kappa}{\pi r}(\cos(\theta) - j\sin(\theta)) = \frac{\kappa}{\pi r e^{j\theta}} = \frac{\kappa}{\pi Z} \tag{165}$$

Where we have used $e^{-j\theta} = \cos(\theta) - j\sin(\theta)$. This is a bewilderingly simple expression!

You might also wish to derive this straight from a limit in the complex potential. Consider a source at $-a$ and a sink at a, then the source is based on $\ln(Z-(-a))$ and the sink is based on $\ln(Z-a)$.

$$W = \frac{\Lambda}{2\pi}\left(\ln(Z+a) - \ln(Z-a)\right) \tag{166}$$

$\Lambda a = \kappa$ so

$$W = \frac{\kappa}{2\pi a}\left(\ln(Z+a) - \ln(Z-a)\right) \tag{167}$$

$$W = \frac{\kappa}{2\pi a}\left(\ln(Z) + \ln(1+\frac{a}{Z}) - \ln(Z) - \ln(1-\frac{a}{Z})\right) \tag{168}$$

$$W = \frac{\kappa}{2\pi a}\left(\ln(1+\frac{a}{Z}) - \ln(1-\frac{a}{Z})\right) \tag{169}$$

At which point we can use expansion of the logarithm about zero (a is vanishing and Z is finite, so the expansion is valid to use)

$$\ln(1+Z) = Z - \frac{Z^2}{2} + ... \tag{170}$$

to give (truncating series)

$$W = \frac{\kappa}{2\pi a}\left(\frac{a}{Z} - \frac{a^2}{2Z^2} - \left(-\frac{a}{Z} - \frac{a^2}{2Z^2}\right)\right) \tag{171}$$

$$W = \frac{\kappa}{2\pi a}\left(\frac{2a}{Z}\right) = \frac{\kappa}{\pi Z} \tag{172}$$

Note that no assumption was made that a was a purely real number. If a is imaginary, then so is κ since $\Lambda a = \kappa$, which means we can write $\kappa = \kappa_0 e^{j\alpha}$ to give $\frac{\kappa_0 e^{j\alpha}}{\pi Z}$. An imaginary a corresponds to the limit of the source and sink being taken along a line that is not parallel to the real axis, ie. at an angle - which is α. Whether there is a minus simply depends on the direction of the doublet (from sink to source) and the reference line for the angle. As written here, this corresponds to the form of the doublet needed for a lifting flow with angle of attack α.

It is worth pointing out that you can use the conjugate trick to find the strength of a doublet that gives a radius R. The radial velocity, which we want to be zero on $R = Re^{j\theta}$, is (because $e^{j\theta}$ is radial)

$$\frac{dW}{dZ}e^{j\theta} = e^{j\theta}\left(Ue^{-j\alpha} - \frac{\kappa_0 e^{j\alpha}}{\pi R^2 e^{2j\theta}}\right) \tag{173}$$

Setting the real part of this, which is given by $U\cos(\theta-\alpha) - \frac{k_0}{\pi R^2}\cos(\alpha-\theta)$, to zero gives $\kappa_0 = \pi R^2 U$, and so the final complex potential is $W = \frac{R^2 U e^{j\alpha}}{Z}$.

21.7 Linearised C_p

Material here is for information - not examinable.

$$C_p = \frac{2}{\gamma M_\infty^2}\left(\frac{p}{p_\infty} - 1\right) \tag{174}$$

Adiabatic flow gives

$$T_\infty\left(1 + \frac{\gamma-1}{2}M_\infty^2\right) = T\left(1 + \frac{\gamma-1}{2}M^2\right) \tag{175}$$

$$\frac{T}{T_\infty} - 1 = \frac{\gamma-1}{2}\left(M_\infty^2 - \frac{TM^2}{T_\infty}\right) = \frac{\gamma-1}{2a_\infty^2}\left(V_\infty^2 - V^2\right) \tag{176}$$

$$\frac{T}{T_\infty} = 1 - \frac{\gamma-1}{2a_\infty^2}\left(V^2 - V_\infty^2\right) \tag{177}$$

$$\frac{T}{T_\infty} = 1 - \frac{\gamma-1}{2a_\infty^2}\left((V_\infty + V')^2 - V_\infty^2\right) = 1 - \frac{\gamma-1}{2a_\infty^2}\left(2V_\infty V' + V'^2\right) \tag{178}$$

$$\frac{T}{T_\infty} = 1 - \frac{\gamma-1}{2}M_\infty^2\left(2\frac{V'}{V_\infty} + \frac{V'^2}{V_\infty^2}\right) = 1 - \epsilon \tag{179}$$

from isentropic relation

$$\frac{p}{p_\infty} = \left(\frac{T}{T_\infty}\right)^{\frac{\gamma}{\gamma-1}} \tag{180}$$

$$\frac{p}{p_\infty} = (1-\epsilon)^{\frac{\gamma}{\gamma-1}} \approx 1 - \frac{\gamma}{\gamma-1}\epsilon \tag{181}$$

and

$$C_p \approx \frac{2}{\gamma M_\infty^2}\left(1 - \frac{\gamma-1}{2}\frac{\gamma}{\gamma-1}M_\infty^2\left(2\frac{V'}{V_\infty} + \frac{V'^2}{V_\infty^2}\right) - 1\right) \tag{182}$$

$$C_p \approx \frac{2}{\gamma M_\infty^2}\left(\frac{1}{2}\frac{\gamma}{1}M_\infty^2\left(2\frac{V'}{V_\infty} + \frac{V'^2}{V_\infty^2}\right)\right) \tag{183}$$

$\frac{V'^2}{V_\infty^2}$ may safely be ignored to give

$$C_p \approx -2\frac{V'}{V_\infty} \tag{184}$$

References

[1] C.N.H. Lock. The ideal drag due to a shockwave. Technical report, A.R.C., 1946.

[2] C.S. Morawetz. On the non-existence of continuous transonic flows past profiles I. *Communications on Pure and Applied Mathematics*, 9(1):45–68, 1956.

[3] W. Mason. Analytic models for technology integration in aircraft design. AIAA paper no. 1990-3262, AIAA/AHS/ASEE Aircraft Design, Systems and Operations Conference September 17-19, 1990, Dayton OH.

[4] B. Göthert. Plane and three-dimensional flow at high subsonic speeds. Technical report, NACA TM-1105, 1946.

[5] K. Oswatitsch. *Advances in Applied Mechanics, vol. VI: Similarity and Equivalence in Compressible Flow*. Academic Press, 1960.

[6] O. Gur, W.H. Mason, and J.A. Schetz. Full configuration drag estimation. AIAA paper no. AIAA 2009-4109, 27th AIAA Applied Aerodynamics Conference, 22 - 25 June 2009, San Antonio, TX.